CRANFIELD UNIVERSITY

PARASKEVI CHRISTOGIANNI

MANUFACTURING AND CHARACTERISATION OF
PHOTORESPONSIVE COMPOSITES FOR DEFENCE
APPLICATIONS

CRANFIELD DEFENCE AND SECURITY

CENTRE FOR DEFENCE CHEMISTRY

PhD

Academic Year: 2015 - 2016

Supervisors: Dr Mohammed Moniruzzaman

and

Dr Guillaume Kister

June 2016

CRANFIELD UNIVERSITY

CRANFIELD DEFENCE AND SECURITY

CENTRE FOR DEFENCE CHEMISTRY

PhD

Academic Year 2015 - 2016

PARASKEVI CHRISTOGIANNI

Manufacturing and Characterisation of Photoresponsive Composites
for Defence Applications

Supervisors: Dr Mohammed Moniruzzaman

and

Dr Guillaume Kister

June 2016

This thesis is submitted in partial fulfilment of the requirements for
the degree of Doctor of Philosophy

ABSTRACT

The development of composites with improved mechanical and impact resistance properties has attracted considerable attention within the defence and aerospace industries. These composites are finding applications in vehicle or aircraft structures which are frequently exposed to impact from bird strikes, hailstorm, dropped tools and runway debris. In addition, exposure to extreme conditions such as high levels of UV light exposure or extreme temperatures increases the brittleness of the polymer matrix, ultimately leading either to the loss of mechanical properties such as compression strength or even to the catastrophic structural failure of the composites.

The aim of this PhD project was to develop toughened and self-healing composites in which delamination and crack growth can be managed to an acceptable level. This was attempted using a new epoxy-based resin modified with photoresponsive azobenzene. Mechanical properties of the composites, toughened by azobenzene, were improved as a result of the photo-induced changes in the azobenzene structures. Initial works were to identify, synthesise and characterise appropriate photoresponsive resins that were thought to offer composites with enhanced properties. The synthesis of azobenzene acrylic- and epoxy-based polymers were accomplished using conventional wet chemistry. Their properties were triggered by different stimuli and characterised using ^{1}H NMR, UV/Vis and FTIR spectroscopy, DSC, GPC, rheology, and nanoindentation.

The azobenzene/acrylic-based copolymer films showed a significant photomechanical behaviour. Nanoindentation analysis demonstrated a maximum increase in stiffness of 19% with an optimum azobenzene loading of 30 mol%. Such an enhancement in stiffness was attributed to the photoinduced reorganisation of the polymer chains by geometrical isomerisation (*trans* to *cis* isomers) of the azobenzene chromophores.

ABSTRACT

Analysis of the thin films by optical microscopy demonstrated a healing effect of the indented region under UV irradiation suggesting that this class of polymers can be used as self-healing materials.

Ultrasound was also found to trigger *cis → trans* isomerisation in the solid state at a much slower rate (120-150 min) than by visible light (30-60 s).

Azobenzene-modified epoxy resins were synthesised by optimising an existing synthetic route and their responses to light and curing behaviour with a common amine hardener (a curing agent for epoxy resin, used to initiate curing/hardening) were assessed. The resulting kinetic reactions were investigated using isothermal (95°C) and dynamic heating scans (30-180°C) in a DSC and by simultaneously monitoring the spectral information using a NIR-FTIR spectrometer. The modified epoxy azobenzene resin proved to be reactive enough to form a network that can withstand temperatures of up to 200°C.

The azobenzene-epoxy resins exhibited high dimensional stability, stiffness enhancement and healing behaviour when they were exposed to UV light. Gas pycnometer studies demonstrated constant volume and density values of the resins before and after UV irradiation.

Optical and atomic force microscopes were used to assess and quantify the healing effect of damaged azobenzene-based polymer films. An intrinsic healing (73% of the total damaged area) was caused by the UV-induced molecular mobility of azobenzene in a 3D crosslinked network. The influence of UV light and the effect of azobenzene loading on the epoxy-based polymeric matrices were also evaluated after fracture mechanics analysis and it was found that an 11% increase in fracture toughness was observed with 10 mol% azobenzene (without exposure to UV light). On the contrary UV light increased the brittleness of the matrix with higher azobenzene loading.

The azobenzene-modified epoxy resin was used to produce glass fibre-reinforced composites. Their photo-induced properties were investigated by compression, impact and post-impact compression testing. The composites

ABSTRACT

exibited an increase (3-16%) in compressive strength after exposure to UV light due to the *trans* → *cis* isomerisation. Moreover, it was demonstrated that the introduction of a small fraction of azobenzene (10 mol%) into the composites enhanced their impact resistance by 10% when subjected to high velocity impacts (190 m/s). The absorbed energy of the azobenzene composites which had been previously exposed to UV light was also increasing linearly with the azobenzene loading.

Keywords: Photosensitive polymers; mechanical properties; azobenzene; self-healing; epoxy glass fibre composites

ACKNOWLEDGEMENTS

ACKNOWLEDGEMENTS

ACKNOWLEDGEMENTS

"One becomes two, two becomes three, and out of the third comes the one as the fourth."

TABLE OF CONTENTS

LIST OF FIGURES

LIST OF FIGURES

LIST OF FIGURES

LIST OF FIGURES

LIST OF TABLES

LIST OF FIGURES

LIST OF EQUATIONS

LIST OF ABBREVIATIONS

^{1}H NMR	Proton nuclear magnetic resonance
AB	Azobenzene
ACN	Acetonitrile
AFM	Atomic force microscopy
AIBN	Azoisobutyronitrile
AOAB	4-acryloyloxyazobenzene
ATRP	Atomic transfer radical polymerisation
CAI	Compression after impact
CC	Column chromatography
DGOAB	Diglycidyloxyazobenzene
DMA	Dynamic mechanical analyser
DMF	Dimethyl formamide
DMOAB	Dimethacryloyloxyazobenzene
DMSO	Dimethyl sulfoxide
DSC	Differential scanning calorimetry
ELVIS System	Explosive (or Extremely) Low Velocity Impact System
FTIR	Fourier transform infrared
gamma-BTLC	gamma-butyrolactone
GOAB	Glycidyloxyazobenzene
GPC	Gel permeation chromatography

LIST OF ABBREVIATIONS

HPLC	High performance liquid chromatography
HR	Healing ratio
HV	Hardness Vickers
IR	Infrared
LC	Liquid-Crystal
m.p.	Melting point
MMT	Montmorillonite
MOAB	4-methacryloyloxyazobenzene
PB	Polybutadiene
PC	Polycarbonate
PD	Polydispersity
PEMA	Polyethylmethacrylate
PMAA	Polymethacrylic acid
PMMA	Polymethyl methacrylate
PS	Polystyrene
PVC	Polyvinyl chloride
PVE	Polyvinyl ether
RAFT	Reversible addition fragmentation chain transfer
SEBN	Single edge notched beam
SEC	Size exclusion chromatography
SEM	Scanning electronic microscope
SMASH	Shape memory assisted self-healing

SMP	Shape memory polymers
SRG	Surface relief gratings
TEA	Triethylamine
THF	Tetrahydrofuran
TLC	Thin layer chromatography
TMA	Thermal mechanical analyser
UV/Vis	Ultraviolet-visible

LIST OF SYMBOLS

A	absorbance
b	path length
c	concentration
d	diagonal of the diamond indenter
E_i	elastic modulus of the indenter
E_r	reduced modulus of the indentation contact
F	force
h	indentation depth under applied force
I	light intensity
K_{IC}	Critical stress intensity factor
m	mass
M_n	number average molecular weight
M_w	weight average molecular weight
pK_a	acid dissociation constant
T	transmittance
T_g	Glass Transition Temperature
T_m	Melting Point Temperature
v_i	Poisson's ratio of the indenter
v_s	Poisson's ratio of the sample
Δl	length difference
γ	shear rate

LIST OF SYMBOLS

η	viscosity
μ	reduced mass
ν	frequency
τ	shear stress
$\emptyset$	diameter

1 INTRODUCTION

1.1 General Overview

Polymer matrix composites are common and used in many engineering applications, such as commercial and military aircraft structural components.[1-3] Their uses are advantageous due to their high specific strength, high specific stiffness and light weight properties in comparison to metals.[4] Composites that are used as primary structures in defence and aerospace applications, are well known to undergo extensive matrix cracking and delamination damage during impact. Bird strikes and hail ice in the case of aircraft platforms, as seen in Figure 1.1.1, are some examples of impact events after which the compressive strength of fibre-reinforced polymer composites is reduced.[5, 6] Furthermore, out of all of the environmental effects (such as temperature, ultraviolet (UV) light or erosion by the air stream), UV irradiation is one of the most damaging parameters to polymeric materials. Exposure to these extreme conditions weakens the resin component of the composite, reducing their overall strength before the composite part cracks or delaminates. According to Kumar *et al.* the formation of micro-cracks in the epoxy matrix occurs due to the increased cross-linking from photo-oxidation reactions that are activated by UV light which induces the polymer matrix to become more brittle.[7] The consequence of this damage is the loss of mechanical properties such as compression strength and can even lead to catastrophic structural failure of the composites.

For this reason composite parts with the ability to exhibit tolerance to delamination, damage and impact when they are subjected to harsh environmental conditions such as UV light or extreme temperatures are required.

One of the methods used to develop composites with enhanced stiffness, impact strength and fracture toughness is the incorporation of nano fillers such as nano clays, nano fibres and nano tubes.[8] Avila *et al.* demonstrated that the dissolution of 5% montmorillonite (MMT), which is a colloidal layered silicate mineral, into an epoxy system has led to an increase in stiffness (by 11%) and

INTRODUCTION

energy absorption (by 4%) for 80 J impact energy.[9] The authors attributed these changes to the presence of nanoclays which affected the failure mechanism from interlaminar to an intralaminar failure and enhanced the mechanical properties of glass fibre composites.

Nevertheless a big disadvantage of this approach is the possibility for agglomeration of the nano fillers inside the matrix due to the absence of chemical bonding between the polymer and the particles or improper dispersion that can result in stress concentration and might lead to the composites' failure.[10]

The studies presented here aim to moderate the deterioration of the composite's mechanical properties and to reduce the formation and growth of micro-cracks with a new approach.

Figure 1.1.1 Plane's fuselage and wings are made largely from carbon-fibre composite (Taken from Ref.[5]), b) and c) damage due to bird strike (Taken from Ref.[6])

This will be accomplished by incorporating stimulus-triggered materials, such as photoresponsive (or photosensitive) polymers into laminated composite systems.[11] Photoresponsive polymers are defined as polymers that respond to UV or visible light by undergoing changes in their chemical structures

INTRODUCTION

(geometrical isomerisation, ring-opening, etc.) and/or their physical properties (absorptivity, polarity, pH etc.).[12, 13] Their inclusion into a polymer composite will have a direct effect on the latter's mechanical properties, such as stiffness or hardness, once they are exposed to sunlight or other stimuli. These polymers, whose strength is expected to increase after exposure to UV radiation, may have the ability to improve the mechanical properties of composites. The beneficial results of the enhancement of the polymer composites with photoresponsive character will be highlighted by evaluating the post-impact mechanical properties of the composites. The combination of increased toughness and healing characteristics will improve the structural integrity of the composite structures, hence increase safety and reduce down time and maintenance costs of any application into which the modified material is incorporated.

In this work, the synthesis of light triggered polymers and formulation of composite materials are addressed in an attempt to generate photomechanical responses that will improve the mechanical properties of the materials. Azobenzene was the photoresponsive molecule that was chosen as the focus of this study. It has the ability to change its geometrical structure reversibly from *trans↔cis* by undergoing a photoisomerisation reaction, after exposure to specific wavelengths of light. More significantly, azobenzene functionalised molecules were synthesised, characterised, then polymerised or co-polymerised prior to the manufacture of epoxy/glass fibre composites with a strong interfacial bonding that can effectively transfer the load from the matrix to the reinforcement.

Two kinds of polymers were investigated: the acrylic-based, which belong to thermoplastic elastomers, and the epoxy-based, which belong to thermosetting polymers. The thermoplastics have the ability to be remoulded, by heat or solvents, as their curing process is reversible. They can be used for recyclable, reshaping or high-impact resistance applications. On the other hand, the thermosetting polymers do not exhibit a reversible curing process, as they

3

contain a cross-linked network of polymer chains and can be used for applications that require high temperature or deformation resistance.[14] Understanding the effect of azobenzene photoisomerisation, when incorporated into acrylic or epoxy resin matrices, on the mechanical properties of the materials is of high importance. This information may contribute to the improvement of composite structures.

Polymethacrylic copolymers with azobenzene in the side chains and a loading range of between 0-100 mol% were synthesised using a free radical polymerisation. Their optical, spectral, thermal and mechanical properties were examined with respect to the changes that are provoked by UV radiation. Investigations into reversible or repeatable behaviour of the synthesised light-triggered azobenzene polymers are summarised. In addition, the influence of different stimuli, such as heat and ultrasound waves, was investigated by UV/Vis, nuclear magnetic resonance (NMR) spectroscopy and high performance liquid chromatography (HPLC) analyses. The generation of simple polymeric thin films gave the opportunity to perform nanoidentation experiments that allowed a more in-depth and detailed understanding of the photo-induced changes in the mechanical properties as a function of the concentration of azobenzene.

Studies investigating the healing effect upon the indented areas of the polymer films containing azobenzene, were performed using optical and digital microscopy after being subjected to UV irradiation. These polymers belong to the un-reinforced acrylic resins and they have possible applications in the cosmetic repairing of vehicle bodies for instance where fast action is required to prevent crack propagation.[15]

Regarding the epoxy-based polymers, a modified resin, consisiting of a difunctional epoxy azobenzene monomer was synthesised. It was used at different molar ratios (1–10%) in a common bi-resin (epoxy/hardener)/glass fibre reinforced composite system. The azobenzene modified resin was mixed with the bi-resin system and the composite panels were manufacturing by the

autoclave process. Fracture mechanics and nanoindentation tests of the cured azobenzene resins were conducted before and after exposure to UV light as initial tests to understand whether or not the photo-induced mechanical changes of the polymers can be transferred into the whole composite matrix and affect the stiffness of the composite.

Healing of damaged areas after exposure to UV light was analysed using an atomic force microscope (AFM). Compression tests of the azobenzene composite panels and impact and post-impact tests on non-UV and UV irradiated specimens were performed in order to identify the effect of photoisomerisation on the propagation of the caused damage.

For the first time the use of azobenzene in composite materials with glass fibre reinforcement has been demonstrated and their effects on physical and mechanical properties of the composites after exposure to various stimuli, like light, heat and ultrasound waves. Those materials and methods might be beneficial for future applications in manufacturing composites with enhanced impact damage tolerance and improved resistance to deterioration of structures in harsh environments.

1.2 Aims and Objectives

The aim of this PhD project was to develop toughening and healable composites where delamination and crack growth can be managed. This was achieved by incorporating photoresponsive polymers into the composite matrix. With the aid of these polymers the mechanical properties of the composites should be improved even after UV irradiation. The main objectives of the programme were:

- Synthesis of a series of azobenzene precursors, monomers, homopolymers and copolymers
- Characterisation and identification of azobenzene monomers and polymers

INTRODUCTION

- Formulation of photoresponsive composites by incorporating azobenzene-based polymers
- Characterisation of the mechanical properties of composites before and after UV irradiation
- Investigation and evaluation of the impact tolerance of the composites before and after UV irradiation

The first part of the project was to synthesise and characterise photosensitive polymers whose stiffness and strength is expected to increase after exposure to UV radiation. It was necessary to synthesise these polymers because the photosensitive molecules cannot make a significant contribution to photo-induced changes in the matrices when they are only doped. However, these changes are profound when they are covalently attached to a polymeric chain. When the photosensitive molecules are doped, their influences are more local, whereas when they are attached to a polymeric backbone, they affect the whole chain. Upon selection of a suitable photoresponsive polymer, the next step was the formulation of composite materials by incorporating the monomer into the resin prior to consolidating the composite. The toughening and healable characteristics of the photosensitive polymeric composites were assessed by monitoring their post-impact behaviour before and after exposure to UV radiation. It was expected that when the photosensitive and resin molecules are well-bonded together, the delamination in the composites would be reduced and their strength and rigidity would be improved.

1.3 Innovation of project

1.3.1 Existing knowledge:

Previous researchers have demonstrated that using doped or chemically incorporated photosensitive azobenzene into polymers leads to changes in the physical and mechanical properties of the whole polymeric matrix after

exposure to light.[16-20] Very few studies though have considered the incorporation of azobenzene-based polymers into composites.

Umeyama *et al*. reported for the first time in 2010 the dispersion of azobenzene polymers with carbon nanotubes and demonstrated photoresponsive behaviour, with geometrical changes, by spectroscopic analysis.[21] Later, Vijayakumar *et al*. and Imin *et al*. confirmed the photo-induced spectroscopic changes of different azobenzene-based polymers reinforced with carbon nanotubes.[22, 23] The next study was published by Kawata *et al*. in 2015 using composite gels that consisted of doped azobenzene molecules and polymer silica particles.[24] The authors observed a gel-sol transition in the composite gels, upon UV irradiation, which was attributed to the azobenzene that underwent the *trans→cis* isomerisation. Moreover the azobenzene in the composite gels acted as a repairing mechanism for surface cracks.

1.3.2 What is unknown?

An area of study is the effect of the azobenzene on the behaviour and properties of the fibre-reinforced polymer composites. Can the azobenzene toughen the composites under impact? Can the physical changes in azobenzene occur within the composites, resulting in improvement of the matrix-dominated mechanical properties and healing of the damage? Among various stimuli that trigger isomerisation in azobenzene molecules, sonication is one that has not been examined in solid materials.

1.3.3 What is the novelty of this project?

In this project there were seven new and significant studies that were conducted, aiming to understand the behaviour of azobenzene and its modifying effect when incorporated into polymers and composite materials. These are as follows:

- Sonication [irradiation with ultrasound waves] as a stimulus on solid-state azobenzene-based polymers

- The optimum amount of azobenzene within the polymeric matrices corresponding to the maximum photo-mechanical effect
- Reaction kinetics of epoxy azobenzene resins with common hardeners
- The influence of azobenzene on fracture mechanics of polymeric matrices
- Investigation of the compression properties of azobenzene-based epoxy resin/glass fibre composites before and after exposure to UV light
- Investigation of the healing effect of azobenzene in polymeric matrices and azobenzene-based epoxy resin/glass fibre composites before and after exposure to UV light
- Investigation of the impact tolerance of azobenzene-based epoxy resin/glass fibre composites before and after exposure to UV light

1.4 Outline of Thesis

This dissertation consists of five chapters. The present chapter, Introduction, provides a general overview of the project, the problem statement and the ultimate aims of this PhD project. The Theoretical Background chapter follows, where a review of azobenzene photosensitive polymers and composites is presented. The third chapter, Experimental Methods, outlines the materials and the characterisation techniques for the polymers, including their theory and the mechanical testing methods used for the composites. Results and Discussion is the fourth chapter, where all the results from the characterisation of the synthesised polymers, the mechanical testing of the azobenzene polymers and epoxy/glass fibre composites are presented and discussed. The last chapter is the Conclusions, which contains the main outcomes from the PhD project and suggestions for future studies. Figure 1.4.1 presents the overall structure of this thesis.

INTRODUCTION
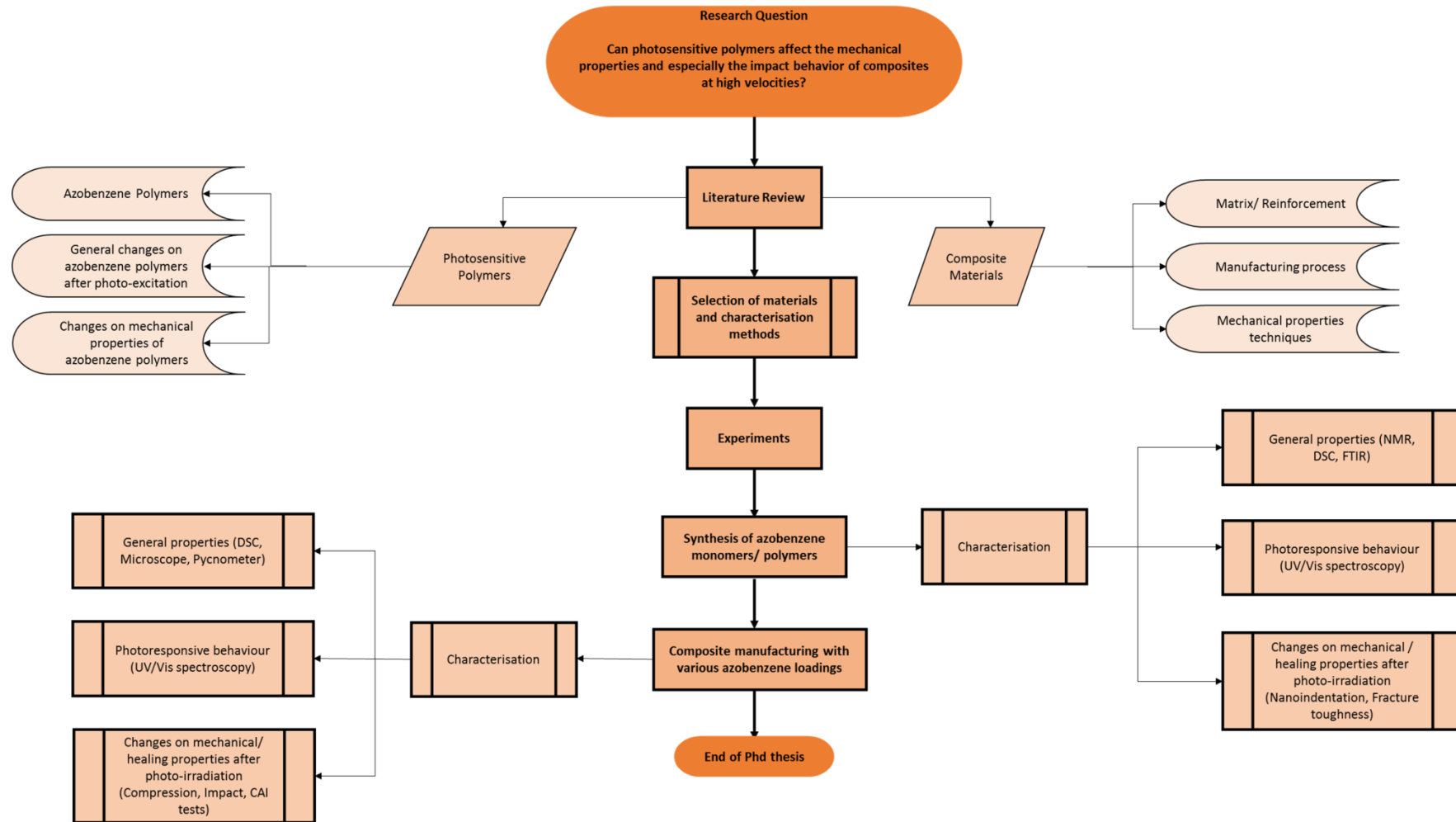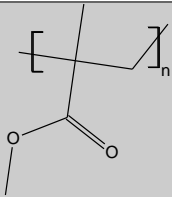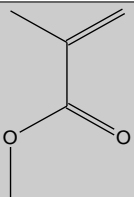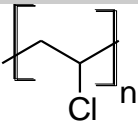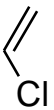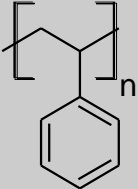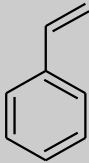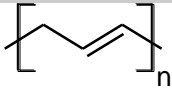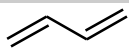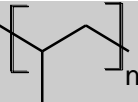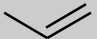
Figure 1.4.1 Thesis flowchart

2 THEORETICAL BACKGROUND

2.1 Fundamentals of synthetic polymers

A polymer is a large molecule built up by the repetition of small units, called monomers.[2, 25] Monomers have either multiple covalent (double or triple) bonds or reactive functional groups, which permit them to connect to each other to produce polymers.[26]

Table 2.1.1 Synthetic polymers and their applications

Polymer	Repeat Unit	Monomer	Applications
Polymethyl methacrylate (PMMA)			Aircraft and aquarium windows, lenses, human tissues, etc.
Polyvinyl chloride (PVC)			Pipes, plastic cards, cables, etc.
Polystyrene (PS)			Food packaging, cups, CD cases, etc.
Polybutadiene (PB)			Tyres, rubbers, etc.
Polypropylene (PP)			Carpets, baby bottles, food containers, bags, etc.

Polymers are molecules of great importance that have a large variety of applications in modern life. They are segregated in two main categories, natural

and synthetic. Some polymers with their repeated unit and their applications are summarised in Table 2.1.1.

Natural polymers have been known and used by people for many years. They are natural molecules such as DNA, cellulose and cotton. On the other hand, synthetic polymers exhibit unique properties like rubber elasticity or high tensile strength. They are used instead of the biological ones, as the basic "ingredients" for the industrial production of clothes, furniture, medical equipment, food packaging, etc.[2, 25]

The common characteristic of all the polymers is the repetition of their monomeric units. They differ in chemical structures and architectures which trigger the variations in their properties. In some cases the repetition of monomers is linear, like a chain, in other cases the chains are branched or cross-linked, forming a network. Different types of polymer chains are schematically shown in Figure 2.1.1.

linear
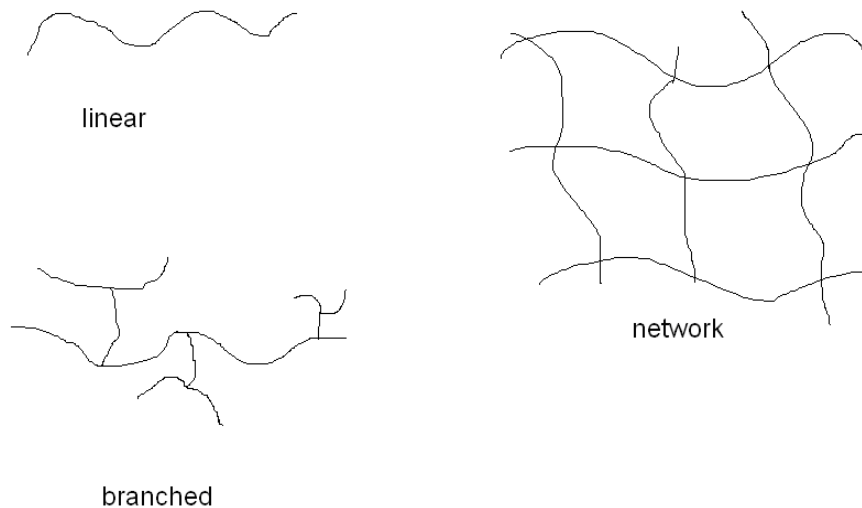
network

branched

Figure 2.1.1 Structure of linear, branched and network polymer chain

The linear polymers are molecules whose repeat units are connected to each other into a linear backbone. Under specific conditions, e.g. if the polymer is heated, free movement can be observed, which explains the elastic or glassy behaviour of elastomers or thermoplastics. For example, polyethylene is a linear

polymer with the following structure generated from CH=CH monomers, where n is the number of the repeat units.

~~CH_2- CH_2- CH_2- CH_2- CH_2-~~   or   -[- CH_2- CH_2-]$_n$-
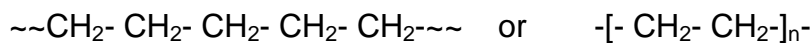
Branched polymers are characterised by more than two linear chains connected at a single or multiple junction point. They can be synthesised from monomers with more than two functional groups. Their intermolecular forces are weaker than those of linear polymers because the branched molecules are linked with one another more distantly. Thus branched molecules display more flexible properties. For instance, the branched polyethylene is well known for its flexibility, which makes it ideal for the production of grocery bags.[27]

Network or cross-linked polymers are formed when linear polymers react with a multifunctional reactive agent, known as cross-linking agents. Polymers with a greater number of crosslinks are harder, more rigid and more tolerate to deformation. They cannot be dissolved in solvents due to the presence of strong covalent bonds. On the other hand, those with less crosslinks and more flexible branches tend to exhibit more reversible properties, like reshaping after heating or when subjected to solvents.[25, 26] Polymers with linear structure have the potential to become stiffened and strengthened by the cross-linking mechanism, where linkages are formed between the chains. Difunctional epoxies are a key example of cross-linking polymers.

Polymers are also divided into two other important groups, as has been previously mentioned within the Introduction Chapter, depending on their thermal behaviour. These are the thermoplastics and the thermosets. The thermoplastic polymers are formed from one kind of polymer chains, while the thermosets are synthesised by cross-linking multifunctional units of the same or different monomers.[3] When thermoplastics are heated, their thermal energy overcomes the weak bonds between chains, so the substance becomes softer until it melts. Thermosets are synthesised by the reaction between a multifunctional hydrocarbon molecule, more specifically a resin, and a hardener,

which attaches the resins together. Thermosets are stronger and more thermally stable than the thermoplastics and cannot be deformed by heat due to these rigid bonds between the polymer chains.[28] For example PMMA, a typical thermoplastic polymer, consists of only C-C and C-H covalent bonds which are weaker than the –N=C=O bonds present in a polyurethane thermoset.

2.1.1 Overview of polymerisation methods

The method by which monomers are transformed into a polymer is called polymerisation and is divided into two types: step-growth and chain-growth polymerisation. In order to obtain the desired polymer it is necessary to determine which reaction is suitable with respect to the repeated monomeric units.

In step-growth polymerisation (e.g. condensation) all molecules (monomer, oligomer and polymer) can react with any other molecule. The reaction proceeds fast at the beginning but the molecular weight increases only slowly and high molecular weight polymers are only obtained at the end of the process.[29] A condensation polymerisation is used for monomers with difunctional or multifunctional groups such as –X, –OH, –COOH, –NH$_2$, etc. This is usually a reaction procedure accompanied by the elimination of a small molecule like H$_2$O, HCl, etc.
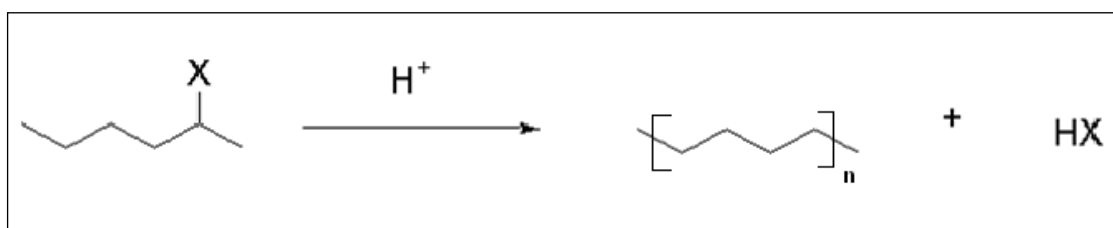
Figure 2.1.2 Reaction scheme for condensation polymerisation.

Condensation reactions occur when a nucleophile attacks a hydrogen rather than a carbon atom. This can be explained by the fact that the nucleophilic

substance acts as a base. In these reactions a small molecule like HBr or H_2O is eliminated as is illustrated in Figure 2.1.2. By this approach there is a fast and a slow intermediate step. The latter one is also the rate determining step.

An example of condensation polymerisation is this between epoxy and amine with elimination of a H_2O molecule. Epoxy is composed of a three-member ring (oxirane or epoxy ring), containing an oxygen atom that is bonded with two carbon atoms. Epoxy resin is a molecule that contains more than one of these epoxy rings and their number per molecule demonstrates the functionality of the resin. Epoxy groups react with suitable curing agents or by homopolymerisation (use of catalyst) to form cross-linked polymeric structure.

An amine as curing agent or hardener is a base, added to an epoxy resin to promote the curing reaction by chemically reacting with each other. They become solidified through a chemical curing reaction shown in Figure 2.1.3.[30] Primary amines react with an epoxy group to form a hydroxyl group and a secondary amine. The secondary amines react further (but with half reactivity than of this of the primary amines) with an epoxy to form a tertiary amine and an additional hydroxyl group.

The liquid epoxy resins are generally the most desirable to use in composite formulations due to ease handling, high reactivity and crosslink density. The crosslink density results in a good heat and chemical resistance to the composite materials.[31]

Azobenzene epoxy functionalised molecules have been synthesised and studied by elementary and spectroscopic techniques but they have not yet been examined with regards to their reactivity or curing behaviour in a composite system.[32] It is of great interest to investigate the use of photoresponsive epoxy resins into composite materials, for the contribution of possible new desired properties. Recently, an azobenzene-based liquid-crystalline polymer/nanotube composite strip showed fast and reversible deformation under UV irradiation.[33] The associated nanotube structure also demonstrated that the composite strip

had much higher mechanical strength compared to the unfilled azobenzene polymer.
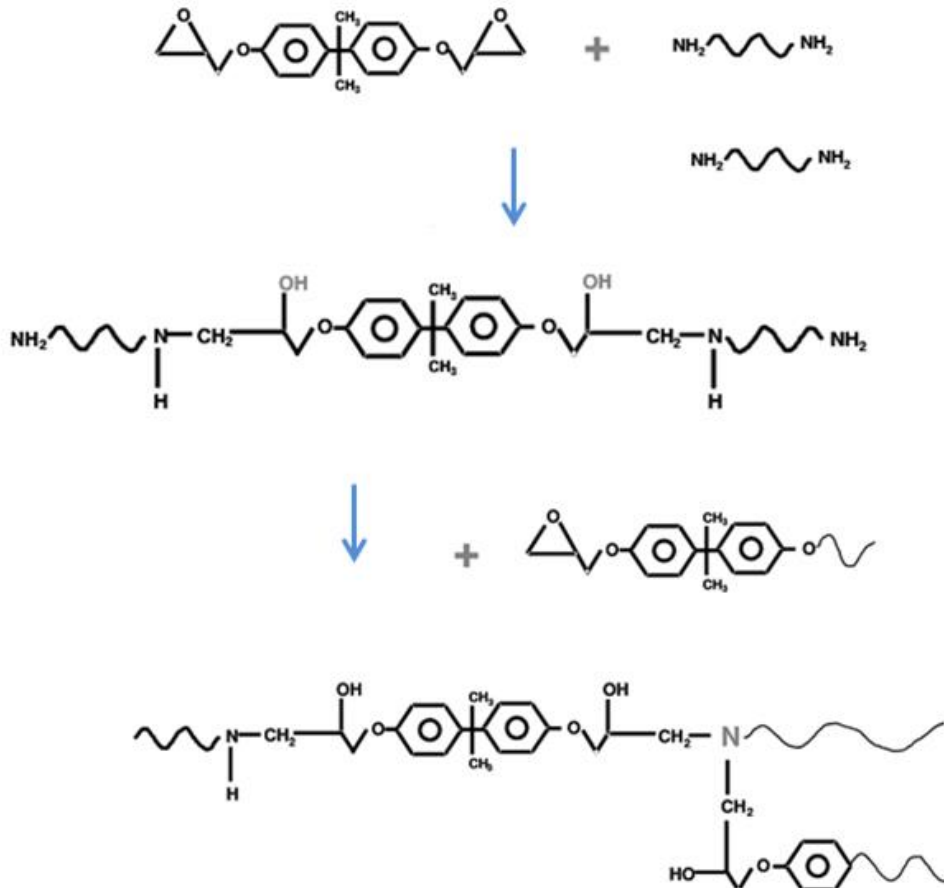
Figure 2.1.3 Representation of curing reaction between epoxy resin and amine (hardener)

On the other hand, chain growth polymerisations (e.g. addition) occur where polymer chains grow by reaction of monomer with a reactive end-group on the growing chain.[29] The reaction speed depends on the concentration of initiator and high-molecular weight polymers form throughout the duration of the reaction. Long reaction times have high degrees of conversion but without

affecting significantly the molecular weight. Addition polymerisations are chain reactions which transfer the monomers into polymers, activated by the opening of the double bond with a free radical or ionic initiator. The repeated unit of the polymer has the same chemical composition as the monomer, e.g. ethylene $CH_2=CH_2$ forms polyethylene $-(CH_2-CH_2)_n-$, without any molecule being eliminated. The monomers should have double or triple bonds for this polymerisation. A free radical polymerisation involves initiation, propagation, and termination steps. The initiation step starts the polymerisation by forming a radical with the aid of an initiator, for example azoisobutyronitrile (AIBN). The propagation step extends the chains by the addition of more repeating units with the initiated radicals, while the termination step involves the deactivation of the radical by combining the radicals or by adding a terminating agent. The route of free radical polymerisation is written as follows:

$I \rightarrow 2R-$ (Initiation)

$R- + M \rightarrow RM-$ (Propagation)

$RM- + M \rightarrow RMM-$

$RM_{n-1}- + M \rightarrow RM_n-$

$RM_n- + RM_n- \rightarrow RM_n-M_nR$ (Termination)
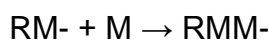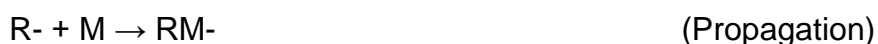
The initiators that are utilised for addition polymerisation are activated thermally or by light irradiation to start the polymerisation reaction. Especially in polyacrylate esters, radical polymerisation happens easily enough due to the intermediate carbon radical which is stabilised by conjugation with the carbonyl group, shown in Figure 2.1.4.
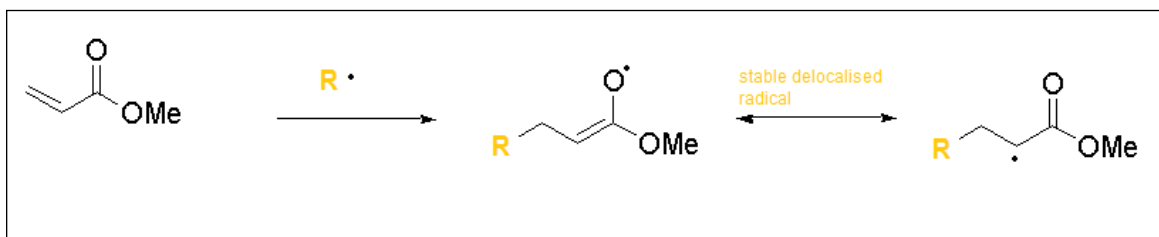
Figure 2.1.4: Reaction scheme for free radical polymerisation

In a wide range of studies conventional free radical polymerisation has been preferred method for the synthesis of azobenzene- based polymers to be studied in this project,[11,12,19, 34, 35] since this method is simple and cost effective. For example, it can be conducted by mixing and heating an appropriate amount of monomer, initiator and solvent (not necessarily). Then the polymerisation process is continued under a specific time and temperature, depending on the kinetics of the reaction. Finally, the polymer should be isolated from the solvent by a more appropriate technique like crystallisation, precipitation or evaporation of solvent. Common organic solvents used for polymerisation are, for example, tetrahydrofuran (THF), chloroform ($CHCl_3$), and dimethylformamide (DMF).

The free radical polymerisation technique is often used for preparation of polymeric films containing azobenzene molecules by photopolymerisation.[36-39] Photopolymerisation involves the use of UV and visible light that produces free radicals leading to the formation of a polymer or its network. The reaction rates can be controlled and increased by turning the light on and off and by changing the light intensity, respectively. Photopolymerisation can be fast and conducted at room temperatures and thus offers cost-effectiveness and environmental benefits.[40]

Not all monomers can be polymerized by a specific chain polymerisation method. On Table 2.1.2 different polymerisation methods can be seen. There is a selectivity factor that depends on the chemical structure of each molecule. As mentioned earlier, if there is a double bond, such as in MMA then radical

polymerisation is more preferable, whereas for instance for the formation of polyethylenimine (PEI) networks, polymerisation occurs via the condensation reaction.

Table 2.1.2 Polymerisation methods used for different azobenzene matrices

Polymeric matrices containing azobenzene	Polymerisation methods	Initiators	Ref.
Cross-linked liquid-crystalline polycarbonate	Photopolymerisation	Irgacure-784	[36, 37, 41]
Graft PMMA	Free radical polymerisation	AIBN	[42, 43]
PCL and PVE	Cationic polymerisation	BF_3-OEt_2	[44]
PMMA brushes	Surface radical polymerisation	AMCS	[45]
Polycarbonate	Free radical polymerisation	AIBN	[46]
PMMA	Free radical polymerisation	AIBN	[19, 34, 35]
PEI, PDADMAC	Condensation polymerisation	-	[47]
PEA networks	Free radical polymerisation	AIBN	[48]
Acrylate elastomeric networks	Photopolymerisation	CBC	[38]

Some new synthetic methods are also available for the preparation of polymers with predetermined conformational structure.[27] Radical polymerisation

19

techniques that can be used in order to achieve a predetermined molecular mass and molecular structure are the "living" polymerisations, like atomic transfer radical polymerisation (ATRP) or reversible addition fragmentation chain transfer (RAFT).

RAFT polymerisation provides the ability to control polymerisation of most monomers by radical polymerisation. These include (meth)acrylates, (meth) acrylamides, acrylonitrile, styrenes, dienes and vinyl monomers. It is tolerant of unprotected functionality in monomer and solvent (e.g. OH, NR_2, COOH, $CONR_2$). The process is compatible with a wide range of reaction conditions (e.g. bulk, organic or aqueous solution, emulsion, suspension). RAFT polymerisation has been successfully applied to the synthesis of carboxyl functional poly(methyl methacrylate) and primary amino-functional polystyrene through the use of appropriately designed RAFT agents.

2.1.2 General properties of polymers

The physical and mechanical properties of polymers are essential in determining their uses for specific applications. Generally, the mechanical behaviour of polymers that indicates their deformation under stress is the leading selectivity factor for their application.

The molecular mass and molecular mass distribution govern the properties of polymers, and especially are related to their mechanical properties.[26] The term molecular mass is used to define the size of a polymer from the ratio of the average mass per chain unit of a substance to 1/12 of the mass of an atom of ^{12}C. As can be seen in Figure 2.1.5 there is a curve to describe the correlation of mechanical strength with polymer molecular weight. The mechanical strength of a polymer starts at a certain value and increases linearly with its molecular weight until reaches a particular point where the polymer with high molecular weight exhibits high strength and then gradually approaches a final value.
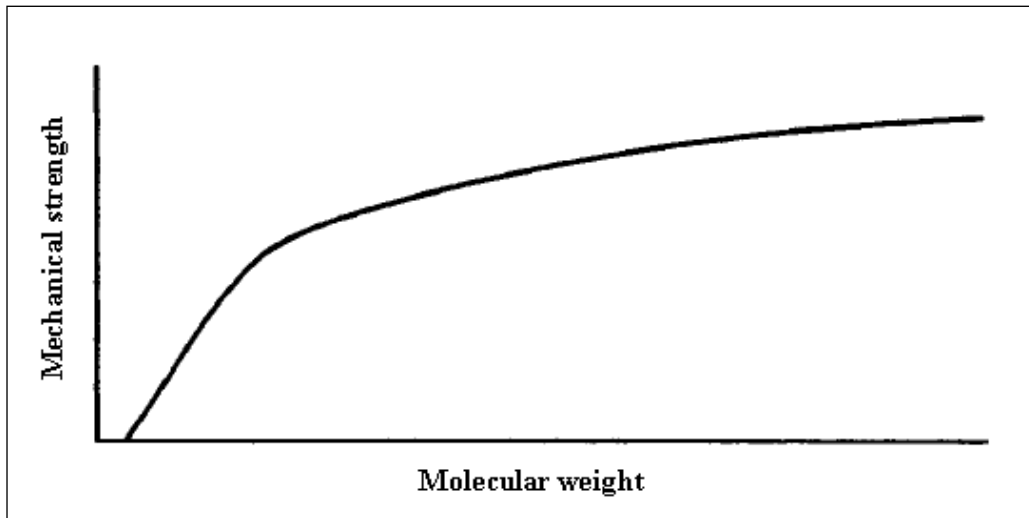
Figure 2.1.5 Plot showing the correlation between mechanical strength and polymer molecular weight (Taken from Ref.[28])

The mechanical properties of a polymeric material can be characterised by stress vs. strain plots, as seen in Figure 2.1.6.a. Rigid plastics exhibit high strength while the flexible plastics demonstrated at the beginning a linear increase between stress and strain and at a significant point, called the yield point, the material was deformed shown by a parallel straight line to the strain axis. On the other hand, the elastomers are less strong than the other two materials and their strain is increased proportionally to the applied stress. The ultimate or tensile strength that is the stress required to break the polymeric sample and the critical elongation until the rupture of the sample, are the two first characteristics that indicate the mechanical character of the polymers.

As can be seen from Figure 2.1.6.b toughness and strength are different measures. Toughness measures the energy that a sample can absorb before it breaks. The modulus (strength) that expresses the resistance to deformation is measured by the initial stress divided by the ultimate elongation and finally the elastic elongation which is the extent of the reversible elongation.[28] Elastic properties of substances which are elongated or compressed can be described as the ratio of the stress to the strain, a factor called the Young's modulus of a

material. Young's modulus calculates the elongation on condition that the stress is below the strength of a sample.
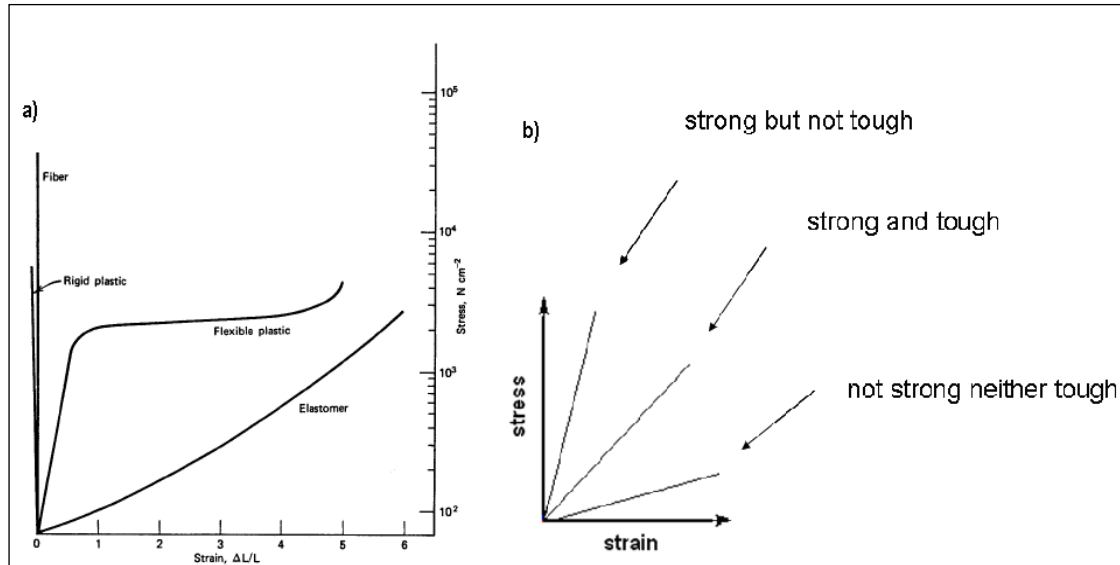
Figure 2.1.6 a) Stress–strain plots for an elastomer, flexible plastic, rigid plastic, and fibre b) stress-strain curve (Taken from Ref.[28])

Deformation and fracture behaviour of polymers can be determined by fracture toughness tests. Typical load-displacement curves are presenting in Figure 2.1.7, demonstrating different material's character from brittle to elastic-plastic.

The impact strength of a polymer can be described as the required energy to break a polymer under a shock loading.[3, 50] Thus the impact behaviour of a polymeric matrix can be strictly correlated with the necessary energy to initiate and to propagate a crack. It can be calculated by measuring the area under the stress-strain curve or by defining the mandatory energy for the occurred damage upon performing an impact test, using a gas gun.
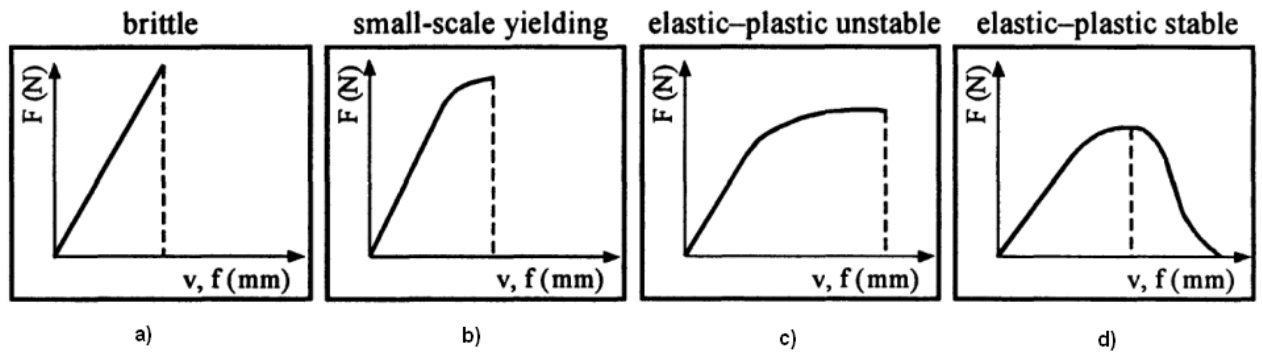
Figure 2.1.7 Load-displacement (f)/crack-mouth opening (v) curves of notched polymeric specimens for ascertaining linear elastic a) and b) and elastic-plastic fracture mechanics parameters c) and d) (Taken from Ref.[49])

The glass transition temperature (T_g) is another noteworthy parameter of polymeric materials.[50] It is the temperature where the polymer changes behaviour from a rubber-like to a glassy state. Above the T_g the polymeric chains exhibit motion, that makes polymers more flexible, while below T_g they indicate a more solid-like behaviour. The polymer chain remains static, like in a solid state. This can be attributed to the free volume theory which explains that a polymer consists of an occupied and a free volume. [27]

When free volume exceeds the significant value of 2.5%, by increasing the temperature, then the polymer reaches the rubbery phase.[1] For example polymers with aromatic groups have a higher T_g than those with aliphatic groups, because their molecules occupy more space and that leads to a decrease of the free volume. Similarly, intermolecular forces from polar groups like carboxylic acid minimise the free volume and increase the T_g of the polymer. Polymethacrylic acid (PMAA) with $T_g=228°C$ and polymethylmethacrylate (PMMA) with $T_g=105°C$ whose repeating units are shown in Figure 2.1.8 indicate an obvious difference that occurs by altering the C-OH bond with C-CH$_3$. Another example is polyisopropene with $T_g=-70°C$ while polybutadiene has $T_g=-90°C$. This can be attributed to the addition of a further

methyl group (-CH$_3$) instead of a hydrogen in the repeating unit, as it can be seen in Figure 2.1.9.[51]
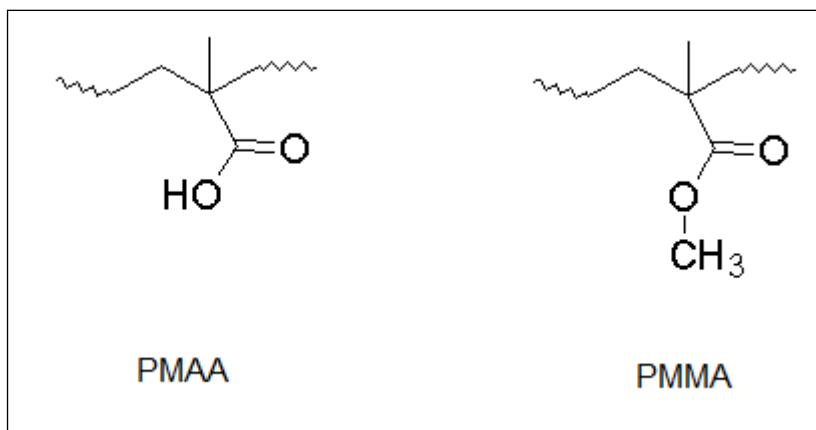
Figure 2.1.8 Chemical structures of polymethacrylic acid (PMAA) and polymethylmethacrylate (PMMA)
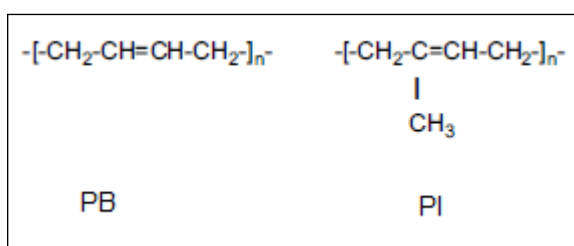
Figure 2.1.9 Chemical structures of polybutadiene (PB) and polyisopropene[11]

2.2 Introduction to photoresponsive polymers

Photoresponsive polymers have been widely studied and have become very popular during the last few decades with applications in holography, camouflage systems, erasable data storage, photo-recording media, drug delivery systems, actuators and bio-chips.[13, 52-60] These polymers are characterised by their ability to respond to light, by altering their physical and chemical properties such as structure, conformation or colour.
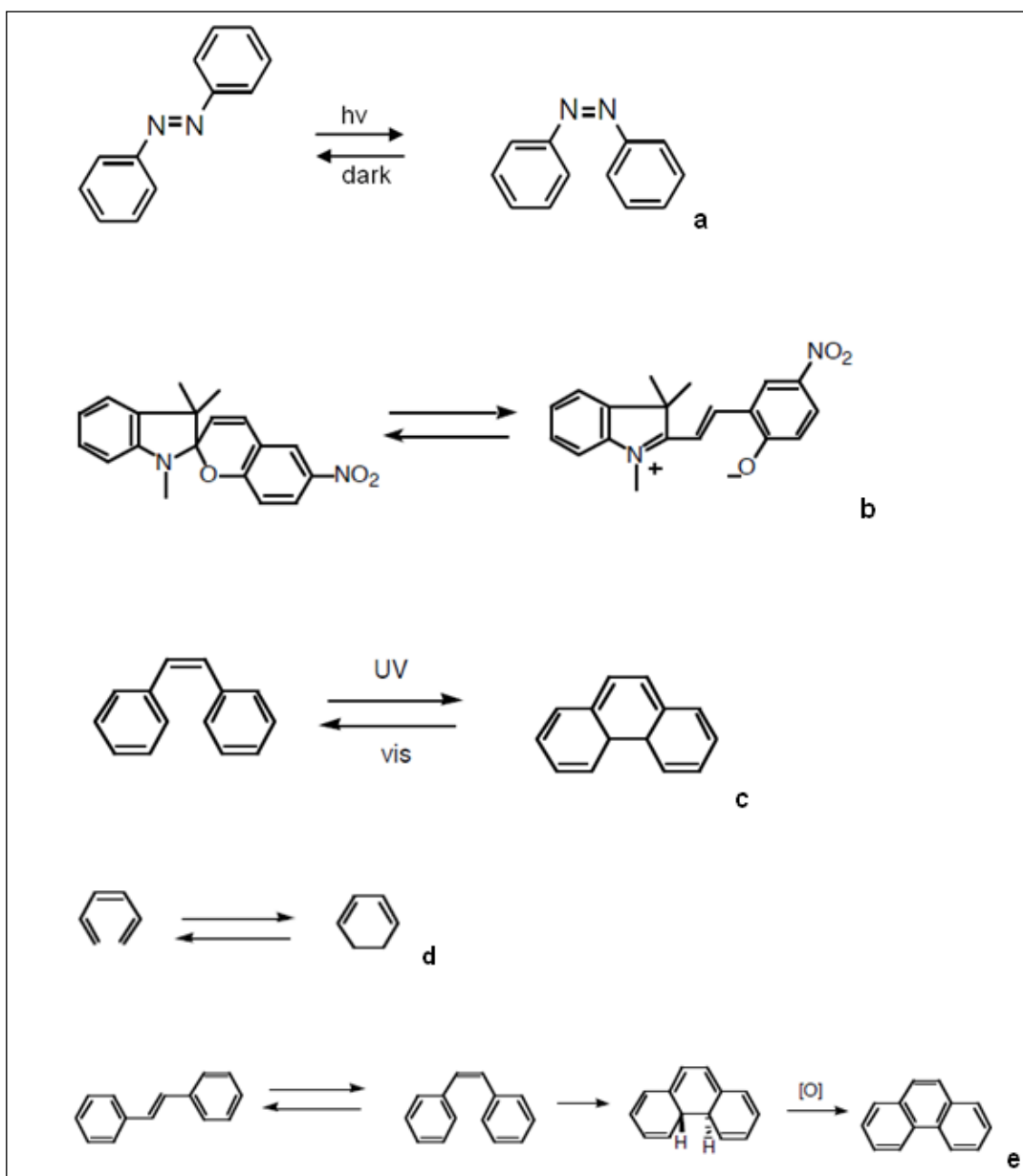
Figure 2.2.1 Schematic tranformations of different photochromic molecules, a) *trans→cis* isomerisation of azobenzene molecules, b) ring-opening reaction of spiropyran compounds, c) pericyclic reactions of diarylethenes, d) fulgides and e) stilbenes

THEORETICAL BACKGROUND

Photoresponsive systems are generally formed from organic molecules that incorporate photochromic molecules, known as chromophores, within their structures. The presence of unsaturated substances or groups with multiple bonds is the main characteristic of the chromophores.

Photochromic reactions utilise light energy to induce conformational changes. These changes affect the chemical and/or the physical properties of polymeric matrixes. For example, changes of photoresponsive polymers cannot only be observed in the colour but also in the geometric structure, the viscosity or in the electrical conductivity after photoirradiation.[11, 13, 17, 19, 20, 35, 52-56, 58-65] It should be mentioned that studies in photosensitive biomaterials successfully presented chemical and shape changes upon light exposure.[55] Wang *et al.* investigated the changes in wettability of organic based photosensitive surfaces and concluded that this leads to improvements in stability and bio-compatibility.[13] Recent reviews dealing with photoresponsive polymers show rapid development in their synthesis and applications.[17, 52, 58] The variety of chromophores that can be used to form a photoresponsive molecule is wide.[13, 20, 54, 56-58, 60, 64] Typical photochromic molecules that can be attached to polymers are azobenzene, stilbene, fulgide, spiropyran, spirooxazine and diarylethene. These compounds are illustrated in Figure 2.2.1.

In azobenzene and stilbenes compounds the photoresponsive behaviour involves photoisomerisation between the *cis-* and *trans* forms, while in diarylethene, spiropyrane and fulgide molecules, it is due to the change between ring-opening and ring-closing forms.

In particular, azobenzene photochromes induce obvious geometrical changes, followed by structural and viscosity changes. In diarylethene molecules, strong electronic changes occur upon photochemical conversion, which offer thermal stability and high fatigue resistance.[35] On the other hand, spiropyrans assume a more intense dipole moment upon photoconversion of the ring-closed to the opened form, which has been used to control the interaction with charged entities and surfaces.[53, 58, 66]

In general, appropriate photoresponsive molecules can be incorporated in many synthetic polymeric compounds in order to trigger the desired properties with regards to applications.

2.3 Azobenzene and photoisomerisation

Among many classes of light-sensitive molecules, azobenzene based molecules will be the main focus of this project. Azobenzene is one of the most abundant photoresponsive molecules and has the ability to undergo reversible photoisomerisation under the illumination of light of an appropriate wavelength.

Its selection can be justified by the fact that it consists of a simple structure, has a low production cost, and it can be easily fabricated. Azobenzene can also be manipulated to act as a mechanoresponsive material, and this behaviour would attract much attention from the research community.[67]
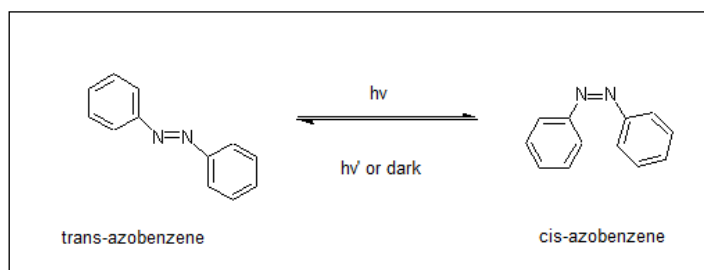
Figure 2.3.1 Isomerisation of azobenzene

The azobenzene molecule, as illustrated in Figure 2.3.1, is composed of two phenyl rings linked via two nitrogen atoms (-N=N-). Azobenzene and its derivatives have two geometric isomers, the more thermodynamically stable, *trans* form and the less stable *cis* isomer which interconvert between each other upon irradiation of light of appropriate wavelength or by heat. The distance between the two phenyl rings of the planar *trans* isomer is 0.9 nm, while for the more twisted, *cis* azobenzene the distance reaches the 0.55 nm. Sekkat *et al.* explained that the *trans* isomer is the thermodynamically more stable form by 50 kJ mol^{-1} than the *cis* counterpart because the latter is less delocalised and

exhibits distorted conformation.[60] *Cis* azobenzene has a bent geometry which increases the steric hindrance and breaks the conjugation of the linear *trans* form and thus is less stable than the *trans*.[68]

Photoisomerisation occurs in both *cis*→*trans* and *trans*→*cis* directions, while for the thermal isomerisation the *cis*→*trans* direction is the only pathway. Thermal reconversion has been found to be much slower than the photochemical isomerisation.[61] The *trans* isomer can be excited by UV light and the *cis* isomer by visible light. Light irradiation of λ=330-380 nm wavelength triggers the *trans* isomers to the *cis* conformation, while λ'=420-450 nm or storage in the dark transfer the azobenzene molecules to the *trans* form.[11, 69] These conversions, under exposure to different light wavelengths explain the reversible character of photoisomerisation process.

Photoisomerisation of azobenzene does not follow one fundamental mechanism. Halabieh *et al*. reported that there is a competition between the two mechanisms that may occur as shown in Figure 2.3.2.[17]

The first possible way is rotation of the -N=N- bond due to the high energy π→π* *trans*ition.[70] On the other hand, isomerisation may occur by the inversion of the one or both nitrogen atoms through low energy n→π* *trans*ition. In both processes the final conformational change is the same, but the required free volume for rotation is more (0.38 nm^3) than what is required for inversion (0.12 nm^3).[11, 60, 61, 69, 71] The inversion process, requires a smaller free volume and this can explicate the isomerisation of azobenzene that occurs even in glassy polymers or in other rigid matrices.

After the isomerisation of azobenzene, considerable changes to various properties are expected. Firstly, the shape changes of the molecule, from a planar to a more twisted geometry. The distance between the two phenyl groups is reduced from 0.9 nm to 0.55 nm when *trans* form is converted to the *cis* counterpart with associated changes in polarity. The dipole moment of the azobenzene increases from 0 Debye for the *trans* form to 3 Debye for the *cis* form giving rise to affinities to other polar molecules or solvents.[11, 13, 59, 60, 69]
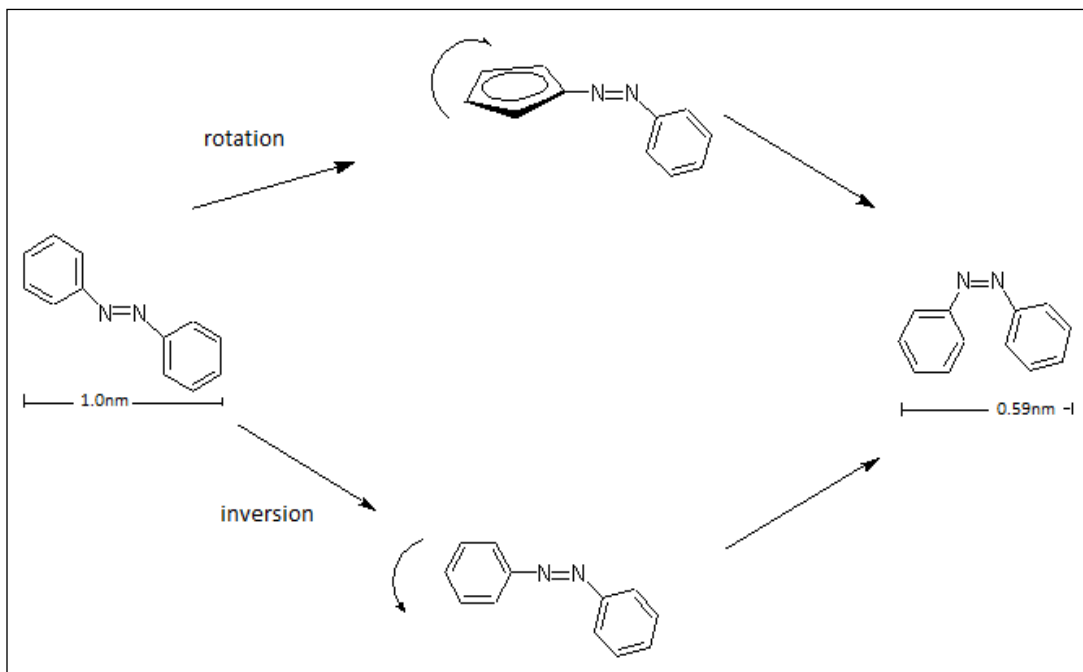
Figure 2.3.2 Mechanisms of photoisomerisation via rotation and inversion

In addition, there are obvious differences in the absorption spectrum. The UV/Vis spectra corresponding to azobenzene molecules display two characteristic absorbance bands which are affected by isomerisation. The first is positioned close the UV region due to the $\pi \rightarrow \pi^*$ electronic transition, attributed to the hydrocarbons and the second absorption band is at the visible region due to the $n \rightarrow \pi^*$ transition attributed to the unpaired electrons of the two nitrogen atoms. When azobenzene undergoes *trans→cis* isomerisation the $\pi \rightarrow \pi^*$ absorption band decreases dramatically and is shifted to shorter wavelengths (hypsochromic effect) while the weak $n \rightarrow \pi^*$ band increases.

These significant microscopic changes that occur after isomerisation are repeatable and reversible after exposure to appropriate stimuli. The activation of isomerisation of azobenzene molecules and polymers and their response to different wavelengths or treatments should be considered and investigated.

2.3.1 Different stimuli inducing azobenzene isomerisation

Azobenzene, as has been previously reported, belongs to stimuli-responsive molecules since it has the ability to respond to external stimuli such as light, pH, heat, etc. The exceptionality of these materials lies not only in the fast geometrical changes occurring in their structure but also in the reversible conversions. Some of the stimuli that trigger azobenzene materials to undergo conformational changes are presented below.[49]

- Light

Trans azobenzene molecules demonstrate a low intensity n→π* band in the visible region (400-500 nm) and a much stronger π→π* band in the UV region (290-320 nm). On the other hand, *cis* azobenzene molecules exhibit a slightly higher intensity n→π* band and a very weak π→π* band in the visible and UV ranges respectively. These two structures are interconvertible by exposure to light of appropriate wavelength.

- UV light

Among all the stimuli that affect azobenzene's geometry, UV radiation (290-320 nm) is the only one who can convert the azobenzene isomers from *trans*→*cis* form. Photo excitation of an electron from the N=N double bond will result in a transition of the azobenzene from the ground state (*trans* form) into an excited state (*cis* form) potential energy surface. When a *trans* azobenzene molecule absorbs a photon with a wavelength in the *trans* absorption band, the azobenzene will convert into the *cis* form.

- Visible light

Visible light (400-500 nm) is responsible for inducing *cis*→*trans* isomerisation. When a photon is absorbed, with a wavelength of light corresponding to the *cis* absorption band, *cis* azobenzene molecules convert to the *trans* isomeric form. It should be mentioned that *cis*→*trans* isomerisation readily occurs at room temperature and can be further accelerated by heating or stimulated by visible light irradiation.

- Heat

Exposure to heat is a well-known stimulus that affects the isomerisation of azobenzene molecules. An increase in the temperature leads to $cis{\rightarrow}trans$ isomerisation of the azobenzene and faster kinetics, while at lower temperature (below 0°C) the kinetics are decreased.[72, 73] This phenomenon can be explained by the thermal relaxation that the cis molecules are undergoing when transformed to their more thermodynamically stable $trans$ form.

- Electric field

Alemani et $al.$ showed for the first time that an electric field can induce reversible isomerisation of azobenzene molecules on Au(111).[51] Both $trans{\rightarrow}cis$ and $cis{\rightarrow}trans$ conversions of azobenzene molecules occurred after applying an increasing bias voltage pulse of 0-9 V and 0-6 V, respectively. The authors attributed these phenomena to the intrinsic dipole moment of the azobenzene and the polarizability at different geometries.

- pH

Dunn et $al.$ demonstrated the influence of the pH on azobenzene monomers undergoing $cis{\rightarrow}trans$ isomerisation.[74] As the pH values of aminoazobenzene were increased from pH 2 to 10, $cis{\rightarrow}trans$ conversion occurred at a faster rate. Tang et $al.$ demonstrated that amino-substituted azobenzene nanoparticles were pH-sensitive, analysing them by AFM and UV/Vis spectroscopy. As the pH values were decreased from pH 6 to 0, the $trans{\rightarrow}cis$ isomerisation rate was increasing, resulting in a colour change from yellow to pink.[75]

- Ultrasound waves

Ultrasound was found to be another stimulus for triggering the azobenzene molecules to undergo conformational change. Quite recently Surampudi et $al.$ demonstrated that by exposing solutions of methacrylic polymers, with azobenzene in the main chain, to ultrasound waves, $cis{\rightarrow}trans$ isomerisation can be induced. This was attributed to a stretching force that causes stress on

the N=N bond resulting in azobenzene isomerisation.[67] There are no reports studying the *cis→trans* isomerisation when azobenzene is located at the side chains of a polymer, and more significantly in a solid state after stimulation by ultrasounds.

2.3.2 Azobenzene derivatives and spectroscopic differences

Azobenzene are especially useful and offer advantages, such as fast response to light and control of properties, due to their reversible processes. By incorporating covalently attached azobenzene groups into polymers, changes in physical and chemical properties could occur at a macroscopic scale.

The variety of azobenzene chromophores as mentioned before is massive and scientists are continuously exploring novel photosensitive azobenzene based molecules for new applications.[34, 38] Spectroscopic changes that arise by the addition of different functional groups into the azobenzene structure have been reported and are of primary interest by being considered for their application.[60, 69] Azobenzene molecules are categorized into three spectroscopic classes, the azobenzenes, the aminoazobenzenes and the pseudo-stilbenes. The absorbance spectra of which are illustrated in Figure 2.3.3.

Azobenzene molecules undergo a low n→π* transition in the visible region (400-500 nm) and a higher level π→π* transition in the UV (290-320 nm). This is attributed to the fact that *trans* azobenzene can be excited by UV irradiation while the *cis* isomer by visible light. Azobenzene and its derivatives are generally yellow in colour as highlighted around the chemical structure in Figure 2.3.3.

The next category is the aminoazobenzene molecules, which have an electron-donating –NH_2 group. This group shifts the π→π* close to the n→π* band therefore any changes after isomerisation can be observed within the

overlapping absorption band (400-500 nm) of the spectrum. Aminoazobenzene compounds have a characteristic orange colour.
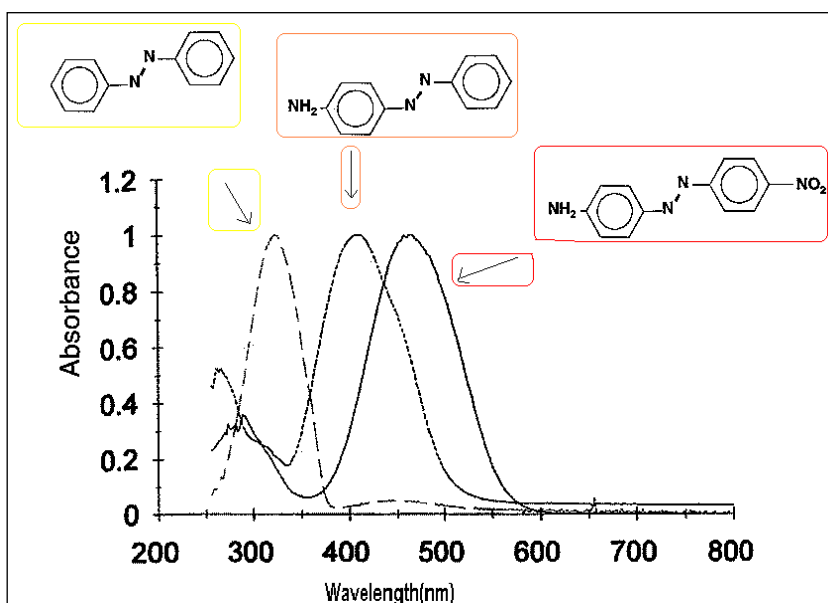
Figure 2.3.3 Absorption spectrum of azobenzene, 4-aminoazobenzene and 4-nitro-4'-aminoazobenzene molecules in a polar solvent (Adapted from Ref.56)

Moreover, the last class of azobenzene molecules are the pseudo-stilbenes. They contain an electron-donating -NH$_2$ group and an electron-withdrawing -NO$_2$ group, and they are characterised by an absence of symmetry. Thus, they absorb lower π→π* energy and higher n→π* and their characteristic band, the intensity of which decreases after *trans→cis* isomerisation, is located at higher wavelengths (400-500 nm) in comparison to the other azobenzene types. These compounds are found to have a red colour.

It should be noted that azo chromophores with electron donor or electron acceptor groups raise the dipole moment of the molecule, which can influence neighbouring dipoles.[17] The advantage of this is unique and plays a key role in all of the material's properties because it explains how the microscopic changes are displayed at the macroscopic level. Some examples of these azobenzene species in the polymeric form are indicated in Figure 2.3.4. The a) and b)

structures present polymers with the azobenzene and aminoazobenzene, respectively, in the main chain. The c) structure shows a polymeric unit with pseudo-stilbene at the side chain.
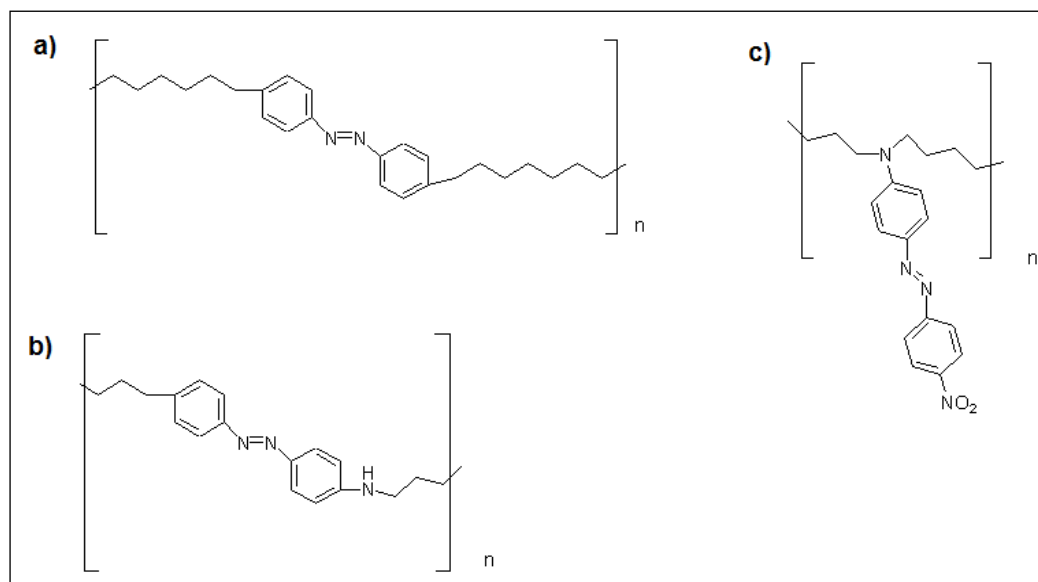
Figure 2.3.4 Molecular structures of a) azobenzene, b) aminoazobenzene and c) pseudo-stilbene based polymers

2.3.3 Effect of azobenzene molecules on mechanical properties

Measurements of the mechanical properties, such as Young's modulus (elasticity), of azobenzene-based polymers were first reported in 2000 by Srikhirin *et al.*[62] Azobenzene-doped (15 wt%) polymer films of polymethylmethacrylate (PMMA) and polyethylmethacrylate (PEMA) were examined separately by quartz resonators for identification of their elastic compliance as a function of time. It was demonstrated that UV illumination caused a reversible and noticeable increase in the material hardness, by 1.5% in the PMMA and 0.2% in the PEMA, which is attributed to the *trans→cis* isomerisation of the azomolecules which locally compressed the matrix and thus formed barriers in response to shear stress. In contrast, after subsequent

irradiation with visible light greater free volume was created by photoisomerisation and thus elastic compliance was observed.

One other approach involves thin films of random copolymers of PMMA and azobenzene-based acrylic monomers.[35] Moniruzzaman *et al.* observed changes in the elastic modulus in the film (115 μm), containing 6 mol% azobenzene, by nanoindentation. Upon exposure to UV irradiation the stiffness of the polymer film showed a notable increase of 10-28%. Upon visible light irradiation the elastic modulus of the film was found to have partially recovered due to reverting *cis→trans* isomerisation. However, according to the authors, this reversion was not complete due to the width of the film, where a significant amount of azobenzene was unable to be irradiated and as a consequence they could not undergo full isomerisation.

Verploegen *et al.* demonstrated that the liquid-crystalline polyvinylmethylsiloxane polymers enriched with 20 mol% azobenzene in the side chains, can reversibly alter their elastic and loss moduli.[63] Small and large amplitude oscillatory shear tests at 100°C were used to measure the elastic and the loss moduli. The authors showed that upon UV irradiation, the elastic modulus decreased by 10% approximately linearly with the irradiation time due to the matrix disruption caused by the isomerisation of azo moieties. Moreover, a recent study confirmed the photo-induced changes on the elastic modulus into liquid-crystalline polymers (LC.) films with 1 mol% doped azobenzene.[76] The oscillatory shear tests at 25°C indicated a decrease of the elastic modulus, after UV irradiation, which recovered to the initial value after cessation of the UV light exposure.

Quite recently Sorelli *et al.* performed statistically nanoindentation experiments looking into the light-induced changes of PMMA with grafted azobenzene molecules (15 mol%), as side chains.[77] They demonstrated that the polymeric films hardness decreased (by 38%), while the creep coefficient value increased (by 39-60%), indicating a significant reinforcement of the viscoplastic response of the film after UV illumination. These changes were completely reversible and

were related to the reorganisation of the polymer chains after *trans* and *cis* isomerisations. It is worth mentioning here that the authors did not perform any nanoindentation tests to pristine films for the purpose of determining the influence of the chromophores.

The conformational changes by photoisomerisation of azobenzene that alter the modulus of the whole polymeric matrix when comparing the effect of azobenzene concentration or the location of azobenzene molecules in the polymer chain have not yet been examined. It may be possible that the mechanical properties could be further improved by having a significant amount of azobenzene chromophores attached in appropriate positions along the polymeric chains.

2.3.4 Shape changes induced by azo-chromophores

The ability of azobenzene chromophores to change the shape of a polymer matrix which they are incorporated in, using light, is attributed to the photomechanical effect and is of tremendous interest to many researchers.[11, 17, 60, 63, 69, 78] The definition of photomechanical effect is, the reversible change in the shape of some molecules by the absorption of light, which results in a significant macroscopic mechanical deformation of the host material.[78]

Eisenbach was the first to report the conversion of electromagnetic radiation into mechanical energy by using azochromophores.[48] He observed, after UV and visible irradiation, an average of 0.15 to 0.25% photomechanical contraction and expansion cycles in the whole solid rubbery films and the process was repeatable. In this study 0.5-2 mol% aminoazobenzene molecules were incorporated as crosslinkers. This phenomenon was explained by the conformational change due to the *trans→cis* photoisomerisation of the azobenzene moiety, which caused a decrease of about 39% in the distance between the two phenyl rings. It should be noted that the local contraction was

even larger because of the rigid bonds between the amino groups of aminoazobenzene and the acryl group.

A more comprehensive study by Finkelmann and co-workers revealed a maximum contraction of 20% in azobenzene containing liquid crystal, elastomeric polymers when they have undergone UV irradiation, which induced the isomerisation of the azobenzene molecules.[79] They synthesised nematic liquid crystals with polysiloxane main chains and azobenzene chromophores at the crosslinking chains. The authors reported that the faint distinction in nematic order upon *trans–cis* isomerisation caused a significant uniaxial deformation of the liquid crystals along the director axis when the molecules are strongly associated by covalent crosslinking to form a three-dimensional polymer network. Moreover, the isomerisation effect has been investigated using azobenzene molecules linked with poly(vinyl ether) in the side chain of a linear polycarbonate film, as a matrix.[46] Tests to the film were conducted using a thermal mechanical analyser under a controlled stress and a constantly increased strain to observe changes in modulus. When the film was irradiated with UV and visible light, the azochromophores were found to undergo photoisomerisation, which created a local free volume, leading to a 0.2% decrease in modulus.[80] The absence of light resulted in the recovery of modulus, due to the complementary fading of the free volume. A decrease in elasticity was observed, which was attributed to the photoisomerisation of azobenzene molecules.

Later, Barrett *et al.* confirmed that the azo compounds, under photo- irradiation undergo elongation below the glass *trans*ition temperature and above the T_g exhibit contraction.[78] They also mention that the azo chromophores, that are doped into an acrylate polymer matrix but not incorporated into main or side chains, do not exhibit the effect. The reason is the mobility and instability that characterise the doped chromophores in the matrix, while those ones joined with covalent bonds exhibit high stability.

One remarkable study by Kondo *et al*. demonstrated the influence of the location of azo-moieties within cross-linked liquid-crystalline polymeric films against the photo-contraction length.[37] Azobenzene moieties, cross-linked to the polymer at two points, were compared with azobenzenes connected to the side chains. The values of contraction length along the alignment direction of the films by UV irradiation were evaluated by an experimental setup shown in Figure 2.3.5a.
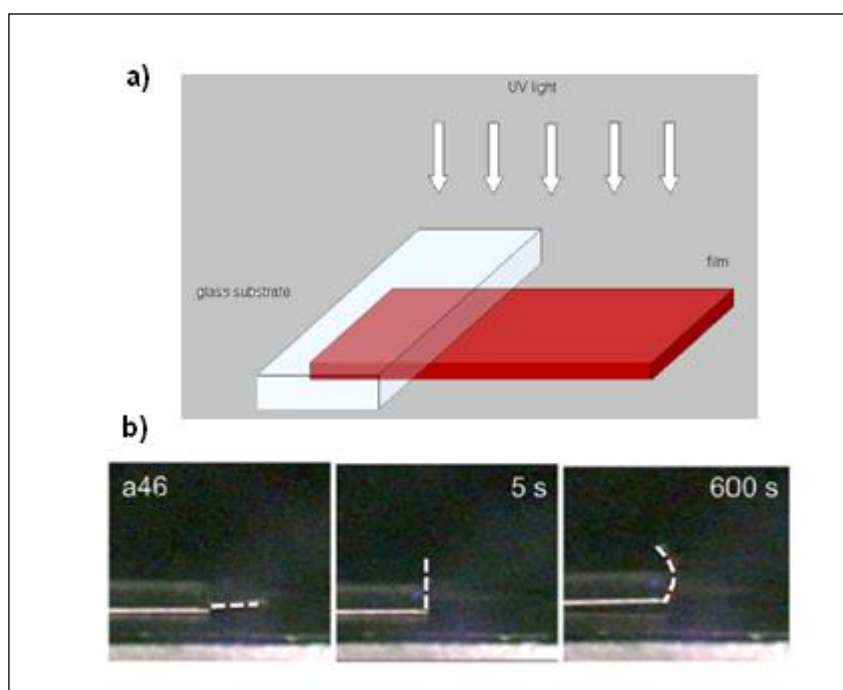
Figure 2.3.5 a) Illustration of the experimental setup used by Kondo et al. [9] and b) series of photographs indicating the motion of liquid-crystalline polymeric films by UV irradiation.

The film with azobenzene cross-linkers exhibited approximately four times higher contraction than observed in the film with azobenzene in the side chains. This difference was attributed to the geometrical restriction that the azobenzene cross-linkers caused to the polymer backbone upon photoisomerisation. The greatest amount of mechanical changes was achieved in a polymer with 20

mol% azobenzene loading. It was also explained that when UV light excites deeper into the surface of the film, photo-induced contraction is caused at the opposite side of the film as illustrated in Figure 2.3.5b.

Table 2.3.1 Various % contractions in different studies as a function of azobenzene loading

Azobenzene concentration (mol%)	Δl contraction (%)	Ref.
30	3.5	[36]
20	2.2	[37]
0.5-2	0.15-0.25	[48]
20	1	[12]
8	20	[38, 79]
8.5-30	12-18	[33]

In another study, the same authors reported that the degree of contraction increases with higher light intensity and with an associated increase in stiffness in an azobenzene cross-linked film.[36] More significantly the highest contraction of about 3.5% was observed with a UV light intensity of 110 mW/cm^2. Studies by Li *et al*. corroborated these results, by demonstrating that the contraction was dependent upon the intensity of the light, and found a contraction of 12% with 20 mW/cm^2 intensity, that reached 17% with a light intensity of 100 mW/cm^2.[38] In both experiments, the contraction was more rapid and of a greater magnitude at temperatures up to 70°C. This was due to the chain mobility at higher temperatures. Full reversal of the contraction occurred in dark because of the *cis→trans* isomerisation of the azobenzene molecules. Table 2.3.1

presents the percentage contractions with various azobenzene loadings in different studies. The results of the table are so different and cannot be compared to each other due to use of different polymer systems.
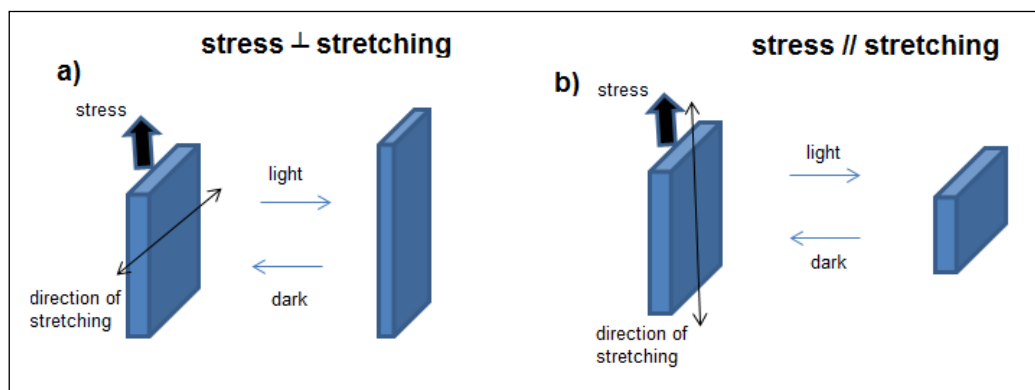
Figure 2.3.6 Schematic examples of a) elongation and b) contraction, reversibly, upon irradiation[44]

A soft polymer film composed of polycaprolactone and polyvinyl ether with azobenzene in the side chains showed faster reversible response to light.[44] The film had undergone rapid deformation and recovery under light irradiation. Moreover, it was observed that the direction of constant tensile stress, under light illumination, plays an important role on the deformation. When the film was stretched in parallel with the tensile stress it became elongated. Contrary, when the stretching direction was perpendicular to the constant stress the film contracted, as can be seen in Figure 2.3.6. Structures in the surface of azo-polymer matrices, due to the mass transport, upon irradiation with a light interference method, were first published in 1995 by Rochon *et al.*[34] These structures, named Surface Relief Gratings (SRG), which look like stripes as illustrated in Figure 2.3.7, are directly formed on the surface and caused by the light excitation of azobenzene molecules. They have been used in photonics and holography applications.[60]
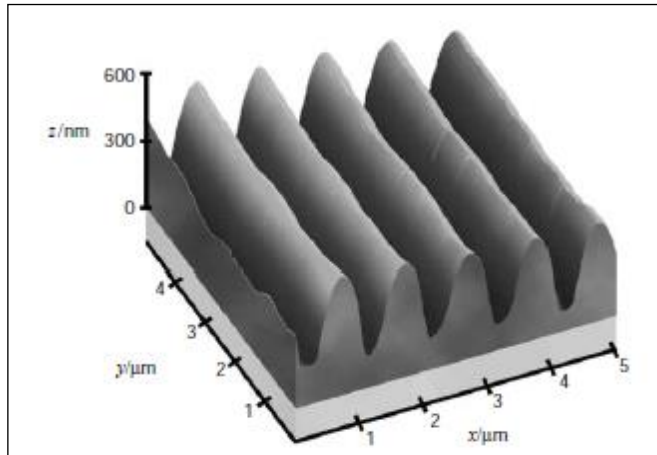
Figure 2.3.7 A typical SRG of an azo-polymer film by AFM image [60]

These gratings are formed by projecting an interference pattern of light into films at temperatures lower than the polymer's glass transition temperature. SRGs resemble hills with valleys, where the former are stiffer and latter less stiff, this was attributed to the azo chromophores that are moved away from the photoirradiated areas. Their mechanism is based on the photomechanical effect that has been mentioned previously.[11, 69, 78]
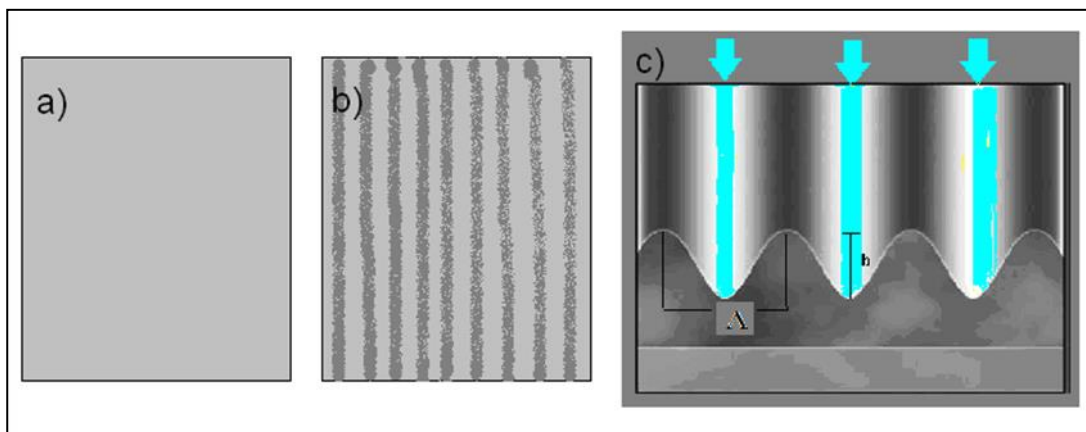
Figure 2.3.8 Schematic examples of a) an azo- film before light irradiation, b) an azo- film with SRG, upon light pattern irradiation and c) SRG with impinging light pattern, where Λ is the periodicity of the gratings and h the height of the SRG [69]

41

Figure 2.3.8.a and Figure 2.3.8.b present an azobenzene containing film before and after the photo-pattern irradiation. The formation of SRG with light pattern is illustrated more clearly in Figure 2.3.8.c, where Λ is the period of the gratings and h their height.[81] The excitement of the molecules induces nano-scale vibratory motion, which leads to a local free volume generation into the polymer film. Thus the material is elongated in the irradiated areas. The term of free volume indicates the empty space between the molecules. In other words, by photoirradiation the molecules can move more easily with an appearance of free volume.[27]

This process of gratings is reversible, because when the polymers with SRG are heated above their glass transition temperature the gratings are erased. The formation of an SRG is strongly affected by the T_g. The higher the T_g of a polymer the more difficult it is to create an SRG.[69]

Recently, researchers have managed to transfer the relief matrix to its initial shape, by adding an appropriate solvent instead of using the thermal erasing method in an azo-poly(methacrylic acid) film.[45] They also investigated the effect of irradiation time and molecular weight on the gratings. They showed that the depth of the stripes of SRG can be controlled by the illumination time. By increasing the UV irradiation time the depth was extended. In parallel, they highlight the importance of the size of polymer chains on the formation of reversible or irreversible SRG. They demonstrated that when the distance of the polymer chains due to the photo-induced motion was smaller than their length, structures with reversible behaviour were produced. Finally, in cases that the lengths of polymer chains were smaller than the periodicity length of the interference pattern, the gratings that formed, were permanent because no chain rupture could occur. Atomic Force Microscopy (AFM) was used in all the above studies to observe the structure of SRG and the photo-induced changes of the films.

The fact that photoisomerisation has a strong relationship with respect to the shape changes of materials has not been disputed. These studies illustrate that shape changes which lead to expansion or contraction, are explained by the photomechanical effect. More specifically, the free volume that is required for the *trans→cis* isomerisation leads to an expansion and in the case of dipole pairing of azomolecules the materials undergo contraction.[69]

2.3.5 The photoviscosity effect

Viscosity, η, is the resistance of a material to flow and is equal to the shear stress τ divided by the shear rate γ, as can be seen in Equation 2-1.

$$\eta = \frac{\tau}{\gamma}$$

Equation 2-1

For liquids, flow is an irreversible deformation (strain) caused by force (stress). In the case of polymers, flow occurs when their chains are moving freely[50]. Viscosity is important for all polymeric studies and for their mechanical properties. For instance, highly viscous polymers can form stiffer and more rigid materials in comparison to those with a lower viscosity.[27]

The photoviscosity effect is defined by changes in polymeric solutions that are related to photo-stimulated conformational changes of the molecule's viscosity. This effect was first observed by Lovrien, who demonstrated possible mechanisms for this effect.[65] He noticed an increase in viscosity in solutions of methacrylic acid and 2,2'-dimethoxyazobenzene acrylamide upon UV irradiation. This increase was attributed to the repulsion of the coulomb forces between the ionic groups, which raised the hydrodynamic volume of the molecule. He also observed a decrease in the viscosity of a non-ionic solution, polymethacrylic acid and chrysophenine solution in water under the influence of

UV light irradiation. The absence of ionic charge causing tight binding of the chromophores has resulted in a decrease in the hydrodynamic volume. Various studies of photoviscosity effects in solutions of azobenzene based polymers have been reported in literature since then.[20, 57] Figure 2.3.9 illustrates a possible mechanism of photoisomerisation of azomolecules that leads to viscosity changes.
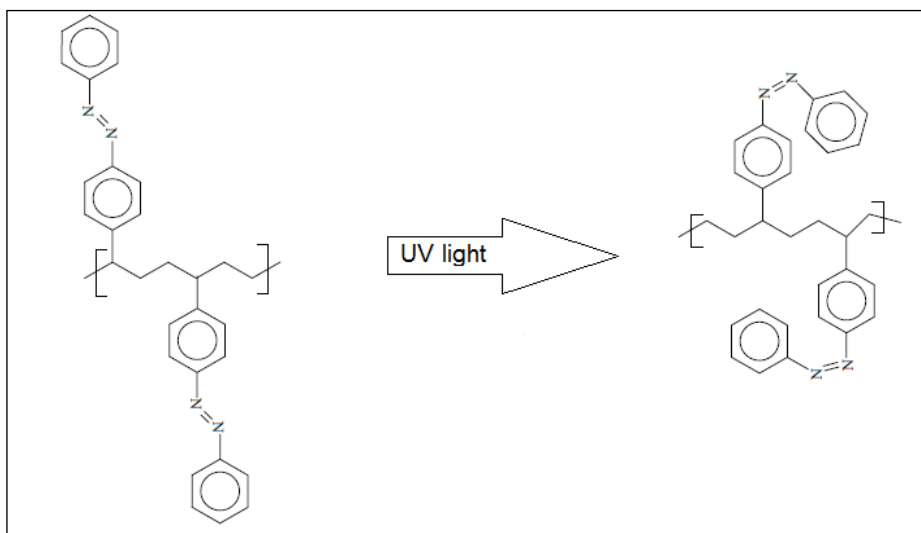
Figure 2.3.9 Possible conformational change of azobenzene polymers upon photoirradiation[32,42]

Copolymers of 4-methacryloyloxyazobenzene with methylmethacrylate were also found to exhibit this effect when they were irradiated by UV light.[19] Their viscosity in DMSO solution was reduced as a consequence of the dipole-dipole interactions caused by photoisomerisation. The experimental results were very precise due to the new technique that the researchers used. They constantly measured the viscosity of the samples by using a cone-and-plate rheometer which was enriched with a solvent trap and improved the accuracy of the measurements. The authors in another study investigated the viscosity behaviour as a function of temperature and demonstrated that photo-induced heating also affects the viscosity of azopolymer solutions.[20] Their experiments

confirmed that the contraction of polymer chains due to the *trans→cis* conversion resulted in a decrease in viscosity.

Measurements of viscosity should be taken into consideration with regards to the creation of a rigid and elastic material as well. Highly viscous molecules, due to the tight crystalline regions, provide toughness compared to the low-viscosity molecules that offer elasticity.[27] Thus, the desired stiffness and elasticity from the azochromophores can be transferred into the macroscopic material through light irradiation and can develop its mechanical properties.

2.3.6 The influence of azo polymers on thermal properties

Glass transition temperature (T_g) is the critical temperature needed in order to induce the brittle, amorphous regions of the polymer to flow.[27] It has a great influence on the viscosity and the mechanical properties of materials. The mobility of polymer chains depends on their T_g. Polymers with high T_g are more attractive to some industries because their intermolecular motion is lower and they exhibit a more "glassy" and resistant character to different temperatures.[27]

It is expected that incorporation of azobenzene moieties into a polymer chain will change the T_g of a polymer. Therefore it is important to understand the azobenzene loading effect on the T_g of azobenzene based polymers.

The influence of concentration of azobenzene molecules on the T_g was examined by Blomquist *et al.*[43] A series of copolymers from methyl methacrylate and 11-(4-ethoxyazobenzeneoxy)undecyl methacrylate (azo-MA) were synthesised. The azobenzene groups were linked at the side chains through a long spacer. The T_g measurements of the polymers were conducted by Differential Scanning Calorimetry (DSC) and Dynamic Mechanic Thermal Analysis (DMTA) and their results revealed a good correlation between the results obtained from both methods.

The graph, shown in Figure 2.3.10, revealed a decrease in T_g almost linearly with azobenzene loading. This decrease was attributed to the flexible methylene spacer, which caused separation of the azobenzenes from the main polymeric chain and enhanced the mobility of the system. However, a control sample of MMA with a methylene spacer (without azo molecules) polymer was not performed, thus this graph cannot represent the quantified effect of azobenzene in terms of T_g.
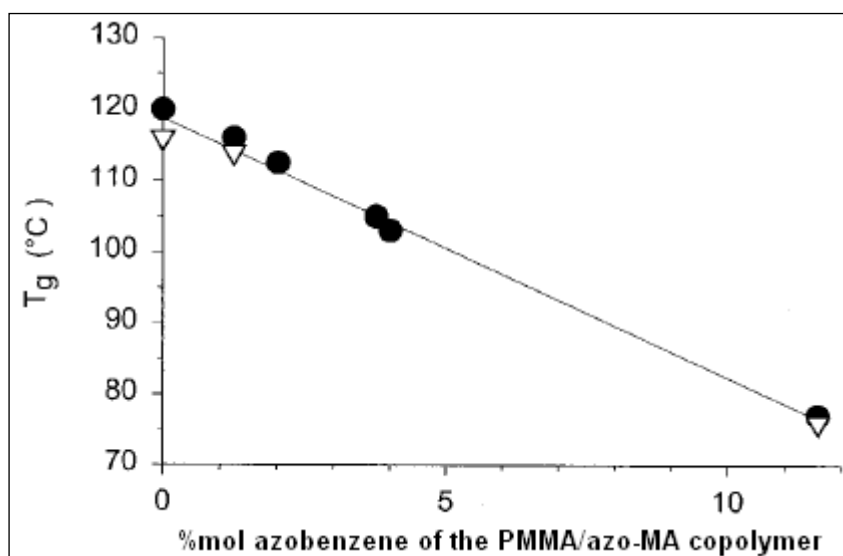
Figure 2.3.10 Glass transition temperature measurements of MMA/azobenzene copolymers by using DSC (cycles) and DMTA (triangles) (Diagram adapted from Ref.[43])

Other studies, support these results, by synthesising graft polymers of azobenzene with PMMA, an increase in the T_g by 20°C was achieved.[42] This is due to a lower azobenzene concentration. As discussed in previous section 2.1.2, polymers with aromatic groups obtain higher T_g and likewise, intermolecular forces, from polar groups that minimise the free volume, can increase the T_g of the polymer. It is clearly demonstrated that T_g of azobenzene based polymers can be changed by manipulating the polymer structures.

2.3.7 The self-healing concept of polymers

Self-healing compounds offer a new solution to damage and failure caused by natural circumstances in a plethora of applications such as aerospace and other modes of transport.[39, 81, 82] These materials have the ability to repair themselves after structural damage and to re-establish ruined or corrupted properties using the resources intrinsically offered to them.[82] The recovery procedure is induced by filling up the empty volume caused by material division upon damage. The repair can either be natural or externally assisted using pressure or temperature for instance.

Self-healing processes are divided into two types: the extrinsic and the intrinsic process. The extrinsic healing procedure relies on the incorporation of external compounds like microcapsules with healing agents into the polymeric materials. When damage occurs, the microcapsules break and these healing agents are released and consequently treat the damage. On the other hand, the intrinsic process does not involve any healing agent but is capable of repairing the damage or cracks of polymers by chain mobility, hydrogen bonding, or ionic interactions. The advantage of this process is the repeatability of the healing effect, attributed to the reversible reactions between the molecules or polymers rather than the single use nature of microcapsules.[82]

Noteworthy studies of the intrinsic healing approach on a cross-linked, furan maleimide, polymer examined the self- healing properties of the fracture at temperatures between 85°C and 95°C.[81] A complete and repeatable healing efficiency was obtained after 30 min at 85°C followed by 30 min at 95°C and then cooling the polymer to room temperature (approximately 6 hrs). The overall fracture resistance of the material after healing was found to be equivalent or slightly enhanced when compared to the initial material state. Photographs of these experiments measuring the fracture toughness are illustrated in Figure 2.3.11.a. Two axially cracks were growing stably on the central hole upon compression. Initially the samples were treated under pressure at 85°C to bring the damaged faces in contact and then the pressure was removed and the

samples were heated at 95°C to exploit the mobility of the pendent chains. The healing treatment was not found to be effective beyond a period of 1 hr. The healing was attributed to the thermally repair of the covalent furan maleimide bond of the polymers at 110°C. The furan maleimide bond can be reformed after have been broken following the reversible Diels–Alder reaction. This bond has also the ability to self-repair at any temperature below 110°C on condition that that the broken moieties come into contact.
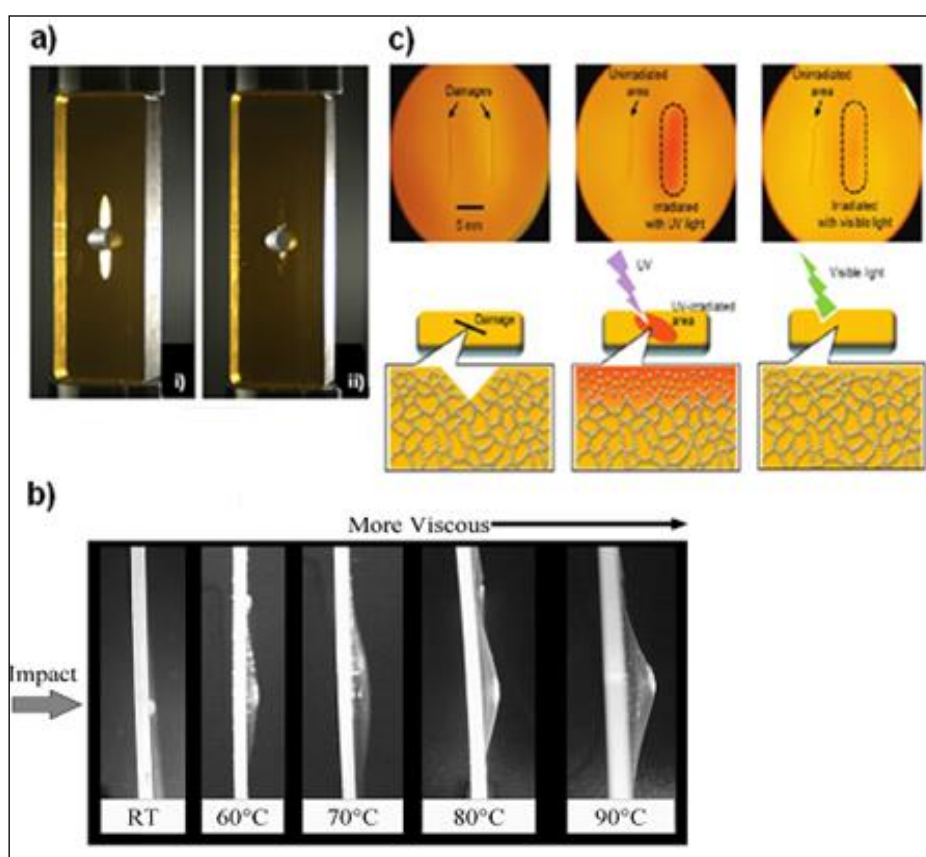
Figure 2.3.11 a) Photographs of specimen upon (i) first fracture and upon (ii) healing treatment [82] b) Films undergoing puncture indicating higher deformation at higher temperatures [39] c) Schematic illustration of the photo-induced healing on azobenzene- containing liquid-crystal composites [76]

Similarly, complete healing results by the above approach were noticed with random poly(ethylene-co-methacrylic acid) films upon ballistic puncture.[39] The research group of Kalista *et al.* demonstrated that the ionic interactions were not playing a major role in the repair of damage. These experiments proved that no puncture restoration occurred at temperatures higher than 60°C, although the chain mobility and the self-bonding were promoted at high temperatures. In Figure 2.3.11.b the profile of the films, impacted at different temperatures, indicated that at low temperatures an elastic mechanism took place while at higher temperatures local deformation occurred, accompanied by a more viscous behaviour. The ability to fill the hole was attributed to the increase in temperature via friction that modified the polymers into viscoelastic melt resulting in a re-bonding of the polymer chains. The melt temperature and even below were found to encourage the interdiffusion of the polymer chains, which resulted in strengthening of the films.

Very recently, Yamamoto *et al.* demonstrated photochemical healing behaviour in a liquid-crystal gel compound, doped with azobenzene moieties, as can be viewed in Figure 2.3.11.c.[76] They made two small cuts of 2 mm deep and 10 mm long on the surface of the samples and irradiated the damaged area with UV light for about 10 sec. This irradiated region altered colour immediately from yellow to orange, which was explained by the photoisomerisation of azobenzene molecules and the cut appeared to be filled. The thermal processes were reversible with a further irradiation of visible light for 10 sec the sample and the cut returned to their original colour and shape respectively. It should be noted that the photochemical healing occurred due to the reorientation of the network induced by the azobenzene isomerisation. Although the healing of the gel films was visually observed, no analysis (e.g. AFM) measuring the depth of the cuts was carried out to calculate the exact healing ratio against irradiation time.

An evolutionary approach, for the self-healing effect of photosensitive polymers, could be the exploitation of covalently incorporated azobenzene molecules into the polymer chains. Their fracture tolerance behaviour will be stronger as they

will be directly linked to the matrix and they will be able to undergo photo-induced healing more effectively than doped systems (localised effect).

2.3.8 Shape memory polymers

Shape memory polymers (SMP) are smart materials, capable of returning back to their original shape after exposure to appropriate stimuli such as heat, moisture or light, etc.[83] The shape-memory polymer consists of netpoints (hard segments), such as covalent bonds, and switching segments (soft segments), flexible polymer chains. The shape memory mechanism lies on the netpoints which they are re-bonding the deformed chain segments without recoiling them. In most cases the stimulus that causes the polymer shape changes is heat. Heating these polymers above their transformation temperature, induces them to undergo a transition stage, as seen in Figure 2.3.12.[84] For both thermoplastic and thermoset SMP, the transformation temperature is usually their glass transition temperature T_g or their melting point T_m.[85]

Rodriguez *et al.* introduced shape memory assisted self-healing (SMASH) polymers, which are polymers with reversible plasticity (shape memory properties) able to completely close and re-bond cracks after thermal treatment.[86] The authors prepared interpenetrating network polymers consisting of cross-linked poly(ε-caprolactone) (n-PCL) and linear poly(ε-caprolactone) (l-PCL) (25 w/w%). They found that the shape memory ability occurred due to the multifunctional crosslinker n-PLC which had acrylate end thiol groups responsible for the rebonding after heating. On the other hand the l-PCL, with a high M_w (65,000 g/mol) for enabling reentanglement after diffusion across the interface, was responsible for the self-healing ability of the system. These synergetic mechanisms helped to close any cracks formed during deformation or damage (shape memory ability) while the chains were diffused to the free surface and eventually across the damaged area at the same heating phase simultaneously with the shape memory function.

The introduction of light irradiation to the SMP that trigger the shape memory effect has been also studied.[83-85] Thermoset polymers with photoresponsive cross-linking cinnamic groups, demonstrated a shape memory effect attributed to the elastic contraction of the polymer chain segments that were activated upon light irradiation.[87]
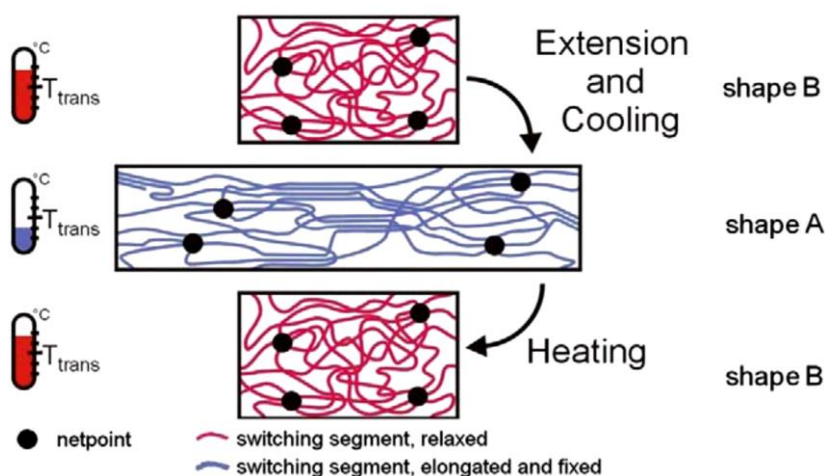
Figure 2.3.12 Thermally induced shape-memory concept, where T_{trans} = thermal transformation temperature related to the switching phase and netpoints = chemical (covalent bonds) or physical (intermolecular) interactions that determine the permanent shape of the polymer. (Taken from Ref.[88])

Azobenzene is one of the most abundant light-responsive molecule, known for its ability to change and control chemical and physical properties of polymers.[80, 89-91] These changes are attributed to the reversible and repeatable azobenzene isomerisation. Irradiation with UV light converts the more thermodynamically stable *trans* azobenzene to its *cis* form. Exposure to heat, visible light or storage in the dark, induce the reversible *cis→trans* isomerisation. The geometrical and polarity changes that occur through this conversion can be transferred to the

macroscopic level, when the azo molecules are attached into a polymeric backbone, which will affect the properties of the whole polymeric matrix.

Very recently, azobenzene was found to be a light-powered healing material for wearable electrical devices.[92] Repetitive recovery of a damaged electrical conductor was achieved only by UV light illumination. The authors attributed this effect to the photoisomerisation of azobenzene which induced the whole polymer matrix to undergo bulk diffusion even below its glass or melting temperature.

The physical changes that occur to a rigid 3D network have not yet being examined. It would be interesting to investigate whether photoresponsive epoxy based thermosets containing azobenzene exhibit any shape memory behaviour after exposure to UV irradiation.

2.4 Overview of composite materials

Composite materials are increasing by being utilised more and more in various applications such as industrial, aerospace and recreational areas. A composite material can be formed by two substances having different properties, the matrix and the reinforcement component, as seen in Figure 2.4.1. The matrix plays an important role in the composites as it is responsible for binding the fibres together. The matrix is usually a polymer thermoset material, like polyimide or epoxy. Common reinforcements are fibres made of glass, Kevlar or carbon that exhibit high strength and stiffness. Although the fibres are brittle, in combination with the polymeric resin they give unique properties to the composite. The optimum result of this combination is that they form tough composites attributed to their heterogeneous structure.[93]
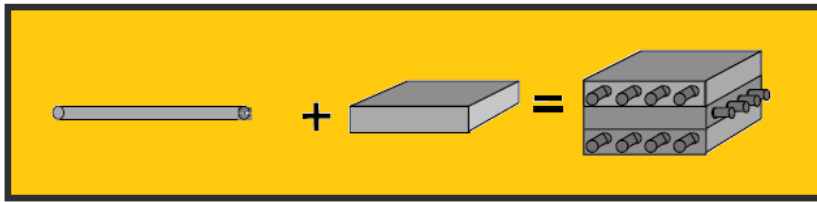
Figure 2.4.1 Illustration of the formation of a composite material

Epoxy/glass fibre composites are produced by different methods such as wet lay-up and compression moulding, vacuum bagging and autoclave curing or filament winding with oven curing.[94] For every application a particular technique is more preferable than the others. The winding process is preferable, for instance, for cylindrical structures, like pipes and can be made with fibres or tapes embedded with resin. Hand lay-up offers low cost tooling, simple handling and a wide range of part sizes. Large panels and relatively complex structures are better formulated by hot-pressing layers of pre-impregnated fibres or by pressurised autoclave.[93] The autoclave curing is the standard production method within the aerospace sector for manufacturing void free composite materials with good mechanical properties. The autoclave process produces denser, void-free materials due to a higher temperature and pressure environment during curing. Autoclaves are heated pressure vessels (usually equipped with vacuum systems) into which bagged lay-ups, are cured at pressures between 50-100 psi.[95]

2.4.1 General properties of polymer composites

Electrical conductivity, chemical resistance and thermal conductivity, fatigue and resistance are some of the main indications that industries are interested in as a first place. Composite materials for aircraft or structure applications can be characterised by various properties, such as thermal, mechanical, physical and chemical. The choice of the desired properties depends on the application's requirements.

The mechanical properties of polymer composites are highly affected by their polymer matrix as well as their reinforcement. The ability of reinforced polymer composites to sustain loads of any kinds, such as tension or compression, and the efficiency of this load transfer is directly related to the quality of the fibre and polymer bond. Weak polymer matrices in combination with brittle fibres contribute to the formation of strong materials. The tensile properties of a composite are dominated by the fibres and its compressional and toughness properties by the polymeric matrix.[3, 27] The material quality is not only the one who affects the mechanical properties. Volume fraction, density and fibres orientation belong to the physical characteristics of the composites and are linked to their properties. High density, high fibre volume fraction and precise filament orientation are responsible for good mechanical properties of composites.[94] Thermal stability might also be linked with the polymer matrices. For instance the matrix of some composites like polyester can sustain up to 50°C while a composite with polyimide matrix can be used at maximum temperature of 280°C.

A key factor driving the increased applications of composites over the recent years is the development of new advanced forms of fibre reinforced polymer materials.[96] This includes developments in high performance resin systems and introduction of smart materials like photoresponsive polymers.

2.4.2 Introduction to composite damages

Damage in composites may be introduced in various forms such as matrix cracks (or microcracks), fibre breakage, radial cracking in fibre or interfacial damage in the region between the matrix and the fibre.[97] Different types of composite damage are shown in Figure 2.4.2. Transverse cracking consists of matrix breaking between fibres in the plies perpendicular to the principal loading direction. Longitudinal cracking is similar to transverse cracking, but this damage induces matrix cracking between fibres in the layers parallel to the loading direction. Cracks or microcracks can be formed during impact,

54

compression, tensile and fatigue stress or after changes in temperature, and during thermocycling. Microcracks can be created in any plies but predominantly in plies off-axis to loading directions. Microcracks in carbon fibre/epoxy laminates are formed instantly across the entire cross-sectional area of the 90° plies. In contrast, cracking in the glass fibre/epoxy decreased partially or totally as the 90° plies get thin. Nairn *et al.* found that complete elimination of microcracks in glass fibre/epoxy laminates required making the 90° plies 5 times thinner than the 0° plies.[98]
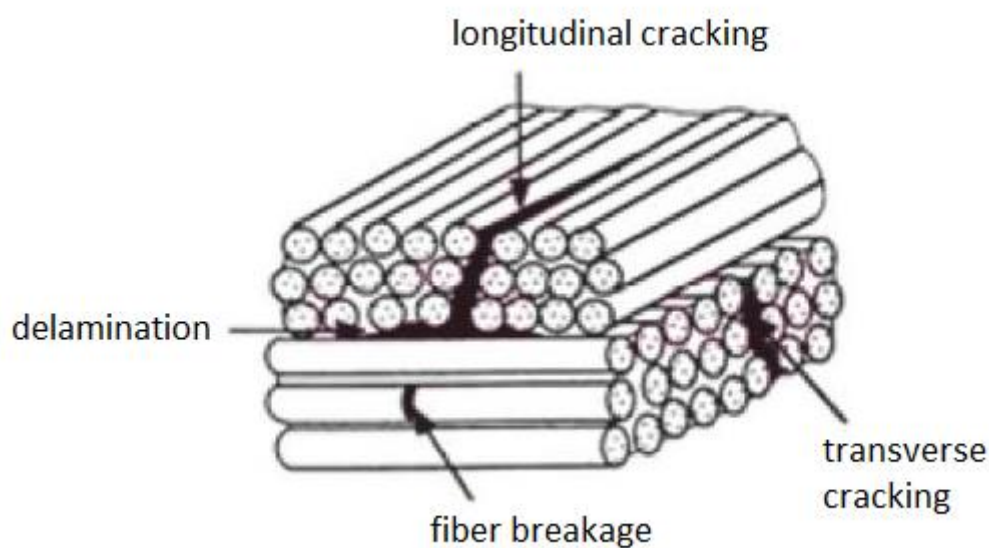
Figure 2.4.2 Damage types of a composite structure (Taken from Ref.[99])

Delamination is debonding between layers with different orientations. Kim *et al* demonstrated that delamination appeared to be mainly governed by either, or a combination of, the tensile stress and size of transverse cracking.[100] Rebière *et al.* investigated the matrix cracking and delamination evolution in composite cross-ply laminates and found that transverse cracking first occurs in the 90° layers.[101] Figure 2.4.3 illustrates a schematic representation of a matrix crack leading to debonding and transverse fibre breakage.

During impact tests, the kinetic energy of the projectile once impacted into the target is scattered and absorbed in various ways by the target. The main energy-absorbing mechanisms throughout the ballistic impact include kinetic energy absorbed due to tensile failure of the fibres, energy absorbed due to matrix cracking and delamination, and frictional energy absorbed in the course of penetration.[102]
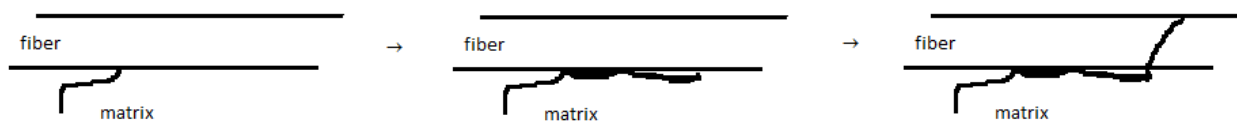
Figure 2.4.3 Crack propagation in composites[103]

2.4.3 The impact tolerance of polymer composites

The impact tolerance is a crucial property of composites. Impact in composites results in creation of large areas of fracture with subsequent reductions in both strength and stiffness.[104] Low-velocity impact response depends on the target stiffness, material properties and the projectile's mass and stiffness. The matrix of the target is of utmost importance as the contact duration is long enough for the entire structure to respond to the impact and in consequence more energy is absorbed elastically.[105] On the other hand, high-velocity impact response is dominated by stress wave propagation through the material, in which the structure does not have time to respond, leading to very localized damage.

The impact resistance is the ability of a material to tolerate shock loading. Impact damage resistance is a matrix-dominated property.[106] The polymeric matrix in a fibre reinforced composite aligns the fibres as well as transfers the stress from one fibre to another. Brittle laminates (such as epoxy resins, PMMA)

have a low crack initiation energy, low crack propagation energy and tend to fail by extensive delamination whereas the tougher systems fail in transverse shear near the impact location.[104, 107] A reduction in the cross-linking density of thermoset matrices also improves the impact resistance of composites.[104]

Fibres can raise the impact strength depending on their nature.[50] They can reduce crack initiation by acting as stress concentrators. Impact resistance is highly dependent to the diameter, length of the fibres and matrix structure. Smaller fibre diameter gives the fibre less surface area, increases the energy absorbing capability of the composite, resulting in lower levels of damage.[108] Long fibres are more preferable. The impact strength can be increased significantly by continuous fibres because they share the shock over the interface area along the fibre. On the other hand, short fibres do not exhibit so clear results.[3] Their use may either enhance or decrease the impact strength.

The selection of the nature and the appropriate size of the fibre reinforcements should be considered very carefully. Previous studies suggest that the presence of reinforced fibres is highly affected to the impact strength of the composite materials.[33, 109] Compression after impact tests are performed here to measure the material residual strength.

2.4.4 Methods to enhance impact resistance of composites

Improving the impact resistance in composites is a vital area of research. There are three main methods to improve the impact resistance properties of composites. The first way is to improve the polymer matrix, the second to enhance the reinforcement and the last one to enhance the adhesion between the matrix-reinforcement.

Incorporation of additives for enhancement of the impact properties is a first approach.[110] The mechanism involves hosting of an elastomeric or rubbery element that can absorb the energy of an impact or dissipate it. Commercially available (DuPond, Dow), impact modifiers (such as Engage 8137, Engage

8100, PARALOID™) have been found to improve the impact resistance of the composites.[111] However these modifiers are responsible for reducing further the tensile strength of composites.

Rubber-toughened epoxies have much higher toughness and impact resistance.[112] In this process rubber or inorganic filler in a minor proportion, typically between 5 and 20%, is incorporated as a dispersed phase in a rigid epoxy matrix. The resulting composite has a higher fracture resistance than the unmodified epoxy resin due to decrease in brittleness.

Another solution is to use high toughness thermoplastics such as polyether ether ketone (PEEK) with a processing temperature of 400°C. The toughness of fibre reinforced PEEK composites is seen to be about ten times that of composites Although it seems an attractive resin, the structural fabrication cost may be prohibitive as a result of the high processing temperature.

Various studies have shown that nano-fillers such as nanotubes, nano-clays and nano-fibres at low concentrations enhance the impact properties and energy dissipation of epoxy-based composites.[113, 114] Fillers act as stress concentrators and the polymer matrix with loading of fillers has less ability to absorb impact energy.[115] Assuming that the bonding strength is significant, the fracture toughness of the brittle epoxy polymer matrix will increase with the addition of MWCNTs, acting as aggregate to improve the critical stress intensity factor, Kc.[116]

Hollow ductile fibres have been also used for improving composites' impact resistance. Epoxy-based composites using hollow polyester fibres were manufactured and led to a lower weight and increased impact damage tolerance of laminates.[117] The explanation for this phenomenon was the flexibility of the hollow fibres. The cylindrical thermoplastic hollow fibres can be easily deformed to an elliptical shape. This capability leads to a decrease in stress concentration at the polymer matrix and subsequently a decrease in the matrix cracking which is the most predominant mode of failure.

Another approach to enhance the impact resistance is by improving the bonding between the polymeric matrix and the reinforcement. Silane coupling agents were used to enhance the adhesion between the polymer and fillers.[118] In an interesting study, better adhesion led to a reduction in delamination under impact loading in composites.

2.4.5 Methods to heal composite damaged areas

Healing of composites damaged areas has been successfully developed by various techniques which are presented in this section.

The autonomic healing concept developed by White *et al.* is presented in Figure 2.4.4.[119] This approach involved a microencapsulated healing agent (dicyclopentadiene) that was embedded in a structural composite matrix containing a transition metal catalyst (Grubbs' catalyst) capable of polymerising the healing agent. As seen in the picture a crack was initiated in the matrix (a) and after propagation (b) the crack ruptured the microcapsules, releasing the healing agent into the crack plane through capillary action. At the end (c), the healing agent came in contact with the catalyst, inducing polymerisation that bonded the crack. The microencapsulation process with self-healing agents has been followed by various researchers.[120, 121] Nevertheless due to some limitations it cannot be applied to every polymer composite. The curing temperature of the composites containing self-healing agents is limited to low values (upto 40°C) for avoiding activation of the catalyst or increased probability of healing agent to be released from the broken microcapsules. Microcapsules need to be fabricated because they are not commercially available. Moreover during the manufacturing of the composites extra care is required. The resins containing microcapsules and catalysts should be prepared by hand mixing avoiding microcapsules rupturing and consequent early, not desired polymerisation.

Another healing mechanism is the hollow-fibre self-healing that was introduced by Bleay *et al.*[122] Hollow glass fibres were used to embed microcapsules because they offer the advantage of being able to store functional agents for composite self-repair systems as well as acting as a reinforcement. A typical hollow fibre self-healing approach used within composite laminates could take the form of fibres containing a one-part resin system, a two-part resin and hardener system or a resin system with a catalyst or hardener contained within the matrix material, as seen in Figure 2.4.5. This repair process helps in reducing the critical effects of matrix cracking and delamination between plies, preventing further damage propagation.[123] Trask *et al.* demonstrated that hollow glass fibres containing a two-part epoxy healing resin can be manufactured and incorporated within a conventional autoclave processing, indicating that this healing approach can be readily applied to other manufacturing techniques.[124] The effect of this healing approach on the mechanical properties was beneficial but insignificant (3%). Another major drawback of this approach is that these fibres are not commercially available.
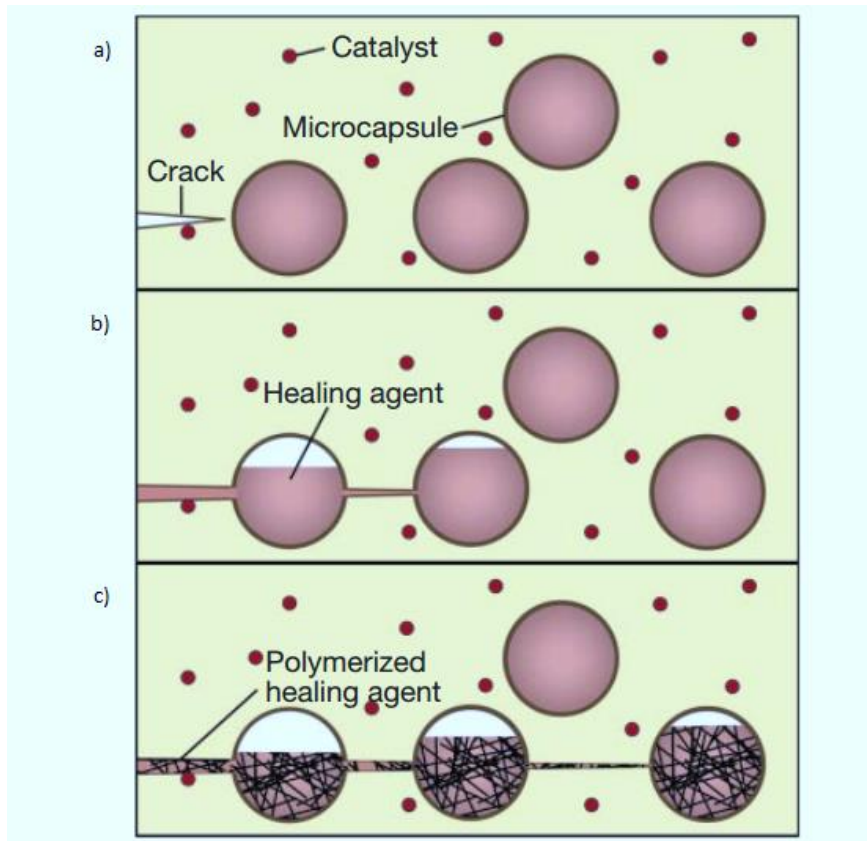
Figure 2.4.4 Autonomic healing mechanism, a) crack initiation, b) dispersion of healing agent and c) polymerisation of healing agent (Taken from Ref.[119])

Finally, Hayes *et al.* demonstrated healing of composites using a self-healing matrix.[125] This self-healing matrix approach involved a thermosetting epoxy resin (blend of Epikote 828 (a diglycidylether of bisphenol A) cured with nadic methylene tetrahydrophthalic anhydride and the mercaptan accelerator, Capcure 3-800) into which a linear polymer (polybisphenol-A-co-epichlorohydrin) (as the healing agent) was dissolved. The linear polymer should be bonded into the cross-linked epoxy matrix through hydrogen bonding but became mobile above a specific temperature, its glass transition temperature (T_g). Thus upon heating, the healing agent was diffused throughout the matrix bridging any cracks within it. In order for this approach to be beneficial heating at high temperatures (>130°C) was required and upto 50% healing efficiency in impact strength and 30% visual healing (optical

microscope) was identified with recovery. Another parameter that should be taken into consideration is that the solubility of the polymer and the healing agent should be matched so that the healing agent remains uniformly dissolved in the matrix, without phase separation.
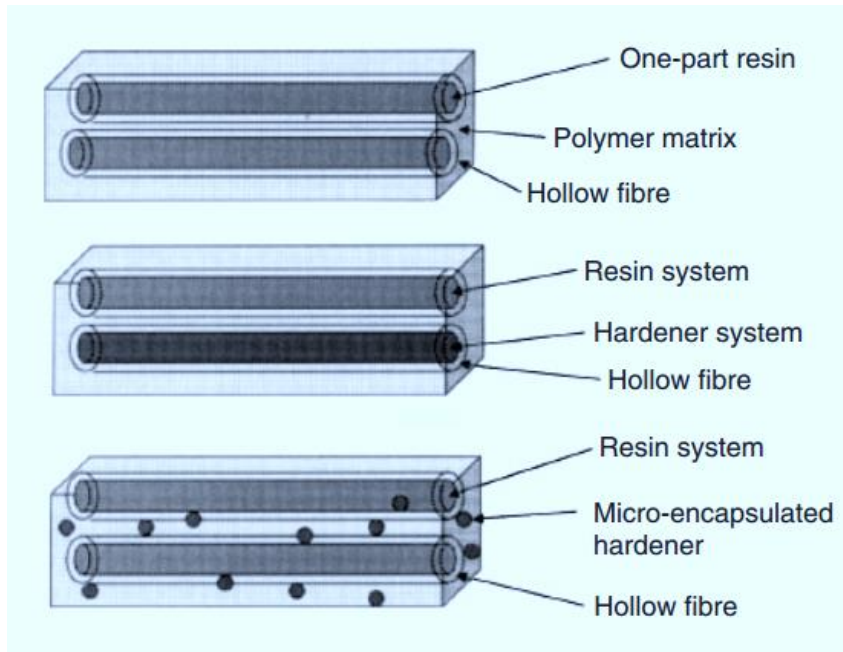
Figure 2.4.5 Hollow fibre self-healing methods (Taken from Ref.[122])

3 EXPERIMENTAL METHODS

The incorporation of photosensitive polymers into glass/epoxy composite materials and the investigation of the modified polymer matrix and the compressive properties of the composites were the main focus of these PhD studies. This Chapter covers all the procedures and equipment used in order to accomplish the sets of experiments that were required to fulfil the remits of this project. Three types of experiment were conducted namely synthesis of polymers, polymers' characterisation and testing of the synthesised materials and azobenzene-based composites.

3.1 Photoresponsive Materials

All the solvents and reagents for the syntheses were purchased and used without any further purification and are listed in Table 3.1.1.

Table 3.1.1 Table of reagents for synthesis

Reagent	Supplier	Purity
2-Aminophenol	Alfa Aesar	99%
4,4-Dihydroxyazobenzene	Sphinx	96%
4-Aminophenol	Alfa Aesar	98%
4-Phenylazophenol	Alfa Aesar	98%
Acetone	Sigma Aldrich	99%
Acryloyl chloride	Sigma Aldrich	97%
Azoisobutyronitrile	Sigma Aldrich	98%
Chloroform	Alfa Aesar	99%
Copper (II) sulfate pentahydrate	Alfa Aesar	98-100%

Dichloromethane	Fischer Scientific	99%
Diethyl ether, anhydrous	Alfa Aesar	99%
Diethylenetriamine	Sigma Aldrich	99%
Dimethyl sulfoxide	Alfa Aesar	99%
Dimethylformamide	Sigma Aldrich	99.8%
Epichlorohydrin	Alfa Aesar	99%
Hexanes	Alfa Aesar	98.5%
Hydrochloric acid	Alfa Aesar	50% v/v aq.sol.
Hydroxylamine hydrochloride	Alfa Aesar	99%
Methacryloyl chloride	Sigma Aldrich	97%
Methanol	Alfa Aesar	99%
Methyl methacrylate	Sigma Aldrich	99%
Petroleum ether 40/60	Alfa Aesar	100%
Sodium nitrite	Alfa Aesar	98%
Tetrahydrofuran	Alfa Aesar	99%
γ-butyrolactone	Sigma Aldrich	99%

3.1.1 Materials synthesis

Azobenzene precursors, monomers and polymers that were used in this research were not commercially available and therefore, their synthesis was a mandatory step. The photoresponsive molecules needed to be functionalised with suitable reactive groups to be able to polymerise or cross-link with other compounds used in this project.

EXPERIMENTAL METHODS

Polymethylmethacrylate (PMMA) was synthesised as a building block of the azobenzene-based copolymers and as a reference sample for comparison. Later syntheses of precursor azobenzene monomers were carried out to obtain 4-4-methacryloyloxyazobenzene (4-MOAB), 4-4-acryloyloxyazobenzene (4-AOAB), 4-glycidyloxyazobenzene (4-GOAB), 4,4´-dihydroxyazobenzene (4,4´-DHAB), 4,4´-diglycidyloxyazobenzene (4,4´-DGOAB) and 4,4´-dimethacryloyloxyazobenzene (4,4´-DMOAB). The monofunctional monomers (4-MOAB and 4-AOAB) were copolymerised with methyl methacrylate [117] and the copolymers were used for the investigation of their photoresponsive properties before and after UV irradiation. Synthesis of an epoxy-azobenzene based monomer, 4-GOAB, was conducted from 4-phenylazophenol and epichlorohydrin.[32] The 4,4´-DHAB was synthesised as the precursor for the synthesis of the 4,4´-DGOAB and 4,4´-DMOAB but the bulk amount of 4,4´-DHAB was purchased from Sphinx company (USA) as the synthetic route used in the laboratory gave a poor yield (<20%). The synthesis of 500 g 4,4´-DGOAB was one of the most important steps in this project as it was used as a cross-linker in the manufacture of the glass/azobenzene-epoxy composites. The synthetic routes involved in material synthesis are presented in the following sub-sections.

3.1.1.1 Synthesis of 4-methacryloyloxyazobenzene (4-MOAB) and 4-acryloyloxyazobenzene (4-AOAB)
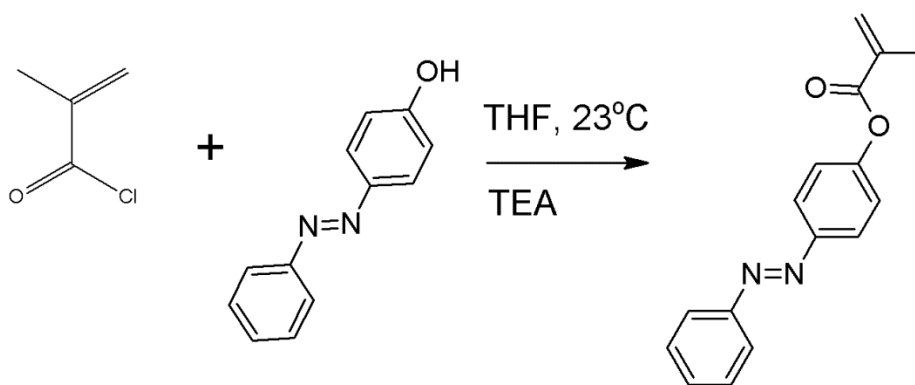
Figure 3.1.1 Synthesis of 4-MOAB[19, 126]

Figure 3.1.1 illustrates the synthetic route for 4-methacryloyloxyazobenzene (4-MOAB). Methacryloyl chloride (1.56 ml, 1 mmol) was added slowly to a 50 ml THF

solution of 4-phenylazophenol (8.8 mmol) and triethylamine (TEA, 2.32 ml,16 mmol) at 5-10°C, under N_2 atmosphere. An ice-bath was used to maintain the low temperature. After 2 hrs, the ice-bath was removed and the mixture was warmed to room temperature and stirred (magnetic stirrer) overnight. The progress of the reaction was monitored by thin layer chromatography (TLC), discussed in detail in section A.3. At the end of the reaction the residue was filtered off with a Buchner funnel and the solvent from the filtrate was evaporated by a rotary evaporator (Rotevapor BUCHI, Vacuum Controller V-805). The product was then dissolved in chloroform ($CHCl_3$, 40 ml), washed with distilled water (4x100 ml) and the organic layer was dried over anhydrous magnesium sulphate ($MgSO_4$) for 18 hrs. After evaporation of the solvent, the product was recrystallised twice from petroleum ether to obtain pure product of 4-MOAB with a 78% yield. The 4-MOAB monomer was then analysed by ^{1}H NMR.[23]

^{1}H NMR δ (DMSO-d_6, 400MHz): 7.92-7.90 (d, 4H), 7.64-7.58 (m, 3H), 7.45-7.43 (m, 2H), 6.34-6.33 (s, 1H), 5.96-5.95 (s, 1H), 2.04-2.03 (s, 3H)
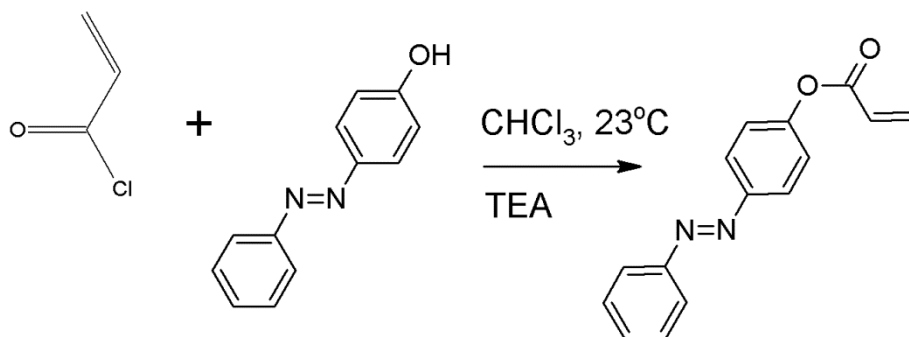
Figure 3.1.2 Synthesis of 4-AOAB[127]

The aforementioned process was repeated to synthesise the 4-AOAB monomer, and its synthetic route is shown in Figure 3.1.2. A solution of acryloyl chloride (2.15 ml, 26.48 mmol) and $CHCl_3$ (10 ml) was added dropwise into a $CHCl_3$ (90 ml) solution of 4- phenylazophenol (5 g, 25.22 mmol) and TEA (3.53 ml, 25.22 mmol) at 5-10°C under N_2 gas. After 2 hrs, the mixture was warmed to room temperature and stirred overnight. The completion of the reaction was monitored by TLC. The reaction mixture was filtered to isolate the triethylammonium chloride salt. The residue was

washed with chloroform to separate the remaining product in the salt. The combined organic phase was washed twice with water to isolate any inorganic products and dried over magnesium sulphate for 18 hrs. The salt was filtered off and the solvent was evaporated from the organic phase using a rotary evaporator. The product was recrystallised twice from petroleum ether to obtain a pure product of 4-AOAB with 72% yield. The authenticity of the 4-AOAB was then characterised by ^{1}H NMR.[127]

^{1}H NMR δ (DMSO-d$_6$, 400MHz): 7.89-7.77 (m, 4H), 7.48-7.39 (m, 3H), 7.26-6.83 (m, 2H), 6.61-6.54 (d, 1H), 6.33-6.22 (t, 1H), 6.00-5.95 (d, 1H)

3.1.1.2 Synthesis of 4-glycidyloxyazobenzene (4-GOAB)
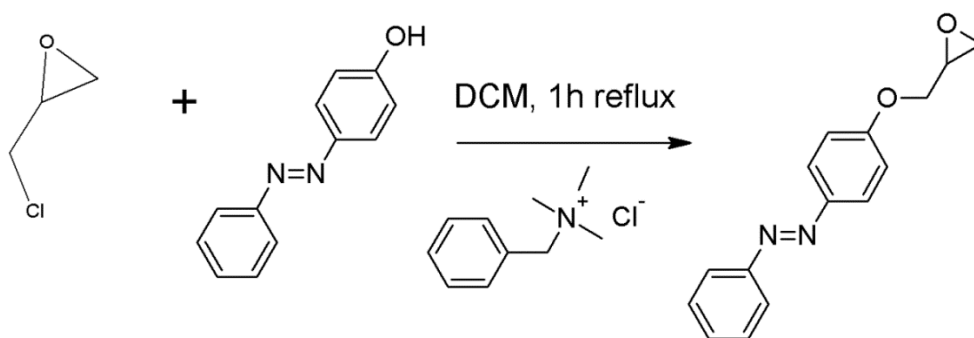
Figure 3.1.3 Synthesis of 4-GOAB[32]

The synthetic route of 4-GOAB is illustrated in Figure 3.1.3. 4-Phenylazophenol (2.00 g, 10.09 mmol), epichlorohydrin (37.34 g, 403.59 mmol) and benzyltrimethylammonium chloride (43.23 mg, 0.05 mmol), with a molar ratio of 1:40:0.05 respectively, were placed in a 100 ml two necked round bottom flask equipped with a condenser and a magnetic stirrer. The reaction mixture was left to reflux under magnetic stirring for 1 hr. The excess of epichlorohydrin was removed using a rotary evaporator and subsequently high vacuum treatment (10^{-2} mmHg). The crude product was characterised by ^{1}H-NMR to check the complete removal of epichlorohydrin. Then the remaining mixture free from epichlorohydrin was dissolved in dichloromethane (DCM, 50 ml) and extracted three times with distilled water (3x120 ml). The organic phase was dried overnight on anhydrous MgSO$_4$ and then filtered. The solvent was evaporated using a rotary evaporator. The resulting solid was dissolved in acetone and reprecipitated from distilled water. After being

dissolved again in DCM, it was recrystallised from petroleum ether to obtain an orange product with a yield of 81%, which was characterised by DSC, IR and ^{1}H-NMR methods, detailed in sections 3.1.2.1, 3.1.2.3 and 3.1.2.5. Furthermore, the obtained orange solid was then subjected to column chromatography since the recrystallized product still showed noticeable "impurities" in the NMR traces. The column was packed with silica gel (Fisher) and DCM was used as the eluent. The purification by column chromatography incurred significant loss of product giving a final yield of 48%. The 4-GOAB monomer from column chromatography was then analysed by ^{1}H NMR and FTIR spectroscopy.[32] DSC analysis showed a melting point of 85.5°C which is in agreement with the literature value.

^{1}H NMR δ (CDCl$_3$, 400MHz): 7.86-7.97 (t, 4H), 7.43-7.53 (m, 3H), 7.02-7.05 (d, 2H), 4.22-4.34 (d, 1H), 4.05-4.07 (d, 1H), 3.50 (s, 1H), 2.92-2.96 (d, 1H), 2.98-2.89 (d, 1H)

FTIR (KBr) cm^{-1}: 3053 (C-H, alkanes), 2927 (C-H, aromatics), 1500 (C-C), 1600 (C-C), 1581 (N=N), 1224-1256 (C-N), 1070-1144 (C-O)

3.1.1.3 Synthesis of 4,4´-dihydroxyazobenzene (4,4´-DHAB)
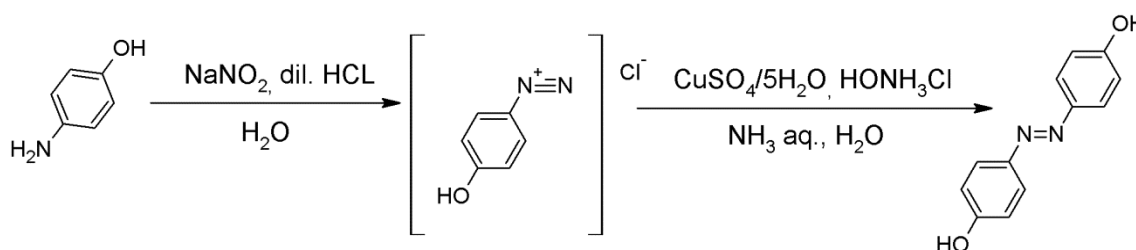
Figure 3.1.4 Synthesis of 4,4´-DHAB[128, 129]

A typical reaction scheme for the synthesis of 4,4´-DHAB is shown in Figure 3.1.4. In a 1 litre beaker, p-aminophenol (4.00 g = 36.68 mmol) and distilled water (40.00 ml) were added. An aqueous solution of 60 ml HCl (3 mM) was added drop wise over 30 min at room temperature. Sodium nitrite (2.6 g = 36.68 mmol) was dissolved in distilled water (216.00 ml), and the solution was slowly added to the former solution in the 1 litre beaker over 2 hrs at 0°C. The low temperature was maintained using an ice-bath.

EXPERIMENTAL METHODS

A solution of copper sulphate pentahydrate (16.3 g = 65.3 mmol), 28% ammonia (10.94 ml = 58.00 mmol) and hydroxylammonium chloride (2.56 g = 36.68 mmol) was added to the former solution in a drop-wise manner. The reaction was carried out for 2 hrs at room temperature. The reaction mixture was filtered, and the crude product was washed with a 1 M hydrochloric acid. Finally, the product was recrystallised from acetone/water and the desired 4,4´-DHAB product was obtained with 24% yield. The purity of the product was checked by NMR and FTIR spectroscopy. The spectroscopy data are listed below. DSC analysis showed a melting point of 185°C which is in agreement with the literature value.[100, 101]

^{1}H NMR δ (CDCl$_3$, 400MHz): 10.05 (s, 2H), 7.73-7.76 (t, 4H), 6.92-6.97 (t, 4H)

FTIR (KBr) cm^{-1}: 3053 (C-H, alkanes), 2927 (C-H, aromatics), 1500 (C-C), 1600 (C-C), 1581 (N=N), 1224-1256 (C-N), 1070-1144 (C-O)

3.1.1.4 Synthesis of 4,4´-dimethacryloxyazobenzene (4,4´-DMOAB)
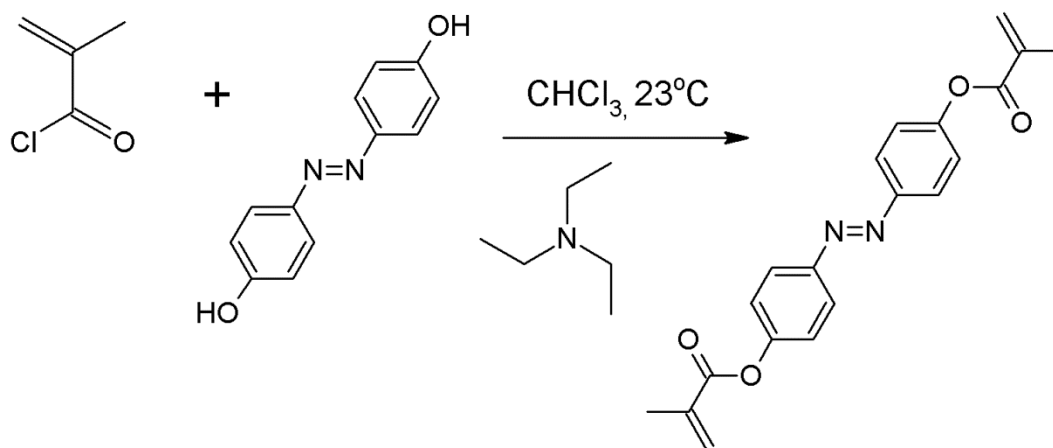
Figure 3.1.5 Synthesis of 4,4´-4,4´-DMOAB[32]

Figure 3.1.5 shows the methacrylation of 4,4´-dihydroxyazobenzene. Methacryloyl chloride (7.35 g = 70.32 mmol) in CHCl$_3$ (10 ml) was slowly added to a CHCl$_3$ (90 ml) solution of 4,4´-dihydroxyazobenzene (5 g = 23.34 mmol) and triethylamine (2.36 g =

23.34 mmol) with continuous stirring at 5-10°C under N_2 atmosphere. After 2 hrs, the reaction mixture was warmed to room temperature and stirred overnight (20 hrs). The progress of the reaction was monitored by TLC. At the end of the reaction the solid residue was filtered off and the $CHCl_3$ solution washed twice with distilled water to remove water soluble materials. The organic layer was dried over anhydrous magnesium sulphate overnight (18 hrs) and the solvent was evaporated using a rotary evaporator. The product was recrystallised twice from DCM/petroleum ether giving a yield of 81%. The purity of 4,4´-DMOAB was verified by NMR and FTIR spectroscopy, and the signals are listed below. DSC analysis showed a melting point of 141°C which is in agreement with the literature.[32]

^{1}H NMR δ (CDCl$_3$, 400MHz): 7.98-7.96 (m, 4H), 7.27-7.03 (m, 4H), 6.39 (s, 2H), 5.80 (s, 2H), 2.09 (t, 6H)

FTIR (KBr) cm^{-1}: 3053 (C-H, alkanes), 2927 (C-H, aromatics), 1500 (C-C), 1600 (C-C), 1581 (N=N), 1224-1256 (C-N), 1070-1144 (C-O).

3.1.1.5 Synthesis of 4,4´-diglycidyloxyazobenzene (4,4´-DGOAB)
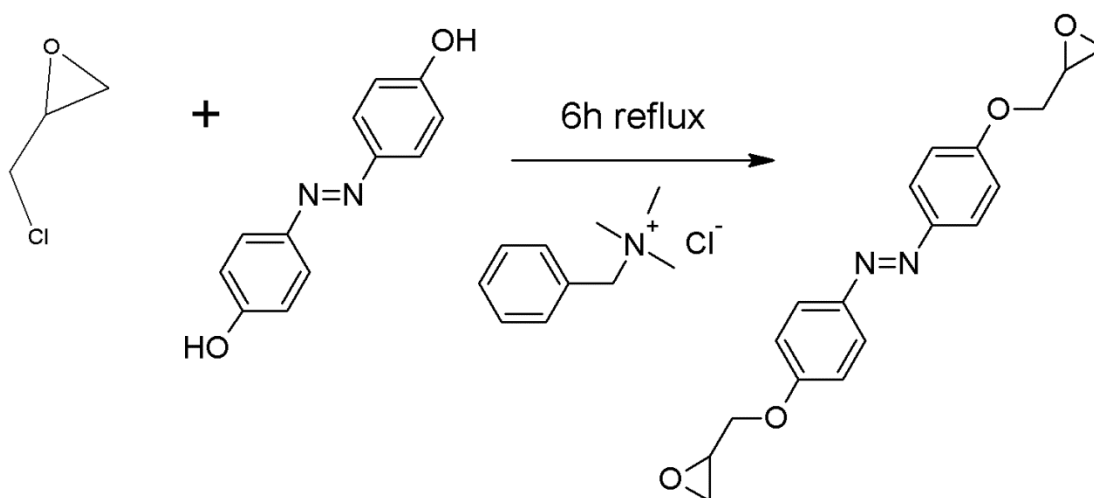
Figure 3.1.6 Synthesis of 4,4´-DGOAB[32]

A difunctional epoxy monomer was synthesised via a condensation reaction between epichlorohydrin and dihydroxyazobenzene. A typical reaction scheme is shown in Figure 3.1.6. 4,4´-Dihydroxyazobenzene (40 g = 122.6 mmol), epichlorohydrin (1.150

L) and benzyltrimethylammonium chloride (1.4 g = 6.13 mmol), with a molar ratio of 1:10:0.05 respectively, were taken in a 2 litre round bottom flask equipped with a condenser and a magnetic stirrer. The reaction mixture was left to reflux under stirring for 6 hrs. After reflux, the excess of epichlorohydrin was removed using a rotary evaporator and high vacuum pump. The residue, free from epichlorohydrin, was dissolved in DCM and then filtrated in order to remove any insoluble material. The DCM solution (50 ml) was washed three times (3 x 120 ml) with distilled water. The organic phase was dried on anhydrous magnesium sulphate, filtered, and the solvent was evaporated using a rotary evaporator. The resulting solid was recrystallised twice from acetone to obtain a yellow product with 75% yield. This synthetic procedure was repeated several times because the 4,4´-DGOAB was the photoresponsive crosslinker for the composite matrix and is not commercially available and a large quantity of approximately 500 g had to be synthesised. The purity of 4,4´-DGOAB was checked by NMR and FTIR and the signals are listed below. DSC analysis showed a melting point of 165ºC which is in agreement with the literature value.[32]

^{1}H NMR δ (CDCl$_3$, 400MHz): 7.89-7.86 (t, 4H), 7.01-7.03 (m, 4H), 4.29-4.33 (t, 1H), 4.02-4.04 (t, 1H), 3.40 (s, 1H), 2.93-2.94 (t, 1H), 2.79-2.80 (t, 1H)

FTIR (KBr) cm^{-1}: 3053 (C-H, alkanes), 2927 (C-H, aromatics), 1500 (C-C), 1600 (C-C), 1581 (N=N), 1224-1256 (C-N), 1070-1144 (C-O)

3.1.1.6 Synthesis of polymethylmethacrylate (PMMA)
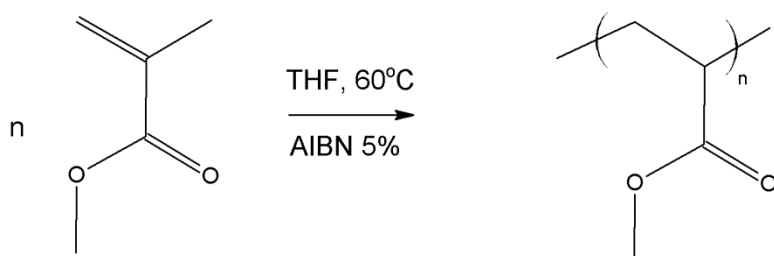
Figure 3.1.7 Polymerisation of MMA

The reaction scheme for the PMMA synthesis is depicted in Figure 3.1.7. A typical synthesis is as follows: methylmethacrylate (5.0 g) was added to tetrahydrofuran

(THF) (20.0 ml) in a 100 ml reaction flask. Azobisisobutyronitrile (AIBN,0.25 g,5 wt%), used as a free-radical initiator, was added to the solution and magnetically stirred until dissolved. The solution was purged with N_2 for 10 min to achieve an inert atmosphere. Polymerisation was carried out at 60°C for 48 hrs. The polymer was precipitated by adding methanol and was dried at room temperature under vacuum for about 4 hrs. The polymer was then analysed for its structure and purity using proton nuclear magnetic resonance spectroscopy (^{1}H NMR). The chemical shifts are listed below.[32] Its molecular weight was determined by gel permeation chromatography (GPC) and its glass transition temperature (T_g) by differential scanning calorimetry (DSC).

^{1}H NMR δ (DMSO-d$_6$, 400MHz): 3.59-3.58 (s, 3H), 1.81-1.80 (s, 1H), 1.63-1.62 (s, 1H), 1.21-1.20 (s, 1H), 1.02-1.01 (s, 1H), 0.85-0.84 (s, 1H), GPC: M_w= 43,000 g/mol, DSC: T_g= 113.5°C

3.1.1.7 Synthesis of poly(MMA-co-MOAB)

The reaction schemes for the synthesis of a series of copolymers of MMA and 4-MOAB in different solvents are illustrated in Figure 3.1.8. These were designed to investigate the effect of solvents on the product's yield.
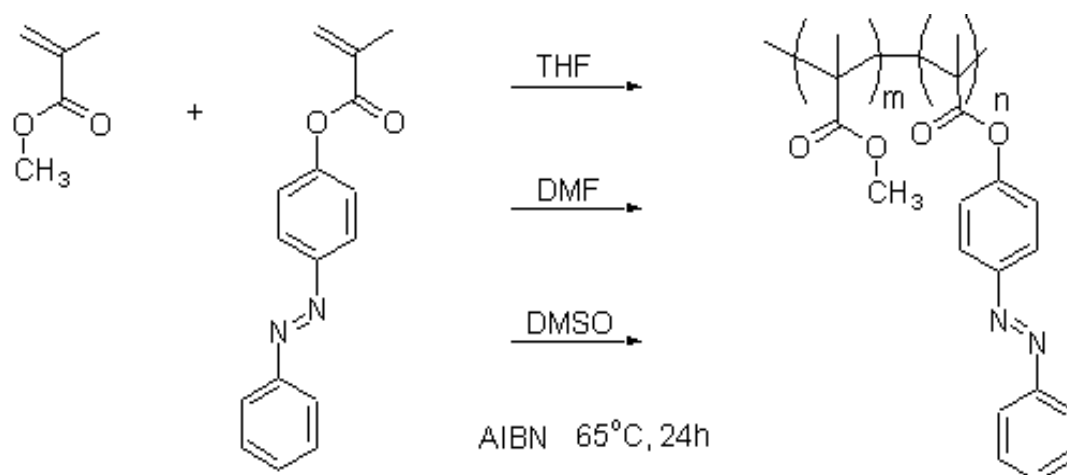
Figure 3.1.8 Synthetic route of poly(MMA-co-MOAB)[19]

EXPERIMENTAL METHODS

A typical synthetic route is as follows: 24.6 mg (0.15 mmol) of azoisobutyronitrile (AIBN) as initiator, 188.95 mg (0.749 mmol) 4-MOAB, 1.5 ml of MMA and 10 ml of solvent were added into a Schlenk flask. The reaction mixture was degassed three times by freeze-thaw cycles. The polymerisation was conducted in an oil bath at 65°C for 24 hrs under continuous stirring. The reaction mixture was then removed from the oil bath and allowed to cool to room temperature. The polymer was precipitated by adding methanol, then dissolved in tetrahydrofuran (THF) and reprecipitated from methanol. Finally, the copolymer was dried under high-vacuum in a desiccator at room temperature until a constant weight was achieved. Similar synthetic routes were followed using dimethyl formamide (DMF) and dimethyl sulfoxide (DMSO) as solvents with yields of 71% (CV2.1/THF), 76%(CV2.2/DMF) and 71%(CV2.3/DMSO). The polymers were characterised by NMR, as seen below, and by GPC and DSC as seen in section 4.1.2.2.[19]

^{1}H NMR δ (CDCl$_3$, 400MHz): 7.97-7.90 (broad s, 4H), 7.52-49 (broad s, 3H), 7.26-7.18 (broad s, 2H), 3.77-3.41 (broad s), 2.35-1.81 (broad t), 1.62-1.52 (s, 6H), 1.25-1.19 (broad s), 1.02-0.85 (broad s)

3.1.1.8 Synthesis of polyglycidyloxyazobenzene (PGOAB)
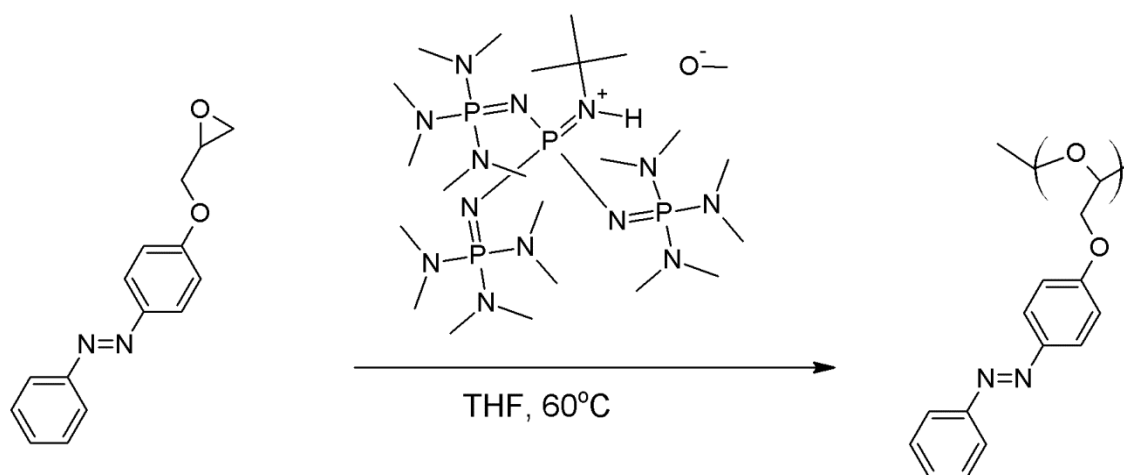
Figure 3.1.9 Synthesis of PGOAB[32, 130]

The homopolymerisation of the 4-GOAB is shown in Figure 3.1.9. In a 100 ml Schlenk flask containing a magnetic following bar, 4-glycidyloxyazobenzene (2 g =

8.043 mmol), methanol (6.408 mg = 0.2 mmol), and 10 ml of anhydrous THF were added. The solution was stirred under N_2 atmosphere for 30 min. Then, 0.2 ml (0.2 mmol) of a 1 M phosphazene base t-Bu-P$_4$ solution in hexane was added and polymerisation was carried out at 60°C for 48 hrs. The polymer was precipitated by adding methanol, hydrochloric acid and distilled water (97:1:2). The precipitate was filtered, then dissolved in 10 ml of THF and reprecipitated from methanol. The filtered polymer was dried at room temperature under high vacuum (10^{-2} mmHg) for 6 hrs and obtained a yield of 35%. The polymer was characterised by NMR and FTIR as seen below.[93] DSC analysis showed a melting point of 58ºC which is in agreement with the literature value.

^{1}H NMR δ (CDCl$_3$, 400MHz): 7.75-7.93 (t, 4H), 7.34-7.52 (m, 3H), 6.75-7.45 (d, 2H), 3.50-4.65 (broad d, 5H)

FTIR (KBr disk) cm^{-1}: 3053 (C-H, alkanes), 2927 (C-H, aromatics), 1500 (C-C), 1600 (C-C), 1581 (N=N), 1224-1256 (C-N), 1070-1144 (C-O)

3.1.2 Materials characterisation

After the synthesis, materials were characterised using various techniques. The basic characteristics of the polymers such as molecular structure, molecular mass or glass transition temperatures were determined using common techniques, such as gel permeation chromatography (GPC), nuclear magnetic resonance (NMR), Fourier transform infrared (FTIR) spectroscopy and differential scanning calorimetry (DSC). UV/Vis spectroscopy was highly used in these studies as the geometrical changes of the azobenzene were related to different absorbance values, and thus were indicating the photoresponsive behaviour of the materials. The investigations of the viscosity and density change due to photoirradiation were conducted using a rotational rheometer and gas pycnometer respectively. The azobenzene polymer films were tested with a nanoindenter in order to identify photoinduced changes in stiffness and hardness.

EXPERIMENTAL METHODS

3.1.2.1 1H NMR spectroscopy

Proton nuclear magnetic resonance (^{1}H NMR) spectroscopy provided information about the composition of polymers and structural information of chemical substances.[130, 131] The NMR absorption is related to differences in the spin nuclei orientation of molecules applied in a magnetic field. Protons have two spin nuclei orientations: those that aligned with the external magnetic field, exhibiting a lower energy state and those against the external magnetic field with a higher energy state. The changes in energy states between different protons in a molecule give rise to a unique signal. Therefore, the sets of equivalent protons that are in a molecule can be determined by the number of signals in the spectrum.

The ^{1}H NMR spectra in this programme were recorded on a Bruker 400 MHz spectrometer using tetramethylsilane (TMS) as an internal reference. The deuterated chloroform (CDCl$_3$) or dimethyl sulfoxide (DMSO-d$_6$) were used as solvents. The spectrum region is read from right to left and a reference compound defines the zero point. Each peak at different chemical shifts indicates different proton environments. The integral that corresponds to the relative area under the peak is proportional to the number of absorbing hydrogen atoms. Different types of functional groups, such as methyl, benzene rings and hydroxyl, can change the chemical shift of the protons. Comprehensive tables that were used for the identification of the molecule structures are found in the literature.[130, 131]

3.1.2.2 Gel permeation chromatography

Gel permeation chromatography (GPC), also known as size exclusion chromatography (SEC), is a chromatographic technique that can separate dissolved polymer molecules according to their sizes by passing through a specific column containing a microporous material. By this technique the weight average molecular mass (M_w), number average molecular mass (M_n) and the molecular mass distribution/polydispersity (PD) of the polymer samples were determined.

EXPERIMENTAL METHODS

The GPC analysis was conducted using a size exclusion chromatograph "Waters" equipped with a 2410 refractive index detector. The 300 mm long and 7.5 mm in diameter column was packed with 10 μm PL-gel (Polymer Laboratories).

Sample solutions were prepared by dissolving polymers in anhydrous THF and leaving them in the dark at room temperature for 2 hrs before being injected. The concentration of the polymeric samples in solution of THF was 1.5 mg/ml. Relative number and weight average molecular masses were determined by eluting the polymer solutions with THF at a flow rate of 1.0 ml/min. A calibration curve was created using narrow dispersed polystyrene standards.

3.1.2.3 Fourier transform infrared spectroscopy

Fourier transform infrared (FTIR) spectroscopy was used for the identification of functional groups that cannot be detected by ^{1}H NMR analysis. A significant example is the -N=N- bond present in an azobenzene molecules, that has no hydrogen linked to it. The combination of infrared (IR) and ^{1}H NMR spectroscopy leads to a faster and more effective identification of compounds.

IR spectra are regular absorption spectra that are produced from the bond vibration motions of a molecule when it is exposed to infrared with different frequencies. For example, according to the Hooke's law, stronger bonds vibrate at a faster rate than weaker bonds. The Hooke's law in Equation 3-1 relates to the bond strength and the frequency of the vibration.

$$v = \frac{1}{2\pi c} \sqrt{\frac{f}{\mu}}$$

Equation 3-1

where c is the speed of light (2.99×10^8 m/s), v is the frequency of the vibration (Hz) and is proportional to the square root of the constant bond strength, f (kg/s^2), and

EXPERIMENTAL METHODS

μ expresses the reduced mass (kg) of the two atoms (m_1 and m_2) that form the chemical bond that can be defined from by the following Equation 3-2.

$$\mu = \frac{m_1 m_2}{m_1 + m_2}$$

Equation 3-2

For the collection of FTIR spectra of the materials, a Vector 22 Spectrometer, was used and the data were analysed by a Bruker Optic's OPUS software. A potassium bromide (KBr) disc was used as a reference. The FTIR spectra were collected at room temperature within the wavelength range of 400-4000 cm^{-1} and with a resolution of 3 cm^{-1}. This wavelength range covered all the visible and near infrared regions.

3.1.2.4 UV/Vis spectroscopy

Ultra-violet and visible (UV/Vis) spectroscopy is another spectroscopic method that leads to the recognition of the composition of chromophore molecules in different structural forms. This technique was extensively used for identifying and quantifying the trans and cis azobenzene isomers. The electrons of molecules at different energy levels cause dissimilar absorption of UV and Vis radiation giving rise to different absorption spectra.

The Beer-Lambert law is useful for the preparation of sample solutions at suitable concentrations. It represents a linear relationship between the absorbance A and concentration c (mol cm^{-3}) of absorbing molecules, as can be seen in Equation 3-3

$$A = \varepsilon b c$$

Equation 3-3

where b is the path length of the sample (m) and ε is the molar extinction coefficient ($M^{-1}m^{-1}$) that expresses the capability of molecules to absorb energy from light at a

specific frequency. Equation 3-4 defines the transmittance T and its correlation with the absorbance,

$$T = \frac{I}{I_o} = 10^{-\varepsilon bc} = 10^{-A}$$

Equation 3-4

where I is the light intensity (A) after it passes through the sample and I_0 is the incident light intensity (A).

The UV/Vis spectra were recorded over 260–600 nm wavelength range using a UV/Visible spectrometer (Zeiss, MCS 522 UV–Vis) equipped with a xenon flash lamp (Zeiss, BLX 500/4). The sample holder was modified to allow complete (total) irradiation of the solid films and liquid samples. The characteristic set-up of a sample chamber for liquid and solid films is illustrated in Figure 3.1.10 and Figure 3.1.11 respectively. The light beam that provided the UV irradiation was positioned at a distance of 12 mm in order to obtain the maximum irradiation area of the materials under investigation.

The azobenzene-based monomers or polymers (15 mg) were dissolved in 25 ml DMSO and used as stock solutions. Each sample solution was diluted further in order to achieve smooth absorbance spectra. The required concentration of the solutions used for carrying out the UV/Vis spectroscopy measurements was 10^{-3} M in DMSO. All the spectra of the solutions were recorded in a quartz cuvette with all sides clear (Photonic Solutions Ltd). To record the UV/Vis spectra of the solid films, their thickness was chosen to be between 7 and 11 μm in order to achieve complete transmission as the azobenzene has a high molar extinction co-efficient ε_{trans} is between 1200 and 2200 and ε_{cis} between 60 and 230 (as seen in Table 3.1.2).[17]
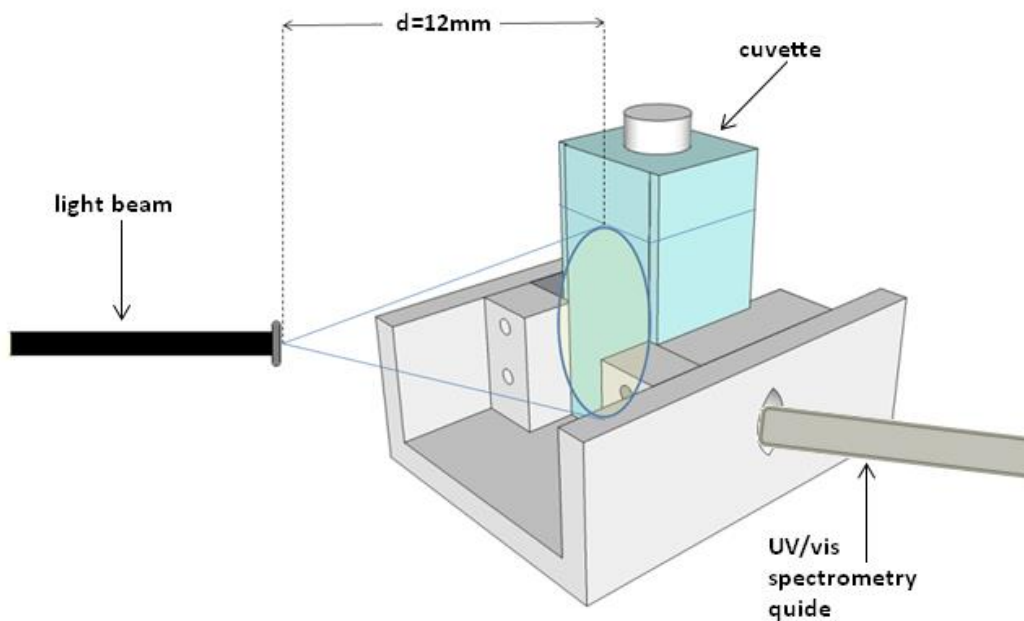
Figure 3.1.10 Setup for irradiating samples in solution
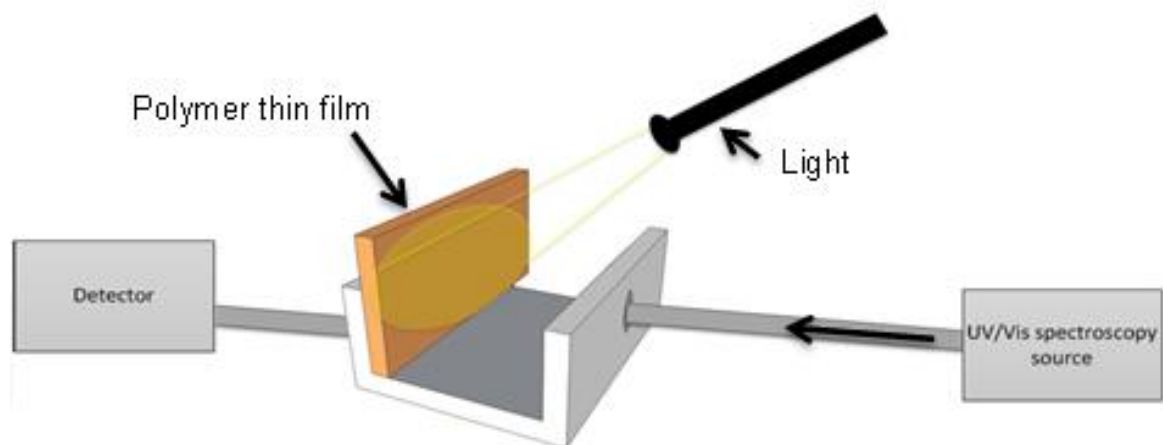
Figure 3.1.11 Typical setup for irradiating polymer thin films

Table 3.1.2 Characteristics, optical absorption values and photo-physical data of azobenzene molecules

Molecules	M_w (g/mol)	C (mol/L)	*trans* (nm)	*trans-*A	$1/C_d$	ε_{trans}	*cis* (nm)	*cis*-A	ε_{cis}
HAB	198.22	0.001261	356	2.037	793	1615.13	436	0.171	135.97
4,4´-DHAB	214.22	0.001167	361	2.124	857	1820.38	447	0.268	229.82
MOAB	266.29	0.000939	324	1.126	1065	1199.90	434	0.053	56.87
4,4´-DMOAB	350.37	0.000714	330	1.560	1401	2186.26	436	0.094	131.38
GOAB	254.28	0.000983	346	0.860	1017	874.49	436	0.214	217.54
4,4´-DGOAB	326.35	0.000766	359	1.727	1305	2254.40	442	0.170	221.96

3.1.2.5 Differential scanning calorimetry

Differential scanning calorimeter (DSC) is a well-known technique for the analysis of thermal properties of materials. DSC measures the heat capacity C_p for transition phases during the changes in enthalpy, and can determine the glass transition temperature of polymers (T_g) and the melting point (T_m) of materials.[132] The T_m of a material is a fundamental point of reference because it directly relates to the bond strength and structure. The higher the T_m, the stronger is the bond.

The DSC analysis was conducted using a DSC METTLER TOLEDO with STAR[e] Software, Version 9.10 under nitrogen atmosphere with a flow rate of 80 ml/min. The calibration of the instrument was accomplished using Indium (In) with a T_m of 156.6°C. The weight of the polymer samples in DSC pans was between 6–9 mg.

Three heating-cooling cycles were used to determine the T_g at a heating rate of 10°C/min, from 25 to 200°C. The T_g of the samples was indicated from the midpoint of the heat flow increase. Alternatively, the identification of T_m required only two heating-cooling cycles within 25-160°C temperature range at a heating rate of 2°C/min for the materials studied in this project.

3.1.2.6 Use of DSC/FTIR for cure monitoring

The reaction kinetic of the monofuctional azobenzene resins (4-GOAB) with a common hardener diethylenetriamine (DETA) was calculated after monitoring the rate of curing of the epoxy-based materials using a DSC and a FTIR simultaneously. The IR spectra were collected during heating of the materials by means of a non-contact optical fibre probe linking a Perkin Elmer DSC to a NIR Nicolet Nexus FTIR. A conventional aluminium pan containing the sample was placed in the sample holder of the DSC. The head of the sample chamber was modified to accommodate the optical fibre probe. The aluminium pan cover on the DSC holder was replaced by a borosilicate cover to allow transmission of the NIR wavelength onto the materials surface. The spectral information of the curing reaction was monitored using the reflectance mode. The non-contact probe was placed above the glass cover at a distance of 1 mm from the sample surface. The background NIR spectrum was obtained using an empty aluminum DSC pan in aerobic atmosphere. The NIR spectra were collected with a resolution of 4 cm^{-1}. The temperature of the DSC was set to 30°C for a minute and then dynamic scans were performed between 30 to 180°C with a heating rate of 5°C/min. The molar ratios of 3:1 and 5:1 (4-GOAB/DETA) were chosen for the DSC/FTIR cure-monitoring experiments. The reaction mixture was prepared by adding 1.71 μl of DETA to a 20 mg of 4-GOAB or 2.85 μl of DETA to a 20 mg of 4-GOAB in a DSC pan at room temperature.

3.1.2.7 Irradiation of materials

The isomerisation of the azobenzene in solid films and solutions was triggered by irradiating the samples using a Novacure M2100 light source (EXFO, Photonic Solutions Ltd). The solutions or films were irradiated at room temperature with a 5 mm diameter light guide, made of fused silica. The output light was extracted using a filter of a wavelength range of 320-390 nm for UV and 400–500 nm for visible light. The intensity of light was 1000-2800 mW/cm^2 for UV and 2800 mW/cm^2 for visible irradiation.
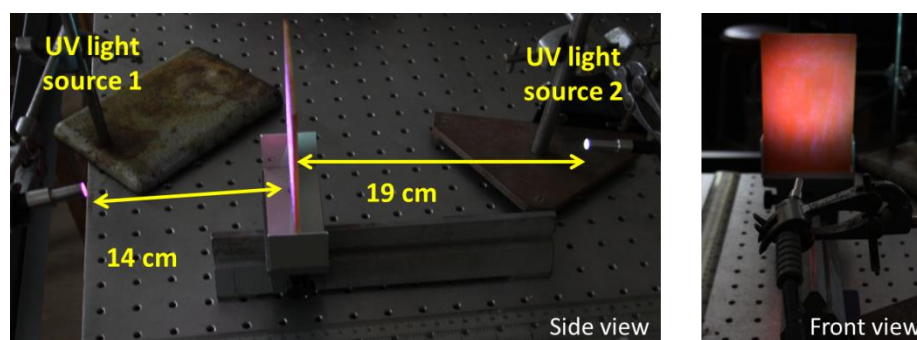
Figure 3.1.12 Experimental set-up of the composites during UV irradiation

The composite specimens were irradiated by two M2100 Novacure light sources in order to expose the specimen to light from the front and rear sides. The wavelength ranges of 320–390 nm for UV and 400–500 nm for visible light were selected for this experiment. Figure 3.1.12 shows the experimental set-up during UV and visible irradiation of all the composite samples. The selected intensities and distances between the specimens and light guides are listed in Table 3.1.3. These values were chosen to ensure maximum exposure of the samples under investigation.

Table 3.1.3 Characteristics of the light sources

	Light source 1		Light source 2	
	UV	Visible	UV	Visible
Intensity (mW/cm^2)	1000	2800	1000	2800
Wavelength range (nm)	320-390	400-500	320-390	400-500
Light beam diameter (mm)	10		5	
Distance between light source and sample (cm)	14		19	

EXPERIMENTAL METHODS

All the specimens were irradiated with visible light for 30 min prior to testing in order to ensure that all the azobenzene chromophores are in the *trans* form. It was expected that irradiation increased the specimen temperature, as discussed in details in section 4.2.1, therefore the irradiated specimens were allowed to cool to room temperature for minimum1 hr before being subjected to further experiment.

3.1.2.8 Rotational rheometry

Rotational rheometry is a technique for the measurement of complex shear rheology. It is sensitive enough to measure the viscosity of dilute polymer solutions, and yet robust enough to measure the viscoelasticity of high modulus polymers or composites. Therefore, this technique was used to investigate if there were any photoinduced changes in viscosity of azobenzene polymers due to the isomerisation. Rotational rheometry is ideal for discerning structural and compositional changes in materials.

The photoviscosity measurements were conducted using a Bohlin C-VOR 150-HR rheometer with a customised sample chamber. The sample chamber, that contained a quartz plate surrounded by a water jacket, had an opening at the bottom, as shown in Figure 3.1.13, to permit irradiation by a light guide. All the viscosity measurements were performed using a 40 mm diameter 1° cone-plate that was positioned 3.8 cm away from the light guide. It should be mentioned that the measurements were collected at a controlled temperature of 25°C. A KTB30 water bath (Julabo, Seelbac) was used to control the temperature of the solution in the cell during irradiation. The shear stress applied to the investigated samples was 0.5-1 Pa.

The required sample volume for each test was 340 μl and the concentrations of the acrylic azobenzene-based polymer solutions were between 15 and 40 mg/ml. Non-volatile solvents such as DMSO and γ-butyrolactone were used in order to avoid solvent evaporation during the viscosity measurements. Additionally, providing solvent in the solvent trap discouraged solvent evaporation. Viscosity data were collected for 5 min in the dark to establish a stable state, 10-20 min under UV

irradiation and a further 10-20 min in order to observe any short-term recovery of the viscosity due to the possible photoinduced heating effect.
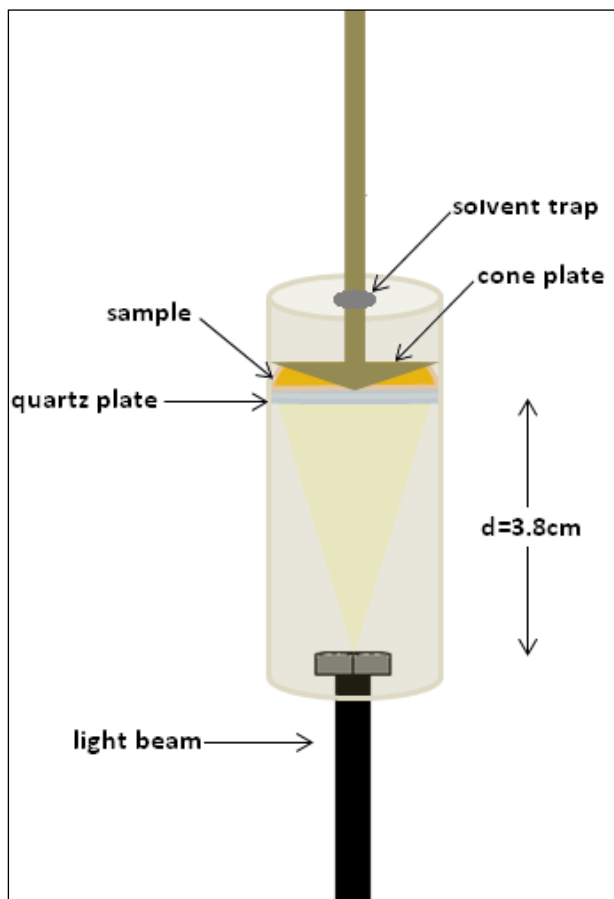
Figure 3.1.13 Setup for rheometer cell

3.1.2.9 Nanoindentation

Nanoindentation experiments were of great importance, as they provided initial information regarding the mechanical properties of the polymers and involved small scale sample testing. Moreover, this technique was found to be very useful for UV-triggered healing investigations on the azobenzene-based polymer films and cured resins, where images of the indented polymeric films were captured before and after UV irradiation. This technique required smaller quantity of solid sample compared to other mechanical testing methods.

EXPERIMENTAL METHODS

Nanoindentation tests measure the hardness of a solid by indenting a very small area of the surface (~64 μm^2) with a nano-Newton (10^{-9} N) force and measuring the depth of the indent.[133] It has a much higher sensitivity and resolution in comparison to the microindentation. With this method, the Vickers hardness (*HV*) of the solid can be calculated from the following Equation 3-5:

$$HV = \frac{2F \sin(\frac{136°}{2})}{d^2} = 1.8544 \frac{F}{d^2}$$

Equation 3-5

where d is the diagonal of the diamond indenter (m), h is the indentation depth (m) under the test force F(N). The actual indentation depth was calculated using the Equation 3-6.

$$\frac{d}{h} = 2\sqrt{2} \tan\left(\frac{136°}{2}\right) = 7$$

Equation 3-6

Taking into account the geometry of the diamond the simplified Vickers hardness formula is shown in Equation 3-7.

$$HV = \frac{F}{26.4236 \, h^2}$$

Equation 3-7

For the determination of the elastic modulus E, Equation 3-8 was employed:

$$E = \frac{1 - v_s^2}{\frac{1}{E_r} - \frac{1 - v_i^2}{E_i}}$$

Equation 3-8

where E_i is the elastic modulus of the indenter equal to 1141 GPa, E_r is the reduced modulus (GPa) of the indentation contact, v_i is the Poisson's ratio of the indenter equal to 0.07 (diamond) and v_s is the Poisson's ratio of the test specimen equal to 0.35 for acrylic/ epoxy polymers.[133]

A schematic representation of polymer films under indentation is illustrated in Figure 3.1.14, where the indenter penetrates the polymeric film onto a glass substrate. Nanoindentation tests on pre- and post-irradiated polymer films were carried out by using a nano-hardness tester from CSM Instruments SA. The system was fitted with a Berkovich diamond indenter with triangle pyramid geometry. The samples were automatically transferred by an electromagnetic spiral from the nanoindenter to an equipped microscope for optical analysis. Force vs. depth curves before and after exposure to UV light were collected and analysed in the indentation software. A maximum load of 2 mN, a relaxation period of 30 s, and loading and unloading rates of 4 mN/min were used in the measurements.
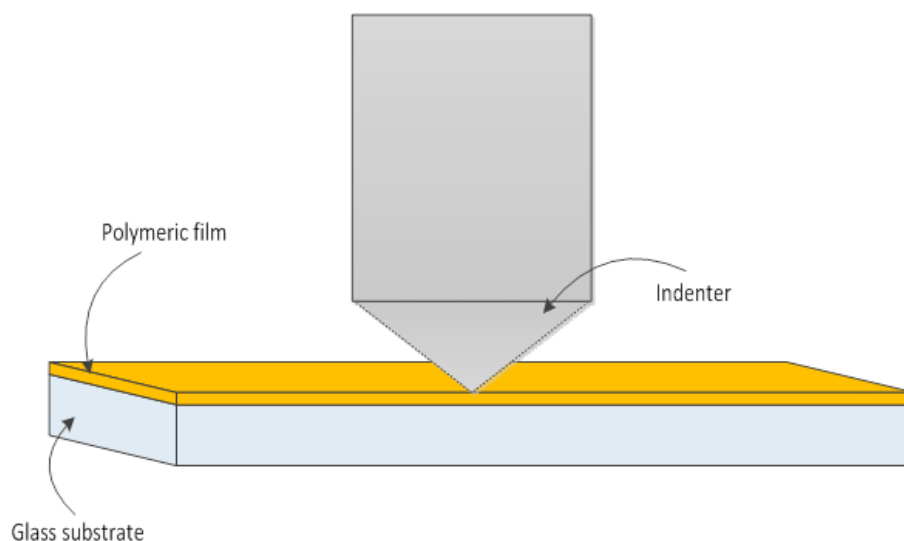
Figure 3.1.14 Schematic representation of indentation

EXPERIMENTAL METHODS

Thin films of the acrylic copolymers with 0%,10%, 15%, 20%, 30%, 45%, 65%, 80% and 100% azobenzene were prepared by casting polymer solutions of toluene (200 mg/ml) onto microscope glass slides at room temperature.[126, 127] The samples were left on a leveled glass table inside a fumehood for three days in order to allow the solvent to evaporate. The films were then placed into a vacuum oven for five more days until the films reached constant weights as confirmed by periodically weighing them. For nanoindentation, the thicknesses of the films ranged between 80–150 mm.

3.1.2.10 Atomic force microscopy

Atomic force microscopy (AFM) is a microscopy technique for studying the morphology of samples at the nanoscale.The AFM provides quantitative information measuring the samples' surfaces using a cantilever with a very sharp tip to scan over. This technique was useful for the UV-triggered healing investigations of the azobenzene-based cured resins as a consequence of the nanoindentation studies.

The morphology of the artificially damaged specimens with a diamond scriber and a pin and the depths of the indents that were created on the films' surfaces pre- and post- UV were investigated by AFM Digital Instruments Dimension™ 3000 scanning probe microscope with a NanoScope IIIa controller (Veeco instruments, Santa Barbara, California, USA) and a NanoScope IIIa software (version 4.42r4). Tapping mode was employed across the surface of the samples at a frequency of 1 Hz. Profiles were taken along a line from the indent's deepest point through the matrix to ensure the same section was being examined. Healing ratio (HR) percentages have been also calculated using the Equation 3-9:

$$HR = \frac{(d_I - d_{UV})}{d_I} \; x \; 100\%$$

Equation 3-9

where d_I is the initial depth (nm) before irradiation and d_{UV} the depth (nm) after 1 hour exposure to UV light.

EXPERIMENTAL METHODS

For these experiments 10% w/w 4,4′-DGOAB were mixed with a bi-resin system Biresin® LS Resin and F4 Hardener (100 parts epoxy/18 parts hardener), provided by Sika®, and cured at 80°C for 2 hrs. Samples as reference were prepared under the same conditions without the addition of the 4,4′-DGOAB. The liquid mixtures after curing were converted into 10 cm x 3.5 cm solid films with thickness range of 3-5 mm.

3.1.2.11 Gas pycnometry

Gas pycnometry is a technique that allows determining the actual density of a sample without taking into account the volume occupied by internal or open porosity. The principle of this method is based on putting a sample of known mass into a cell of known volume. The helium pycnometer determines the density and volume of solid samples by measuring the pressure change in helium in the calibrated volume, according to the following equations, Equation 3-10, Equation 3-11 and Equation 3-12:[134]

$$P_{atm}V_{expansion} = n_{expansion}RT_{atm}$$

Equation 3-10

$$P_i \left(V_{cell} - V_{sample} \right) = n_c RT_{atm}$$

Equation 3-11

$$P_{ii} \left(V_{cell} - V_{sample} + V_{expansion} \right) = n_c RT_{atm} + n_{expansion}RT_{atm}$$

Equation 3-12

where P_{atm} is the ambient pressure (Pa), $V_{expansion}$ the expansion volume (m^3), $n_{expansion}$ the number of moles of gas in the expansion volume, R is the molar gas constant (8.3144 Jmol^{-1}K^{-1}), T_{atm} the ambient temperature (°C), P_i is the initial pressure (Pa) (closed valve) and P_{ii} is the elevated pressure (Pa) (opened valve).

EXPERIMENTAL METHODS

A Micromeritics AccuPyc 1330 gas pycnometer, with helium gas, was used for recording the density values of the azobenzene-based polymeric films before and after UV irradiation and sonication. These tests were conducted to identify if there were any volume changes after the azobenzene had undergone isomerisation. Four samples with different azobenzene loading were tested and for each specimen the average value of density was calculated after five scans. The 300-400 mg films were cut into small pieces in order to fit into the experimental cell. The temperature was continuously recorded and remained constant at 23°C for all the samples during the measurements.

3.1.2.12 Sonication

Since ultrasound waves were found to be another stimulus that triggers the *cis→trans* isomerisation of azobenzene molecules in solution, it was decided to investigate the effect of ultrasound on the *cis→trans* isomerisation in solid polymer films. For this sonication experiment, the PMMA, P(MMA/MOAB) and PMOAB films, prepared as described in section 3.1.2.4, were placed into clear plastic resealable grip seal bags (Fisher Scientific), to ensure that the films did not peel off the glass slides in contact with water in the Grant ultrasonic bath (400 W). The bath was operated at a frequency range of 50-60 Hz; the temperature of the water was recorded using a thermocouple.

3.1.2.13 HPLC analysis of ultrasound-treated samples

High Performance Liquid Chromatography (HPLC) (Waters 2695) was used to analyse the compositions of *cis* and *trans* isomers of 4,4′-DGOAB following sonication. Acetonitrile (ACN) was used as the eluent. The detector wavelength was set to 412 nm, where the isosbestic point of the *trans* and *cis* 4,4′-DGOAB is located.

In order to determine the *trans*/*cis* ratio of 4,4′-DGOAB in ACN solution (1.5 mg/ml), three vials containing ~2 ml solution each from the same stock solution (500 ml), were prepared. The first measurement was accomplished without any further treatment of the solution, the second after 1 min of exposure to UV light and the third

after 1 min exposure to UV light, and then 120 min of sonication in an ultrasound bath. *Cis* and *trans* isomers were calculated by integrating the peaks in the chromatogram.

3.1.2.14 Fracture toughness of epoxy resins

Single edge notched beam (SEBN) tests were performed to characterise the influence of azobenzene and UV light on the fracture toughness of the cured azobenzene-loaded resin. The measurements of the cured epoxy resin (bi-resin system) with 0%, 5% and 10% 4,4´-DGOAB were carried out using a Dartec Series HC25 testing machine (Zwick Ltd). The samples were tested in a 3-point bending mode with a span of 24 mm. The cross-head speed was 3 mm/min, and the force was measured using a load cell of 500 N (RDP Electronics Ltd). The data acquisition was performed at a capture rate of 1000 points per minute. A typical set-up is shown in Figure 3.1.15.
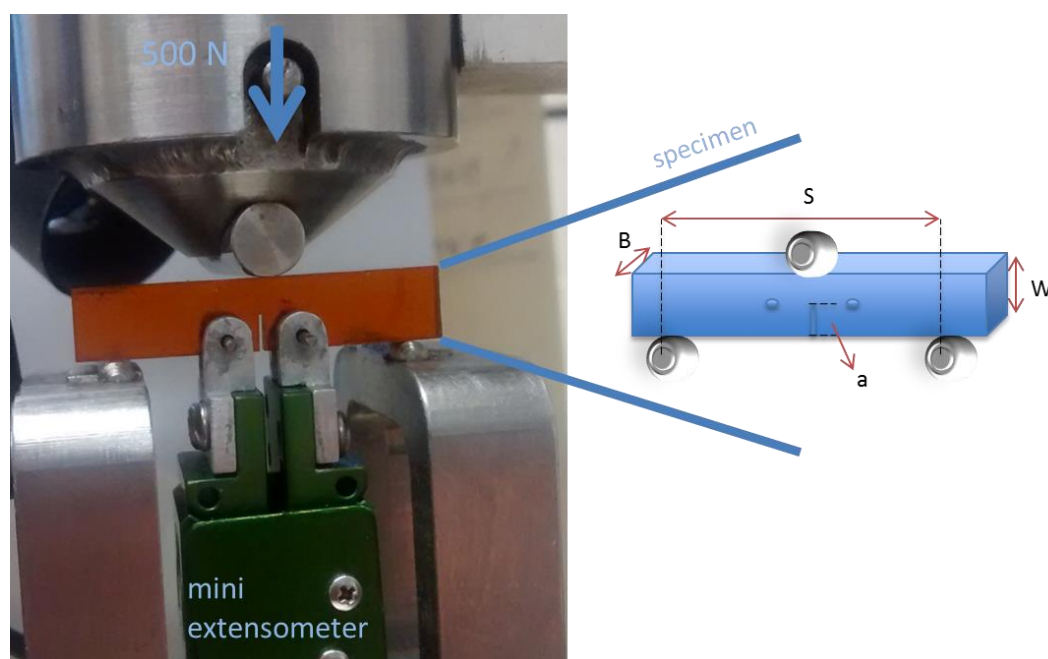
Figure 3.1.15 Representation of 3-point bending test for fracture mechanics tests, with the specimen dimensions

The specimens were prepared following the ASTM E 1820 procedure.[135] Initially, all the specimens were irradiated with visible light (400-500 nm) for 30 min and stored

in the dark for a week prior to testing. The specimens that were exposed to UV irradiation for 30 min were allowed to cool down to room temperature for 1 hr in the dark before testing in order to eliminate the heating effect of irradiation, as discussed in details in section 4.2.1.

The SEBN specimens had the dimensions of 27 mm x 6 mm x 3 mm and a 3 mm long notch was cut in the middle of the specimen's length using a metallurgical saw (Struers® Accutom-2) in order to start the crack propagation. A sharp cut, using a blade, was additionally created in order to narrow the crack at the end tip of the notch. Two extensometer attachment holes were pierced using a 1 mm diameter drill bit in order to allow a miniature extensometer (Model 3442-006M-050ST, Epsilon Technology Corp.) to be fitted. The extensometer recorded the horizontal displacement that occurred during the crack growth. The 9610 Dartec control unit was used for collecting the load, time and crosshead displacement. The fracture toughness (K_{IC}) was calculated from Equation 3-13 for the specific SEBN geometry using the function of Equation 3-14:

$$K_{IC} = \frac{F_c S f(\frac{a}{W})}{BW^{3/2}}$$

Equation 3-13

$$f\left(\frac{a}{W}\right) = \frac{\left[(2 + \frac{a}{W}) \cdot (0.886 + 4.64\left(\frac{a}{W}\right) - 13.32\left(\frac{a}{W}\right)^2 + 14.72\left(\frac{a}{W}\right)^3 - 5.6\left(\frac{a}{W}\right)^4)\right]}{\left(1 - \frac{a}{W}\right)^{\frac{3}{2}}}$$

Equation 3-14

where F_c is the critical force (N), S is the span (m), a is the crack length (m), W is the thickness (m) and B is the width (m) of the specimen.

Videos were also captured using a high-speed camera (V.12 Phantom), with an acquisition rate of 1000 pictures per second and a resolution of 256 x 256 to identify the crack growth in each sample.

3.2 Photoresponsive composites
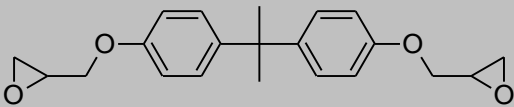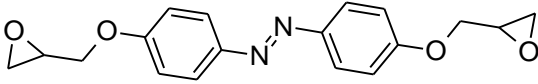
Common manufacturing techniques were used for the preparation of the photoresponsive composite panels. Combined methods of hand lay-up, vacuum bag and autoclave curing were applied. After the composites had been manufactured, the individual panels were cut into appropriate sizes for impact and compression after impact tests.

3.2.1 Materials for composites

The photoresponsive composites were made from glass fibres (unidirectional glass fibre cloth, East Coast Fibreglass Supplies) reinforcing the epoxy resin (Biresin® LS Resin and Biresin® F4 Hardener supplied by Sika®). The fibres were supplied as unidirectional fabric. Prior to processing, 5% and 10% of 4,4´-diglycidyloxyazobenzene (4,4´-DGOAB) were added as the crosslinker. Their structures are depicted in Table 3.2.1. Higher amount of 4,4´-DGOAB could not be added because this would increase the cross-link density of the polymeric matrix leading to a decrease in the resistance to crack initiation and in the plastic deformation capability due to constrained free volume.[136] Reference panels containing no azobenzene in the resin were also prepared using the same experimental techniques as stated above.

Table 3.2.1 Epoxy resins and hardener structures

Product	Chemical name (Abbreviation)	Molecular structure
Biresin LS resin	Diglicydyl ether of bisphenol A (DGEBA)	
Azobenzene resin	4,4´-Diglycidyloxyazobenzene (4,4´-DGOAB)	
Biresin F4 hardener	2,4,4-Trimethylhexane-1,6-diamine	

The bi-resin system was selected based on the following criteria:

- the epoxy part should be mainly Bisphenol A and a liquid

- the pot life should be higher than 1 hr

- the curing or post-curing temperature should be above 25°C

- the curing time should be not more than 8 hrs

- the colour after curing should not be dark (pale yellow or light orange are acceptable).

3.2.2 Composite manufacturing

In order to investigate the role of azobenzene concentration on the composite impact properties, six panels were manufactured with three different azobenzene loadings of 0%, 5% and 10%.

For each panel, eight glass fibre fabrics were cut using a pair of scissors to the desired dimensions (500 mm x 250 mm x 4-5 mm) and were stacked with the following sequence of [0, 90]$_s$ on a steel plate. The mixture of 4,4´-DGOAB/ epoxy

resin was poured and spread using a wooden spatula between every other fabric layer. On completion, the panels were then vacuum bagged as shown in Figure 3.2.1.
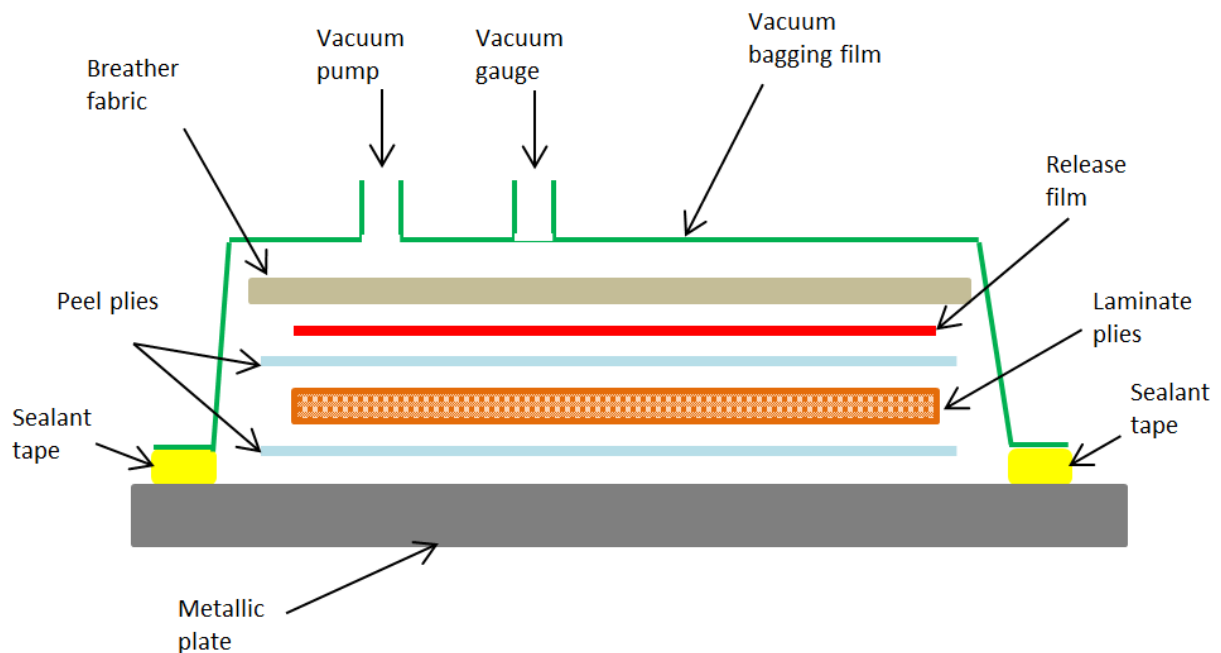
Figure 3.2.1 Illustration of vacuum bagging

The vacuum bagging is a technique used to improve the quality of composites. It is one of the most common procedures for manufacturing various components of aircrafts. A vacuum of about -30 inHg was applied to extract any air trapped during the composites lay-up process. The other benefit of applying vacuum is to remove any volatiles that can be generated during the chemical reaction. The vacuum bagging process was as follows:

- The steel plate (60 cm x 60 cm) was coated with a polytetrafluorethylene (PTFE, Teflon®) film (Tyaflor by Tygavac Advanced Material Ltd) for easy removal of the composite panels after curing.

EXPERIMENTAL METHODS

- Fabrics were placed between two peel plies (made of nylon, Aerovac Cytec plc) on the top of the steel plate. The peel plies that were in contact with the laminate were required to easily peel off the composite panels after solidification.

- On the top of the peel ply, a perforated release film (made of polyolefin, Aerovac Cytec plc) was placed. It was a thin plastic sheet that is perforated to help remove trapped air, solvent, volatiles or excess resin out of the panel.

- Then a breather (Aerovac Cytec plc) was placed on top of the release film. The breather, made of non-woven polyester fabric, was responsible for absorbing any excess of resin and allowing solvent and air to be removed from within the vacuum bag.

- Finally, a bagging film (made of nylon, Tygavac Advanced Material Ltd) was sealed on the steel plate with a tape. The film allowed the vacuum to be applied to the panel during the curing process. Two quick release coupling (plug and socket) valves that were connected to the vacuum pump and the pressure gauge were fitted through the bagging film.

On completion of the vacuum bagging, the composites were cured in a dry autoclave (Aeroform Ltd). This is a large vessel that offers controlled temperature, vacuum and pressure profiles simultaneously, and is used for curing polymeric reinforced composites. The photoresponsive and reference composites were processed in an air atmosphere according to the manufacturer's recommended cure cycle of 2 hrs at 80°C, with a heating rate of 1.67°C/min, under a pressure of 50 psi and vacuum. A typical curing profile is shown in Figure 3.2.2.

After curing, the panels were left in the autoclave to cool down to room temperature overnight. The bagging materials were then removed and the panels were stored in the dark until characterisation.
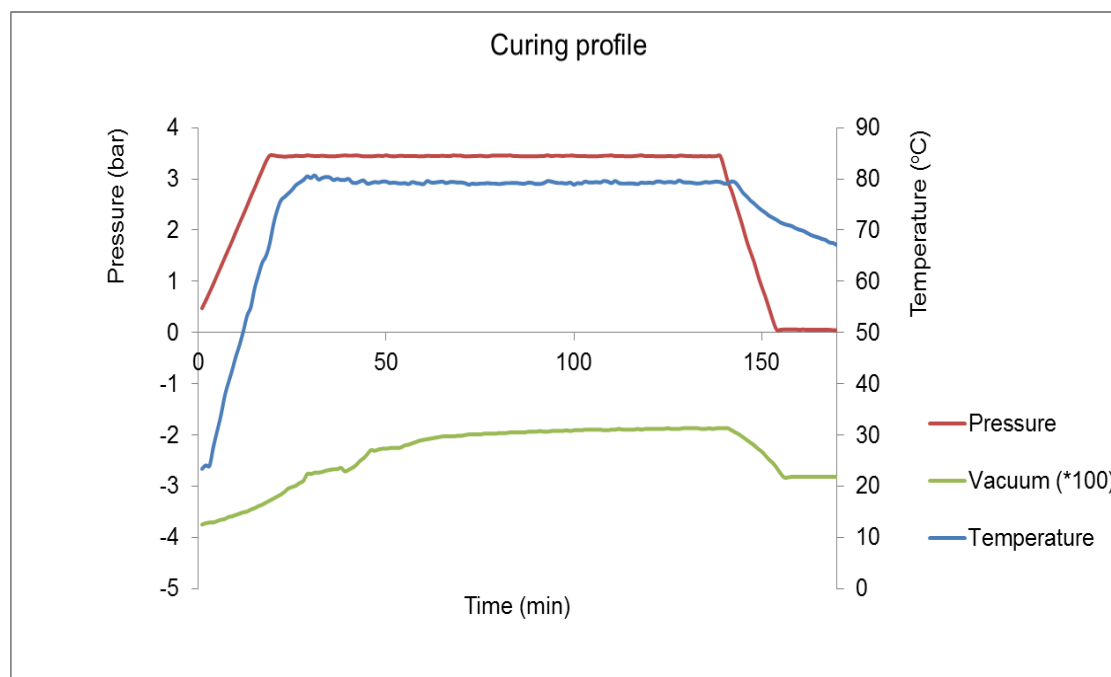
Figure 3.2.2 Typical curing profile of composite panels

3.2.3 Composite characterisation

The influence of azobenzene in the glass/epoxy composites was investigated by carrying out compression, impact and compression after impact (CAI) tests before and after photoisomerisation. The dimensions of all the samples were selected to 150 mm x 100 mm x 3 mm for each test.

3.2.3.1 Microscopy analysis to evaluate void and fibre volume fractions

Microscopic analysis was done to determine the fibre orientation, ply thickness and the fibre and void volume fractions. This was achieved using a Keyence VHX-1000 digital microscope. Off-cuts of the photoresponsive composites were cold mounted in an epoxy resin (EpoFix resin/hardener system, Struers) (of 40 mm diameter) and then polished using a polishing machine (Rotopol-21, Struers). The specimens were ground with 220 grit (for 1 min), 1000 grit (for 1 min) and 2400 grit (for 3 min) SiC abrasive papers (Struers) using water as lubricant, and then polished using 3-μm

and 1-μm diamond suspensions (DP-Suspensions, Struers) for 6 min and 1 min, respectively, to obtain a near to scratch-free surface.

The fibre orientation, the ply thickness and the fibre and void fractions were determined by processing the images using the open-source software ImageJ (developed by Wayne Rasband). Firstly, after capturing a mosaic image from the digital microscope, various areas of the layers of about 2 mm x 0.5 mm dimensions were selected. A selected area under investigation can be seen in Figure 3.2.3.
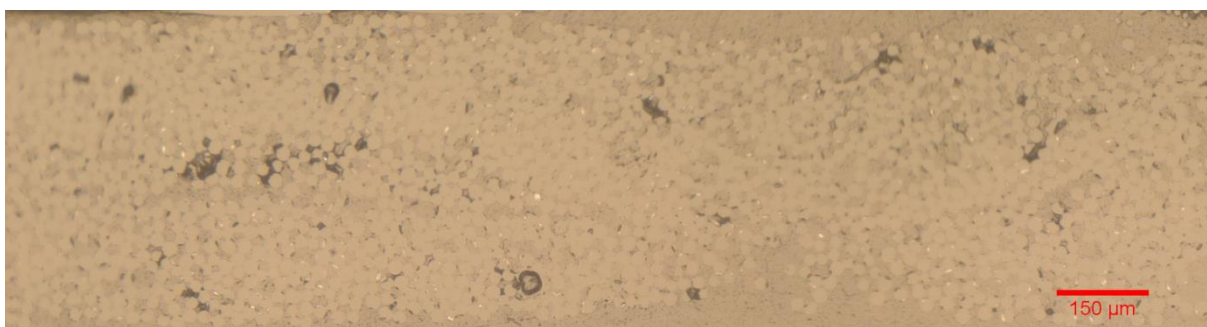
Figure 3.2.3 Initial image of a 90° ply of glass/epoxy composite

The next step was to convert the image to 8-bit. Then an optimum threshold was selected to adjust the contrast of the grey scale image (Figure 3.2.4). The grey, green and blue areas corresponded to resin, fibres and voids respectively. By the percentages obtained in the threshold, the fibre volume fractions were determined.
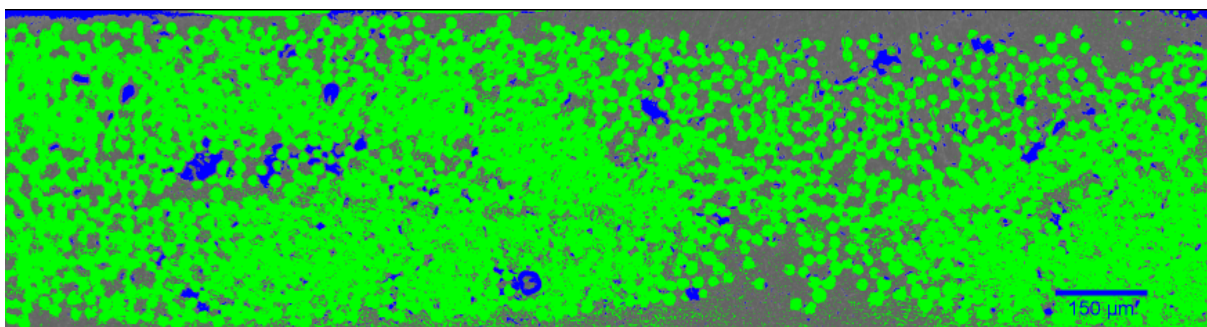
Figure 3.2.4 Green-blue contrasted image of a 90° ply of glass/epoxy composite

EXPERIMENTAL METHODS

The void volume fraction of the photoresponsive composites was measured using the previously described method. Figure 3.2.5 shows a mosaic image of a cross-section of a sample where the different fibres alignment and voids are visible. The 2-D stitching for obtaining a mosaic image was necessary to capture such large objects (voids) since they would not be entirely observed using a scan procedure. Once the selected area was converted to green-blue contrasted image, the voids were apparent (blue colour) and their distribution was measured by the threshold.

9.5mm x 1.7mm cross-section area of
AB_1% composite sample

below: 14.72 %, above: 55.28 %
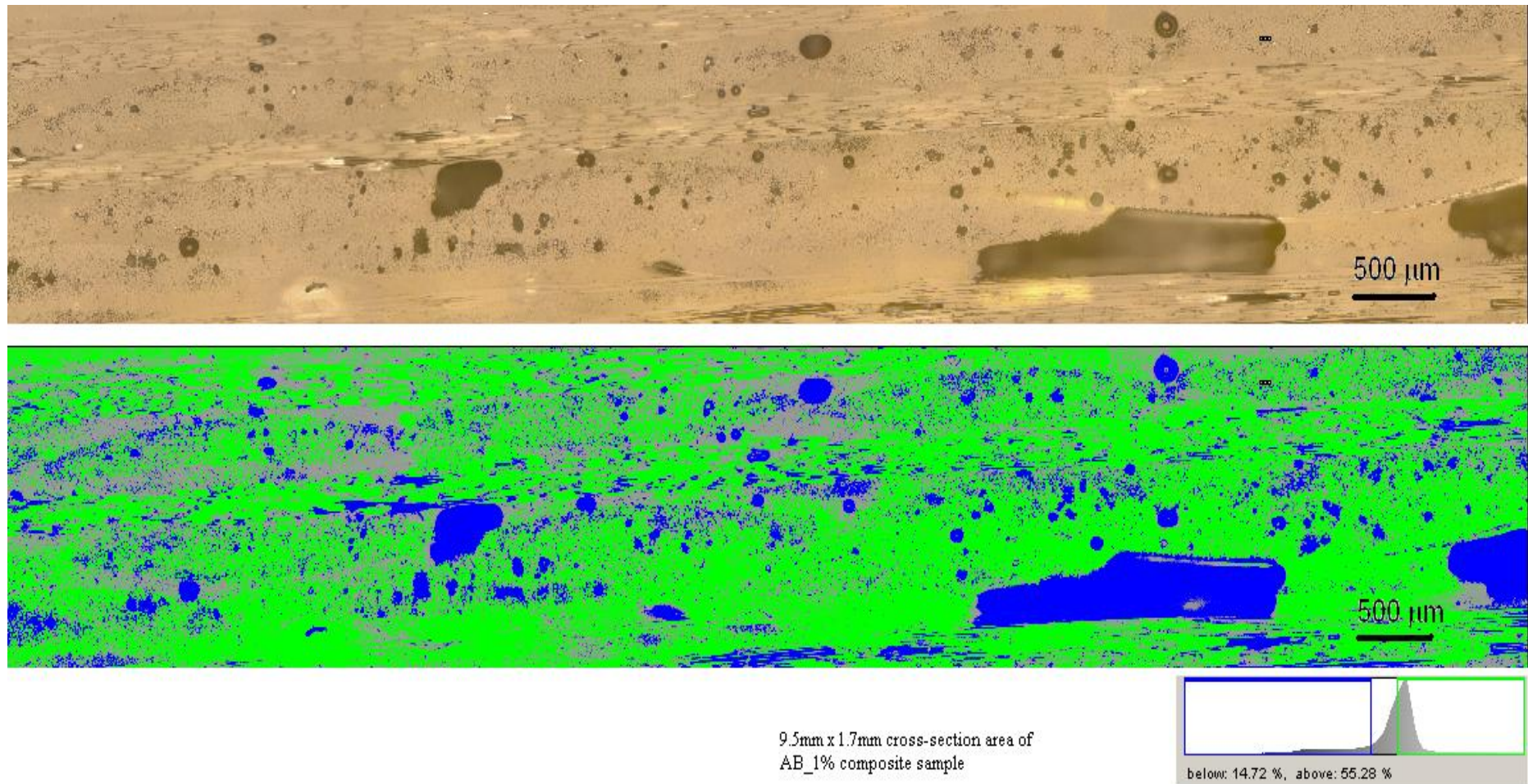
Figure 3.2.5 Initial image and green-blue contrasted image of a cross-section of glass/epoxy composite with its threshold

3.2.3.2 Reflectance CM-700D spectrophotometry

As mentioned in the subsection 3.1.2.9 thin azobenzene polymeric films were required to be able to record the UV/Vis spectra. Because of the high absorption coefficient of the azobenzene chromophores (>21,100),[137] UV/Vis absorption spectroscopy was not a suitable technique to determine the different transition states after isomerisation in thick composite panels. Consequently, reflectance spectrophotometry was used.

This was carried out using a CM-700D spectrophotometer (Konica Minolta) which is a precise, easy to use, portable and lightweight spectrophotometer designed to measure the spectra of solid films using reflection mode.[138] This instrument uses light from a xenon lamp (10 W) to illuminate the specimen uniformly and then the reflected light from the specimen is received by the detector. The intensity of the signals was collected every 10 nm within the wavelength range of 400-700 nm. It was found to be the most suitable method for calculating the *trans* and *cis* isomers ratios of the azobenzene chromophore in the composites. The different excitation states that occurred before and after isomerisation were accompanied with a slight colour change that was monitored by this technique.

3.2.3.3 Thermal imaging

When an object is heated, it radiates electromagnetic energy. The amount of energy is then related to the object's temperature. This energy can be detected by a thermal camera that converts it in to an electronic signal which is then processed to produce a thermal image.[139] A thermal image is an image of the object with different colours, each representing a range of temperature present within the object. The advantage of this technique is that the temperature of the object can be accurately quantified without physical contact by measuring the emitted energy. Bates *et al.* demonstrated that a thermal camera for quantitative in-service and manufacturing process inspection of commercial aircraft

components is another non-destructive testing and is 30 times faster than the ultrasonic c-scanning technique.[140]

Thermal camera mainly senses the wavelengths in the mid (3000-5000 nm) and long (5000-14000 nm) wave infrared (MWIR/LWIR) to deduce the temperature of the emissive body. Emissivity is the material's ability to emit thermal radiation and it varies significantly from material to material with values ranging between 0 and 1.[141] An ideal object which absorbs and emits the maximum amount of thermal radiation has an emissivity equal to 1.

For these studies, a MWIR (SC7600 model, FLIR) thermal imager was used. Its sensitivity of 0.02°C allowed the capture of the finest image details and temperature difference information. The emissivity range was specified to be 0.90-0.92 according to literature for epoxy/glass fibre composites.[142] ALTAIR Version 5© software was used for these experiments, which permitted a very precise comparison of the thermal changes between the samples by setting the desired lower and upper temperature limits to 19.5°C and 26°C respectively for the composites.

3.2.3.4 Compression test

Compression tests can determine the in-plane compressive properties by applying a compressive force on the specimen. It was selected for determining the influence of azobenzene on the mechanical properties of the photoresponsive composites because compressive strength is a matrix-dominant property.[143] These sets of tests are believed to be important for these studies, and sensitive enough to indicate photo-induced changes that may affect the compressive response of composite specimens.

The compression tests were conducted according to the British standard BS ISO 18352, on 3-5 composite specimens with different azobenzene loading or light illumination.[144] All the specimens of 150 x 100 x 3 mm dimensions were tested at ambient temperature. The samples were loaded until failure at a cross-

head speed of 2 mm/min using a universal testing machine Zwick and a 200-kN load cell. The compressive strength of the composites (σ_c) was calculated from the following Equation 3-15:

$$\sigma_C = \frac{F}{b \cdot h}$$

Equation 3-15

where σ_c is the compressive strength (Pa), F is the maximum load (N), b is the width of specimen (m) and h is the thickness of specimen (m).

3.2.3.5 Impact test

High-velocity impact tests were conducted on the photoresponsive composites to study the influences of the incorporated chromophores and the azobenzene isomerisation. The chromophore influence was studied with non-UV irradiated laminates containing 0%, 5% and 10% azobenzene impacted at three different velocities (130, 190 and 340 m/s). On the other hand, the influence of azobenzene isomerisation on the impact behaviour of the epoxy-azobenzene/glass fibre composites was investigated at a single velocity of approximately 190 m/s (125 kJ). The high-velocity impact tests were carried out using an ELVIS (Explosive (or Extremely) Low Velocity Impact System) single stage 22 mm diameter gas gun. The velocities of 130 m/s and 190 m/s were obtained with air at a pressure of 5 bar and 10 bar, respectively, whereas the velocity of 375 m/s was reached with helium at 45 bar. The specimens (150 mm x 100 mm x 3 mm) were clamped from the top and bottom in a target–holding rig (Figure 3.2.6), in order to prevent any improper orientation. A stainless steel sphere (12 mm diameter, 7.04 g) sitting in a cup type sabot, as seen in Figure 3.2.7, was the projectile used for all the tests.
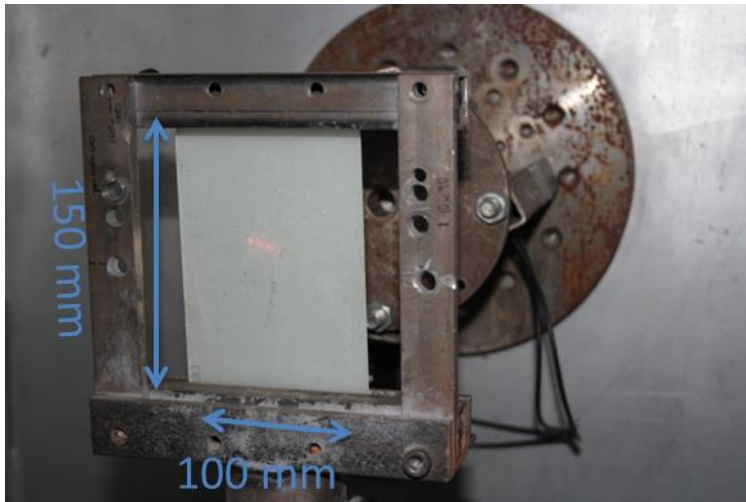
Figure 3.2.6 Target–holding rig
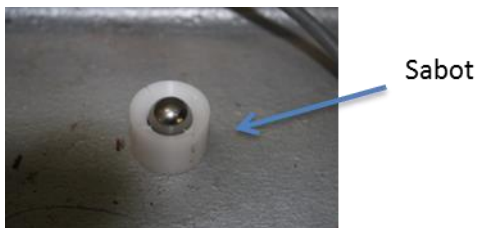
Figure 3.2.7 Stainless steel sphere in its sabot

During the high velocity impact tests the panel behaviour was recorded using a V.12 Phantom high-speed camera (40,000 pictures per second and 608x224 resolution) from which the projectile impact, rebound and exit velocities were extracted. The absorbed energy was calculated from the following Equation 3-16:

$$E_t = \frac{1}{2}m(v_1^2 - v_2^2)$$

Equation 3-16

where m is the mass of the projectile (kg), v_1 and v_2 are the entry and exit velocities (m/s) respectively, and E_t is the absorbed energy (J).

3.2.3.6 Compression after-impact test

Compression after impact (CAI) tests were carried out in order to compare the residual strength of the impacted specimens subjected to UV and visible irradiation. This set of experiments followed exactly the same technique as described in section 3.2.3.4 for the compression test. The only difference here was that the specimens have been previously impacted. In addition to the material's residual strength, CAI tests helped to evaluate whether strengthening and/or healing of the impacted samples occurred after exposure to UV radiation.

These experiments were performed at room temperature using the Zwick universal tester with a 200 kN load capacity. The cross-head speed of the testing machine was set at 2 mm/min until the maximum compressive load was reached. The compression stress, strain, and the maximum stress were measured as a function of the azobenzene loading.

3.2.3.7 Damage and morphology analysis

The high transparency of the epoxy-azobenzene/glass fibre composite panels offered the opportunity to visually observe internal damage such as delamination and large matrix cracks. This was achieved by placing the panels in front of a common light bulb (60 W) and by taking photographs of the illuminated samples using a Canon digital camera. The photographs were then processed through the ImageJ software (open-source developed by Wayne Rasband) for measuring the area of the delamination that was created as a result of the impact.

4 RESULTS AND DISCUSSION

This chapter presents the results and discussion for the azobenzene-based materials before and after they have been subjected to external stimuli such as UV light, heat and ultrasound wave. Synthesis and characterisation of the precursor molecules, monomers and polymers are described. Manufacturing and characterisation of the photoresponsive glass/epoxy fibre composites are discussed.

4.1 Photoresponsive Materials

The polymers that were investigated in this PhD programme were acrylic and epoxy based. The acrylic matrix (thermoplastic) was made from copolymers of MMA and azobenzene functionalised monomers with azobenzene loadings of 0-100 mol%. The physical and mechanical changes of the acrylic polymers were investigated before and after exposure to UV light in solid and liquid states. The epoxy-based materials that were synthesised were made from modified epoxy resins with azobenzene in the main chain. The azobenzene difunctional epoxies, were used as crosslinkers, therefore only up-to 10 w/w% was cured with a common epoxy bi-resin system of bisphenol and a hardener (amine). Their photo-induced properties and healing abilities were also assessed.

4.1.1 Synthesis

Various precursors, monofunctional and difunctional monomers were synthesised in the lab as most of them were not commercially available. Figure 4.1.1 presents the structures of the precursor and monomers with their yields enlisted in Table 4.1.1. Their synthesis, difficulties, scale-up and development processes are discussed below.

RESULTS AND DISCUSSION

Hydroxyazobenzene (HAB)

4,4'-Dihydroxyazobenzene (DHAB)

Methacryloyloxyazobenzene (MOAB)

4,4'-Dimethacryloyloxyazobenzene (DMOAB)

Glycidyloxyazobenzene (GOAB)

4,4'-Diglycidyloxyazobenzene (DGOAB)
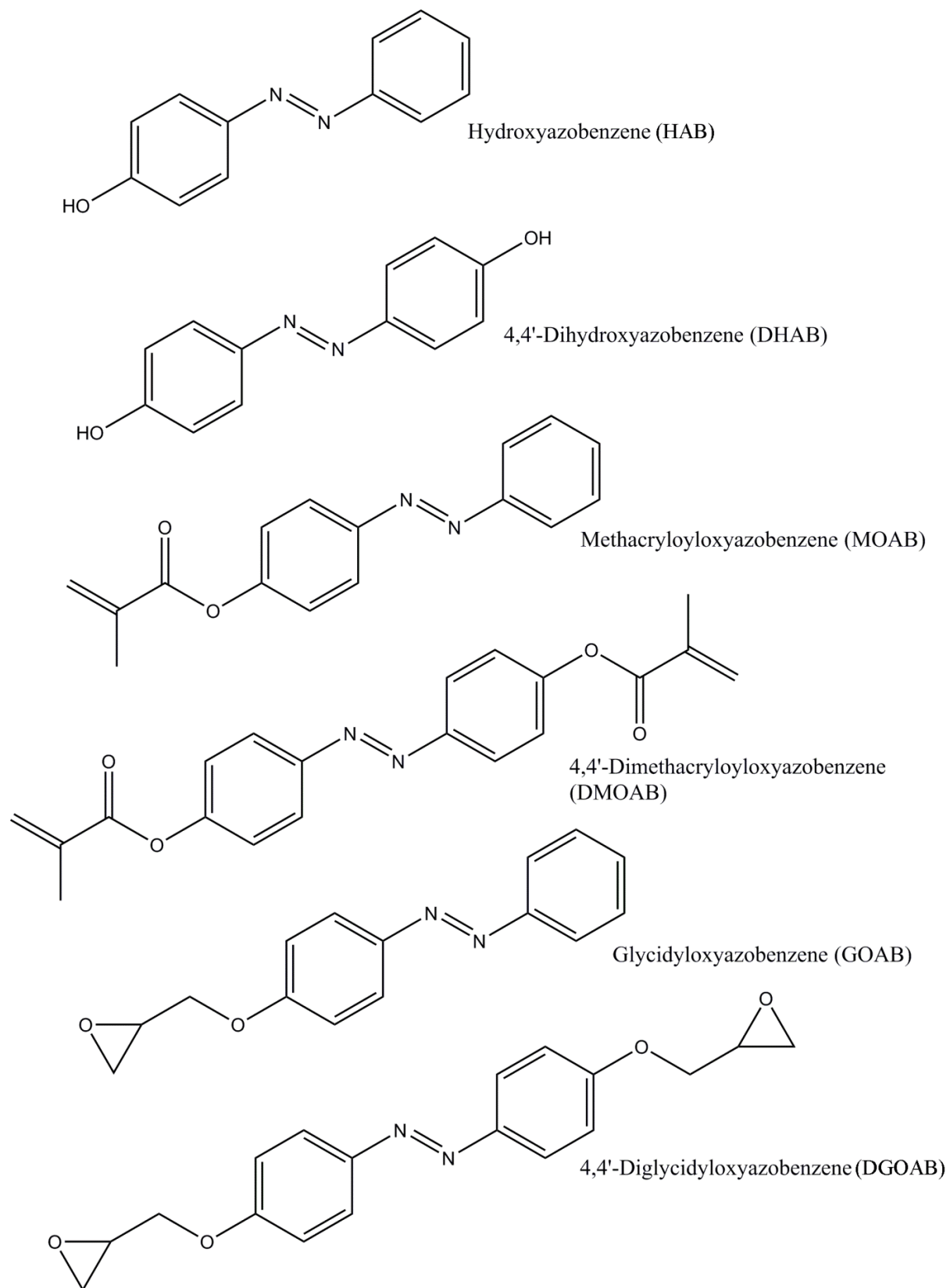
Figure 4.1.1 Structures of mono- and di-functional azobenzene molecules

Table 4.1.1 Synthesised amounts and yields of azobenzene molecules

Molecules	Amount (g)	Yield (%)
4-MOAB	20	78
4-AOAB	10	72
4-GOAB	20	81
4,4´-DHAB	2	24
4,4´-DMOAB	10	81
4,4´-DGOAB	500	75
PMMA	20	90
P(MMA/MOAB)	10/each	71-76
PGOAB	2	88

Azobenzene monomers functionalised with acrylic or methacrylic groups are not commercially available. Therefore, their synthesis as precursor molecules was necessary for obtaining azobenzene-based polymers. The syntheses of approximately 10-20 g of the azobenzene-based monomers 4-methacryloyloxyazobenzene (4-MOAB), 4-acryloyloxyazobenzene (4-AOAB) and 4,4´-dimethacryloxyazobenzene (4,4´-DMOAB) were achieved via the substitution reactions between the commercially available hydroxyazobenzene and the methacryloyl chloride or acryloyl chloride, respectively according to the literature.[23] Extra care was given to the ice-bath for maintaining the temperature of the reaction mixture at 5°C while the methacryloyl chloride was added to the THF solution of the hydroxyazobenzene, as it was an exothermic reaction. Completion of the reaction was achieved within 2 hrs stirring at room temperature (as monitored by TLC) but more time (1 day) was required for purification and solvent removal. Two or three times recrystallisation was required in order to isolate any starting materials from the final product with 71-78% yield. Similar studies in relevant literature state that the reaction was left

stirring at room temperature for 48 hrs and column chromatography was used for the monomers purification, and a lower yield of 70% was achieved.[23]

Polymethacryloyloxyazobenzene (PMOAB) and P(MMA/MOAB) copolymers with 10%,15%, 20%, 30%, 45%, 65% and 85% azobenzene loadings were not commercially available and therefore their synthesis was a mandatory step. The azobenzene-based copolymers (10 g each) were synthesised by a free radical polymerisation of 4-methacryloyloxyazobenzene (4-MOAB) and methylmethacrylate (MMA.) according to the synthetic method described in Figure 3.1.8. The homopolymers and copolymers were produced after 2 days of stirring at 65°C. The removal of impurities (mainly monomers) at the end of the synthesis was an easy step ($CHCl_3/H_2O$ extraction). High yields (>75%) were achieved which was in accordance with relevant literature.[23] On the other hand, a longer reaction time of 64 hrs at 65°C with a similar yield of 80% was reported by other authors.[23]

Furthermore, epoxy-based azobenzene monomers were not commercially available. Therefore 4-glycidyloxyazobenzene (4-GOAB) and 4,4´-diglycidyloxyazobenzene (4,4´-DGOAB) were synthesised in the laboratory following the synthetic route of Peris *et al*.[32] After 1 hr reflux reaction of 4-hydroxyazobenzene and epichlorohydrin with a molar ratio of 1:40 respectively 2 g of 4-GOAB were produced. The product was recrystallised and purified using column chromatography. A significant amount of 4-GOAB was trapped in the column giving a lower yield of 48% compared to a higher yield of 95% reported by Peris *et al*.[32] Different solvents or a mixture of solvents could be used as eluents to collect any left over product but it was unnecessary since it was demonstrated that column chromatography was not needed anymore (details are in section 4.1.2.1).

Although the 4,4´-dihydroxyazobenzene (4,4´-DHAB), used as a precursor for the production of 4,4´-DGOAB, was commercially available, its synthesis was attempted following a method similar to the one reported by Matsumoto *et al*.[145] They obtained a very high yield of 71% producing 2 g of 4,4´-DHAB. Following

step-by-step the same synthetic procedure a yield of 24% was obtained. The reason for this poor yield was attributed to the decomposition of diazonium salt at temperatures above 0°C.[146] Therefore the synthetic route was discontinued and the product (500 g) was purchased from Sphinx.

The 4,4´-DGOAB (500 g) were synthesised by modifying the above procedure of Peris *et al*. and scaling up from 2 g to 40 g.[32] The molar ration of 4,4´-DHAB and epichlorohydrin was decreased from 1:40 to 1:10 by allowing the reaction to reflux over a longer period (6 hrs instead of 1 hr). The purity of the product was verified by TLC. The yield of the product after optimisation of the process and purification was quite satisfactory as it reached 75%.

4.1.2 Materials characterisation

In this section the findings for the photoresponsive materials structures and properties are described in detail. The photo- and ultrasound-induced geometrical changes of the azobenzene are presented. Curing and isomerisation kinetics were determined. The investigations of viscosity and density change due to light irradiation as well as the healing behaviour of the photoresponsive materials are discussed. The influence of azobenzene and UV light irradiation on the stiffness and fracture properties of polymeric films are described in detail.

4.1.2.1 ^{1}H NMR analysis

^{1}H NMR provided information about the structure and functional groups in all the starting materials and chemical substances that were synthesised in the laboratory. All the NMR signals that were identified are mentioned in section 3.1.1, under each corresponding synthetic route. The outcome was that, with this technique, the identification of the composition of azobenzene in polymers was obtained.

A series of polymers assigned as CV.1, CV2.2 and CV2.3 (copolymers of P(MMA/MOAB)) synthesised under the same conditions but in different solvents such as; THF (sample CV2.1), DMF (sample CV2.2) and DMSO (sample

RESULTS AND DISCUSSION

CV2.3). The ^{1}H NMR spectra of the (MMA/MOAB) copolymers (a) CV2.1, (b) CV2.2 and (c) CV2.3 are shown in Figure 4.1.2. The ^{1}H NMR spectra of the three azo-copolymers indicated three characteristic chemical environments due to the aromatic proton signals from azobenzene at 7.89-7.93 ppm, 7.49-7.52 ppm and 6.88-6.90 ppm corresponding to four, two and three aromatic protons respectively. The composition of azobenzene content was determined by using Equation 4-1 (formula for % azobenzene concentration).

$$AB\% = \frac{A_{\delta=7.9}/4}{A_{\delta=7.9}/4 + A_{\delta=3.6}/3}$$

Equation 4-1

In spectra (b) the signal was more intense presumably due to interactions of the copolymer with the DMF residual solvent. The CDCl$_3$ appears clearly with a sharp signal at 7.26 ppm in all the three spectra as the used deuterated solvent. The intense signal at 3.68 ppm corresponds to the protons from the methyl –O-CH$_3$ group. The presence of DMF was identified at 2.88 and 2.61 ppm at (b) spectra, more significantly, but traces of it were also detected in CV2.1 and CV2.3 NMR spectra. This can be explained by the fact that the three samples were drying into the same desiccator, so all the samples might have been contaminated by DMF vapour. The broad doublet at 1.89-2.07 ppm is attributed to the resonance of the CH$_3$ protons of the methacrylate.

The signal at 2.61 ppm corresponds to water; especially at the copolymers CV2.1, CV2.2 synthesised in THF and DMSO respectively and less intense for the CV2.2, prepared in DMF. Finally, the two broad signals at 1.21-1.45 ppm and 0.84-1.02 ppm were attributed to the methylene and methyl group respectively.

RESULTS AND DISCUSSION

^{1}H-NMR analysis confirmed the azobenzene content to be 3.2% in P(MMA/MOAB) CV2.1 synthesised in THF, 2.3% in CV2.2 in DMF and 3% in CV2.3 in DMSO. The amount of azobenzene was expected to be less than 5% (5% target), since 100% yield was not achieved (71-76% yields). The remaining 2% amount of azobenzene monomer could have been homopolymerised or copolymerised but with a very low molecular weight as the chain termination in free radical polymerisation is a random process.[147] The azobenzene monomer or low molecular weight polymers were removed from the final product after purification, as described in section 3.1.1.7.

Since THF was found to be a good solvent for the monomer, easy to remove at the end of polymerisation and gave better yield, it was selected for the synthesis of a series of methacrylic polymers with azobenzene loadings varying between 0-100%. The polymer names with the corresponding azobenzene contents of the synthesised polymers are presented in Table 4.1.2.
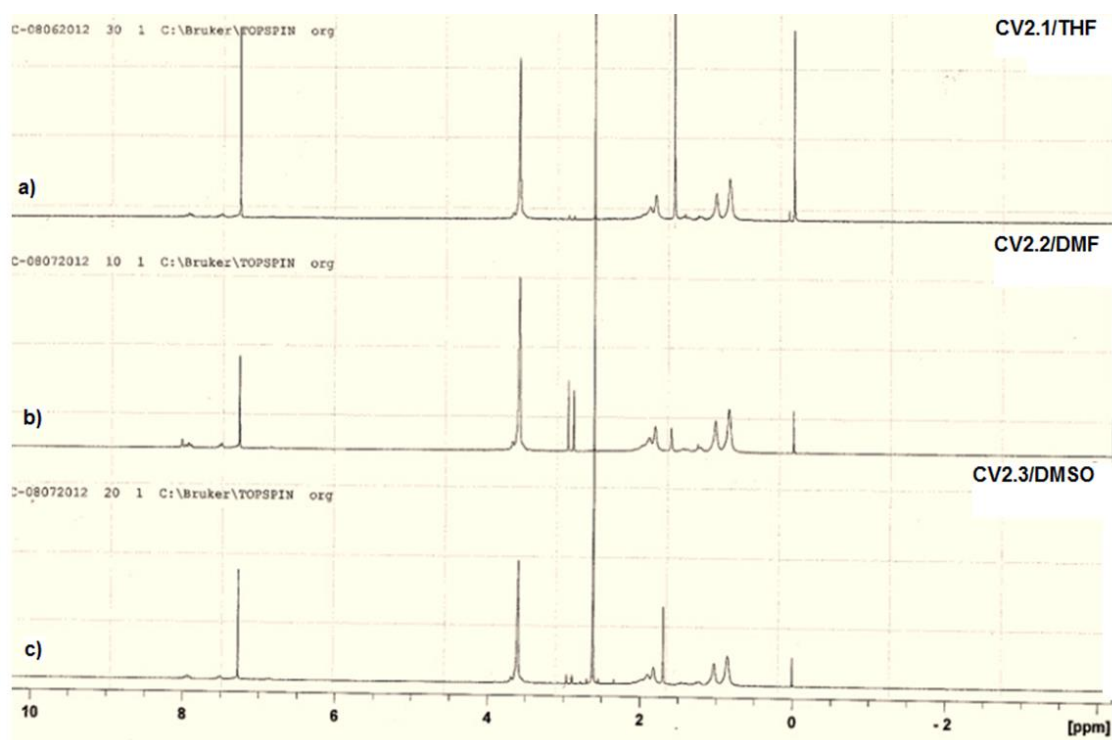
Figure 4.1.2 ^{1}H-NMR spectra of (MMA/MOAB) copolymers in CDCl$_3$

RESULTS AND DISCUSSION

Table 4.1.2 Azobenzene loadings of methacrylic polymers

Names	Azobenzene (% mol)
PMMA	0
10%P(MMA/MOAB)	10
20%P(MMA/MOAB)	20
30%P(MMA/MOAB)	30
45%P(MMA/MOAB)	45
65%P(MMA/MOAB)	65
80%P(MMA/MOAB)	80
PMOAB	100

To study the purity of glycidyloxyazobenzene (4-GOAB) and compositional fluctuation due to UV irradiation and storage in the dark ^{1}H-NMR spectra were monitored.

The ^{1}H NMR spectra of the purified 4-GOAB in $CDCl_3$ at room temperature (a) unirradiated, (b) upon 5 min of UV irradiation, (c) after 1 day and (d) 2 days storage in the dark are presented in Figure 4.1.3. The analyses at different conditions were conducted for the identification of different proton signals that could occur after isomerisation. The azobenzene monomer during its synthesis and purification procedures was exposed to room light (not in the dark), thus existence of *cis* isomers could be possible.
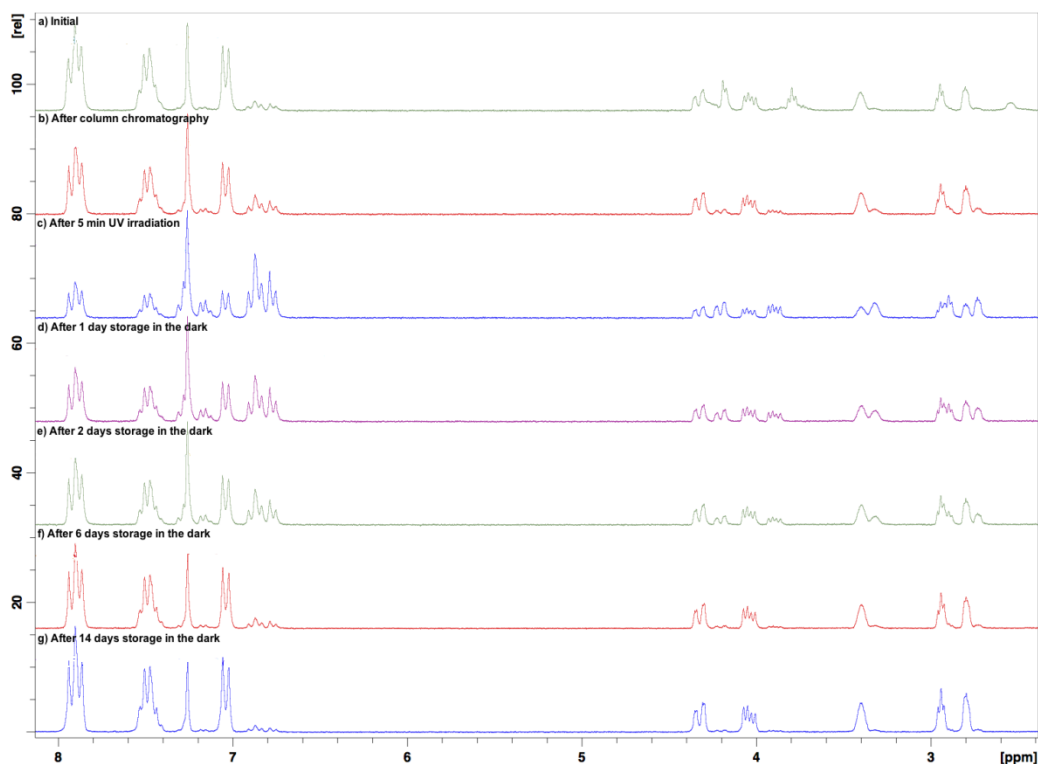
Figure 4.1.3 ¹H NMR spectra of 4-GOAB in CDCl₃ at room temperature a) non-irradiated, b) after purification, c) after 5 min of UV irradiation, and after storage in the dark (d–g).

The spectrum in Figure 4.1.3.a indicated three characteristic signals at 7.86-7.97 (t, 4H) ppm, 7.43-7.53 (m, 3H) ppm and 7.02-7.05 (d, 2H) ppm that resulted due to the presence of two aromatic rings in 4-GOAB. The protons of the methylene group appear at the 4.22-4.34 ppm and 4.05-4.07 ppm region. The broad signal at 3.50 ppm was attributed to the proton of the methylene carbon and the two subsequent chemical shifts of 2.92-2.96 ppm and 2.98-2.89 ppm correspond to the methylene group of the epoxy ring. These stated signals at their specific chemical shifts are in good agreement with the literature, thus the existence of glycidyloxyazobenzene was confirmed.[32]

RESULTS AND DISCUSSION

Nevertheless, additional signals were observed in the NMR spectra labelled with (a) that were assumed to be impurities representing about 18% of the total product at 7.15-7.31, 6.75-6.87, 4.17-4.22, 3.38-3.90, 2.89, 2.92-2.96 and 2.87-2.89 ppm. When the same solution was irradiated for 5 min with UV light the NMR spectrum (b) revealed that the intensity of the so called "impurities" increased while the proton signals of the glycidyloxyazobenzene became weaker. The opposite effect was observed after storage in the dark. By comparing the NMR signals from these four spectra it is believed that the different proton environments were signals of the *cis* isomers and were assigned to the photoisomerisation of the azobenzene. The *trans*-glycidyloxyazobenzene had the chemical shifts described above. On the other hand, the aromatic signals of the *cis* monomer appeared to be shifted upfield.

The spectra (b), (c) and (d) showed an upfield shift in the signals of the epoxy and methylene groups due to the *cis* structure of the azomonomer. The resonance signals at 7.15-7.31 (m, 3H) ppm that interrupted by the characteristic signal of $CDCl_3$, 6.87-6.90 (t, 4H) ppm and 6.75-6.87 (d, 2H) ppm were noticed to shift without having the same order as in the *trans* form. This may be caused by the interaction of the oxygen of the glycidyl ether molecule with the aromatic protons, located next to the two nitrogens. The four protons next to the nitrogen could come closer to the oxygen as they were in the *cis* conformation and thus can explain why their signals overlapped those at the end of the unattached benzene ring. Regarding the epoxy ring, new signals appeared next to each signal from the *trans* conformation of the molecule: for the protons in methylene at 4.17-4.22 (d, 1H) ppm and 3.38-3.90 (q, 1H) ppm, for the chiral another singlet at 2.89 ppm and for the methylene between the epoxy and the ether bond a broader multiplet signal at 2.92-2.96 ppm and another signal at 2.87-2.89 ppm. The signals of the *cis* isomer appear at higher field than the signals corresponding to the *trans* isomer, due to the anisotropic effect of the π cloud of the aromatic ring.[70]

The *cis* signals were found next to the *trans* ones but with lower intensity due to different proportional proton environments of the *trans* and *cis* forms. By analysing the integrals of the NMR spectra it was possible to calculate the loading of each isomer.

Another study has already indicated that the ^{1}H NMR spectra of 4-methacryloyloxyazobenzene after UV irradiation presented new additional sets of not only aromatic but also vinyl signals due to the *cis* conformation of the azobenzene.[148] Peris *et al.* demonstrated different chemical shifts due to the *trans* and *cis* configurations of the 4-GOAB monomer.[32] Here for the first time the changes in the proton signals of an epoxy group linked to azobenzene due to the reversible azo-isomerisation were investigated.

The graph in Figure 4.1.4 illustrates the percentage of the two geometric isomers in CDCl$_3$ at ambient, upon 5 min of UV irradiation, after 1 day and after 2 days in the dark respectively. In each situation the blue columns express the percentage of the *trans* and the red ones the percentage of the *cis*-GOAB.
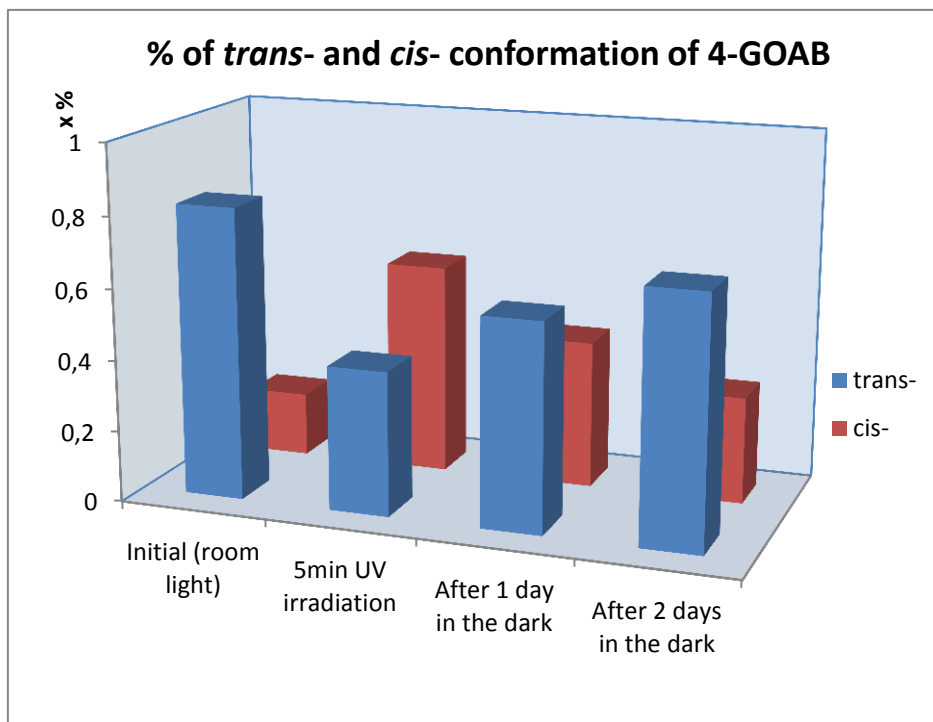
Figure 4.1.4 Graph of proportional *trans*- and *cis*-GOAB molecules based on NMR spectra

From the first NMR data it was observed that about 18% of *cis* isomers were formed presumably by the influence of the room light in the laboratory during the synthetic and purification procedures. Upon 5 min UV irradiation the intensity of the *trans* peaks decreased by 51% and a parallel 60% increase in the *cis* isomers was noticed. After keeping the sample in the dark for 1 day a reversible behaviour was noticed, which was expected due to the reversion of the *cis* isomers to the more stable *trans* forms. A 45% increase of *trans* molecules was observed after storage in the dark the first day, while subsequent storage in dark for a second day led to a 75% increase of the *trans* isomers. In parallel, 30% and 49% decreases of *cis* molecules were noticed after storage in the dark for 1 and 2 days subsequently.

Further studies for determining the reversible *trans*→*cis* isomerisation kinetics were carried out (section 4.1.2.4.1) in order to obtain a better view about the reaction kinetics.

4.1.2.1.1 Curing analysis by ^{1}H NMR

The first molecule under investigation for its reactivity, with a common amine, diethylenetriamine (DETA), was the monofunctional epoxy monomer the glycidyloxyazobenzene (4-GOAB). Its photoresponsive behaviour was evaluated after curing in order to confirm that photo-induced changes can occur in a rigid network at liquid and solid forms.
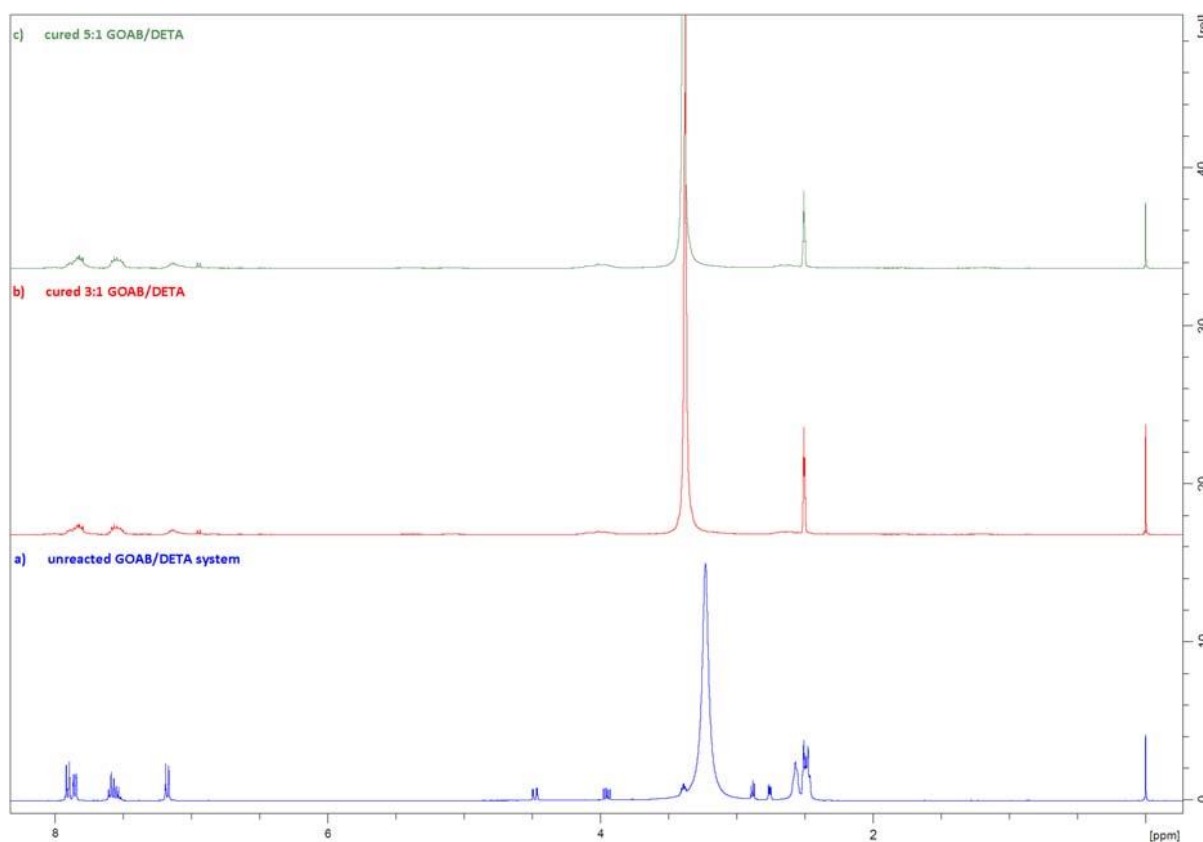
Figure 4.1.5 ^{1}H NMR spectra of 4-GOAB/DETA at room temperature as (a) unreacted system, (b) cured with 3:1 molar ratio system, and (c) cured with 5:1 molar ratio system

^{1}H NMR spectra of unreacted and reacted 4-GOAB/DETA systems are presented in Figure 4.1.5. The chemical shifts for the mixture of 4-GOAB with DETA in dmso-d_6 are illustrated in the spectrum (a). The spectra of cured

samples with a 3:1 and 5:1 molar ratio of 4-GOAB/DETA are presented in Figure 4.1.5 (b) and (c) respectively.

It was observed from the spectrum (a) that there are three strong multiplets at 7.91-7.84 ppm (m, 4H), 7.61-7.53 ppm (t, 3H) and 7.19-7.17 ppm (d, 2H) corresponding to the benzene rings of the 4-GOAB. In both cured samples these resonance signals became broader, indicating polymeric character, and signals shifted slightly downfield. Two sharp signals at 4.50-4.46 ppm (d, 1H) and 3.97-3.93 ppm (q, 1H) corresponding to the methylene of the epoxy disappeared and instead a broad multiplet appeared at 4.08-3.96 ppm, showing that the epoxy ring has been opened. The other two sharp signals at 2.89-2.87 ppm (m, 1H) and 2.77-2.75 ppm (m, 1H) corresponding to the methylene group next to the ether linkage and the broader ones at 2.57-2.46 ppm disappeared completely. For the cured solutions the NMR spectra (b) and (c) indicated a new weak multiplet peak in the middle at 2.67-2.50 ppm, confirming the formation of a new amino bond with the opened epoxy ring.

Moreover, the rate of the reaction was calculated by quantitative analysis of the integrals corresponding to the reacted amines. It was found that for the 3:1 system, about 2.76 molecules of (~3) 4-GOAB reacted with each DETA molecule. Similarly, 3.07 molecules of 4-GOAB were attached to each DETA molecule in the 5:1 (4-GOAB/DETA) system. It is clear that even though the DETA has five functional protons, only a maximum of three molecules of 4-GOAB can react with it. Once 3 4-GOAB molecules are attached to a DETA molecule the cured system becomes too crowded to be able to accommodate any more 4-GOAB molecules. The reactivity decreases due to steric hindrance and most probably the positions of the amine that reacted with the 4-GOAB are one secondary and two primary amines. Two newly formed secondary amines after reaction are thought to be steric less favourable for addition to any further 4-GOAB molecule as can be seen in Figure 4.1.6. Other authors reported that electron density and steric hindrance affect the reactivity of amines as curing agents.[149, 150]

The ^{1}H NMR studies confirmed that the reaction had occurred from the disappearance of the oxirane group and the amine protons.
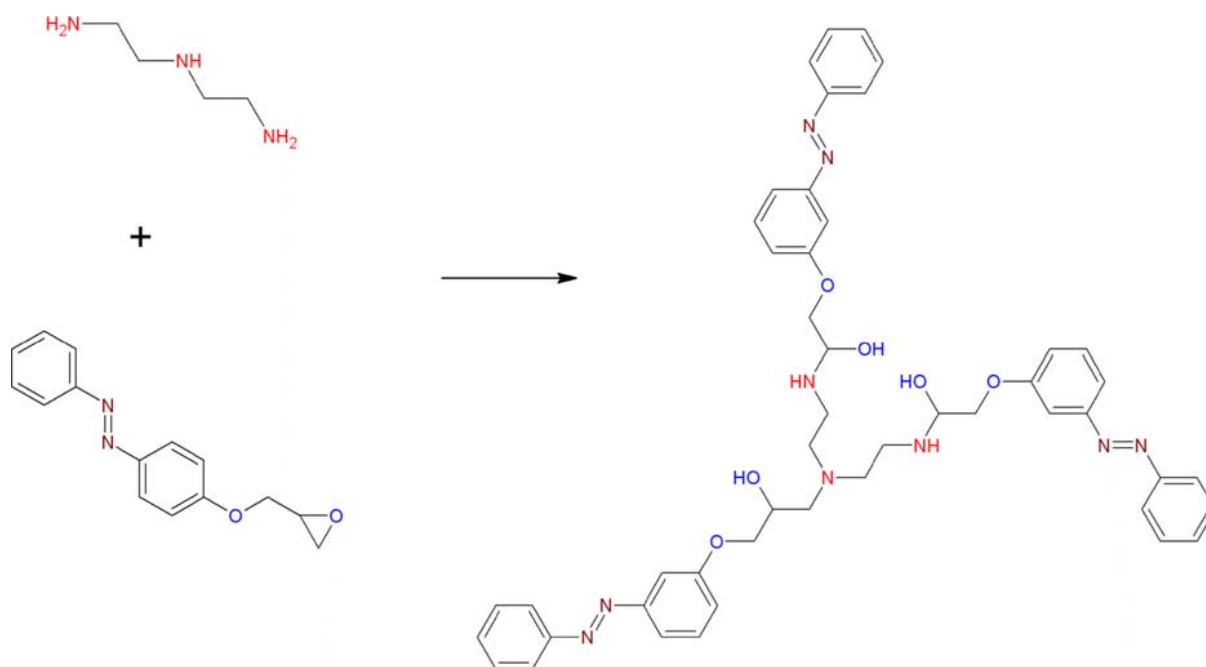
Figure 4.1.6 Proposed 4-GOAB/DETA reaction scheme

4.1.2.2 GPC analysis

After the structural information of the polymers obtained by ^{1}H NMR, the next characterisation technique that was followed was the gel permeation chromatography (GPC), for investigation of the polymers' molecular weight and polydispersity.

In Table 4.1.3 the synthetic yields and the GPC results of the (MMA/MOAB) copolymers are illustrated. It has been shown that synthesising PMMA with different solvents can affect the mechanical and thermal behaviour of the polymer.[126, 127] The molecular chain properties of azobenzene based polymers synthesised by using THF (sample CV2.1), DMF (sample CV2.2) and DMSO (sample CV2.3) were investigated. All the accomplished copolymers were

produced with very reasonable yields. CV2.1 and CV2.3 achieved 71% yield, while CV2.2 polymerised in DMF obtained 76% yield. The GPC chromatogram of the copolymers recorded a single broad peak without the appearance of any shoulders. The presence of only one peak in the chromatogram ensured the polymerisation synthesis. If an additional narrower peak was apparent the existence of homopolymers or very low or high molecular weight polymers within the copolymers could be determined.

Table 4.1.3 Yields, molecular weight and polydispersity obtained from (MMA/MOAB) copolymers using different solvents

Names of poly(MMA/MOAB)	CV2.1	CV2.2	CV2.3
Solvents	THF	DMF	DMSO
Yield	71%	76%	71%
M_w	77,190	65,785	114,096
M_n	49,275	36,846	69,217
PD	1.56	1.78	1.64
Units/chain	457	342	642

It is apparent that the solvents were also affecting the M_w of these copolymers. The highest polymer molecular weight was obtained with DMSO, a highly polar aprotic solvent. THF and DMF were responsible for a lower but quite satisfactory weight average molecular mass. The M_w of the CV2.1, CV2.2 and CV2.3 copolymers were found to be 49,275 g/mol, 36,846 g/mol and 69,217 g/mol respectively. Their molecular weight distributions (M_w/M_n) ranged between

RESULTS AND DISCUSSION

1.56 and 1.78. From these results it was found that each CV2.1, CV2.2 and CV2.3 polymer chains consisted of 457, 342 and 642 total monomer units of which approximately 22, 17 and 32 will be the 4-methacryloyloxyazobenzene units.

Table 4.1.4 Molecular weight data of polymers with various azobenzene loadings

Names	AB (%mol)	M_w (g/mol)	Units/chain
PMMA	0	43,000	434
10%P(MMA/MOAB)	10	78,000	677
20%P(MMA/MOAB)	20	87,000	664
30%P(MMA/MOAB)	30	57,000	379
45%P(MMA/MOAB)	45	63,000	356
65%P(MMA/MOAB)	65	42,000	200
80%P(MMA/MOAB)	80	44,000	186
PMOAB	100	77,000	306

The azobenzene loadings between 0-100% weight-average molecular mass and the number of units per chain of the (MMA/MOAB) polymers are presented in Table 4.1.4. Similarly to the CV2.1, CV2.2 and CV2.3 polymers, the presence of only one peak in the GPC chromatogram reassured the success of polymerisation reaction and product's purity. As it can be seen from the table there is not any apparent trend related to the azobenzene loading and the average molecular weights of the polymers. This was not a surprise since each polymer was synthesised via free radical polymerisation where there is no

control over chain growth or termination reaction. Different polymerisation routes like RAFT for instance would produce polymers with controlled M_w.[28] From these findings it was estimated that azobenzene units in 0% (PMMA), 10%, 20%, 30%, 45%, 65%, 80% and 100% (PMOAB) polymer were about 0, 67, 132, 113, 160, 130, 148 and 306 respectively.

4.1.2.3 FTIR analysis

Furthermore, after the ^{1}H NMR and GPC analysis, the characterisation of the monomers and copolymers by Infrared spectroscopy proved the existence of bonds of the methyl methacrylate and 4-methacryloyloxyazobenzene. The results of the wave numbers corresponding to characteristic linkages are presented in Table 4.1.5 and Table 4.1.6. They suggest that monomers are joined together to form copolymer and they are in agreement with literature.[32]

Table 4.1.5 Transmittance frequencies by Infrared spectrometry of PMMA

Bond	Compound Type	Wave number (cm^{-1})
C-H	Alkanes	2844
C=O	carboxyl	1745
C=C	aromatic rings	1490
C-O	ether	1060-1113

4-GOAB and 4,4´-DGOAB were analysed by FTIR spectroscopy as well. Specific fingerprint regions corresponding to characteristic linkages verified the existence of bonds of the azobenzene epoxy monomers and are presented in Table 4.1.7. These results and those of ^{1}H NMR, in section 4.1.2.1, support that the examined products are pure 4-glycidyloxyazobenzene and 4,4´-diglycidyloxyazobenzene.[32]

Table 4.1.6 Transmittance frequencies by Infrared spectrometry of 4-MOAB, 4,4´-DMOAB, P(MMA/MOAB) and PMOAB

Bond	Compound Type	Wave number (cm^{-1})
C-H	aromatic rings	2952-2999
	alkanes	2844
C=O	carboxyl	1745
C=C	aromatic rings	1490
N=N	diazo-	1595
C-N	amine	1148-1275
C-O	ether	1060-1113

Table 4.1.7 Transmittance frequencies by Infrared spectrometry of 4-GOAB and 4,4´-DGOAB

Bond	Compound Type	Wave number (cm^{-1})
C-H	aromatic rings	3053
	alkanes	2927
C=C	aromatic rings	1500, 1600
N=N	diazo-	1581
C-N	amine	1224-1256
C-O	ether	1070-1144

The disadvantage of this technique was that *trans→cis* isomerisation could not be identified. Isomerisation occurs after rotation or inversion of the -N=N- bond (1581 cm^{-1}) which belongs to the fingerprints region and the changes of the azobenzene materials after exposure to UV light were not apparent and neither could be quantified.[151]

4.1.2.4 UV/Vis spectroscopic studies

UV/Vis studies were performed for demonstrating the photoresponsive behaviour of azobenzene monomers and polymers in solid (thin films) and liquid (solutions) phases.

4.1.2.4.1 UV/Vis spectroscopy of the 4-GOAB monomer and cured (4-GOAB/DETA) system

The photo-isomerisation and the reversible reaction of 4-GOAB monomer in DMSO studied by UV/Vis are shown in Figure 4.1.7 and Figure 4.1.8. 15 mg of 4-GOAB were dissolved in 25 ml DMSO and used as stock solutions. The sample solutions were diluted further in order to achieve smooth and clear absorbance bands without noise and cutting off the peak. The required concentration of the solutions used for carrying out the UV/Vis spectroscopy measurements was 10^{-3} M in DMSO.
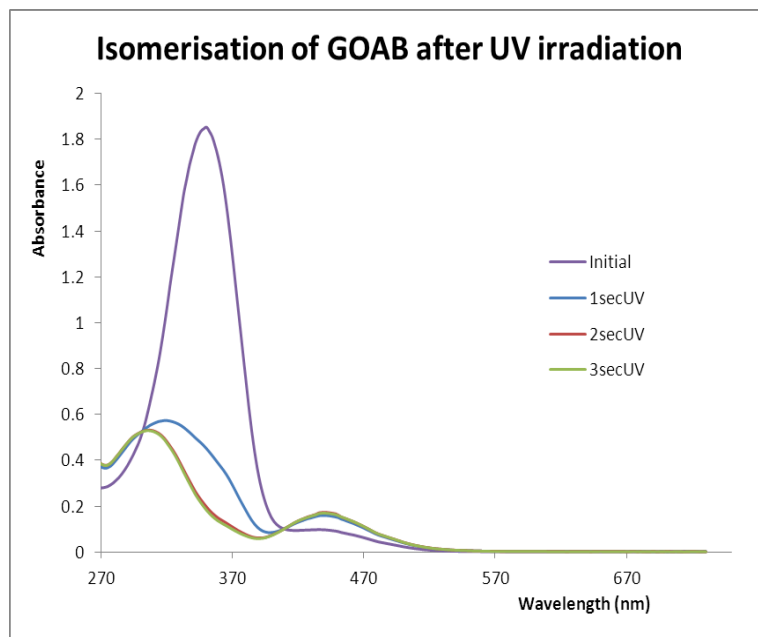
Figure 4.1.7 UV/Vis absorption spectrum of 4-GOAB monomer in dmso solution before after 3 sec of UV irradiation

In Figure 4.1.7 the UV/Vis absorbance spectra of the azobenzene monomer in DMSO against irradiation time is illustrated. The non-irradiated solution exhibited two absorption bands at 378 nm attributed to the *trans* azobenzene molecules with $\pi \to \pi^*$ energy level and at 440 nm due to its forbidden *cis* geometric isomers with $n \to \pi^*$ transition. Upon UV irradiation (320-390 nm) for 1 sec, the peak at 378 nm decreased and finally disappeared at 3 sec, demonstrating that all the *trans* isomers were converted to their *cis* conformation. Similarly the intensity of the absorbance peak at 440 nm, corresponding to the *cis* configuration, increased. The levels of increase and decrease are not proportional because of the forbidden $n \to \pi^*$ transition.

The reversible photoisomerisation was examined by visible light irradiation and is shown in Figure 4.1.8. The already *trans*-azobenzene isomers from the dark of the 4-GOAB monomer at the beginning indicated an intense broad peak at 375 nm. The absorbance band at 440 nm for the *cis* isomers was hardly apparent. Upon 5 sec of visible light irradiation for the thorough transformation

127

of the azobenzene molecules to their *trans* geometrical structure the only noticeable change was a further decrease at the 440 nm peak. Immediately after 5 sec of UV irradiation the *trans* absorbance band of the 4-GOAB decreased dramatically while the intensity of the band corresponding to the *cis* isomers indicated a significant hyperchromic shift. The sample solutions were then exposed to visible light and within 2 sec, the magnitude of the two characteristic bands changed reversibly and completely due to the photoisomerisation.
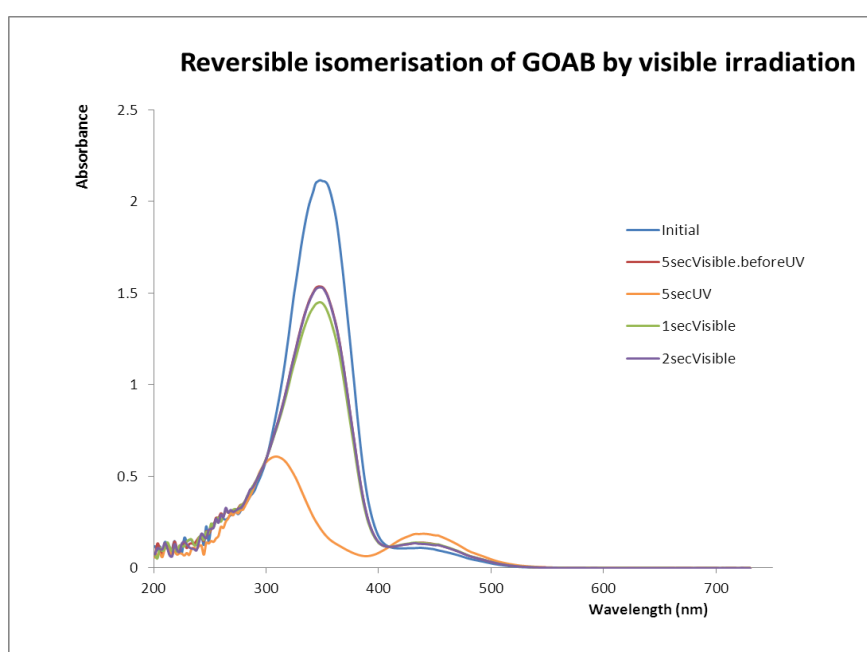
Figure 4.1.8 UV/Vis absorption spectrum of 4-GOAB monomer in DMSO solution before after 2 sec of visible light

The graph plotted in Figure 4.1.9 demonstrates the percentage of the *cis* 4-GOAB monomers against the UV irradiation time. It is obvious that the isomerisation process of these monomers is very fast in solution. Upon 1 sec of UV light irradiation the *cis* isomers from 0 value were increased to 96% and after 2 sec they reached 99%. The required UV irradiation time for the accomplishment of photoisomerisation was demonstrated to be 3 sec.
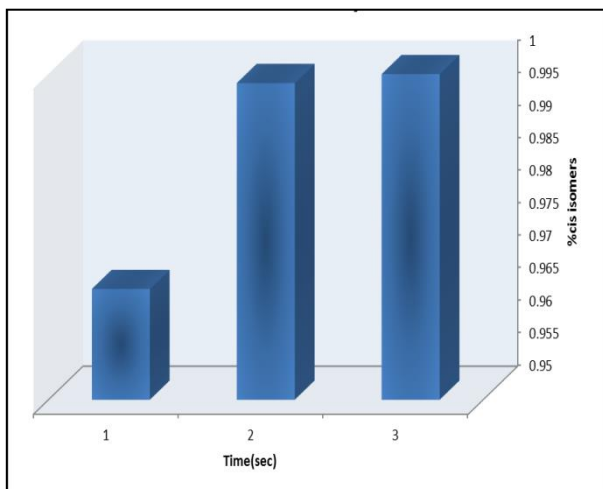
Figure 4.1.10 Isomerisation of GOAB monomer in DMSO solution after exposure to UV light
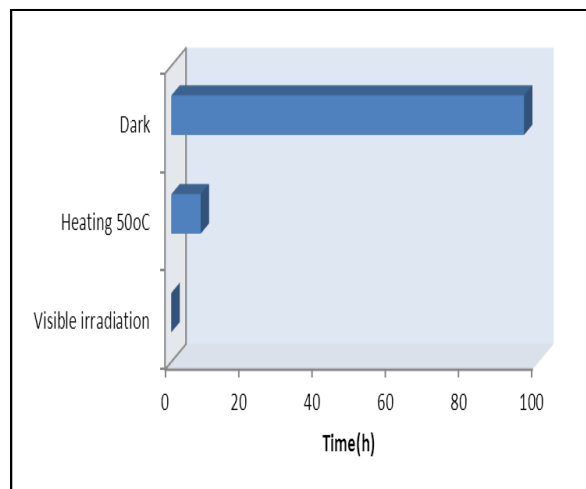
Figure 4.1.9 Reversible isomerisation of GOAB monomer in DMSO solution after different treatments against time

Additionally the reversible transformation reaction was examined in three different ways against time, by placing them in the dark, by heating them up and by irradiating them with visible light. The required time for complete isomerisation after each different treatment is presented in Figure 4.1.10. The DMSO solution samples of 4-GOAB monomers went back to their *trans* form after keeping them in the dark for 4 days. By heating them at 50°C the reversible isomerisation was accomplished after 8 hrs. Finally, only 2 sec of visible light were sufficient for the reversible conversion of the *trans* azobenzene monomers. These findings were expected as storage in the dark is considered as thermal relaxation and heat is a well-known stimulus for triggering the *cis→trans* isomerisation in azobenzene molecules.[67, 68]

The isomerisation of the cured system was investigated by UV/Vis spectroscopy in order to compare the required time to interconvert *cis* and *trans* isomers of monomer (4-GOAB) and cured systems. Figure 4.1.11 shows the UV/Vis spectra of the cured system (4-GOAB/DETA) in DMSO solution against the UV

irradiation time. It can be observed from the graph that the absorbance band at 350 nm for *trans* isomer (π−π*) decreased gradually with irradiation time and after 5 sec the decrease slowed down. Further irradiation spectrum for 20 sec showed complete conversion of *trans* isomer to the *cis* form. This can also be confirmed by the increase in the second absorption band at 440 nm corresponding to the forbidden −π* electronic transition.
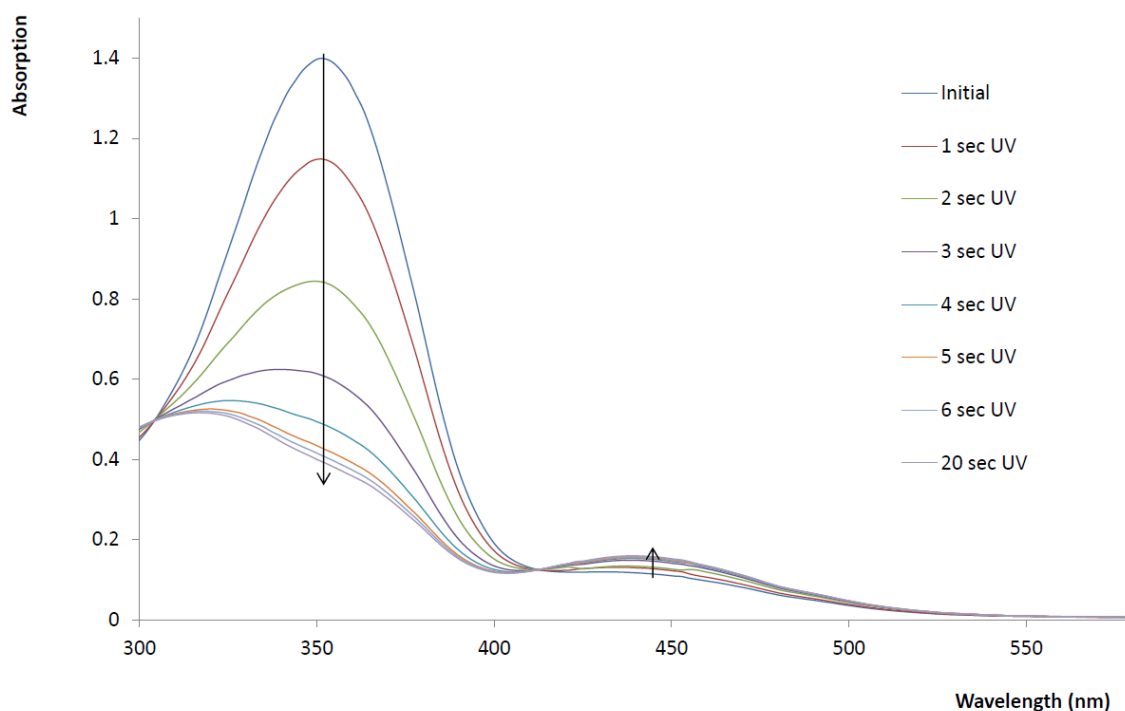
Figure 4.1.11 UV/Vis absorption spectra of 4-GOAB/DETA in DMSO solution before and after 20 sec of UV irradiation

Absorption spectra of the cured *cis* 4-GOAB/DETA by irradiation with visible light are illustrated in Figure 4.1.12. Almost 91% of the *cis* isomers reverted back to the *trans* form within 1 sec as evidenced by the drastic increase of the absorption peak at 440 nm. After 2 and 3 sec of irradiation with visible light, 98% and 99% of the *cis* form was converted to *trans* isomer respectively. It took

about 4 sec for the cured system to completely transfer to its *trans* form by visible irradiation. The results suggest that the isomerisation of azobenzene can be triggered by UV light even it is in the cross-linked form. However, the conformational change from *trans→cis* isomer in the cured system was three times slower than that in the 4-GOAB monomer. Moreover, the cured 4-GOAB/DETA system reverted to the *trans* form by visible irradiation two times slower when compared to its monomeric counterpart (4-GOAB). The differences in the isomerisation times between the monomer and cured system were expected due to the formation of new bonds between amine and epoxide. The new bonds restricted the movement of the azo-molecules, since the isomerisation occurs by rotation or inversion between the two nitrogen atoms.
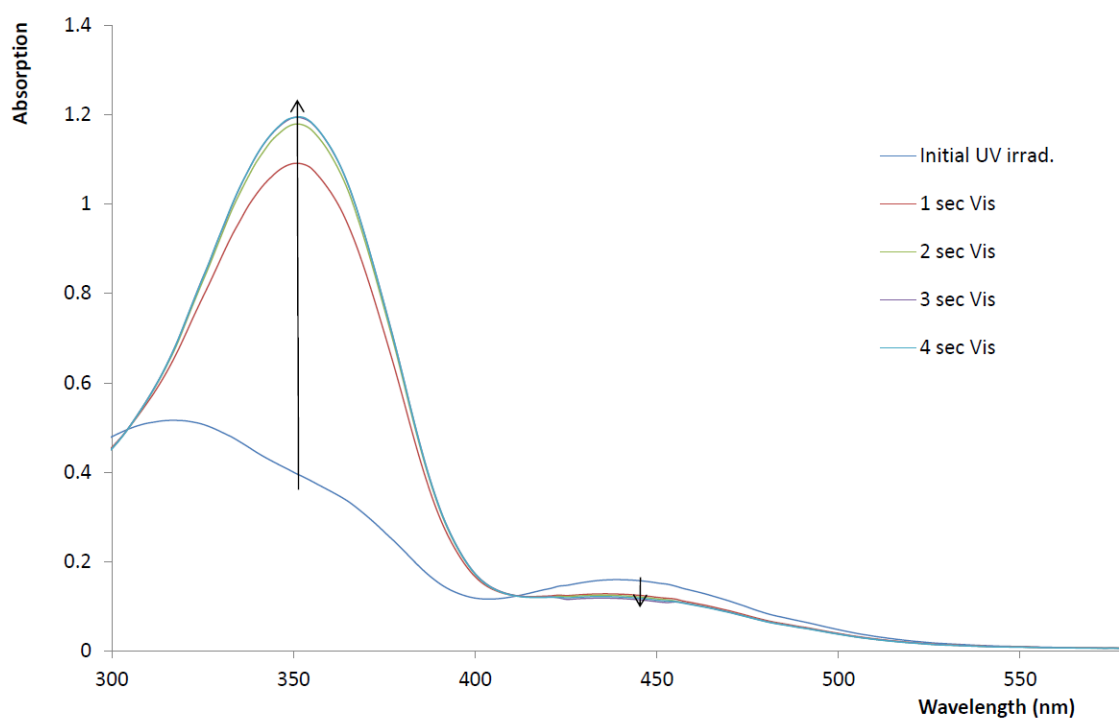
Figure 4.1.12 UV/Vis absorption spectrum of 4-GOAB/DETA in DMSO solution irradiated with UV and visible light

RESULTS AND DISCUSSION

4.1.2.4.2 UV/Vis spectroscopy of azobenzene methacrylic polymers

All the (MMA/MOAB) polymer films with various azobenzene loadings (0-100 mol%) were analysed by UV/Vis spectroscopy during *in-situ* light irradiation. Figure 4.1.13 and Figure 4.1.14 show the reversible photoisomerisation of azobenzene in the polymer films as a function of irradiation time. It should be mentioned that the UV/Vis spectra for all the polymers exhibited the same trend with irradiation time, but here the spectra of a copolymer containing 20 mol% azobenzene is presented.

Figure 4.1.13 clearly shows two absorption bands at 318 nm and 440 nm which correspond to the *trans* isomers for $\pi-\pi^*$ electronic excitation and *cis* isomers for forbidden $n-\pi^*$ excitation respectively. The intensity of the absorption band at 318 nm decreased noticeably after UV irradiation, while the intensity at 440 nm increased. This increase is much clearer in the enlarged view as shown in the insert (Figure 4.1.13). Nevertheless, this band was not utilised for quantitative analysis of the isomers due to smaller changes in the absorption intensity of the forbidden $n-\pi^*$ transition for *cis* isomers. Hence the changes in the absorption band at 318 nm were used to calculate the amount of isomerisation. It was found that after 6 min of UV irradiation the absorption peak at 318 nm decreased by 59%.
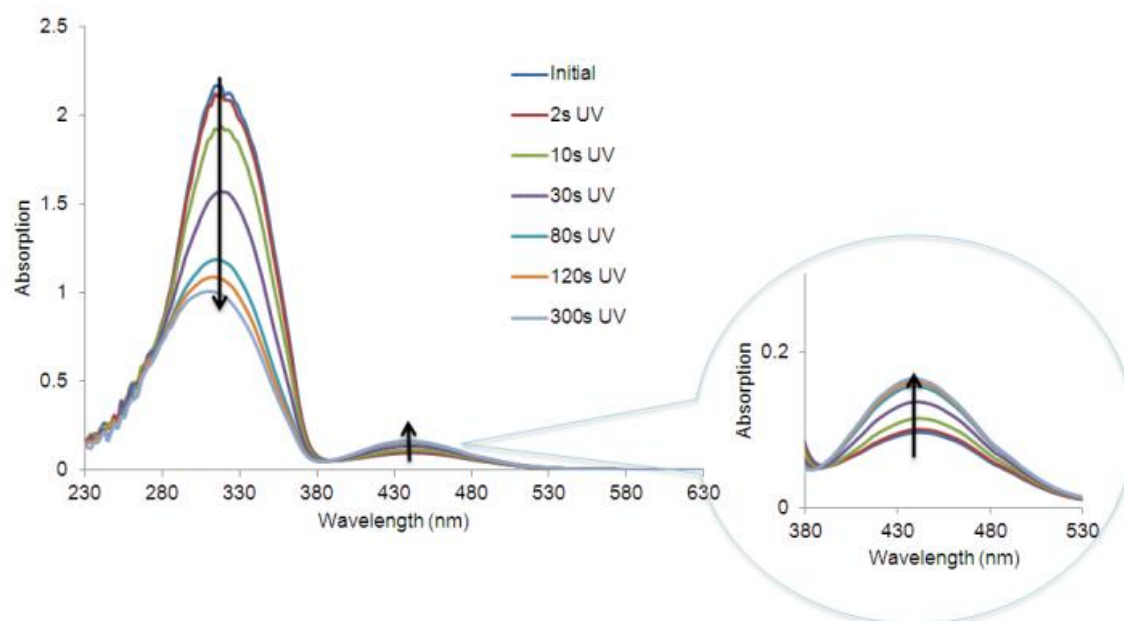
Figure 4.1.13 UV/Vis spectra of 20% P(MMA/MOAB) film during UV irradiation.
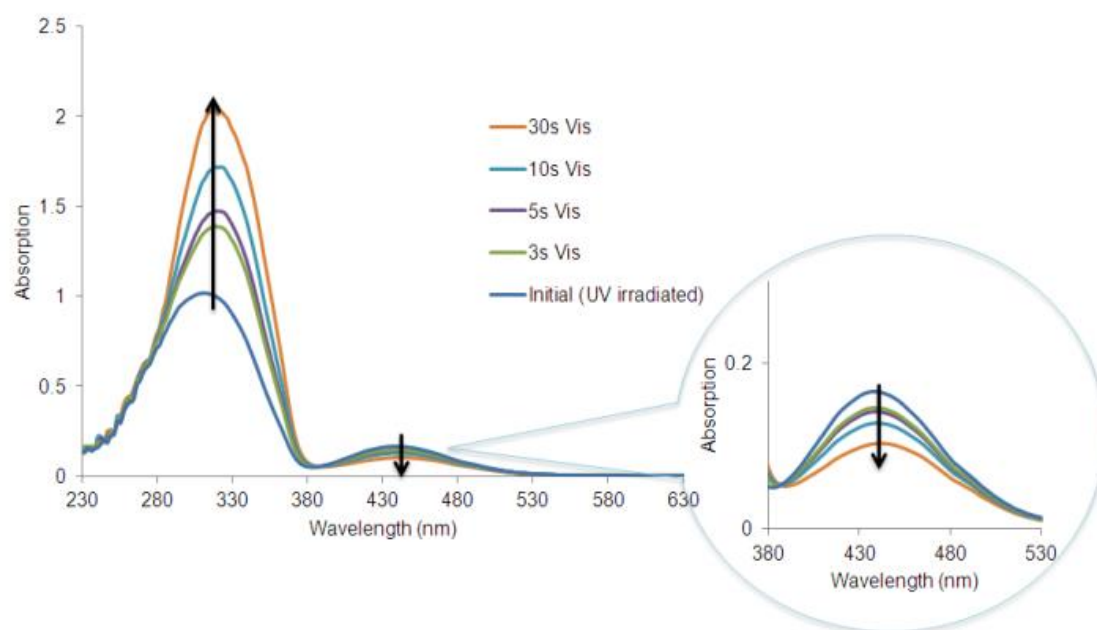
Figure 4.1.14 UV/Vis spectra of 20% P(MMA/MOAB) during Visible irradiation.

The UV/Vis spectra in Figure 4.1.14 demonstrated a typical absorption graph of the reversible *cis→trans* conversion upon exposure of the films to visible light.

The initial, first spectrum was collected immediately after UV irradiation (6 min) to make sure that all the azobenzene was in *cis* isomeric form. After visible irradiation the peak at 318 nm gradually increased, whilst the peak at 440 nm decreased (enlarged view, Figure 4.1.14), indicating an increase in the *trans* azobenzene isomers. Subsequent irradiation of the film with visible light showed a complete recovery to the *cis* form within 30 sec.
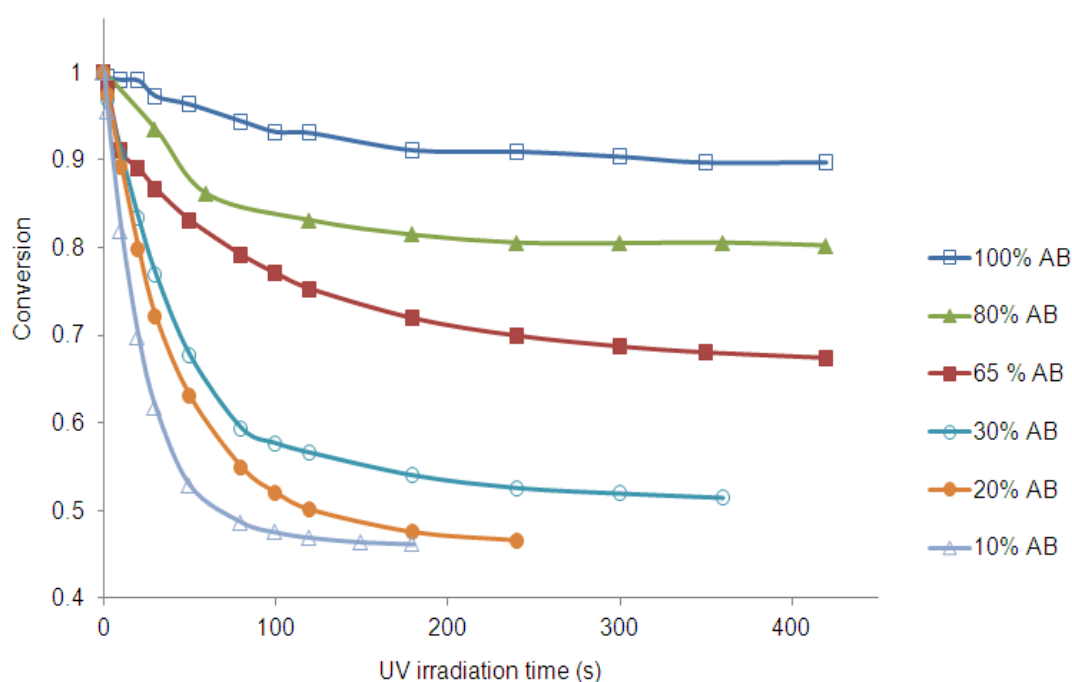
Figure 4.1.15 *Trans→cis* conversion in P(MMA/MOAB) films vs. UV irradiation time

Figure 4.1.15 indicates the conversion rates of reversible *trans→cis* isomerisation as a function of UV irradiation time for the polymers with different azobenzene loadings. The rates of *trans→cis* isomerisation increased almost linearly up to 80 sec of irradiation but above this time the conversion rates showed plateau behaviour. Maximum irradiation time for the completion of the

trans→cis isomerisation in the polymer thin films was found to be 7 min. The *trans→cis* conversion increased with decreasing azobenzene loading (Figure 4.1.15). Note that 100% conversion of *trans* isomers to their *cis* counterparts was not possible to achieve and above 65 mol % azobenzene loading the *trans* to *cis* conversion was found to be less than 33%. This phenomenon could be explained in terms of freedom of rotation of azobenzene chromophores in the polymer. The distance between the neighboring chromophores decreases with increasing azobenzene loadings in the polymer chains, thus restricting their rotations for *cis* isomerisation to occur. Another possibility may be the reversion of the *cis→trans* isomers immediately after irradiation was ceased.

4.1.2.5 Thermal properties of acrylic azobenzene polymers

Heating-cooling-heating experiments were performed at a rate of 10°C/min, for each sample from 25 to 200°C. Figure 4.1.16 shows the DSC traces of three cycles for P(MMA/MOAB) prepared from THF, DMF and DMSO. Generally the T_g range of PMMA is considered to be around 100°C. Thus higher Tg in azo-copolymers is expected due to the presence of bulky aromatic rings in the side azobenzene.[43]

The heating cycles of the copolymers, synthesised from THF are illustrated in Figure 4.1.16.a. The first curve showed a considerably lower T_g at ~113°C with respect to the other scans. The DSC of the 2nd and 3rd heating cycles of the azobenzene copolymer CV2.1 (synthesised in THF) indicated a T_g of about 126°C. Some irregular features before the broad exothermic peaks can be noticed in these three traces, confirming the presence of residual THF or H_2O, which was observed in NMR in section 4.1.2.1. This increase of T_g at the 2nd and 3rd scans might be the case that the THF evaporated during the 1st cycle. The presence of THF in the 1st cycle favoured the polymer chain to relax easily.

The DSC heating cycles in Figure 4.1.16.b present the glass transition temperature of the azo-copolymer CV2.2 synthesised in DMF. The T_g appeared

to be at around 110°C. During all the heating cycles the temperature was observed at the same level and without major differences. This stable behaviour could be attributed to the strong hydrogen bonding in PMMA chains assigned to the DMF solvent which reduced the evaporation rate of DMF and thus it contributed to the polymer softening.
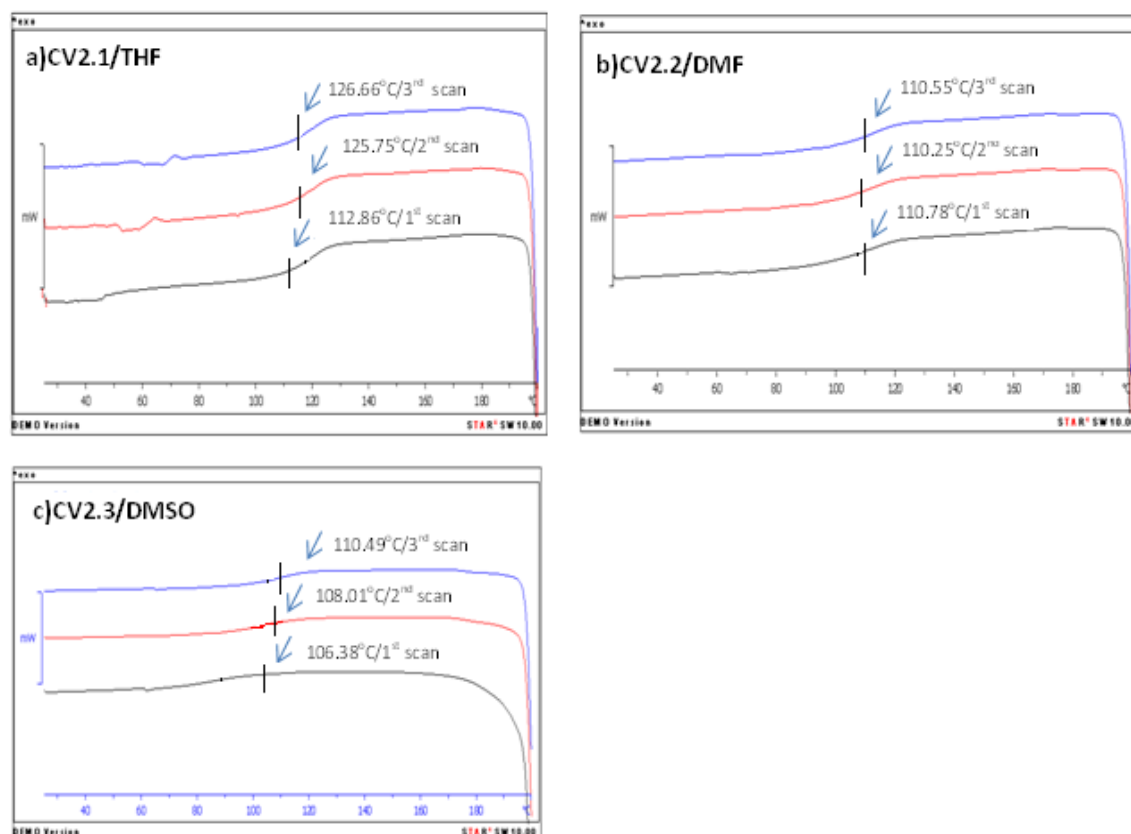
Figure 4.1.16 DSC thermal traces, in three consequent heating-cooling cycles, of copolymers (MMA/MOAB) synthesised from three different solvents (a) CV2.1/tetrahydrofuran, (b) CV2.2/dimethylformamide and (c) CV2.3/dimethyl sulfoxide

Likewise the thermal analysis of the azo-copolymers prepared from DMSO is presented in Figure 4.1.16.c with a range of T_g= 106-110°C. The first scan exhibited a lower T_g of 106°C comparing to the CV2.2. Between the second and third heating scans the T_g rose from 108 to 110°C, demonstrating that during

the two subsequent heating cycles the polymer chains were organised in a more ordered form.

Table 4.1.8 Glass transition temperature, weight average molecular weight and number of units per chain of polymers with various azobenzene loadings

Names	AB (% mol)	T_g (°C)	M_w (g/mol)	Units/chain
PMMA	0	113.5 ± 0.7	43,000	434
10%P(MMA/MOAB)	10	128.4 ± 0.3	78,000	677
20%P(MMA/MOAB)	20	130.5 ± 0.2	87,000	664
30%P(MMA/MOAB)	30	133.4 ± 0.3	57,000	379
45%P(MMA/MOAB)	45	131.3 ± 0.4	63,000	356
65%P(MMA/MOAB)	65	126.2 ± 1.1	42,000	200
80%P(MMA/MOAB)	80	121.0 ± 1.2	44,000	186
PMOAB	100	149.1 ± 1.0	77,000	306

In Table 4.1.8 all the molecular characterisation data (T_g, M_w, units/chain) of the (MMA/MOAB) polymers with various azobenzene loadings of 0-100% are presented. The presence of only one T_g and the absence of any metling point at the thermograms confirmed the completion of the polymerisation and product's purity. As it can be seen from the table there is no apparent trend relating to the glass transition temperatures and the average molecular weights of the polymers. After plotting the T_g values of the polymers versus their corresponding azobenzene loadings a correlation was identified, as seen in Figure 4.1.17. The polymers' T_g appeared to increase with the azobenzene content upto 30% loading where it reached a maximum temperature of T_g= 133°C. Then it started

to decrease with the azobenzene content until 80% loading. The homopolymer PMOAB with 100% azobenzene loading did not follow this pattern. It appeared to have the highest T_g= 149°C. This behavior could be attributed to the different polymer chains rearrangement and/or due to different solvent loss in each polymer. Isotactic rearrangement of polymers corresponds to higher T_g values compare to atactic or syndiotactic polymers.[152] The polymers in this study did not have any controlled chain rearrangement because they were synthesised via free radical polymerization. Additionally, these results demonstrated also that in this class of materials the T_g and M_w are not related.
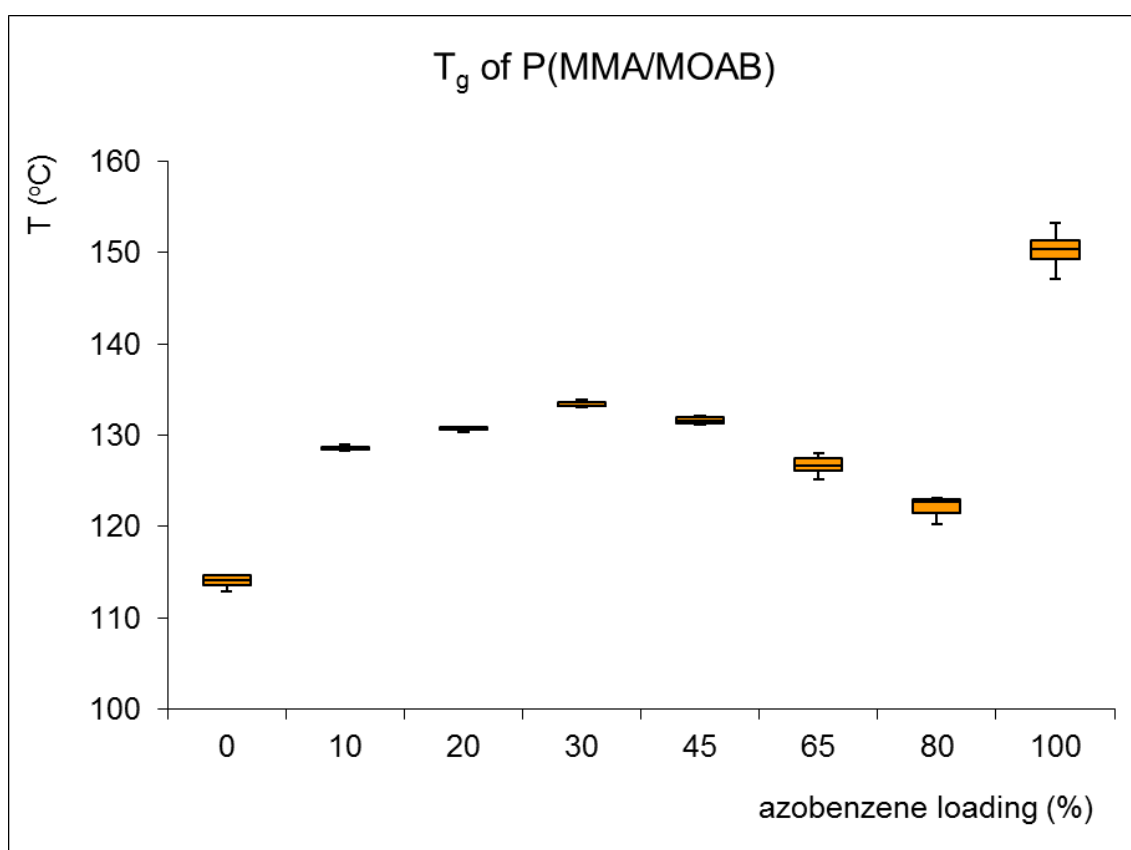
Figure 4.1.17 Influence of azobenzene loading on the thermal properties of acrylic copolymers

4.1.2.6 Photoviscosity effect

Viscosity measurements of the CV2.1 poly(MMA/MOAB) in DMSO solutions were recorded using a modified cone and plate rheometer as described in previous section 3.1.2.8. In situ UV irradiated viscosity data in a temperature controlled atmosphere were collected. The viscosities of DMSO and of PMMA solution were tested before and after UV irradiation but no changes were observed.
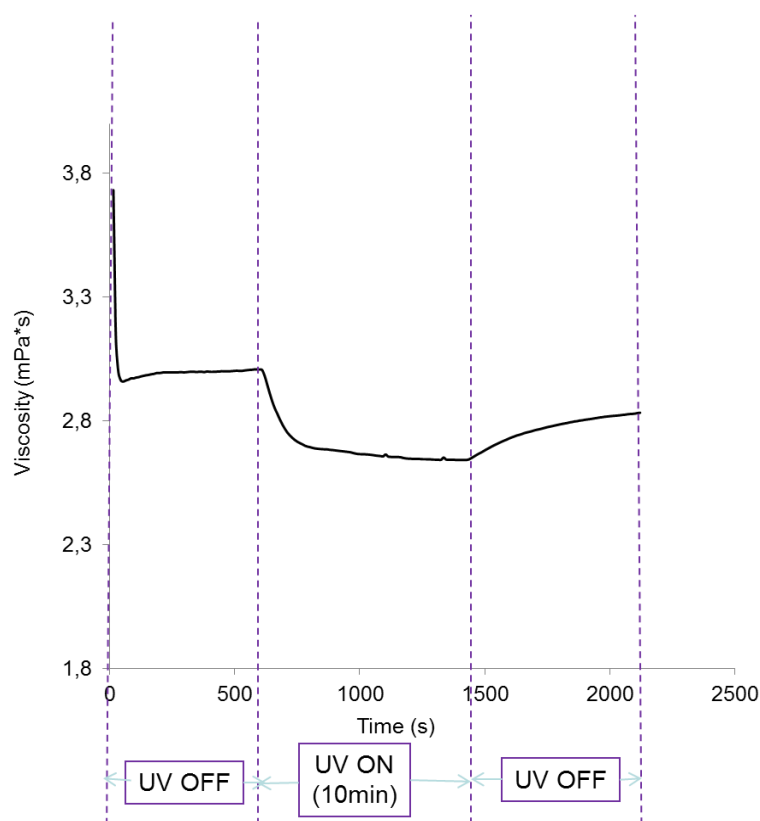
Figure 4.1.18 Viscosity vs. time of CV2.1 azobenzene copolymer in 15 mg/ml DMSO solution (10 min in the dark, 14 min exposed to UV light and 10 min in the dark), σ=1Pa, T=25°C.

A typical viscosity-time graph for the azobenzene copolymer solution is depicted in Figure 4.1.18. A short time of 5-10 min was required at the beginning of the

experiments for the system to achieve a stable rotation. The viscosity did not decrease even though the solutions were under continuous shear. By irradiating the solutions with UV light the viscosity appeared to decrease dramatically by 6.5% within a couple of minutes. The apparent changes revealed the completion of photoisomerisation that occurred during that short period of time and were also confirmed by UV/Vis spectroscopic studies in the previous section 4.1.2.4. After 14 min of exposure time the solution managed to reach a minimum level of viscosity. When the solution stopped being irradiated, the viscosity data continued to be collected until a steady level was reached. The viscosity increased gradually almost by 3% due to the rearrangement of the azopolymer chains caused by the UV-induced isomerisation. Therefore, the net photoviscosity decrease of the poly(MMA/MOAB) solutions with 3.2% azobenzene loading came at 5%.
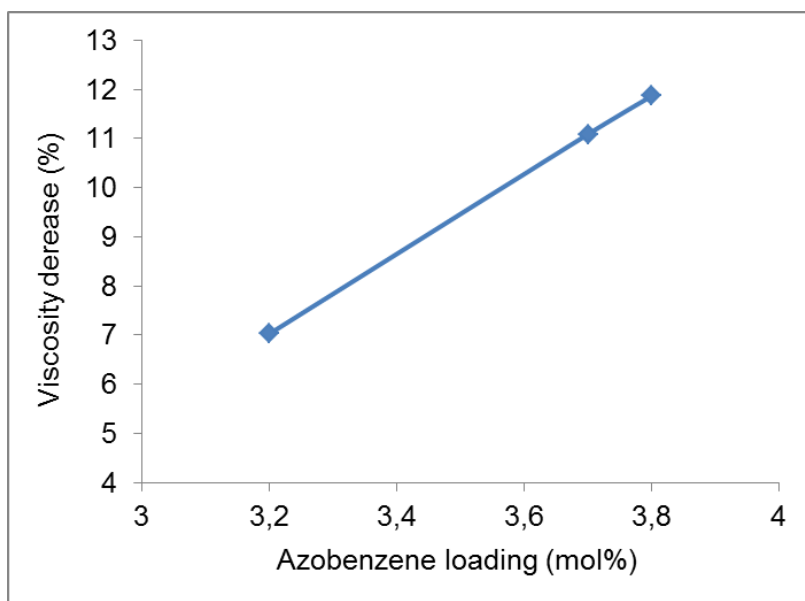
Figure 4.1.19 Viscosity decrease vs. azobenzene loading

Since the experiments were performed in a temperature controlled environment no significant heating effect was there. Therefore the photoinduced changes in

viscosity were attributed clearly to the *trans→cis* isomerisation by UV light which is already examined and reported in previous studies by capillary type rheometer.[60, 65, 69] Furthermore the noticeable changes were influenced by the amount of the azobenzene loading in the polymeric side chains. This behaviour was found to be in accordance with previous investigations in MMA/MOAB copolymers.[19] The graph in Figure 4.1.19 presents the positive and linear correlation between % decrease of viscosity and the % mol of the azo-molecules. The photoviscosity effect appears higher by increasing the azobenzene mol% within the loadings studied in this programme.

Table 4.1.9 Comparison of photoviscosity data of azobenzene copolymers, 15 mg/ml concentration in DMSO with respect to their M_w, after 10 min UV irradiation

Polymer	AB loading (mol %)	η decrease %	η increase %	M_w	PD
CV2.1	3.2	7.03	2.71	77,190	1.56
CV2.2	3.7	11.09	0.29	65,785	1.78
CV2.3	3.8	11.87	1.04	114,096	1.64

From the viscosity measurements that were conducted, the decrease of viscosity upon UV irradiation and its increase after pausing the UV irradiation were calculated. The results of the three different copolymers dissolved in DMSO are shown in the Table 4.1.9. The overall decrease of the photoviscosity (after the UV light was switched off) was found to be 10.8% for the CV2.2 and CV2.3 and 5% approximately for the CV2.1. The concentration of azobenzene affected the changes as discussed above. On the other hand, the weight

average molecular mass did not show any influence on the viscosity decrease of the copolymers.
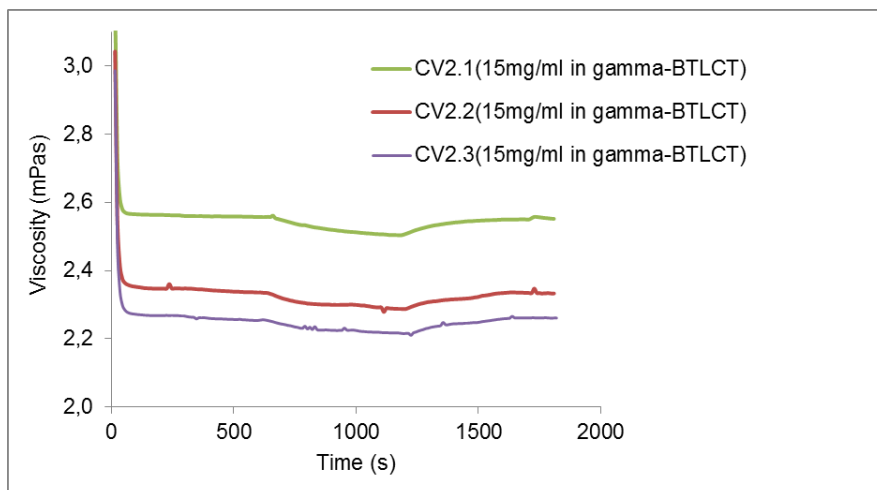
Figure 4.1.20 Solutions of CV2.1, CV2.2 and CV2.3 in 15mg/ml γ-BTLC solution after 5 min UV irradiation

The viscosities of CV2.1, CV2.2 and CV2.3 samples were further investigated in γ-butyrolactone (BTLC) in order to explore the photoviscosity effect in a different solvent. This solvent was selected due to its non-volatile character and tested before and after UV irradiation without any observed viscosity change. In Figure 4.1.22 the rheological results from the MMA/MOAB copolymer solutions in BTLC with 15 mg/ml concentration are demonstrated. Upon UV irradiation a significant 2% decrease in viscosity was observed. The total recovery of the viscosity after a pause of the UV light irradiation indicated that this solvent may not be suitable for photoviscosity measurements.

4.1.2.7 Nanoindentation measurements

4.1.2.7.1 Effect of azobenzene loading on acrylic polymer's hardness and stiffness

Initial experiments for the investigation of photoinduced changes in stiffness were conducted on a P(MMA/MOAB) film with 3.5 mol% azobenzene loading. Figure 4.1.24 illustrates a representative load-depth curve of an azobenzene copolymer film that was examined by nanoindentation. The initial (red color) curve corresponds to a film before irradiation. After 10 min of exposure to UV light the load-depth curve (blue) shifted to the left indicating an increase in the material's hardness. It should also be noted that the elastic modulus of the film increased significantly upon UV irradiation.

 The increase of the Vickers Hardness and of the elastic modulus is plotted in Figure 4.1.23. It can be observed that the hardness of the polymeric film with 3.5% azobenzene loading increased by 29% upon 10 min of UV irradiation. Previous studies explored the changes in hardness in SRG azobenzene films with homopolymers (100 mol% azobenzene) and found a 20% increase.[153]

The larger increase was probably due to higher azobenzene loading. Furthermore the overall stiffness of the film achieved a noticeable increase by about 5%, from 3.84 GPa to 4.04 GPa. Nanoindentation studies of 4-methacryloyloxyazobenzene/ methylmethacrylate copolymer films showed a 10% increase in stiffness corresponding to 6 mol% azobenzene concentration

which is in good agreement with the obtained data.[35]

In order to determine the elastic modulus and its changes upon exposure to UV and visible light a series of nanoindentation tests (6-10 measurements for each sample) were performed. The effect of azobenzene loading on the polymeric films of PMMA and the copolymers of methymethacrylate and methacryloyloxyazobenzene with 10%, 20%, 30%, 45%, 65%, 80% azobenzene loadings was evaluated under identical conditions. Polymer films with more than 65% azobenzene loading were too brittle to be suitable for nanoindentation experiments. The brittleness of the polymers with high

azobenzene loadings is thought to reflect their liquid-crystalline behaviour. [36, 41, 52]
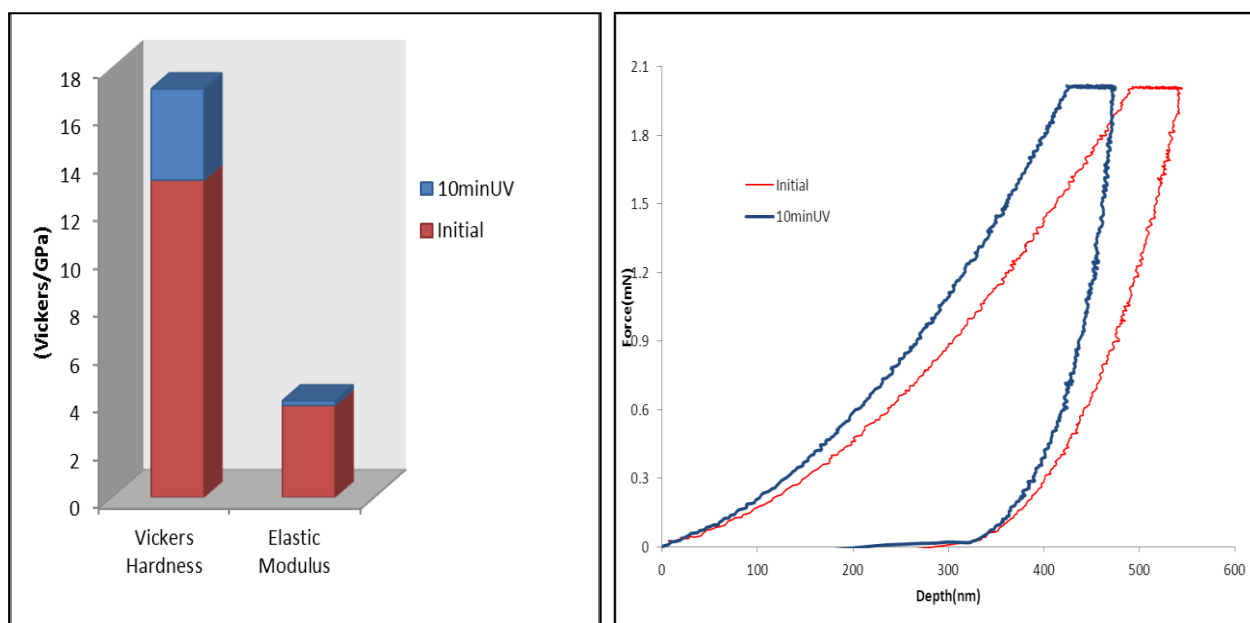
Figure 4.1.21 Increase in hardness (Vickers) and in elastic modulus (GPa) after 10 min of UV exposure

Figure 4.1.22 Loading and unloading vs. indentation depth in P(MMA/MOAB) film before and after 10 min UV irradiation

Typical nanoindentation curves of the 30% P(MMA/MOAB) film are shown in Figure 4.1.23 before and after UV irradiation. After 1 hr of exposure to UV light the loading curve remains almost unchanged, indicating no significant change to the hardness of the film. Contrariwise, the *dP/dh* slope of the curve, upon unloading, changed significantly after irradiation justifying the increase in stiffness.[153]

The films in this investigation were kept in the dark for a week in order to ensure that all the *cis* isomers, formed during material processing and handling under ambient light, were reverted to their *trans* form. The nanoindentation experiments were carried out on the virgin films and after irradiation with UV light for 1 hr. In order to exclude the photoinduced heating effect the irradiated

films were allowed to cool for 2 hrs, in the dark, to allow the films to reach room temperature before being subjected to the nanoindentation experiments.
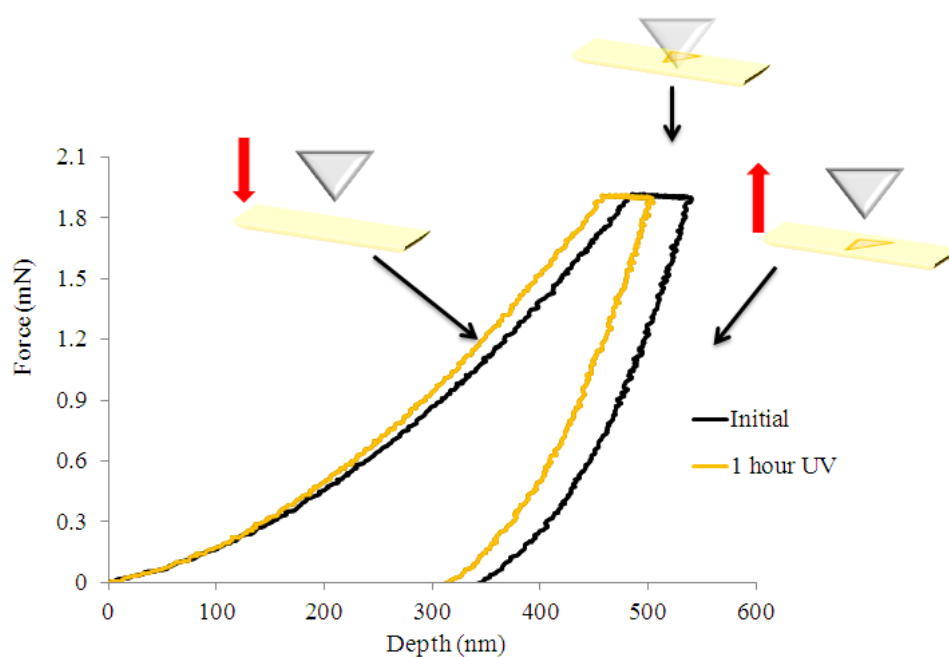
Figure 4.1.23 Characteristic loading-pause-unloading vs. depth curve of 30% P(MMA/MOAB) film before and after 1 h UV irradiation. The black line corresponds to the non-irradiated azobenzene film and the orange line to the irradiated film.

After the tests the films were left in the dark for 16 hrs and a third round of nanoindentation tests was performed to observe the recovery of the *cis* isomers to their *trans* form. Finally, the films were exposed to visible light for 30 min to allow a total conversion of the *cis* isomers to their *trans* form. Table 4.1.10 enlists the nanoindentation measurements of all the films with different azobenzene loading including their increase after UV and visible irradiation. The results are demonstrated better in the following Figure 4.1.25 and discussed in details.

Table 4.1.10 Stiffness measurements from nanoindentation testing of solid films with various azobenzene loading

Names	10%P(MMA/MOAB)	15%P(MMA/MOAB)	20%P(MMA/MOAB)	30%P(MMA/MOAB)	45%P(MMA/MOAB)	65%P(MMA/MOAB)
Initial stiffness (GPa)	3.60 ± 0.07	3.65 ± 0.06	3.71 ± 0.07	3.16 ± 0.08	3.52 ± 0.15	3.72 ± 0.02
Stiffness after 1 h UV irradiation (GPa)	3.67 ± 0.13	3.87 ± 0.10	4.09 ± 0.03	3.78 ± 0.05	3.84 ± 0.14	4.03 ± 0.05
Stiffness after storange in the dark (GPa)	3.79 ± 0.09	3.67 ± 0.09	3.85 ± 0.06	3.38 ± 0.06	3.72 ± 0.06	3.91 ± 0.06
Stiffness after 30 min visible irradiation (GPa)	3.52 ± 0.09	3.63 ± 0.14	3.86 ± 0.05	3.53 ± 0.07	3.95 ± 0.07	3.93 ± 0.05
Increase in stiffness after UV irradiation	2%	5%	10%	19%	9%	6%
Increase in stiffness after visible irradiation	-	-	4%	12%	11%	8%

Figure 4.1.24 shows how the elastic modulus of P(MMA/MOAB) film containing 30% azobenzene varies under exposure to different stimuli. Upon irradiating with UV light for 1 hr, the elastic modulus showed a significant increase. Upon storage in the dark the modulus decreased and after visible irradiation it reached a final value higher than the initial one. The observed changes of modulus were expected to occur due to the photoisomerisation of azobenzene chromophores in the polymer and are in agreement with the literature.[35] When

the polymers were irradiated with UV light, the *trans* isomers transformed to their *cis* forms with an associated reorganization of the polymer chain,[153] resulting in an increase in the elastic modulus. When the azobenzene chromophores reverted back to the *trans* form, the film became slightly softer as a result of a density decrease and reorganisation of the polymer chains. It is apparent that the modulus did not reach the initial value presumably because of
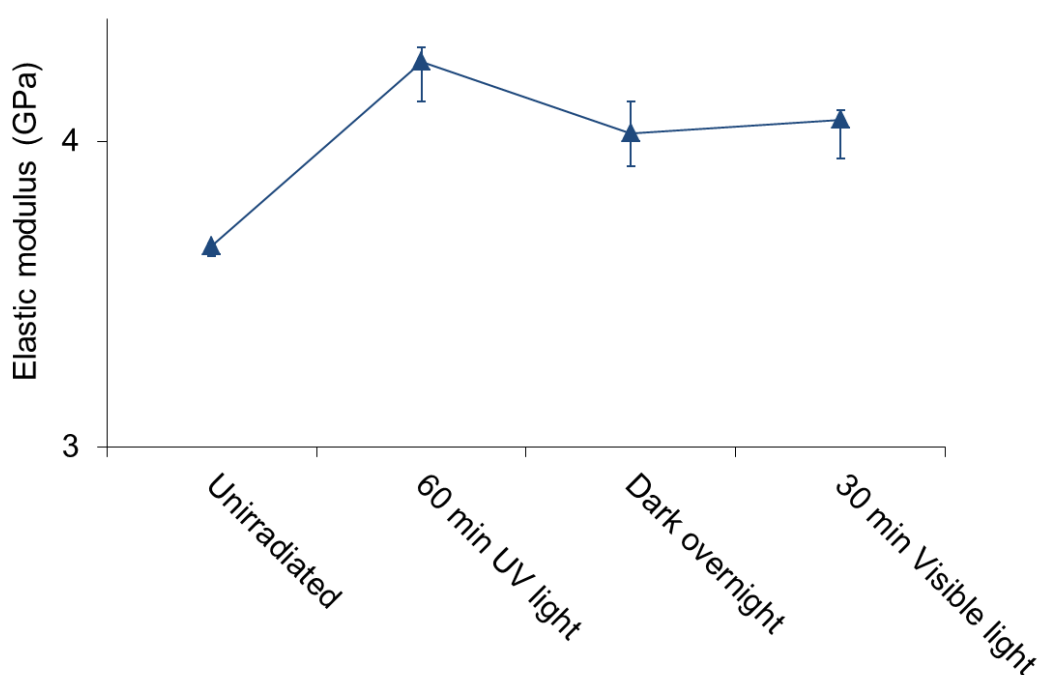
Figure 4.1.24 Typical graph of stiffness vs. time of 30% P(MMA/MOAB) film

the incomplete rearrangement of the polymeric chains in the solid film, although complete *cis→trans* isomerisation was achieved.

Figure 4.1.25 presents the percentage increase in stiffness of the MMA/MOAB copolymer films compare to their initial unirradiated values within the specific azobenzene loadings. It is clearly shown that the photo-driven stiffness is

147

influenced by the amount of chromophores in the polymers. Following UV irradiation for 1 hr, the elastic modulus increased linearly up to 30 mol% azobenzene loading, reaching a maximum value of 19%. Above 30 mol% loading the stiffness changes started to decrease and reached a low value for 65 mol% loading. This suggests that maximum stiffness increase can only be achieved with 30 mol% azobenzene loading. A previous study demonstrated a maximum of 10% increase of stiffness with 10 mol% azobenzene loading.[35] The authors did not investigate the effect using higher azobenzene loading and they attributed the mechanical changes to the photoisomerisation of the azobenzene chromophores.
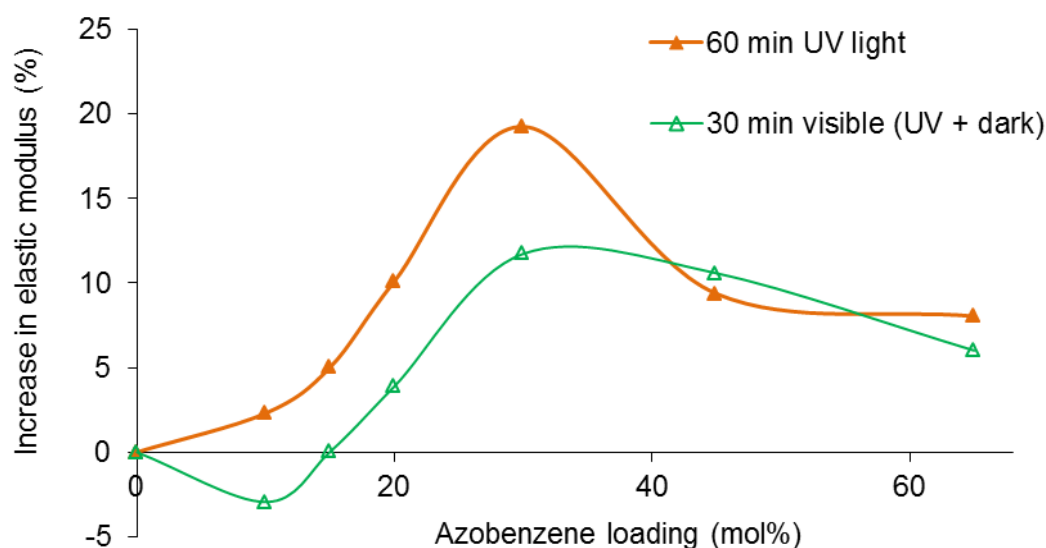
Figure 4.1.25 Photo-stiffness after UV (filled symbol) and a cycle of UV, dark and visible light (unfilled symbol) at various chromophore loadings

Variation of increase in stiffness after a further 30 min of visible irradiation of the films that were previously irradiated with UV light for 1 hr and stored in the dark

for 18 hrs, are shown in Figure 4.1.25. Theoretically the samples irradiated with visible light should have the same stiffness values as the virgin (non-irradiated) films. Nevertheless it was observed that the azobenzene molecules in their *trans* isomeric form enhanced the initial values (non-irradiated). The increase in elastic modulus after visible irradiation followed a trend similar to the one after UV irradiation. As seen in the graph in Figure 4.1.25, the elastic modulus increased linearly up to 30 mol% azobenzene loading, achieving the highest value of 12%. The polymers without azobenzene did not exhibit any significant stiffness changes after visible irradiation. The films containing 10 mol% azobenzene demonstrated a 3% decrease in elastic modulus compare to the virgin films. This decrease could be due to exposure of the virgin films to room light which would lead to the coexistence of both *trans* and *cis* azobenzene isomers into the polymeric matrix. Polymers containing 15 mol% azobenzene loading recovered completely (0% increase in stiffness). Presumably this (15 mol%) chromophore amount is the limit that can induce reversible changes to the whole polymeric matrix after exposure to UV and visible irradiation respectively. The polymers with azobenzene loadings above 30 mol% demonstrated higher stiffness values after visible irradiation (*trans* azobenzene) than the non-irradiated polymers but lower values than after UV irradiation (*cis* azobenzene). The results suggest that the concentration of the azobenzene chromophores in a polymer matrix plays a major role in the modulus changes.

The photoinduced changes in elastic modulus are attributed to the intra-molecular conformational changes of the azo-polymers due to the reversible *trans* to *cis* photoisomerisation, which is confirmed in the section below. After 30 min of visible irradiation, all the polymers consisted only of *trans* azobenzene isomers. Complete recovery of the elastic modulus was not achieved by visible light although reversible isomerisation was completed possibly due to the fact that UV-induced isomerisation forced the polymer chains to be coiled up but they could not be reorganised to their relaxed state in solid film within the experimental time available.[154]

RESULTS AND DISCUSSION

The *trans* isomers are changing their structure due to UV irradiation to *cis* form with associated reorganisation of the polymeric chains. Moreover the azobenzene units of the polymeric films may form cross-linkings upon UV irradiation and thus could explain the increase in stiffness and in hardness.[153] PMMA films do not indicate any increase upon UV irradiation.[35, 153] Therefore the effect is believed to be caused purely by isomerisation of azobenzene. Finally it should be noted that no heating effect was involved in the changes. During the UV exposure it is expected a temperature rise which could induce softening of the films by lowering the stiffness and the hardness.[69] However these results are opposite to that because the samples were left for 1 to 2 hrs to cool down to room temperature and then were tested. Another factor that should be considered in addition to these results is that each polymer has different chain length and T_g as presented in sections 4.1.2.2 and 4.1.2.5. These properties might affect the polymer's stiffness regardless the azobenzene loading.

4.1.2.7.2 Nanoindentation analysis of the azobenzene epoxy resins

After ensuring that the azobenzene molecules were capable of reversible isomerisation within a polymeric network in solid phase, induced by light, the following step was to characterise the epoxy-based polymer matrix that the composites were consisted of. The azobenzene resins' mechanical properties and their ability to recover back to their initial shape after the creation of indents were investigated. The nanoindentation tests were performed to pristine and subsequently UV irradiated azobenzene films with 0%, 5% and 10% loading. The results are tabulated in Table 4.1.11, showing not-significant change on the elastic modulus (stiffness) and an apparent softening after UV irradiation of the epoxy resin films. The hardness of the 5% and 10% azobenzene films decreased by 23-26%, an effect that is in agreement with the literature because of the light-induced free volume formation due to photoisomerisation.[16, 155]

RESULTS AND DISCUSSION

Table 4.1.11 Hardness data from nanoindentation of azobenzene films before and after UV irradiation

	Stiffness (GPa)	Hardness (MPa.)
Initial reference film (0% AB)	3.87 ± 0.19	278.55 ± 96.54
UV irradiated reference film (0% AB)	3.84 ± 0.14	281.42 ± 82.89
Initial 5% AB/ epoxy resin film	3.71 ± 0.06	273.91 ± 56.42
UV irradiated 5% AB/ epoxy resin film	3.66 ± 0.12	202.17 ± 36.53
Initial 10% AB/ epoxy resin film	3.73 ± 0.11	255.62 ± 31.45
UV irradiated 10% AB/ epoxy resin film	3.75 ± 0.10	188.67 ± 19.77

The most appealing photoinduced changes that were produced during nanoindentation experiments were the physical. After penetrating the specimens by the indenter, images were captured before and after UV irradiation. Figure 4.1.26 illustrates the indents of the reference sample before and after irradiation with UV light. The reference sample was an epoxy resin film that did not contain any azobenzene molecules. No differences were apparent after the UV treatment. The indents on the two images were very similar to each other.

Remarkably, in Figure 4.1.27 three indentation marks are presented that were generated on the epoxy resin film containing 10% azobenzene before and after UV irradiation. Unlike the reference film, the highlighted indents of the azobenzene film showed a physical change after the film was exposed to UV light.

151
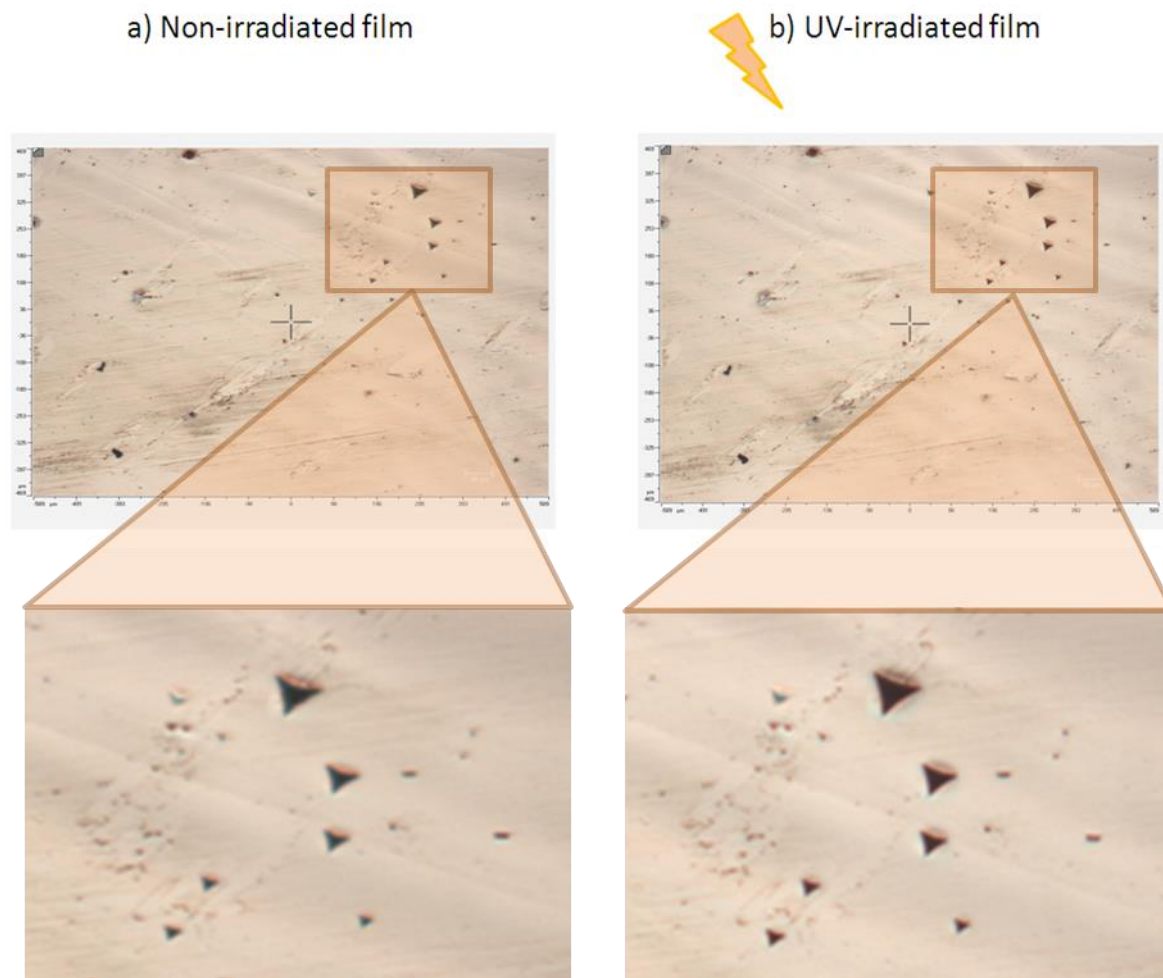
Figure 4.1.26 Images of indentation marks of an epoxy resin film a) before and b) after UV irradiation with their enlarged views.

All the three indents appear to have disappeared and only the triangle outline was slightly apparent. This effect is assumed to occur due to the *trans→cis* photoisomerisation of the azobenzene molecules. The latter could initiate an additional motion of the polymeric chains and pull them together to recover to a more relaxed state after the stress that was produced after the indentation. The interactions of azobenzene molecules in a polymeric system for assisting the achievement of a complete healing effect have been previously reported.[24, 76] The healing mechanism occurred after UV light irradiation that induced a

transition from a heterogeneous (gel.) to a homogeneous (sol) state of silicon-based composites with doped azobenzene molecules (5-10 mol%). The microparticle/liquid crystal gels were reconstructed in the homogeneous (fluidic) sol state.
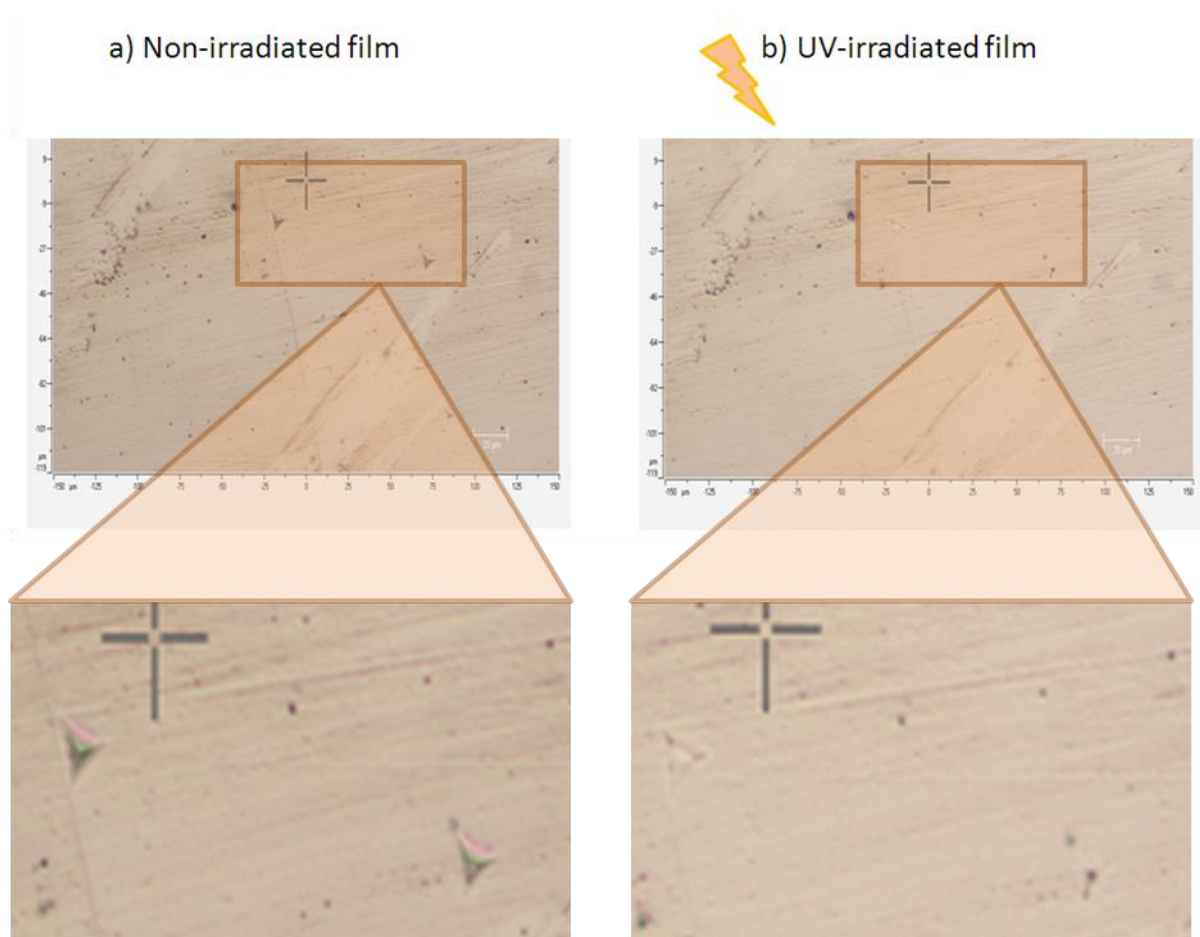
Figure 4.1.27 Images of indentation marks of an azobenzene-based epoxy film a) before and b) after UV irradiation with their enlarged views.

In order to exclude the possible recovery of the azobenzene films by thermal effect, the cured films with and without azobenzene content were analysed by DSC. It was found that their T_g is quite similar, 81°C (reference) and 83°C (azobenzene epoxy). The UV light exposure with a 1000 mW/cm^2 intensity was not capable of producing these temperature values during the specific period (1

hr) of irradiation time. Therefore it was assumed that the free polymer chains between the crosslinks gained higher mobility due to the *trans→cis* isomerisation of the azobenzene, triggered by the light.

These studies demonstrated that UV light can also induce physical shape changes when a polymeric film contains azobenzene.[18, 156]

4.1.2.8 Healing behaviour of the azobenzene thermoplastic and thermoset films

After the nanoindentation experiments where healing of the indents was observed in cured epoxy (thermoset) films containing azobenzene after UV irradiation, further investigation on P(MMA/MOAB) copolymers (thermoplastics) was conducted. In order to observe the physical changes due to UV irradiation, indented images of the films of PMMA and azobenzene-based copolymers were captured with a conventional optical microscope.

Figure 4.1.28 a and b show the pre- and post-irradiated indents of a P(MMA/MOAB) film containing 45 mol% azobenzene in the polymer side chains. Comparison of Figure 4.1.28 a and b confirms that the depth of the indent decreased when the film was subjected to 1 hr UV radiation.

The healing of the indent could be attributed to photo-heating effect that softened the irradiated region leading to material movement to the voids in the film or the *trans→cis* isomerisation which offered a volume change in the film, which consequently contributing to the movement of the material in the void region. However, irradiation of the indented virgin film with visible light did not show any healing effect although visible light irradiation increased the film temperature more than the UV irradiation suggesting that the healing effect was not due to photo-thermal effect. Irradiation of the healed films with visible light did not revert the healed region to the indent shape although *cis* isomers were converted to the *trans* counterpart, signifying that the healing is not reversible.
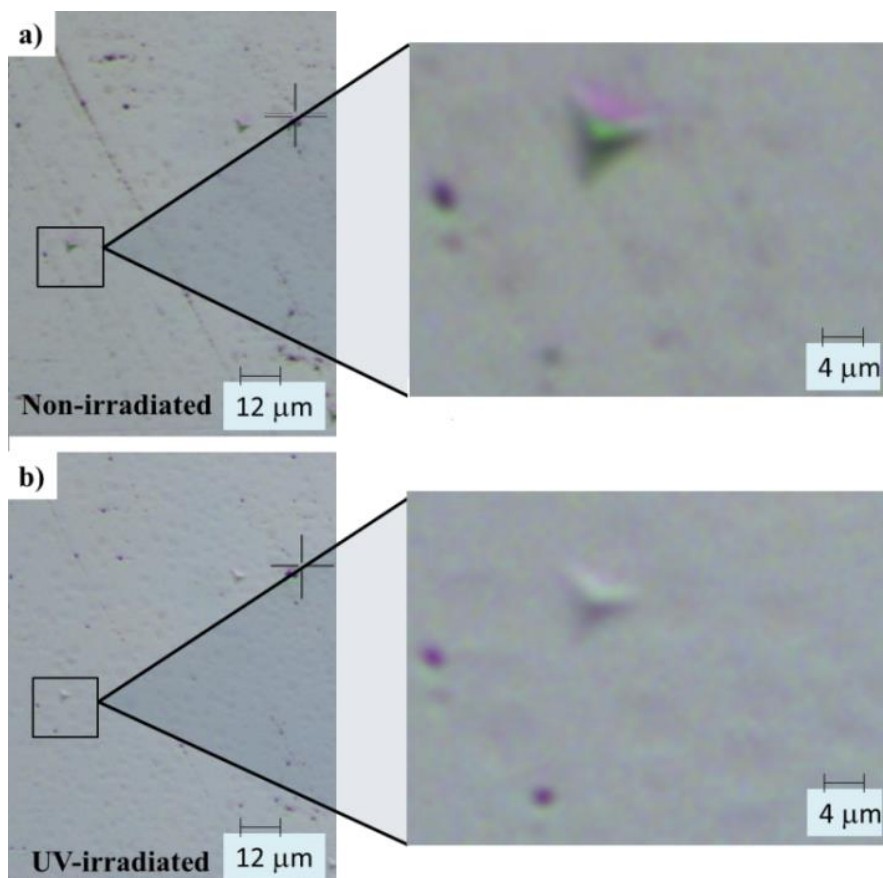
Figure 4.1.28 Image of the 45% P(MMA/MOAB) film after nanoindentation before and after exposure to UV light a) non-irradiated and b) after 1 h UV irradiation with their enlarged views,

Figure 4.1.29 a and b show the indents of a pre- and post-irradiated PMMA film with no azobenzene. No healing of the indent was observed in Figure 4.1.29 b when the film was irradiated with UV light for 1 hr suggesting that the healing behaviour in Figure 4.1.28 was not caused by the photo-thermal softening of the materials but instead it was the effect of photoisomerisation of azobenzene in the film. If this had been caused by the photo-thermal effect the indent in the PMMA film would also have been healed. This finding suggests that this class of polymers can be used as a self-healing agent for damage repair by UV light. Partial healing of photochromic polymer films has been reported previously but in softer, gel-like materials.[76]
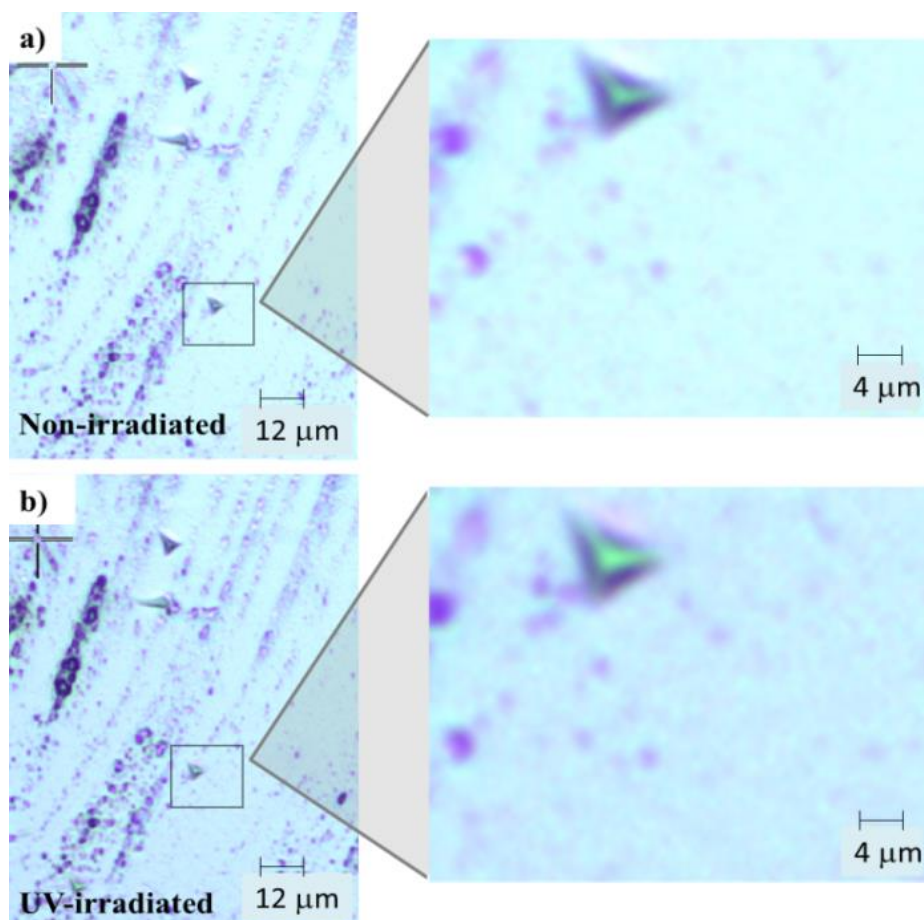
Figure 4.1.29 Image of the PMMA film after nanoindentation before and after exposure to UV light a) non-irradiated and b) after 1 h UV irradiation with their enlarged views

This experimental method was then extended to indentation conditions to obtain quantitative recovery data after exposing the thermosetting films containing azobenzene to UV light. The calculations of these ratios were established by AFM measurements after the creation of various penetrations at a nano- and micro-scale level. Some scratches on the surface of the films were applied using a diamond tip scriber and a pinhole was created with a common pin made

of steel. Initially, the reference sample was examined for ensuring that the physical changes were not attributed to the epoxy polymeric matrix. In Figure 4.1.30 the 3D images of the cured epoxy resin film that does not contain any azobenzene molecule, before and after UV irradiation, are illustrated. Two scratches of 56 nm and 105 nm depth were created initially and after the UV treatment no significant recovery was observed. Therefore it can be confirmed that this epoxy system does not exhibit any shape memory or healing behaviour.

The depths of the indents that were created on the films' surfaces pre- and post- UV irradiation can be found in Table 4.1.12. Profiles were taken along a line from the indent's deepest point through the matrix to ensure the same section was being examined.

The healing ratio (HR) percentages have been also calculated using the Equation 4-2, where d_I is the initial depth (nm) before irradiation and d_{UV} the depth (nm) after 1 hr exposure to UV light.

$$HR = \frac{(d_I - d_{UV})}{d_I} \; x \; 100\%$$

Equation 4-2

The 10% azobenzene-based epoxy films were analysed under the same conditions, but this time the penetration depths were even higher or larger than the ones in the reference film. Figure 4.1.31 depicts 3D images of the azobenzene film before and after exposure to UV light accordingly. The scratches with initial 948 nm and 400 nm depth heights, after 1 hr UV irradiation presented a smoother surface profile. Their healing ratios were found to be 55% (948 nm) and 68% (400 nm) respectively. Similarly, two additional scratches of 772 nm and 132 nm depth, as shown in Figure 4.1.32, confirmed the healing behaviour of the azobenzene thermosets, demonstrating a 73% (772 nm) and 72% (132 nm) healing ratio after exposure to UV light. The observed recovery

that the films presented can potentially be attributed to the *trans→cis* photoisomerisation of the azobenzene, as explained in the previous section 4.1.2.7.2 (nanoindentation).
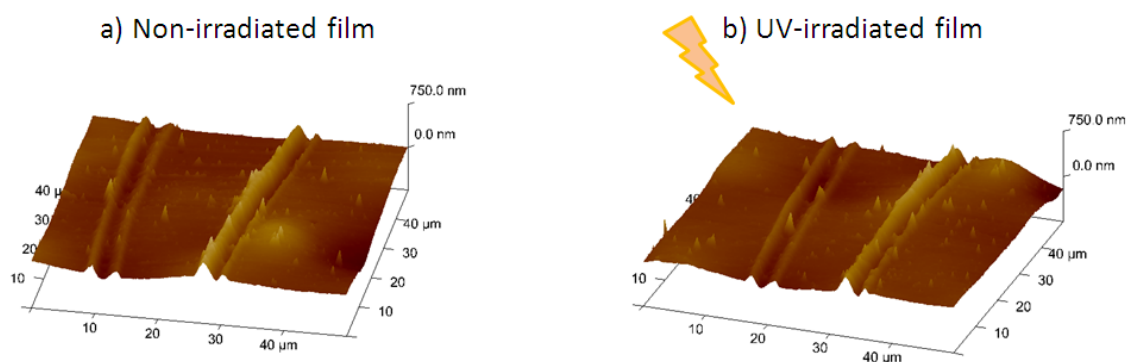
Figure 4.1.30 3D AFM topographic images of two scratches on an epoxy resin film (reference sample) a) before and b) after 1 hour UV irradiation, with Z-range of inset images at 750 nm for comparative purposes
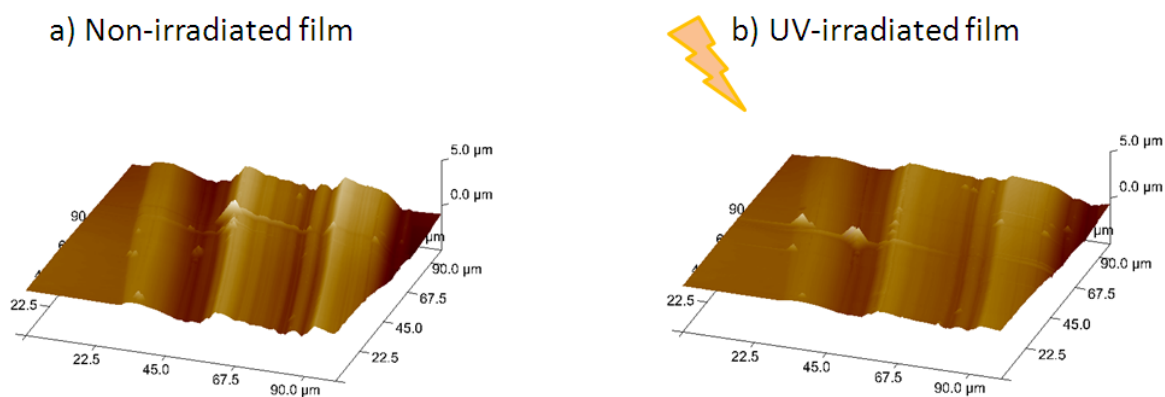
Figure 4.1.31 3D AFM topographic images of two scratches on a 10% azobenzene-based epoxy resin film a) before and b) after 1 hour UV irradiation, with Z-range of inset images at 5 μm for comparative purposes
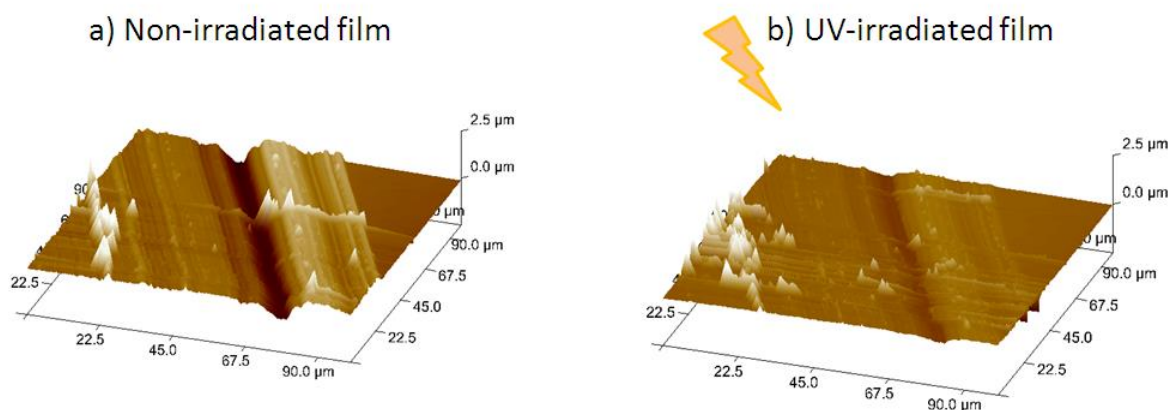
Figure 4.1.32 3D AFM topographic images of two extra scratches on a 10% azobenzene-based epoxy resin film a) before and b) after 1 hour UV irradiation, with Z-range of inset images at 2.5 μm for comparative purposes
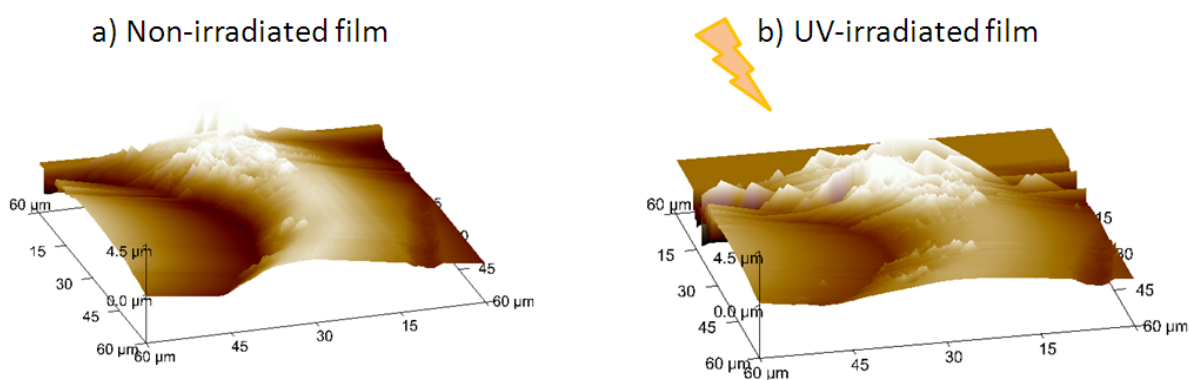
Figure 4.1.33 3D AFM topographic images of a pinhole on a 10% azobenzene-based epoxy resin film a) before and b) after 1 hour UV irradiation, with Z-range of inset images at 4.5 μm for comparative purposes

A further indent of a pinhole on the azobenzene film is illustrated in Figure 4.1.33. The initial depth that occurred at a maximum of about 2.7 mm. In this case, after the UV treatment the healing ratio was found to be 40%. The recovery effect was smaller here possibly because the damaged area was too large.

159

Table 4.1.12 Depths and healing ratio measurements of indents (scratches and pinhole) of epoxy based films

	10% AB/ epoxy resin (scratch 4)	10% AB/ epoxy resin (scratch 2)	10% AB/ epoxy resin (scratch 3)	10% AB/ epoxy resin (scratch 1)	10% AB/ epoxy resin (pinhole)
Initial depth (d_I, nm)	132.39	400.19	771.65	947.80	2675.01
Depth after 1hr UV irradiation (d_{UV}, nm)	37.36	127.62	208.46	430.07	1607.49
Healing ratio (HR, %)	72%	68%	73%	55%	40%

Here for the first time, the healing ratio of an azobenzene rigid network was identified and quantified. Previous authors observed a gel-sol transition in azobenzene composite gels, after UV irradiation, which was attributed to the azobenzene and acted as a repairing mechanism for surface cracks.[24]

4.1.2.9 Density measurements of azobenzene polymers

After demonstrating the healing behaviour of azobenzene polymers it was necessary to investigate if the photo-induced physical changes occurred due to volume changes after the azobenzene isomerisation. Therefore the densities of all the films containing 0%, 10%, 20%, 30%, 45%, 65%, 80% and 100% azobenzene were measured before and after exposure to UV light. The mass

and density of the samples remained constant before and after UV irradiation (Table 4.1.13) suggesting that the films were completely dried before the analysis and the volume of the solid films did not change due to reversible isomerisation. Thus there were no volume changes after reversible *trans→cis* isomerisation.

It should be noted here that other authors attribute the photo-induced changes to volume changes that occur after azobenzene isomerisation but none of them have presented any quantitative data with high-precision volume measurements (±0.02%) and true density calculations, such as pycnometry results.[157-159]

Table 4.1.13 Characteristic density data of the azobenzene polymeric films

Names	Mass before UV light (g)	Mass after UV light (g)	Density before UV light (g/cm^3)	Density after UV light (g/cm^3)
0% PMMA	0,958	0,957	1,199	1,202
10% P(MMA/MOAB)	0,929	0,927	1,208	1,206
20% P(MMA/MOAB)	0,953	0,952	1,200	1,202
30% P(MMA/MOAB)	0,946	0,944	1,194	1,191
45% P(MMA/MOAB)	0,955	0,953	1,213	1,211
65% P(MMA/MOAB)	1,205	1,204	1,206	1,208
80% P(MMA/MOAB)	0,948	0,947	1,210	1,212
100% PMOAB	0,967	0,965	1,200	1,197

4.1.2.10 Ultrasound wave as a stimulus for *cis→trans* isomerisation

4.1.2.10.1 Ultrasound treatment of polymer thin films

In this study the effect of sonication on the possible switching behaviour of the azobenzene chromophores in the solid copolymer films was investigated. Surampudi *et al.* very recently demonstrated that by exposing solutions of methacrylic polymers, with azobenzene in the main chain, to ultrasound waves, *cis→trans* isomerisation can be induced.[67] This phenomenon was attributed to a stretching force that causes stress on the N=N bond resulting in azobenzene isomerisation. Surampudi's studies were based on spectroscopic analyses and any temperature rise due to ultrasound treatment was not taken into consideration.

For this PhD project, the temperature effect due to ultrasound waves was taken into account and described here, for the isomerisation of azobenzene polymers in solid and liquid states. Studies on the effect of different temperatures for *cis→trans* isomerisation were conducted and enabled the identification of *cis→trans* isomerisation of azobenzene in all P(MMA/MOAB) thin films for the first time.

The UV/Vis spectra of the 20 mol% P(MMA/MOAB) thin films exposed to UV or visible light or ultrasound waves are shown in Figure 4.1.34. Figure 4.1.34a presents the *trans→cis* isomerisation in the thin films exposed to UV radiation. The spectrum has two distinct absorption bands at 318 nm which is attributed to the *trans* isomers due to π−π* transition state, and at 440 nm corresponding to the *cis* isomers due to the forbidden n−π* transition. The absorbance band at 318 nm sharply decreased and the weak band at 440 nm slightly increased after UV irradiation confirming *trans→cis* isomerisation. Complete *trans→cis* isomerisation was accomplished within 300 s of UV irradiation.
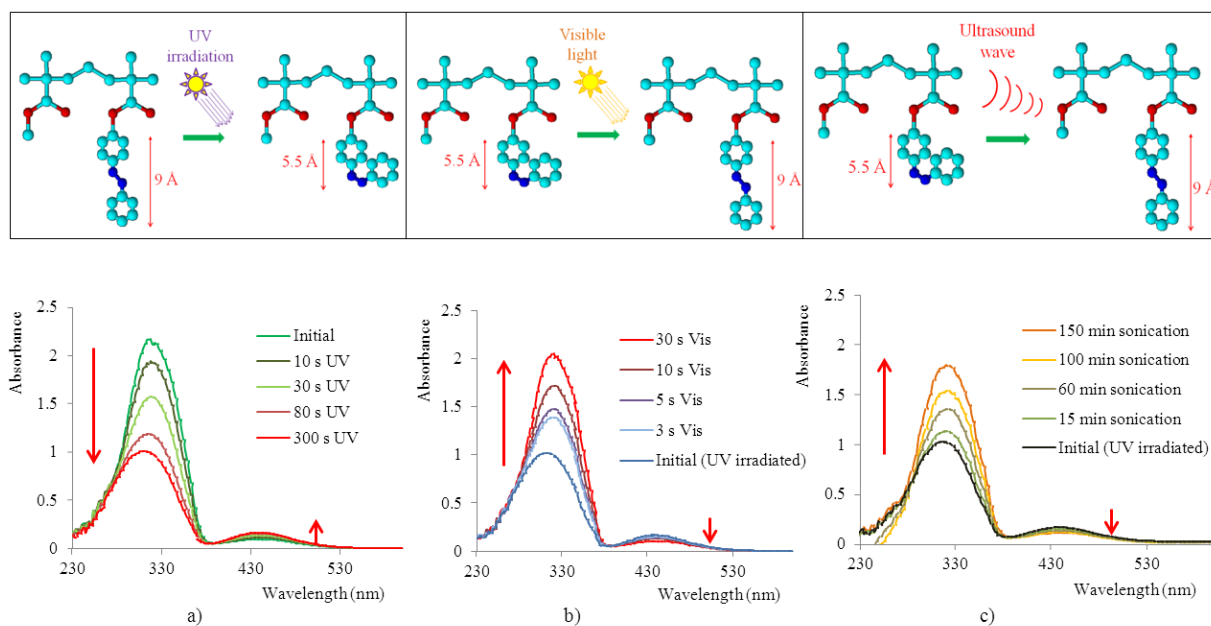
Figure 4.1.34 UV/Vis spectra of the 20%P(MMA/MOAB) film after a) UV irradiation, b) visible irradiation and c) exposure to ultrasound waves

Figure 4.1.34b presents the *cis→trans* isomerisation of azobenzene in the 20 mol% P(MMA/MOAB) films exposed to visible light. The intensity of the band at 318 nm increased noticeably after visible irradiation and the band at 440 nm decreased with irradiation time suggesting a reversion of *cis* isomers to their *trans* counterparts. Complete *cis→trans* isomerisation of the azobenzene in the polymers was accomplished after 30 s of exposure to visible light. The rate of *trans→cis* conversion was expected to be slower than the *cis→trans* conversion because: the intensity of the visible light (1000 mW/cm^2) was higher than that of the UV (500 mW/cm^2), and the *trans* form is thermodynamically more favourable (50 kJ mol^{-1} energy difference) than the *cis* form with twisted geometry.

A virgin film containing 20 mol% azobenzene chromophores in the *trans* form was subjected to ultrasound in order to study the possible *cis→trans* isomerisation by vibrational force. Figure 4.1.34c shows the UV/Vis spectra of the films exposed to ultrasound waves. The intensity of the *trans* peak at 318

163

nm increased with sonication time, while the intensity of the peak at 440 nm decreased suggesting that ultrasound induced switching of the *cis* azobenzene to the *trans* form in the solid films. Complete recovery of the *cis* isomers to the *trans* conformation in a copolymer with a 20 mol% azobenzene was achieved within 150 min which is significantly longer than the recovery time by visible light (30 s). Similar recovery behaviours were observed in all the polymer films containing different azobenzene loadings, and the results are shown in Figure 4.1.35.
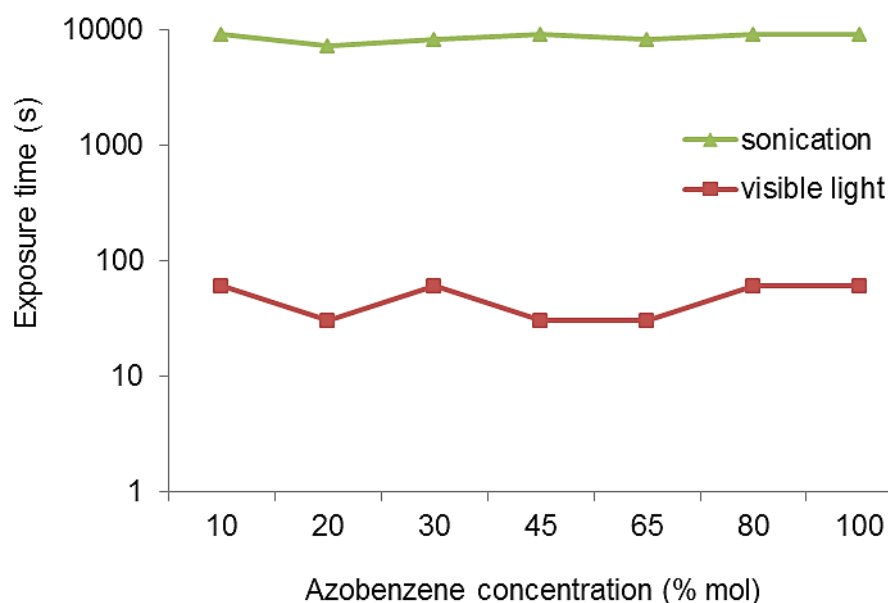
Figure 4.1.35 Required exposure time (logarithmic scale) to ultrasound waves and visible light for *cis→trans* isomerisation of thin copolymer films vs. azobenzene loading.

The graph combines the sufficient irradiation times for *cis→trans* conversion for all the polymers against their azobenzene concentration. The green triangles correspond to the sonication times and the visible irradiation times are represented by the red squares. The results suggest that in both cases the exposure time is independent from the azobenzene concentration of the

polymers. All the azobenzene copolymers were converted within 30-60 sec after visible irradiation while after exposure to ultrasound more time was required 120-150 min. The *cis→trans* isomerization of azobenzene films by visible light was noticeably much faster than by sonication. This could be explained by the fact that sonication is used to accelerate chemical reactions and because isomerisation can be considered as a two-sided reaction (*cis→trans*, *trans→cis*) of which both may occur simultaneously during sonication.[160] Since the *trans* isomer is predominant in the dark at room temperature and the energy barrier of the photoexcited state is ~23-50 kcal·mol^{-1}, the azobenzene molecules of the copolymers will convert to their *trans* form, as the more relaxed and stable isomeric form.[70]
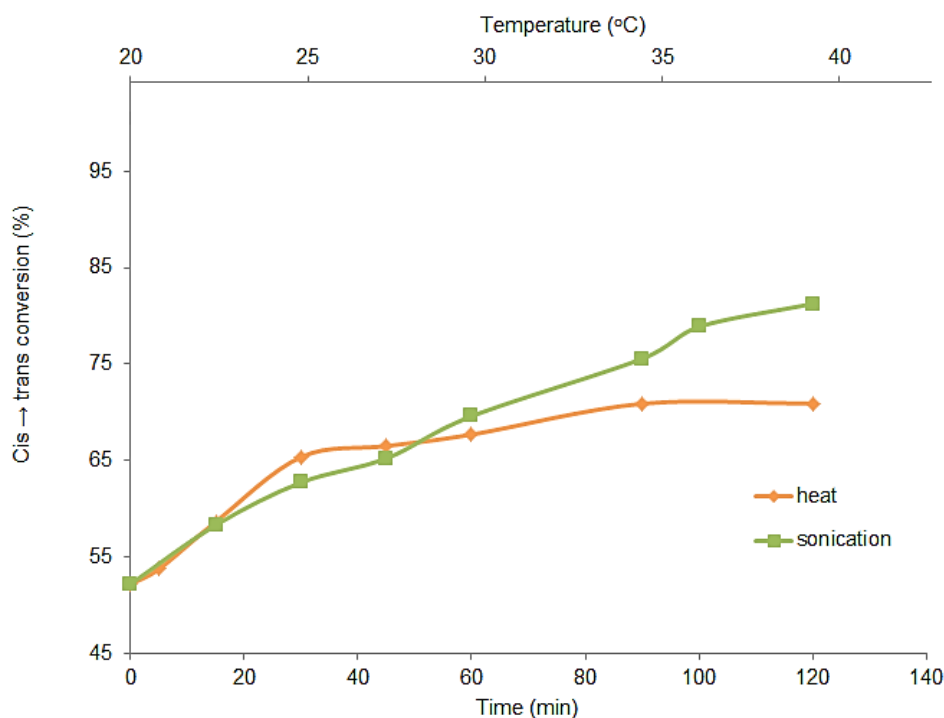
Figure 4.1.36 *Cis→trans* conversion (%) of 20%P(MMA/MOAB) thin films after exposure to heat and sonication

While temperature does not significantly alter the quantum yield of *cis→trans* isomerisation the quantum yield of *cis→trans* is significantly influenced by

thermal treatment. Thus it is necessary to quantify the *cis→trans* conversion by ultrasound induced temperature rise and ultrasound itself. Upon ultrasound treatment of the polymer films, the ultrasound bath showed a temperature rise by about 19 °C in 2 hrs. In order to identify how much *cis→trans* isomerisation was activated due to thermal relaxation and separate the isomerisation by ultrasound; experiments were repeated in a water bath at the same temperature windows (20-39°C) followed by periodic measurement of their UV/Vis spectra.

The progress of the thermal and ultrasound induced isomerisation as function of time are presented in Figure 4.1.36. The squares correspond to films that were in a sonication bath and the rhombuses to the films that were heated in a water bath. It was observed that only 20% of the *cis* isomers were converted to the *trans* form by ultrasonic agitation for 2 hrs whilst an additional 36% were isomerised by the associated temperature rise. It is clearly seen that both thermal and ultrasound treatments triggered the *cis→trans* isomerisation with the exposure time. The ultrasound triggered isomerisation was much faster than the thermal isomerisation. This is possibly due to a combined effect of ultrasound and associated heating effects by the rises in temperature of the polymer films. After sonicating for 120 min of the azobenzene films the *trans* isomers reached 81%, while the *trans* isomers reached 70% upon gradual heating the films from 20°C to 39°C for 2 hrs. This finding confirms that major *cis→trans* isomerisation during ultrasound agitation is triggered by the heating effect and a relatively lower portion was isomerised by ultrasound wave. Surampudi *et al.* reported 100% recovery of *cis* isomers to their *trans* counterparts.[67] The authors did not discount the possible temperature rise and associated *cis→trans* isomerisation from their findings. By discounting the ultrasound-induced heating effect it was confirmed that *cis→trans* isomerisation can be triggered by the treatment of ultrasound wave on solid polymer films.

The structural changes in the copolymers after sonication were confirmed by ^{1}H NMR spectroscopy. Deuterated dimethyl sulfoxide (DMSO-d_6) was used as the solvent. Typical ^{1}H NMR spectra of the pre- and post-treated P(MMA/MOAB) copolymer films are shown in Figure 4.1.37.
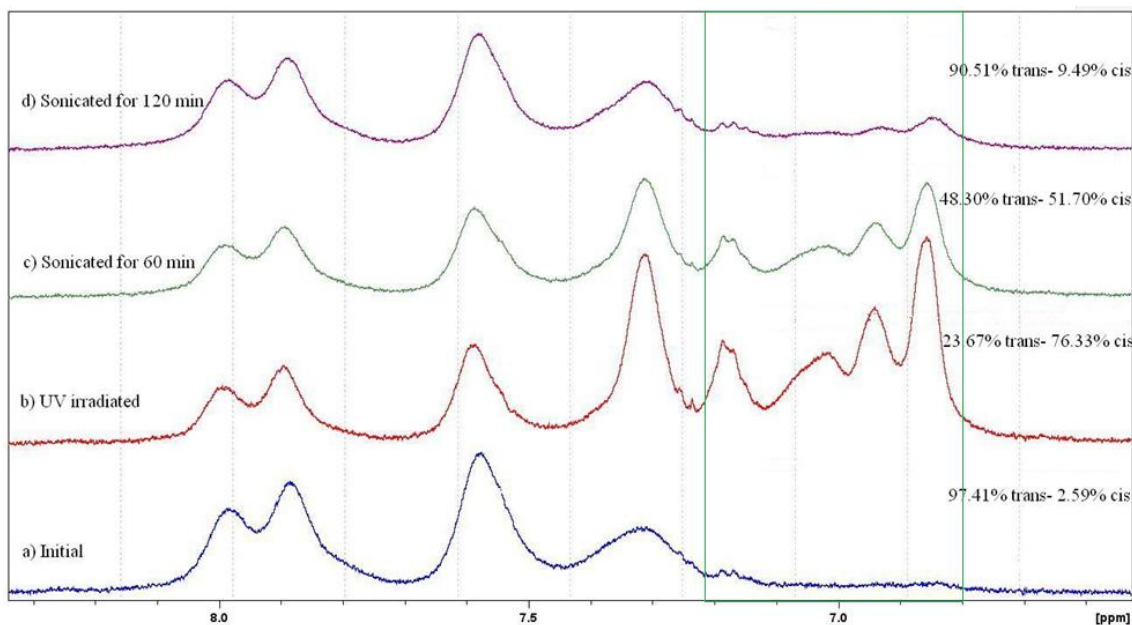
Figure 4.1.37 ¹H NMR spectra of the 20% P(MMA/MOAB) film a) un-treated film, b) 10 min UV irradiated film, c) 60 min sonication and d) 120 min sonication.

The spectrum of pre-treated film (Figure 4.1.37 a) showed three broad signals in the aromatic region. These resonance signals at 7.87–8.05 (4H) ppm, 7.48–7.62 (3H) ppm, and 7.20–7.43 (2H) ppm correspond to the protons from benzene ring of the *trans* azobenzene pendant chain. Upon 10 min of UV irradiation, additional signals appeared at 6.75-7.20 ppm (green region in Figure 4.1.37 b) while the intensity of the signals due to *trans* isomers decreased by 76.33%. These new signals (green region) are attributed to the aromatic protons from the *cis* configuration of the azobenzene in the polymeric chain. When UV treated film with 76.33% *cis* isomer was exposed to ultrasound waves for 60 min, the intensity of the chemical shifts at 6.75-7.20 ppm (Figure 4.1.37 c) decreased to 51.70% suggesting *cis→trans* isomerisation in the solid film. Further treatment of this film with ultrasound demonstrated a full recovery of the *trans* isomer from the *cis* form within 120 min as seen in Figure 4.1.37d. The UV/Vis and ¹H NMR spectroscopic results were found to be in good agreement

and demonstrated clearly that ultrasound waves can trigger the *cis→trans* isomerisation in methacrylic thin films containing azobenzene in the side chains.

No volume changes of the films were noticed before or after ultrasound treatment. The mass and density of all the polymers was measured and both values remained constant after exposure to ultrasound waves, with the same values as tabulated in Table 4.1.13 (previous section 4.1.2.9).

Until very recently isomerisation of azobenzene polymers was usually achieved by photo- and thermal-treatments. This study demonstrated that *cis→trans* conversion in solid azobenzene-based P(MMA/MOAB) films can also be achieved by exposure to ultrasound waves.

4.1.2.10.2 Ultrasound response of 4,4´-diglycidyloxyazobenzene determined by HPLC

4,4´-Diglycidyloxyazobenzene (4,4´-DGOAB) is a relatively new monomer, which was synthesised by Rusu *et al.* in 2012 for the first time, and can be used as a difunctional epoxy crosslinking agent.[161] 4,4´-DGOAB contains azobenzene, a well-known stimuli-responsive molecule that undergoes reversible *trans↔cis* isomerisation under light irradiation at specific wavelengths, heat and more recently ultrasound waves irradiation was found to be another stimulus.[67] This photoresponsive crosslinker has been selected to be one of the main components of the photosensitive composites and its response to ultrasound waves should be determined.

From ^{1}H NMR and UV/Vis analysis we have demonstrated that ultrasound treatment of UV irradiated 4,4´-DGOAB molecules induces *cis→trans* isomerisation. More significantly, a new peak in the UV/Vis spectra was identified at the epoxide region (300 nm) that could be ascribed to the opening of the epoxy ring of the monomers. The purpose of this study was to investigate the effect of ultrasound waves on the 4,4´-DGOAB and to determine the *trans* and *cis* ratios by HPLC.
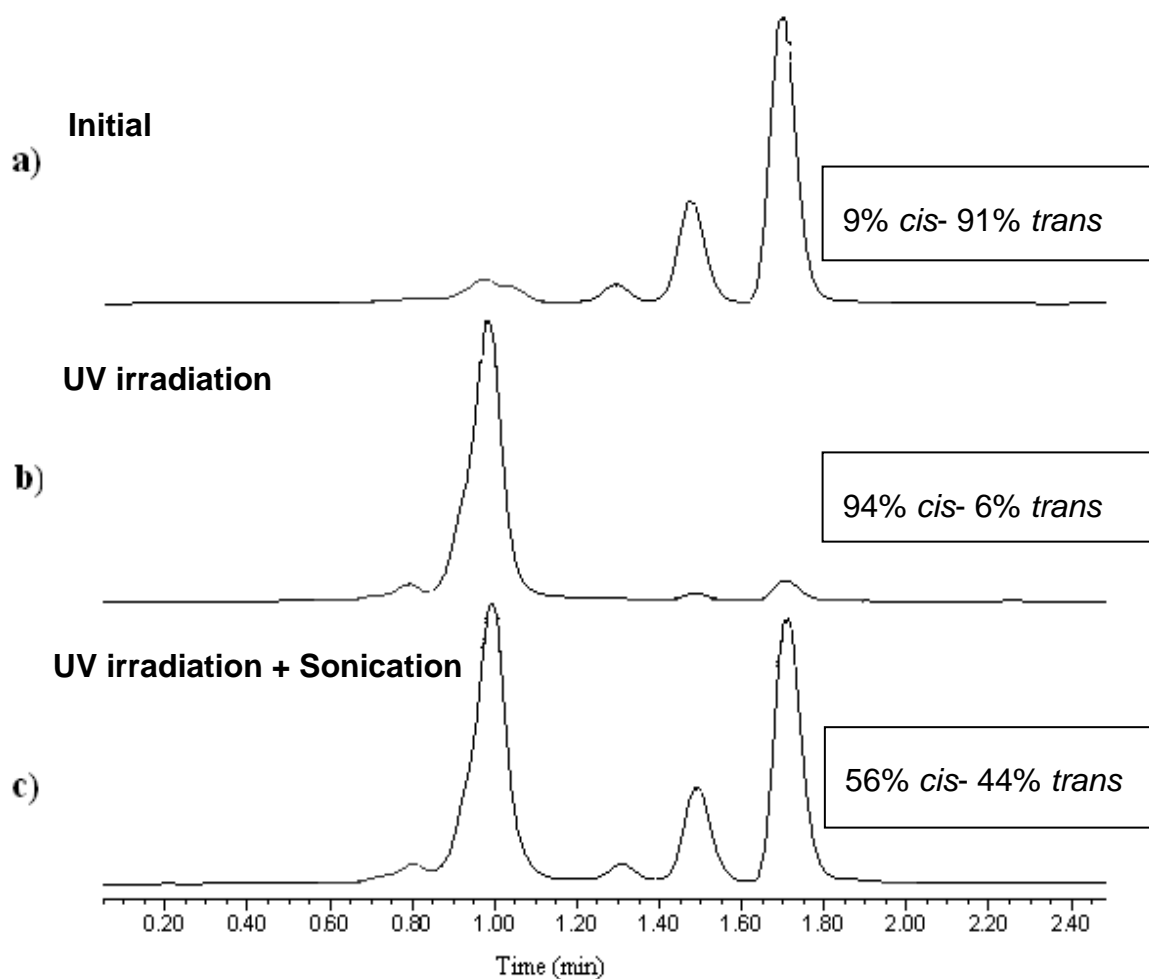
Figure 4.1.38 HPLC chromatograms of 4,4´-DGOAB in acetonitrile (1.5·10⁻⁵ M) at room temperature (~21°C) with *trans* and *cis* molar ratios a) initial, b) after UV irradiation for 1 min and c) after subsequent UV irradiation and sonication.

The chromatograms of the 4,4´-DGOAB without irradiation, after UV irradiation and sonication are shown in Figure 4.1.38. In Figure 4.1.38.a, four HPLC elution peaks were observed at 1, 1.3, 1.5 and 1.7 min. The appearance of more than one peak gave us the impression that our samples were contaminated with impurities, although they have been analysed by ^{1}H NMR and were found pure. In this case the impurities were found to consume 9% of the main product. The ACN solvent that has been used and the starting material 4,4´-dihydroxyazobenzene were also analysed by HPLC, as seen in 5.1A.5, but

none of them looks like to have been responsible for the elution peaks of the 4,4´-DGOAB solution. After irradiation with UV light for 1 min (Figure 4.1.38.b), the two intense peaks at 1.5 and 1.7 min retention time almost disappeared and in parallel the peak at 1 min increased dramatically by obtaining 94% of the main product. Furthermore a new weak peak at 0.8 min appeared.

This proves that the *trans* isomeric form of 4,4´-DGOAB has one elution peak at 1.7 min and the *cis* isomeric form is eluted faster at 1 min.[162] The existence of the weak peaks at 1.5 min and 0.8 min implies that some oligomers were formed with *trans* and *cis* conformation respectively. Investigation of both *trans* and *cis* isomers and reversibility of isomerisation by HPLC have been reported previously.[163] The new peak at 1 min corresponds to the *cis* isomeric form of 4,4´-DGOAB. The shorter elution time of the *cis* form was expected, since the acetonitrile polarity is measured at about 3.92 D and the azobenzene from 0 D at the *trans* form reaches 3 D dipole moment when it converts to the *cis* form.

The chromatogram of the last sample that had subsequently been subjected to UV light irradiation (1 min) and ultrasound waves (120 min) is illustrated in Figure 4.1.38.c. As can be observed all the five peaks are apparent. The molar ratio of the *trans* and *cis* 4,4´-DGOAB was found to be 44% and 56% respectively. The quantitative analysis for all the samples was calculated by integrating the elution peaks at 1 min (*cis* form) and at 1.7 min (*trans* form). In Figure 4.1.39, the peak heights of the differently treated solutions were compared with the retention time. It can be seen that when the molecules are in their *trans* form the elution peak at 1.7 min reaches the maximum, while the 1 min peak reaches the minimum value. The opposite effect occurs when the azobenzene monomer is in *cis* form. The HPLC analysis verified that sonication is able to induce *cis*→*trans* isomerisation to 4,4´-DGOAB molecules. The longer the samples were exposed to ultrasound waves the more 4,4´-DGOAB molecules were converted to their *trans* form.
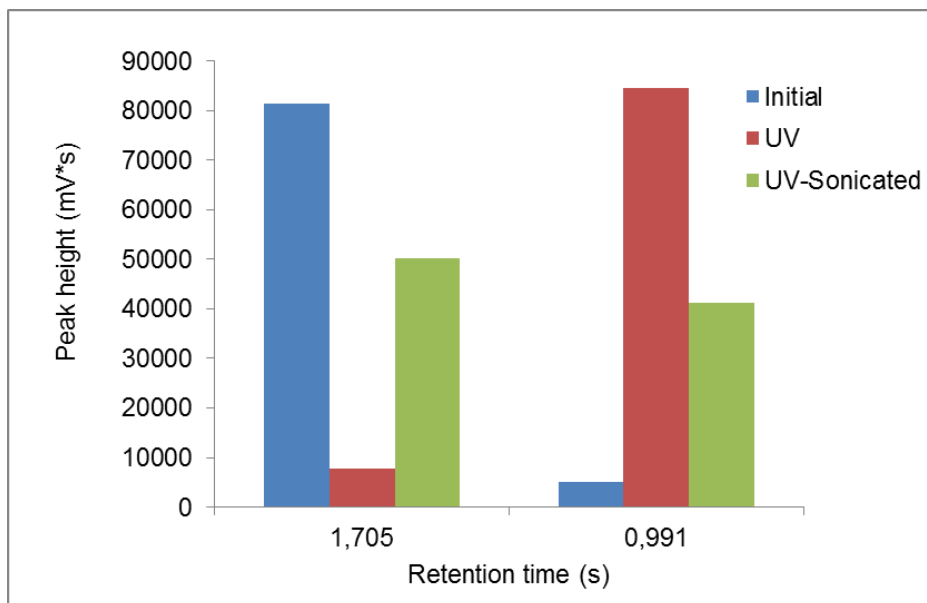
Figure 4.1.39 Peak heights of 4,4´-DGOAB samples vs. retention time

The appearance of 4,4´-DGOAB oligomers was attributed to the sonication effect. Further analysis should be conducted after additional irradiation with visible light to the samples that have been subjected to UV irradiation and at the end of sonication to ensure complete *cis→trans* conversion.

4.1.2.11 Thermal effect due to light irradiation on azobenzene films

The entire experimental work undertaken in this research required the samples (monomer and polymer solutions, cured epoxy films and epoxy/glass fibre composites) to be subjected to UV and visible irradiation. Thus, it was of high importance to quantify how much the irradiated specimens were heated by the radiation and also to ensure that they went back to ambient temperature before performing any experiments. In this section the temperature of the cured epoxy-based films was recorded using a high sensitivity MWIR thermal camera.
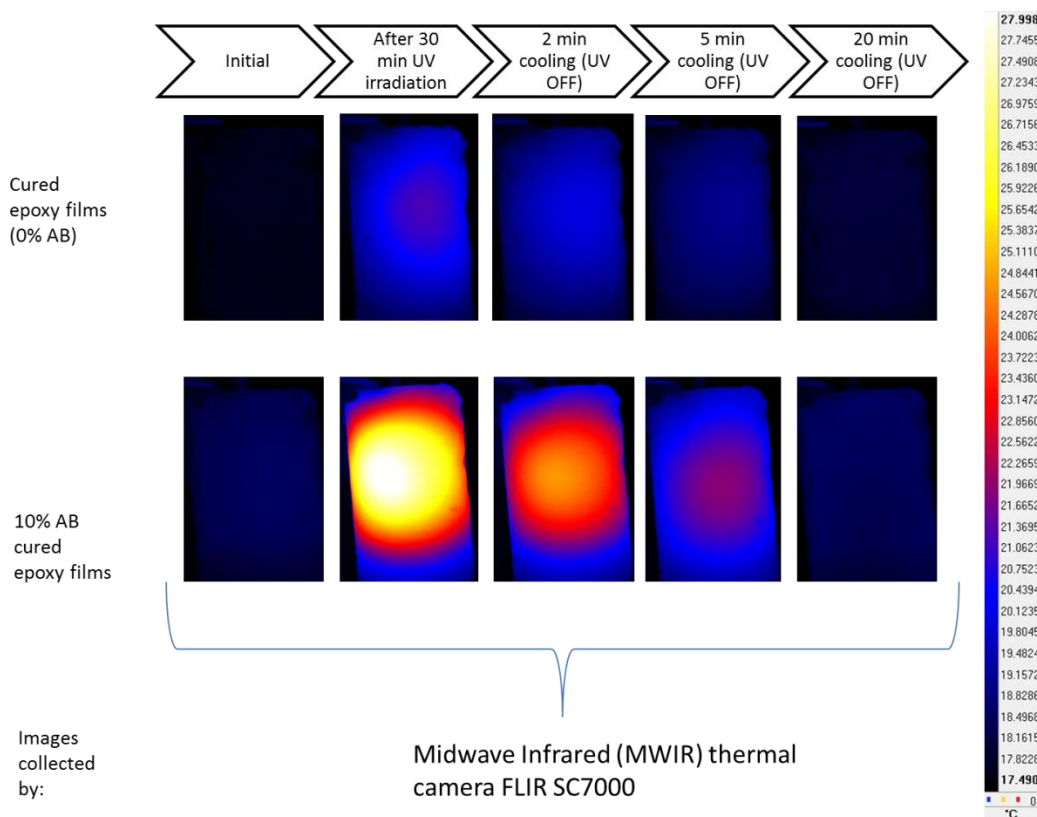
Figure 4.1.40 Thermal analysis cured epoxy-based films

Figure 4.1.40 illustrates a series of thermal images of the cured epoxy resins with 0% and 10% azobenzene loadings before and after (when light is turned off) exposure to UV light for 30 min (required time for the *trans→cis* isomerisation in cured films). The temperature-colour scale, on the right side of the image, provides the temperature values with their corresponding colours. At the temperature of 17.5°C the colour appears blue and as the temperature increases it goes gradually to purple (21°C), red (23°C), orange (24.5°C) and at higher temperature of 27°C the colour is bright yellow. From the images it was obvious that UV light irradiation increased the temperature in all the films.

The epoxy films after 30 min UV irradiation (2nd column) present a spot (radius ~ 15 mm) with higher temperature in the centre. This spot is attributed to the

172

heat dissipation from the light source that produces light in the centre and therefore heats the sample in the centre more intensely.[164] The temperature gradient on the surface is following a Gaussian distribution. The spot does not appear to be homogeneous because the films were irradiated from both sides (front and rear) with light beams of different radius (2.5 mm and 5 mm) as described in experimental section 3.1.2.7.
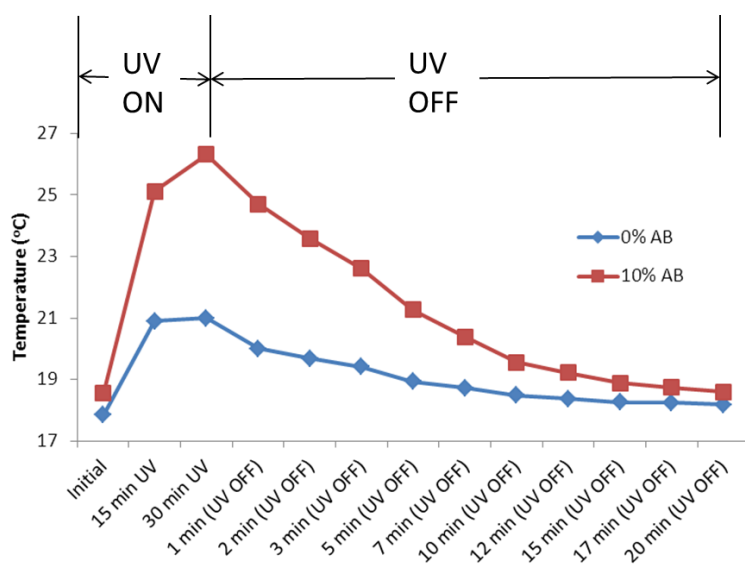
Figure 4.1.41 Temperature values of cured epoxy films containing 0% and 10% azobenzene after switching the UV light source on and off.

The graph in Figure 4.1.41 demonstrates a 3-8°C temperature rise from the plot of temperature values vs. time, after UV irradiation. Rhombuses correspond to the films without azobenzene and squares to the films with 10% azobenzene. When the UV light was switched off thermal images were taken periodically until a constant temperature was reached. The film with the modified resin (10% azobenzene loading) exhibited a temperature 5°C higher after UV irradiation than the control film. The specimens reached their initial temperature in 20 min after the UV light source was switched off. The 5°C temperature difference can

be explained by the presence of azobenzene (with molar absorption coefficient of 30,000 M^{-1} cm^{-1}) that absorbs more light than the DGEBA epoxy resin (with molar absorption coefficient of 0.926 $M^{-1}cm^{-1}$).[165] When a molecule absorbs light, it is raised to an excited electronic state. In this excited state, it can react either by dissociation or by reacting with another molecule or by isomerisation (photochemistry). It can also return to the ground state either by releasing the excess energy as heat or by emitting a photon of light (fluorescence). The additional temperature rise in the polymeric films with 10% azobenzene loading can also be due to the exothermic *cis→trans* isomerisation that Bushuyev *et al.* have demonstrated in the solid state (33-37 kJ mol-1, DSC exothermic peak).[166]

The temperature rises that were observed in the cured epoxy films are not significant compared to the T_g of the polymers (81-83°C).

4.1.2.12 Influence of azobenzene and UV light on fracture toughness of epoxy based polymers

The reason for measuring the fracture toughness of the polymeric materials was to understand the influence of azobenzene concentration and UV light on the crack propagation in the polymeric matrices that were planned later to be reinforced with glass fibres. Fracture toughness measurements of the azobenzene polymers have never before been assessed therefore the investigation of the effect of the azobenzene loading and/or the UV irradiation influences was crucial.

Figure 4.1.42 presents photos of non-irradiated SEBN examples with 0%, 5% and 10% azobenzene loadings at various times during 3-point bending test. These photos depict at the beginning a region of cavitation (microcracks) and plastic yielding ahead of the notch.[167] The cavitated region (5-16 s) appeared as a darkened area at the end of the notch. The size of this area increased when the samples demonstrated higher fracture toughness.[168]
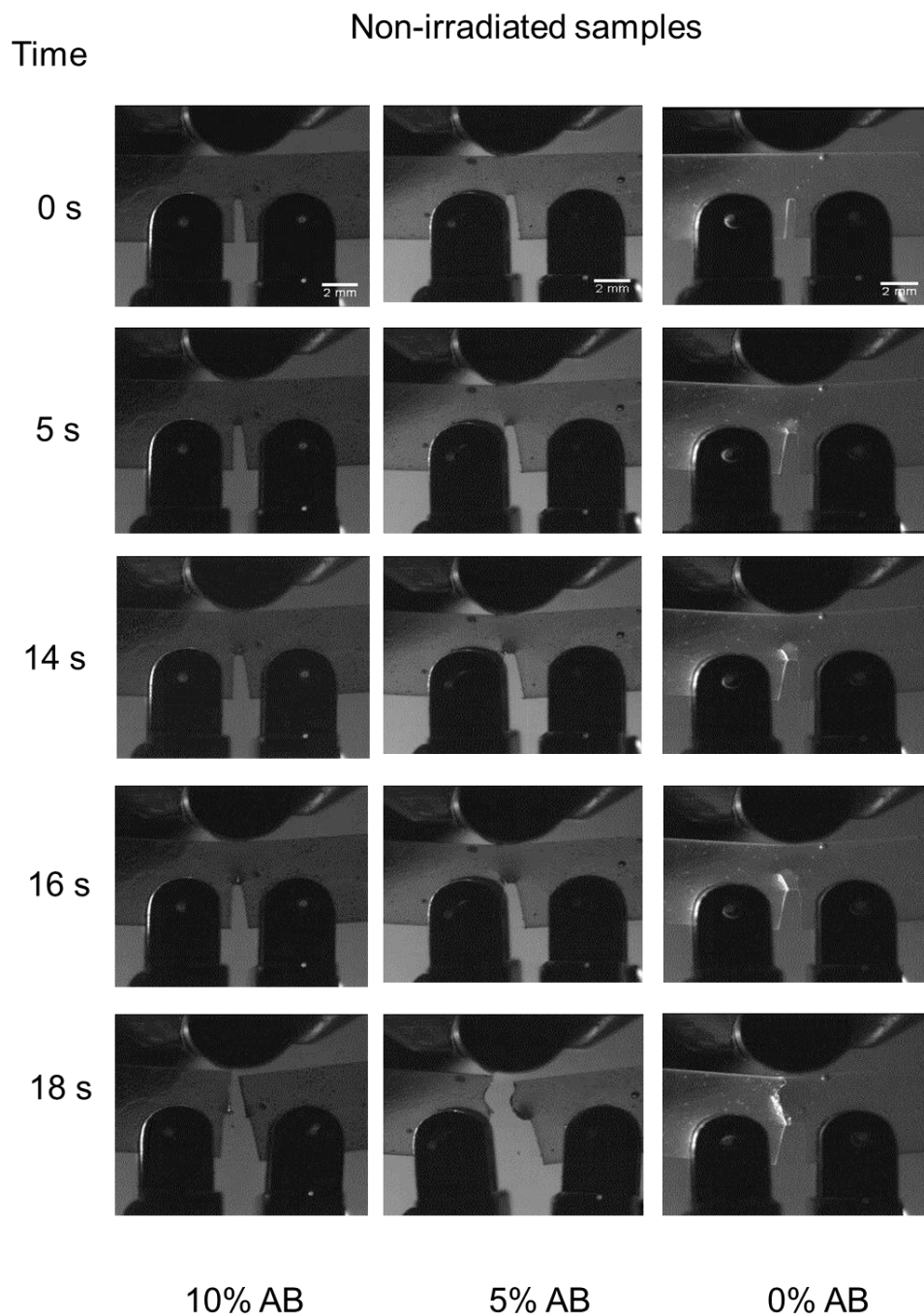
Figure 4.1.42 Photos of epoxy resin samples to test by the SEBN method as a function of the azobenzene loading, applied load and test duration (captured by high-speed camera).

RESULTS AND DISCUSSION

As can be seen from the photos of Figure 4.1.42 and from a typical load vs. time plot, in Figure 4.1.43, the energy of the samples was dissipated as pre-failure damage (micro-cracks) and then suddenly as a fast-moving fracture. This behaviour is expected from brittle materials such as epoxy resins and PMMA.[169]
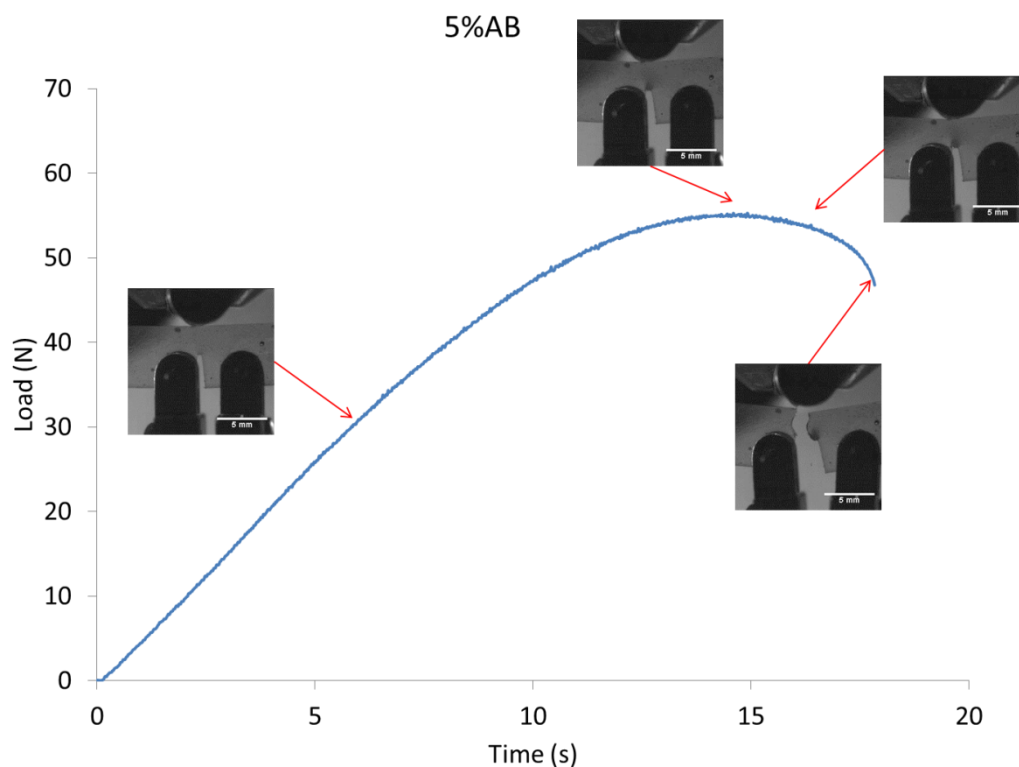
Figure 4.1.43 Typical load vs. time graph of fracture toughness with real-time images from high-speed camera.

The fracture toughness (K_{IC}) of polymeric epoxy resins as a function of the azobenzene loading of non-irradiated and UV-irradiated specimens is presented in Figure 4.1.44. The details of the specimens' dimensions, maximum loads and fracture toughness are listed in Table 4.1.14. Samples that were not exposed to UV light, showed an 11% increase in K_{IC} which was observed with 10% azobenzene. The improvement in resistance to crack growth may have occurred due to the azobenzene molecules which require more energy to

"break" when they are in their more thermodynamically stable, *trans*, isomeric form. Another possibility could be that the *trans* azobenzene molecules exhibits a more rubber-like behaviour in comparison the *cis* azobenzene with a more brittle behaviour due to their twisted/folded structure. Garg *et al.* have demonstrated that the addition of rubber to a brittle resin causes a reduction in stiffness and a significant increase in fracture resistance by plasticising the matrix [112]
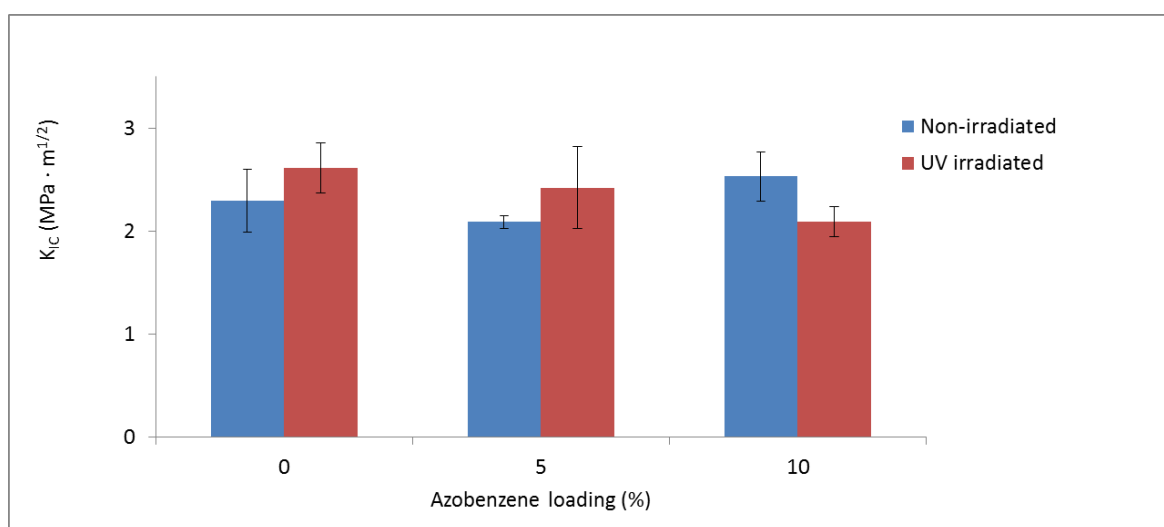
Figure 4.1.44 Fracture toughness of UV and non-irradiated specimens vs. azobenzene loading (%).

After exposure to UV light the fracture resistance linearly decreased with increasing azobenzene loading. This decrease in fracture toughness with the azobenzene loading could be attributed to the *trans→cis* isomerisation that requires free volume space for rotation of the azo bond.[170] During the *trans→cis* conversion, residual stress with subsequently mini-cracks could occur within the polymer matrix, as the azobenzene molecules are covalently attached to a crosslinked network. Such localised stresses act as a driving force for crack growth and facilitate the notch crack to propagate.[171] Therefore the higher the

azobenzene loading the more likely is the stress from the isomerisation to affect the whole epoxy resin matrix' fracture toughness properties.

Table 4.1.14 Dimensions, maximum loads and fracture toughness of cured epoxy resin specimens with and without exposure to UV light

Epoxy resin samples	Width (mm)	Thickness (mm)	Crack length (mm)	Maximum load at elastic-linear region F_Q (N)	Failure load F_C (N)	Fracture toughness K_{iC} (MPa m$^{1/2}$)
0%AB_Ref	6.02 ± 0.01	2.87 ± 0.02	3.03 ± 0.06	51.44 ± 7.35	69.10±12.26	2.29 ± 0.30
5%AB	6.04 ± 0.00	2.87 ± 0.08	2.98 ± 0.04	43.69 ± 0.97	60.48 ± 2.71	2.09 ± 0.06
10%AB	6.03 ± 0.02	2.93 ± 0.09	2.96 ± 0.10	53.69 ± 7.09	77.34 ± 9.43	2.53 ± 0.24
UV_0%AB_Ref	6.05 ± 0.02	2.83 ± 0.09	2.94 ± 0.14	50.30 ± 6.02	77.62 ± 10.60	2.62 ± 0.24
UV_5%AB	6.02 ± 0.01	2.88 ± 0.13	2.92 ± 0.12	53.08 ± 13.84	73.23 ± 14.53	2.42 ± 0.40
UV_10%AB	6.02 ± 0.02	3.00 ± 0.14	2.98 ± 0.10	54.39 ± 12.59	64.51 ± 8.27	2.09 ± 0.15

By comparing the effect of UV irradiation for each sample separately, it can be noticed that an increase in fracture toughness occurs at the specimens with 0% and 5% azobenzene loading. A significant 20% decrease in K_{IC} was reached with 10% azobenzene loading after UV irradiation compared to the non-irradiated polymeric matrix. This increase can be explained by the photo-oxidation of the polymer matrix after exposure to UV light that decreases the overall crosslinking density of the matrix as a consequence of the chain scission reactions.[172] Reduction of the mechanical properties, such as stiffness, of the UV irradiated specimens was expected but the fracture toughness properties

were enhanced due to the lower crosslinked density than the virgin specimens. On the other hand, the decrease in fracture toughness seen with the 10% azobenzene loading samples can be justified by the polymer chain rearrangement or the stress that occurs after the UV-induced *trans→cis* isomerisation as explained in the previous paragraph.
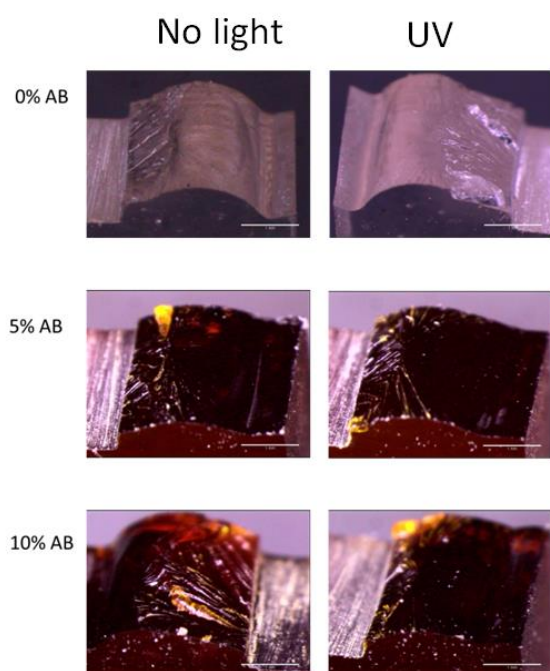
Figure 4.1.45 Fracture morphologies after failure (images taken from optical microscope, 1mm scale-bar)

Figure 4.1.45 illustrates micrographs of the fracture surface of specimens showing the matrix ductility. The features on the samples' surfaces are quite similar and no significant differences were noticed between samples with different azobenzene loadings or between UV and non-irradiated samples.

The incorporation of azobenzene as a crosslinker of the polymeric matrix was aimed to contribute to the enhancement of the fracture properties. It was demonstrated that 10% azobenzene (in *trans* form) improves the fracture

resistance of the polymeric matrix. On the other hand, when the modified resins with azobenzene are exposed to UV irradiation (*cis* isomers) the fracture mechanic properties are affected negatively with increasing azobenzene loading.

4.2 Photoresponsive composites

In this chapter characterisation of the epoxy/ glass fibre reinforced composite panels, with photoresponsive azobenzene resins at different loadings (0%, 5% and 10%), and investigation of their compressive properties, impact tolerance at high-velocities and damage evaluation before and after UV irradiation have been discussed. It was expected after impact testing that some of the kinetic energy of the projectile would be absorbed by the azo-molecules and thus it might lead to smaller deformations or other types of failure at the polymer matrix after photo-isomerisation. Further to those studies, compression after impact (CAI) tests followed in order to compare the UV irradiated and non-irradiated impacted specimens on residual strength with regards to the azobenzene loading. Figure 4.2.1 depicts clearly the hierarchy of the experiments at different light treatments.
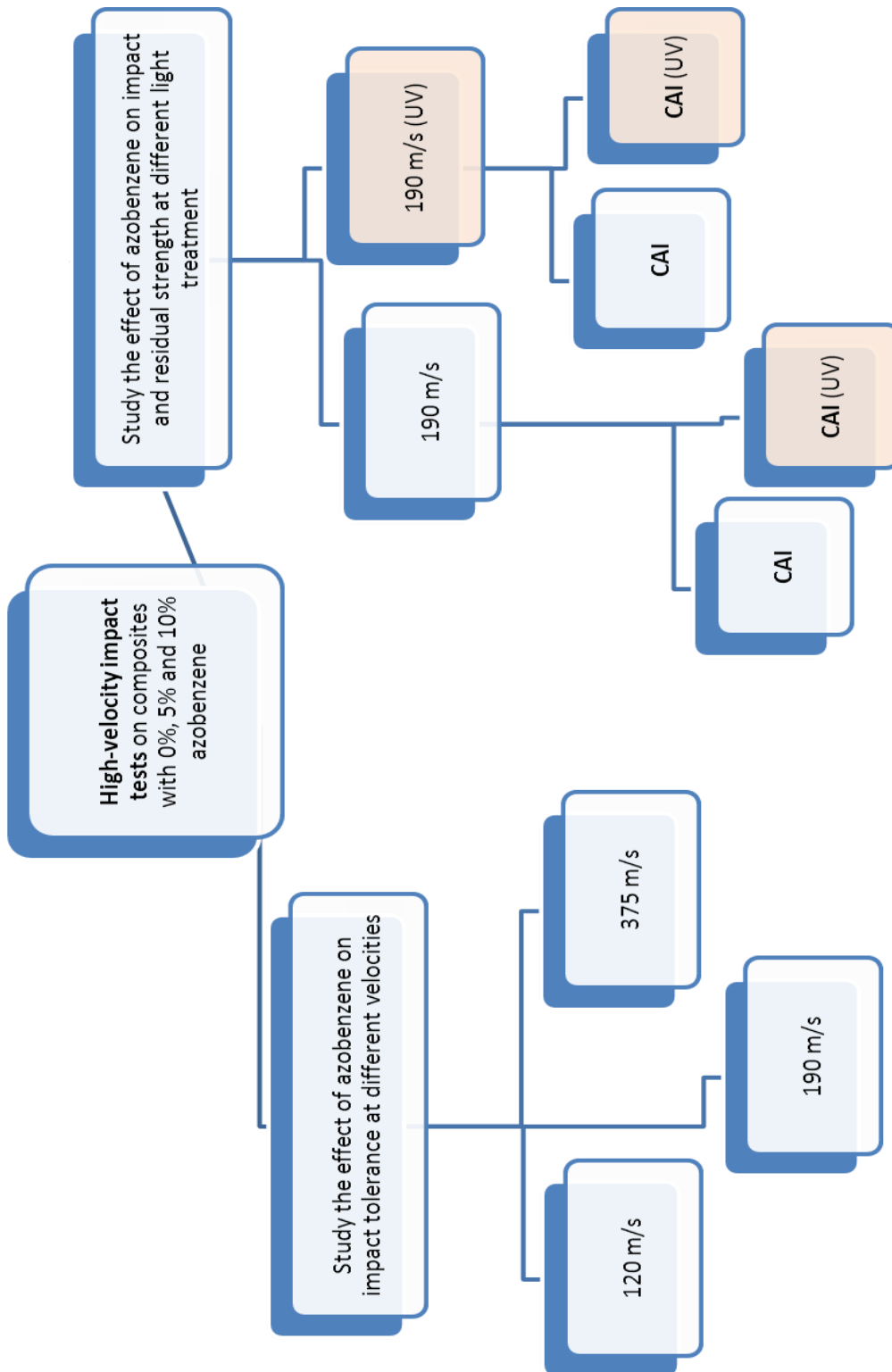
Figure 4.2.1 Hierarchical progress of the performed experiments at different velocities and light treatment from top to bottom

4.2.1 Composites manufacturing and quality

Photoresponsive azobenzene-based pre-impregnated materials or resins are not commercially available. Therefore, the photoresponsive composites were manufactured as described in section 3.2.2. The manufacturing of the photoresponsive composites was a straightforward process with some limitations and challenges.

The photoresponsive crosslinker, 4,4´-DGOAB, was a solid powder and required full dispersion with the viscous epoxy resin prior to blending with the hardener. Due to the high viscosity of the liquid resin (Viscosity at 23°C = 1,250 mPas), the 4,4´-DGOAB powder was not fully dissolved in the resin after mixing with a magnetic stirrer. It was found that heating at 40°C improved the dispersion of the 4,4´-DGOAB but this temperature raise could initiate the curing after the addition of the hardener. Therefore it was necessary for homogeneous mixing of the 4,4´-DGOAB with the epoxy to take place a day before the composite manufacturing to allow the photoresponsive resin to cool to room temperature. Another challenging part of the process was identified when the mixture of 4,4´-DGOAB/ epoxy resin was poured and spread using a wooden spatula between the glass-fibre layers. The mixture was getting thicker with the addition of the hardener and spreading between the fibres without changing their orientation required slow and very careful moves. In parallel there were some time and temperature limitations. The handling time at room temperature before the mixture was starting to gel or cure was 80 min. The increase in temperature (above 25°C) might initiate the curing before the 80 min. Therefore the hand lay-up and vacuum bagging processes needed to be accomplished within this time at room temperature conditions for each panel before being placed in the autoclave.

After the composites were manufactured, they were placed in front of a lamp to check for gross manufacturing defects, visually. The quality of each panel was examined further using optical microscopy, for evaluation of its void and fibre volume fractions. Usually all the composites have amounts of voids regardless

the raw materials or manufacturing technique, due to trapped air or any volatiles or incomplete consolidation. Acceptable void values for industrial applications are approximately 1-5% v/v.[173] Lower content of voids is desirable in composites as the formers act as crack initiators.[174] Fibre volume fractions typically are ranged between 50% and 80%.[135, 136]
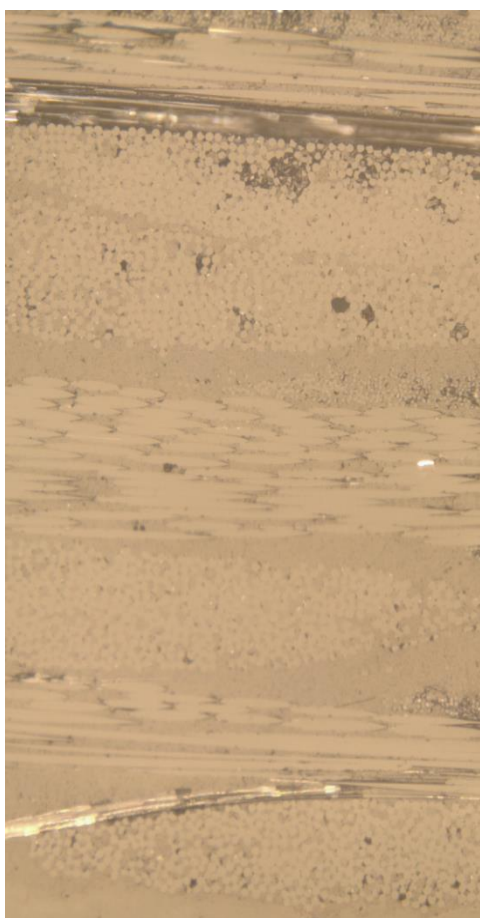
Table 4.2.1 Thicknesses of plies of the composite's cross-section

No. of ply	Fibre orientation	Thickness (μm)
1	0°	392
2	90°	418
3	0°	434
4	90°	487
5	90°	384
6	0°	405
7	90°	363
8	0°	412

Figure 4.2.2 Cross-section of 0% azobenzene composite panel

All the panels with 0%, 5% and 10% azobenzene loading consisted of balanced and symmetrical laminate with a combination of 0° and 90° layers, as can be seen in Figure 4.2.2. The thickness, fibre and void fractions were calculated according to section 3.2.3.1 and the results are presented in Table 4.2.1 and

Table 4.2.2. As it can be seen, the fibre volume fractions in all the composites were within 31-43% which represent typical values according to the literature.[135]

The amount of voids that were present in the composites was higher than the limit of 5% for composites with acceptable qualities. Composites without azobenzene had 6-9% void volume fractions and composites with 5% and 10% azobenzene 7-16% void volume fractions. The increase of voids in composites with azobenzene might be attributed to the existence of any insoluble azobenzene as a solid powder. Pawar *et al.* showed that the inclusion of filler particles increased the void fraction of composites.[114] These values were taken into consideration for the following experiments.

Table 4.2.2 Fibre and void volume fractions and thicknesses of photoresponsive composites

Composite panels	Fibre volume fraction, V_f (%)	Void volume fraction, V_v (%)	Thickness (mm)
0% AB_Ref 1	38	9	2.3
0% AB_Ref 2	41	6	2.2
5% AB _1	43	7	2.4
5% AB_2	33	13	2.5
10% AB_1	31	11	2.5
10% AB_2	35	16	2.6

The disadvantage of optical microscopy, for V_v and V_f identification, is the small observed area which increases the measurement uncertainty. Finally, it should be mentioned that a non-instrumental, visual inspection was conducted for each panel after manufacturing. By placing the composites in front of a light bulb

(where any defects could be observed due to the composites' translucency) it was possible to verify whether the panels were homogeneous after manufacture.

4.2.2 Photoresponsive behaviour of the azobenzene-based composites

The initial goal of these studies was to demonstrate whether or not the azobenzene molecules were capable of reversible isomerisation within a cross-linked polymeric network reinforced with glass fibres. The use of the reflectance spectrophotometer to record the photoisomerisation of composites and thick azobenzene films (>1 mm) was found to be suitable in this case, as the colour of the specimens changed visually from dark yellow (*trans* form) to orange (*cis* form) reversibly. In the following paragraphs the spectra of the composites after UV and visible irradiation are discussed.

Figure 4.2.3 illustrates the spectra of a composite with 10% azobenzene loading after UV and visible irradiation. The first spectrum was collected from a non-irradiated specimen, which previously had been stored in the dark for two weeks, and represented the film containing 100% *trans* azobenzene molecules. After 30 and 60 min of exposure to the UV light a decrease in the reflectance at 570 nm (yellow colour) was noticed and attributed to the *trans→cis* isomerisation. Longer exposure than 60 min of the specimens to the UV light did not induce any further change in the spectrum. Therefore the outcome from the complete *trans→cis* geometrical conversion suggests a maximum reflectance decrease of 23% for the specific azobenzene loading.

Subsequent irradiation with visible light for 30 and 60 min demonstrated the opposite effect. As can be seen in the spectra the reflectance of the composites was increased with the irradiation time, resembling to a recovery to the more thermodynamically stable *trans* azobenzene form. The almost total 94.6% *cis→trans* isomerisation was achieved after 60 min of visible irradiation.
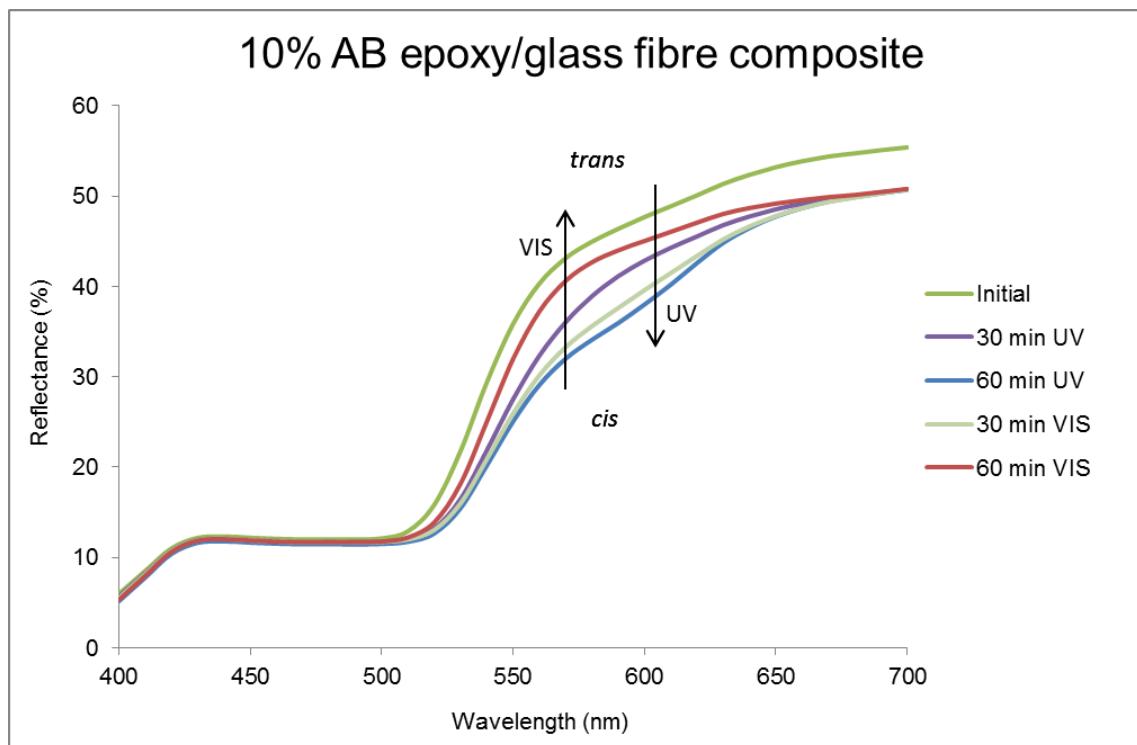
Figure 4.2.3 Reflectance spectra of a 10% azobenzene-based epoxy/glass fibre composite during exposure to UV and visible light irradiations

Finally, it should be noted that the reference specimens which did not contain any azobenzene did not present any spectral variations after the different light treatments. As can be seen in Figure 4.2.4 the reflectance spectra of the reference epoxy/glass fibre composite were collected before and after exposure to UV and visible light every 30 and 60 min. Longer exposure than 60 min of the specimens to the UV light did not induce any further change in the spectrum. The reflectance of the reference specimen remained almost stable at 69-71% after the different light treatments. These findings are in agreement with the previous UV/Vis studies discussed in section 4.1.2.4, that were conducted on acrylic films containing 0-100% azobenzene loading. The analysis of the PMMA film that did not contain any azobenzene did not exhibit any spectral variations before or after exposure to UV light. Thus the photo-induced changes in

reflectance of these materials are attributed to the *trans→cis* isomerisation of the azobenzene chromophores.
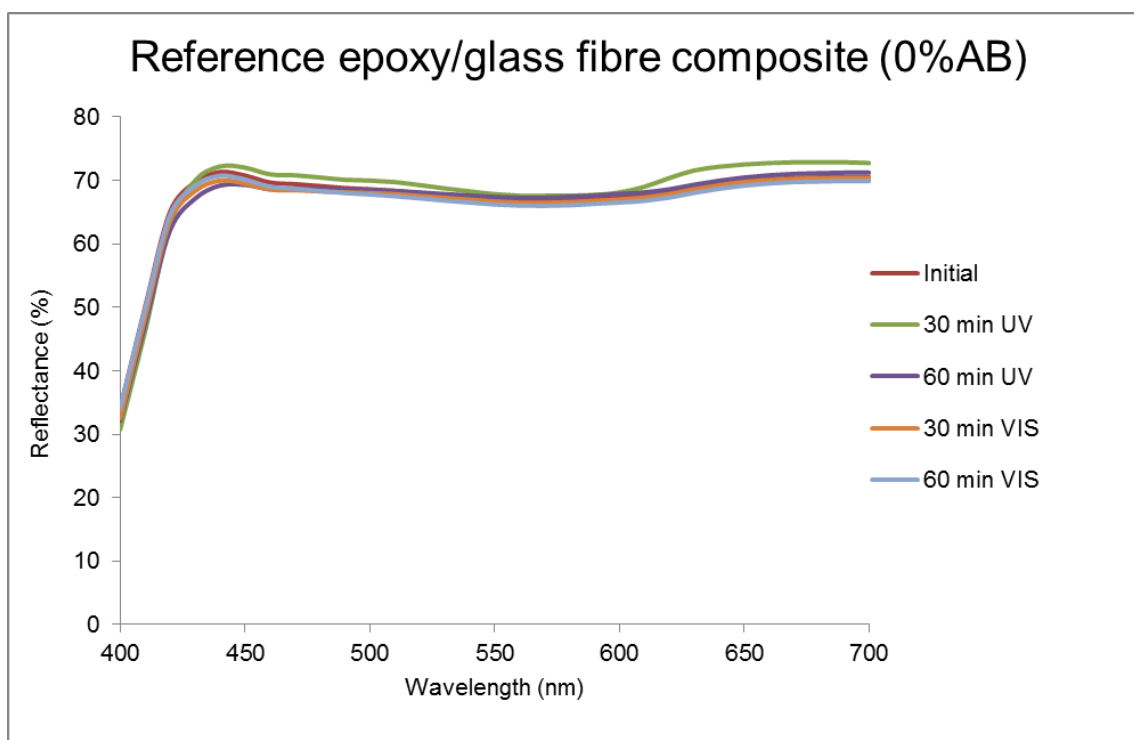
Figure 4.2.4 Reflectance spectra of a reference epoxy/glass fibre composite without azobenzene after exposure to UV and visible light irradiations

The results suggest that azobenzene molecules are capable of reversible isomerisation within the glass fibre composites and require 1 hr UV exposure for complete *trans→cis* conversion. As reflectance spectroscopy is a technique where the measurements are collected only from the surface of the specimens, it was necessary to ensure that *trans→cis* conversion was achieved within all the layers of the composites; therefore spectra were collected from the top and bottom of the specimens.

4.2.3 Thermal effect due to light irradiation on photoresponsive epoxy/glass fibre composites

For the requirements of this PhD, the photo-induced changes in the molecular structures that alter the physical and mechanical properties of polymeric matrices were the main focuses of this research and therefore, any thermal effect should have been excluded. In order to achieve this, a high sensitivity MWIR thermal camera was used for recording the temperature rises of the samples being irradiated.
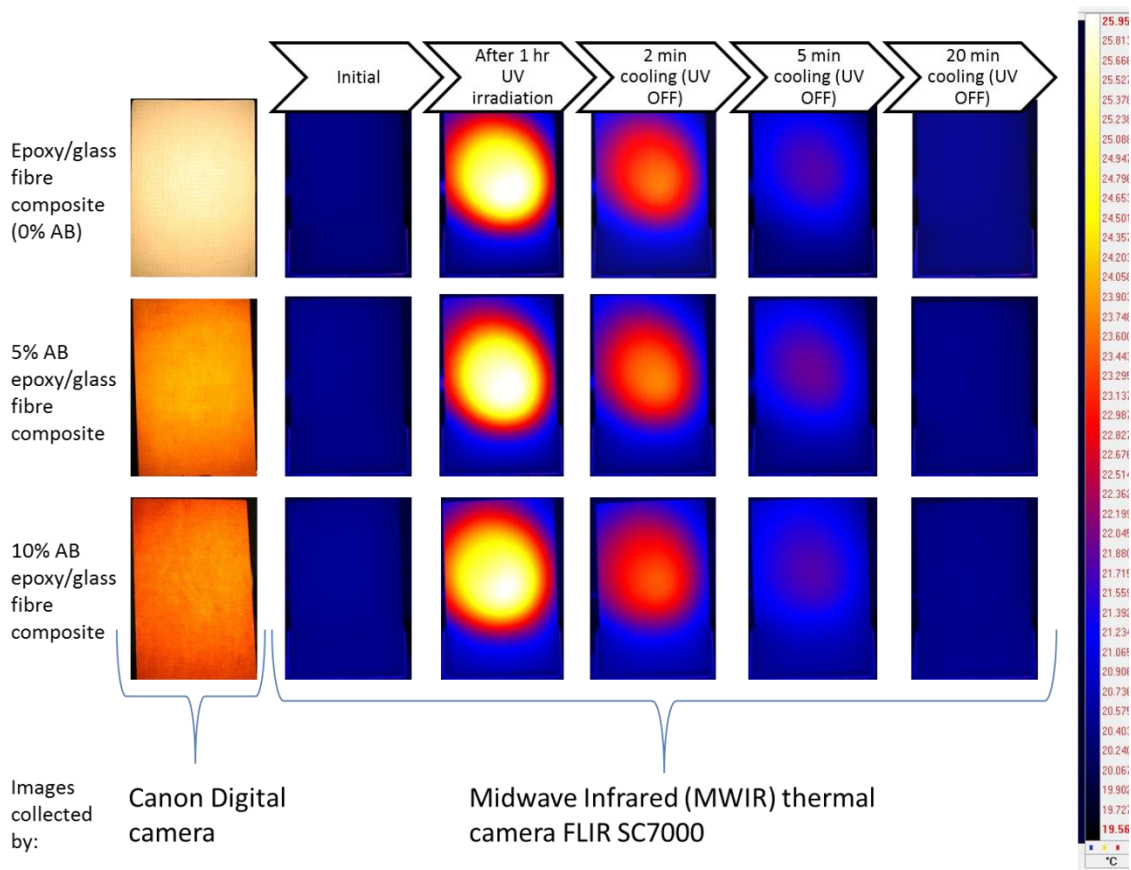
Figure 4.2.5 Thermal analysis of glass fibre composites

Figure 4.2.5 illustrates a series of photos and thermal images of epoxy/glass fibre composites with 0%, 5% and 10% azobenzene loadings before and after

(when light is turned off) exposure to UV light for 1 hr (required time for *trans→cis* isomerisation in composites). On the right side of the image there is a temperature-colour scale providing the temperature values with their corresponding colours. At low temperatures of 19.6°C the colour appears blue and as the temperature increases it goes gradually to purple (22°C), red (23°C), orange (24°C) and at higher temperatures of 26°C the colour is bright yellow. From the images it is obvious that UV irradiation increased the temperature in all the composites.
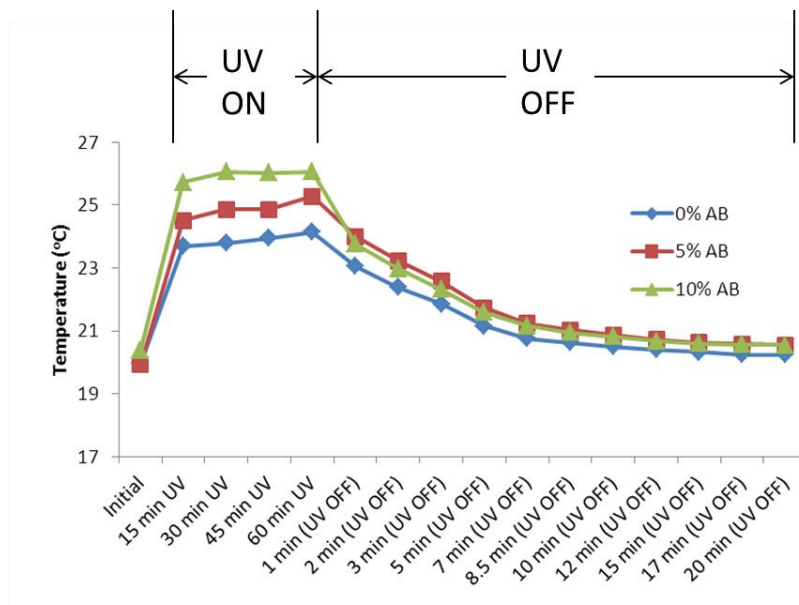
Figure 4.2.6 Temperature values of epoxy/glass fibre composites containing 0%, 5% and 10% azobenzene after switching the UV light source on and off

In Figure 4.2.5 all the composites after 1 hr UV irradiation (3rd column) present a spot (radius ~ 45 mm) with higher temperature in the centre. As has been previously explained in section 4.1.2.11, this spot is attributed to the heat dissipation from the Gaussian beam intensity profile of the light source that creates a hot centre with a colder periphery. The spot is not homogeneous because the light beams, that the composites were exposed to both sides (front

and rear), have different radius (2.5 mm and 5 mm), as described in experimental section 3.1.2.7.

After plotting the exact temperature values vs. the time a 3.5-6°C temperature rise depending on the azobenzene loading was identified after UV irradiation, as seen in Figure 4.2.6. In the graph, rhombuses correspond to the composites without azobenzene and squares and triangles to the composites with 5% and 10% azobenzene respectively. When the UV light was switched off thermal images were taken periodically until a constant temperature was reached. It was apparent that all the samples demonstrated the same behaviour during and after irradiation. Initially a sharp increase of the temperature was noticed after 15 min exposure to UV and then an almost constant temperature with a gradual temperature increase was reached after 60 min of UV irradiation. After the UV light was switched off the temperature gradually decreased. The more interesting result was that the temperature after 60 min increased as a function of the azobenzene loading (1°C increase for 5% azobenzene loading and 2°C increase for 10% azobenzene loading). The additional temperature rise of the composites with higher azobenzene loading was assumed to occur due to the *cis*→*trans* isomerisation reaction.[137] Bushuyev *et al.* have demonstrated that the exothermic *cis*→*trans* isomerisation can take place in the solid state (33-37 kJ mol^{-1}, DSC exothermic peak).[166] From the studies of this PhD project it was demonstrated that 20 min were required for the composites to reach the initial temperature after the UV irradiation was switched off.

The difference between the temperature increase in the cured resins (section 4.1.2.11) with 10% azobenzene (8°C) and the temperature increase in the epoxy/glass fibre composites with 10% azobenzene (6°C) could be attributed to the reinforcement of the composites since the composites consisted of 65-69 w/w% polymeric resins, (with 10% azobenzene). It was expected the temperature rise of the composites to be lower than that of the pure polymeric resins also due to the different focuses of the light beams (distance between the light beam and the specimen) on the films and composites. Samples closer to

190

the light source get hotter.[175] The distances between the light sources and the films (12 cm and 14 cm) were shorter between the light sources and the composites (14 cm and 19 cm), as can be seen in section 3.1.2.7.

4.2.4 Compression tests of photoresponsive epoxy/glass fibre composites

The first tests that were performed on the composites for evaluating the influence of azobenzene on the mechanical properties were compression tests, as the compressive strength is a matrix-dominant property.[143] The compressive properties of the epoxy/glass fibre composites with 0%, 5% and 10% azobenzene loading before and after exposure to UV irradiation for 1 hr are presented in Figure 4.2.7. The red columns correspond to the UV irradiated samples and the blue to the non-irradiated samples. The influence of azobenzene on the compressive properties of the non-irradiated composites, was negative in composites with 5% azobenzene (a 20% decrease in the compressive strength) and 10% azobenzene loading (a 7% decrease). On the other hand, when the composites containing azobenzene were subjected to UV light for 1 hr and then tested an enhancement of their compressive properties was observed. The reference epoxy/glass fibre composites (without azobenzene) demonstrated a decrease in strength by 10% after exposure to UV light. It has already been demonstrated that UV irradiation degrades the mechanical properties of epoxy resin composites (brittleness occurs due to the increased cross-linking from photo-oxidation reactions of the polymeric matrix that are activated by UV light).[7] However from the nanoindentation experiments of this PhD (4.1.2.7.2), no significant changes in stiffness were observed in the cured epoxy resins before and after exposure to UV light.

The UV treated composites exhibited an increase in compressive strength with higher azobenzene loading. More significantly, there was a 3% and 19% increase of strength (compare to the reference samples, 0% azobenzene) for the composites with 5% and 10% azobenzene loading respectively.
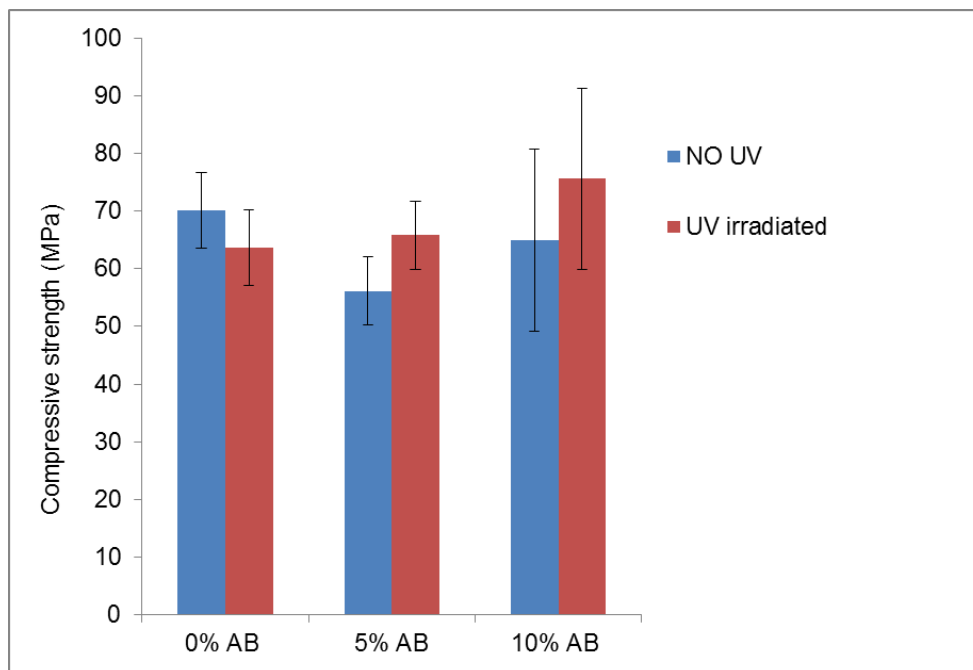
Figure 4.2.7 Compressive strength of epoxy/glass fibre composites with 0%, 5% and 10% azobenzene loading

Although the standard deviation of the composites with 10% azobenzene is too high (10%) previous nanoindentation findings (in section 4.1.2.7.1) have shown a similar trend. A 2% increase in nanoindentation stiffness after UV irradiation of polymer films with 10% azobenzene loading was observed. This increase could be attributed to the more twisted geometry of the azobenzene which enhances the mechanical properties (stiffness) of the whole polymeric matrix, as has being previously demonstrated by other studies.[35] The enhancement of composites' compressive properties might have occurred due to the polymer chain rearrangement caused by the photoinduced *trans→cis* isomerisation. The compression strength depends on the polymer matrix and fibre-matrix adhesion.[176] Xie *et al*. has demonstrated that by improving the interfacial adhesion using treated glass fibres the compressive strength was enhanced too.[177] In addition, it has been shown that the increase in polarity of phenolic epoxy resins leads to better adhesive properties due to higher bond strengths.[178] Therefore, increase in the compression strength might have

occurred due to a better adhesion between the polar, *cis* azobenzene epoxy resins, with 3 Debye dipole moment, and glass fibres or because the polymeric matrix containing *cis* azobenzene chromophores demonstrate better compressive properties than with the non-polar, *trans* azobenzene with 0 Debye polarity.[154]

4.2.5 High-velocity impact experiments of photoresponsive azobenzene epoxy/glass fibre composites

After the compression tests, impact experiments were followed for evaluating the impact resistance of the composites at high velocities.

4.2.5.1 Light-induced energy changes

A single velocity of 190 m/s was applied to the composites (2 replicates each) with 0% (as control), 5% and 10% azobenzene loading in order to compare their kinetic energy differences before and after exposure to UV light. The entry and exit velocities, v_1 (m/s) and v_2 (m/s) respectively, the inlet and absorbed energy values, E_i (J) and E_t (J) respectively, and the energy difference percentage ΔE_f (%) are listed in Table 4.2.3.

The difference in absorbed energy of the composites with 0-10% azobenzene loading between the non- and UV irradiated composites are plotted on the graph shown in Figure 4.2.8. The squares correspond to the results of the UV irradiated specimens and the rhombuses to the non-irradiated composites. Comparing the energy values of the specimens it can be observed that there is a very similar trend between the non- and UV irradiated samples with regards to their azobenzene loading.

RESULTS AND DISCUSSION

Table 4.2.3 Results after impact (190 m/s) of non- and UV- irradiated composites

	v_1 (m/s)	v_2 (m/s)	E_i (J) †	E_t (J) ‡	ΔE_f (%) §
0% AB (No UV)	186.9±1.0	129.6±0.3	123.0±1.3	63.8±1.6	51.9±0.7
5% AB (No UV)	188.3±0.9	126.0±3.9	124.7±1.2	68.9±2.2	55.2±2.3
10% AB (No UV)	187.2±1.3	123.3±1.8	123.3±1.8	69.8±3.3	56.6±1.9
0% AB (UV)	186.4±0.9	126.5±2.7	122.4±1.2	66.0±1.2	54±1.5
5% AB (UV)	187.7±5.2	124.6±1.1	124.1±6.9	69.4±5.9	55.9±1.7
10% AB (UV)	183.5±0.3	114.5±2.2	118.5±0.4	72.4±2.2	61.1±1.7

† $E_i = \frac{1}{2}mv_1^2$ ‡ $E_t = \frac{1}{2}m(v_1^2 - v_2^2)$ § $\Delta E_f = \frac{E_t}{E_i} \cdot 100\%$

The energy that was absorbed after impact from the non-irradiated composites was approximately the same for the targets containing 5% and 10% azobenzene with values 8% and 9.5% respectively higher than the energy absorbed by the control. These findings suggest that the azobenzene is able to reduce the transferred energy from the projectile to the target at 190 m/s. Nielsen *et al.* have demonstrated, likewise, that the enhancement of ceramic composites with encapsulated armour-grade materials results in higher absorption and reduction of the transferred impact energy from most types and sizes of projectile.[179] This was justified by the high energy absorption of the armour-graded materials that caused increase of the dwell time of the projectile. High energy absorption materials are supportive for composites to withstand extreme loading conditions. Azobenzene here possibly absorbs some energy resulting in less kinetic energy to be transferred when the projectile penetrates the specimens.
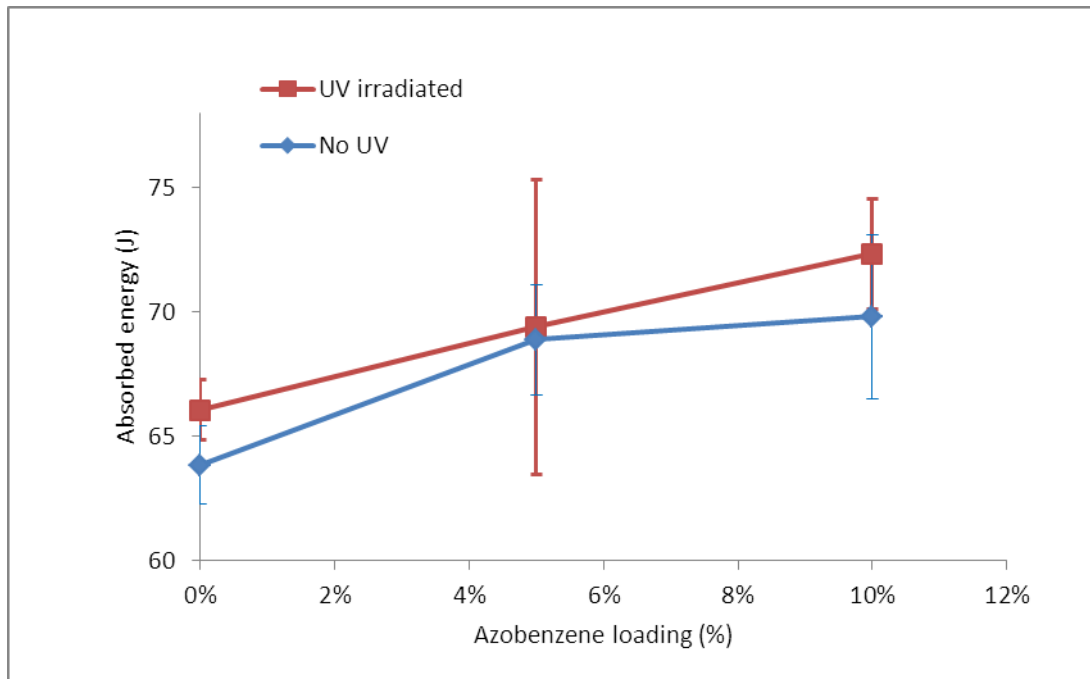
Figure 4.2.8 Absorbed energy at 190 m/s velocity impact vs. azobenzene loading at UV and non-irradiated composites

In the same way, the energy that was absorbed by the targets which had being previously exposed to UV light linearly increased with the azobenzene loading. The average absorbed energy values of the samples containing 5% azobenzene were 5% higher than the control and those with 10% azobenzene 10% higher accordingly. Improvement in energy absorption may have occurred because *cis* azobenzene led to improvement in interlaminar shear strength (maximum shear stress between layers of a composite) which increases the delamination resistance of polymer composite, a dominating mechanism in absorption energy of polymer composite laminates during high-velocity impact test.[180] Thus the energy level at the control samples (0% azobenzene) indicated lower values in contrast to those containing 5% and 10% azobenzene. Another parameter, apart from the matrix system, that should also be taken into consideration for the response of polymer composite materials subjected to

195

high-velocity impact is the fibre volume fraction. It has been demonstrated by Thomason *et al.* that increase in void content of glass fibre composites leads to a reduction in modulus.[181] In these studies the fibre volume fraction varies between 31-43%, as seen in section 4.2.1, and also it should be taken into consideration that each composite panel was prepared separately and differences in structure might occur. The panels with 10% azobenzene loading appeared to have lower amounts of reinforcement and more voids, compared to the composites with 0% and 5%, which might have led to reduced impact properties.

High-velocity impact results indicated better ballistic performance (by 10%) for specimens containing azobenzene (5-10%) by showing higher energy absorption in particular after UV irradiation.

4.2.5.2 Azobenzene effect in energy changes

After the addition of azobenzene indicated a higher energy absorption at 190 m/s, further studies were conducted to investigate its effect at two additional velocities. Figure 4.2.9 presents the absorbed energies of the non-irradiated composites with 0%, 5% and 10% azobenzene loading after impact at the 130, 190 and 370 m/s velocities. It should be noted here that at 130 m/s impact the projectile bounced back, in contrast to the 190 m/s and 370 m/s impacts where perforation occurred, but more details will follow in section 4.2.6 regarding the damage modes.

The graph in Figure 4.2.9 clearly shows an increase in absorbed energy with increasing impact velocities. In these studies, all the specimens were not subjected to UV irradiation, thus the azobenzene molecules were in their *trans* form. The absorbed energies at 130 m/s and 190 m/s for the control (rhombuses) and the composites with 5% (squares) and 10% (triangles) azobenzene loading were quite similar. Important differences appeared after impact at 370 m/s. The composites with 5% azobenzene loading demonstrated a capability of absorbing 57% more energy than the control. Likewise, 32%

more energy was absorbed by the 10% azobenzene composites than the samples without azobenzene.
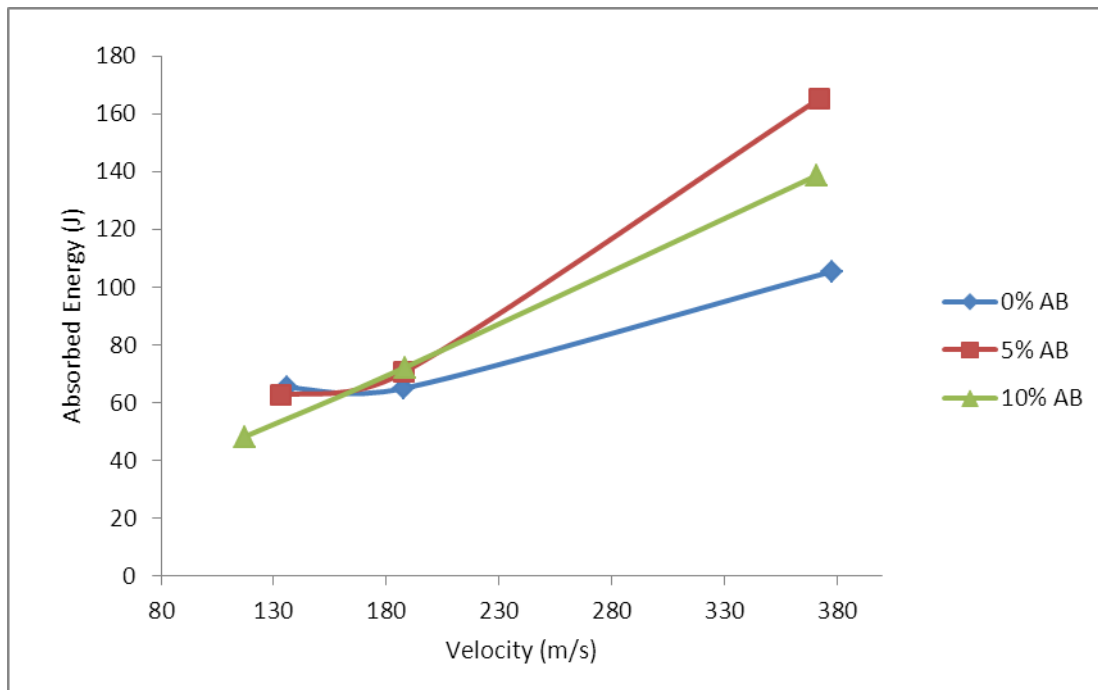
Figure 4.2.9 Absorbed energies of non-UV irradiated samples at different velocities

Theoretically, the absorbed energy with increasing impact velocity (beyond the perforation velocity) should remain constant.[182] This can be explained by the fact that when faster projectiles penetrate the targets in a shorter time, it is more likely that the targets have not enough time to undergo any further, progressive deformation. Furthermore, it has been demonstrated by Hazell *et al.* and Garcia-Castillo *et al.* that the increase of the areal density of composites leads to an increase in absorbed energy due to a longer contact time between the projectile and the target.[183, 184] Other studies confirmed that as the volume fraction was increased, the absorption energy from the total impact energy was increased in composites with upto 65% fibre volume fraction due to fibre breakage. Above this point (V_f=65%) the absorbed energy was decreased since

the interlaminar crack was propagated without any fibre breakage due to the decrease of the interlaminar shear strength.[185] In these PhD studies the differences in absorbed energy could correspond to the stressed-induced isomerisation of the azobenzene but more studies are required to verify this phenomenon. Therefore it is more likely any significant variation in the specimens' quality (thickness, V_f, V_v) might have led to this linear relationship between the impact and absorbed energy.

4.2.6 Damage assessment of impacted photoresponsive composites

From the impact tests the damaged areas, whose morphologies are described in detail below, of the 0%, 5% and 10% azobenzene composites were measured at different velocities and are presented in Figure 4.2.10. The kinetic energy of the projectile once impacted into the target is scattered and absorbed in various ways by the composites.[102] The main energy absorbing mechanisms of the ballistic impact include kinetic energy absorbed due to fibres' failure, due to matrix cracking and delamination and frictional energy absorbed during penetration.

These samples were not subjected to any light exposure therefore the effect of the azobenzene loading at different impact energies was studied. The results showed that after impact at 130 m/s and 370 m/s the created damaged area was quite similar for all the composites. At 190 m/s impact, the level of the damage was increased by approximately 50% for the 0% and 5% azobenzene composites. Especially the 10% azobenzene composite presented 19% more damage than the 0% and 5% composites.
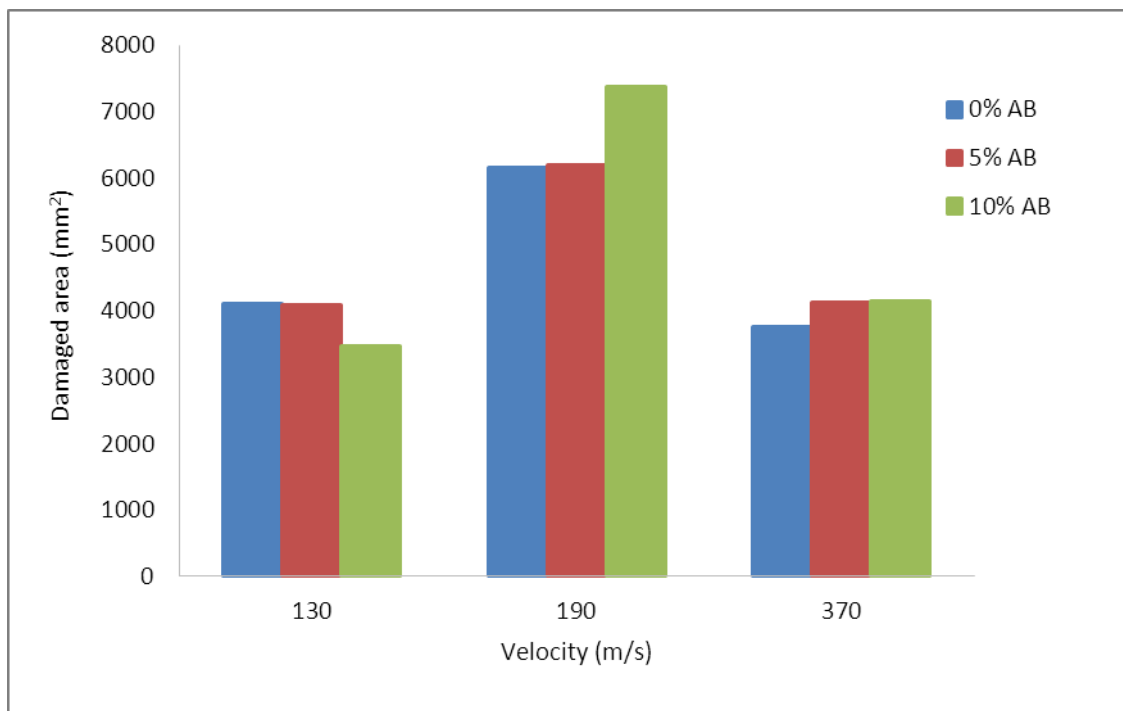
Figure 4.2.10 Damaged areas of non-irradiated composites at different velocities

It would have been expected a positive linear relationship between the size of the damage zones and the impact energy.[102] If higher amount of ballistic energy was absorbed by the same energy absorbing mechanism, the damaged area should be larger. Nevertheless, it has been found that the level of damage increases with increasing impact energy up to the penetration velocity, at which point the projectile perforates the target due to the decreased contact time that induces limitations to the failure modes.[186] Therefore, at increasing impact energy levels, greater than the penetration velocity, the level of damage decreases. In these findings it can be assumed that the penetration velocity is 190 m/s, which can justify the correlation between the damaged area and velocities. These experiments are highly related to the composites quality and since composite panels with 10% azobenzene indicated higher void volume fraction, as seen in previous section 4.2.1, an increase in delamination would have been more likely to occur.[185]
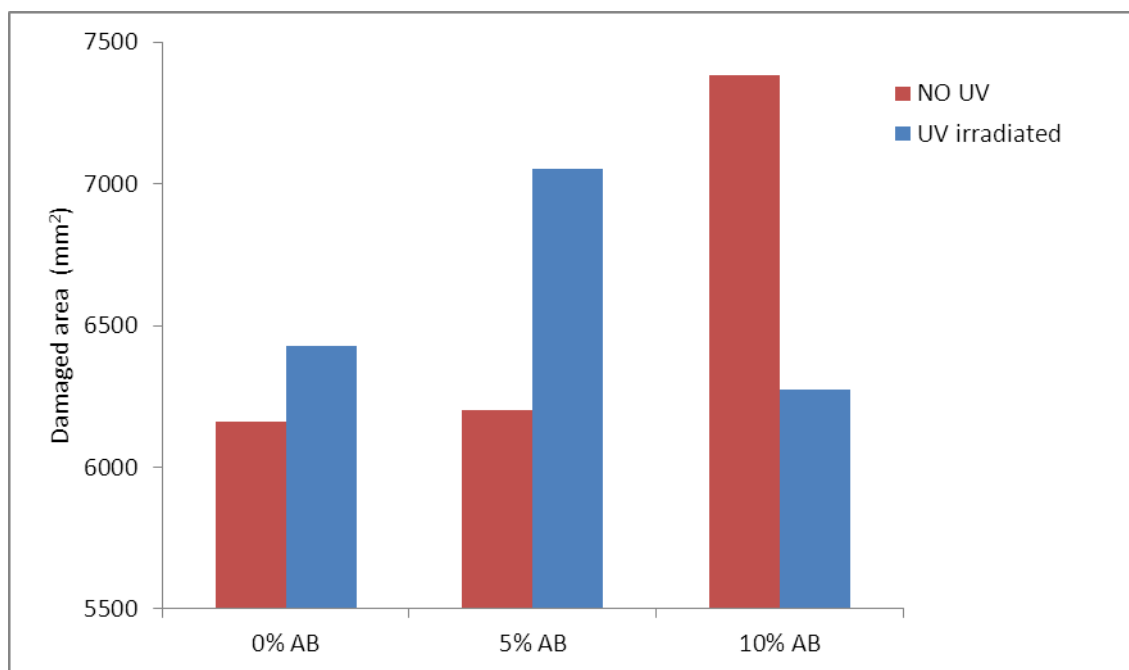
Figure 4.2.11 Comparison of damaged area between UV and non-irradiated specimens after impact at 190 m/s

Further analysis on the damaged area was conducted for the non and UV irradiated samples containing 0-10% azobenzene and previously impacted at the same velocity (190 m/s). Figure 4.2.11 illustrates the damaged area vs. the azobenzene loading by demonstrating the influence of UV light. It is apparent that the damage of the non-exposed samples became larger with the azobenzene loading. The damaged area is expected to increase with increased absorbed energy after impact at a single velocity.[102] Therefore, this effect came in accordance with the findings from the absorbed impact energy vs. azobenzene loading, in the previous section 4.2.5.1 which indicated an increase in absorbed energy with higher azobenzene loading. On the other hand the damaged areas of the UV irradiated composites were not found to have any correlation with the azobenzene loading. An important increase by 10% of the damage was noticed at the UV irradiated 5% azobenzene composite compare to the non-irradiated specimen. These results came in accordance with the fracture toughness findings of the polymeric matrices in section 4.1.2.12. When

the modified resins with azobenzene were exposed to UV irradiation (*cis* isomers) the fracture toughness of the materials was decreased due to localised stresses after *trans→cis* isomerisation which facilitate and propagate any crack growth.[171]
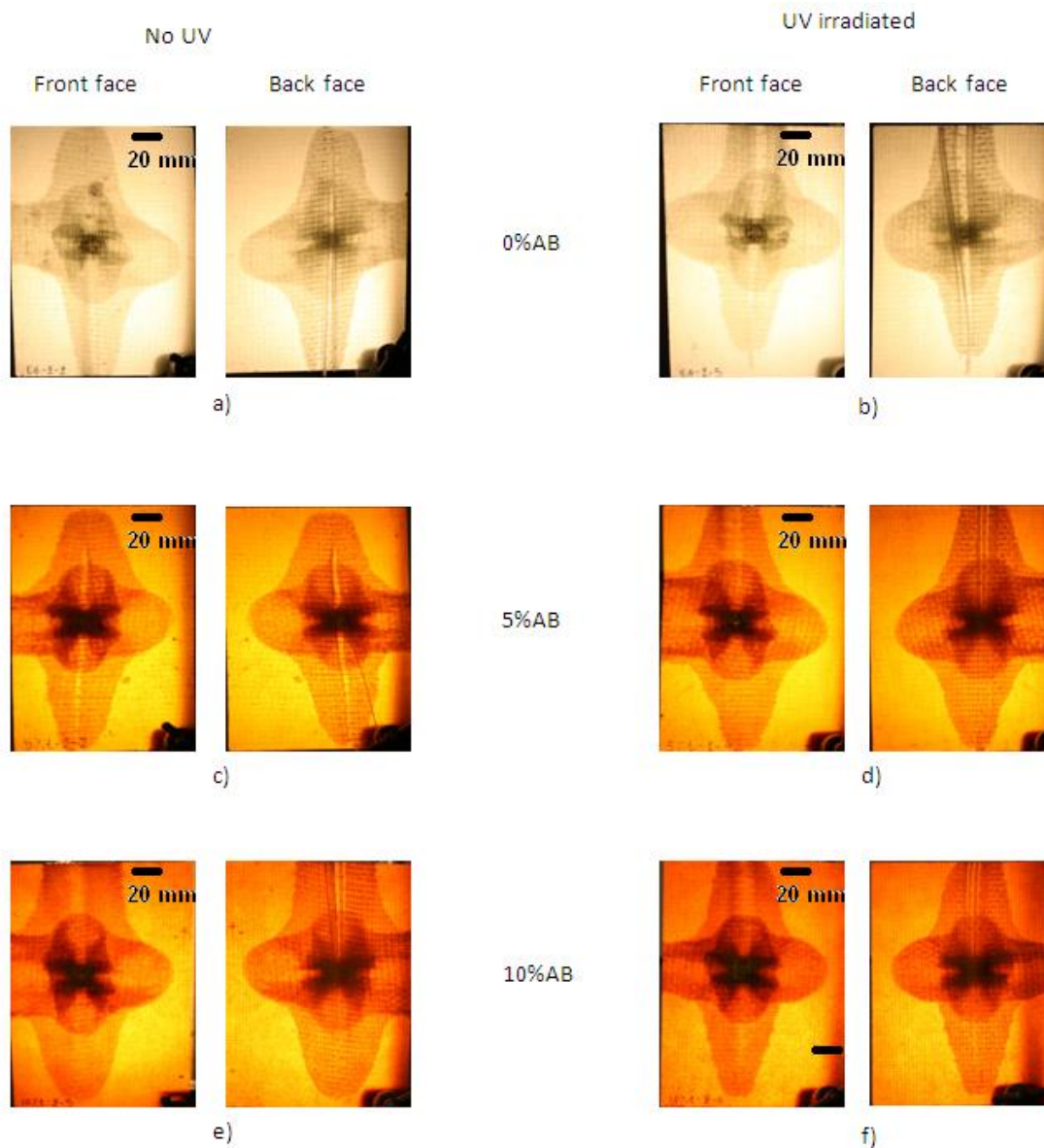
Figure 4.2.12 Front and back faces (left and right respectively) of composites with 0%, 5% and 10% azobenzene loading UV and non-irradiated after 190 m/s impact

Figure 4.2.12 illustrates a selection of front and rear faces of composites containing 0%, 5% and 10% azobenzene, with and without being exposed to UV light. Impact at 190 m/s produced quite similar large delamination areas with perforation and fibre fracture to all the specimens regardless the azobenzene loading. The delaminated areas of the epoxy based glass fibre reinforced composites formed a cross-shape zone in all the cases. The cross-shape is a common damage shape, observed in reinforced fibre composites with [0/90]$_{ns}$ cross-ply stacking sequences.[187, 188] The directions of cracks are perpendicular to the direction of fibres. As the specimen in the bulge on the rear side is further penetrated by the projectile, its tensile strength is eventually exceeded and a star-shaped crack develops around the tip of the projectile. At the rear sides of the specimens rearward petalling was also observed.[189] Petalling is produced by high radial and circumferential tensile stresses after passage of the projectile and is accompanied either by large plastic flows and/or permanent flexure.[189] These images (Figure 4.2.12) indicated that delamination is the major energy absorption mechanism in these specimens.[180]

As can be seen in Figure 4.2.13 the composites with different azobenzene loading exhibited the same type of impact damage when penetration (130 m/s) and perforation (190 and 370 m/s) occured. The damage modes caused by the impact varied with the applied impact energy. The a), d) and g) photos correspond to the specimens with 0%, 5% and 10% azobenzene respectively after impact at 130 m/s. The projectile did not manage to perforate the targets, although petalling, delamination, fibre pull out, fibre breaking and matrix cracking were observed. On the other hand, at 190 m/s the sphere perforated successfully all the targets, leaving again a petalling damage morphology, as seen in Figure 4.2.13 b), e) and h) for 0%, 5% and 10% azobenzene composites. Different failure morphologies were noticed at the highest velocity. In Figure 4.2.13 c), f) and i) the petalling is being decreased while a well-defined hole became obvious for all the samples. The failure morphologies came in good agreement with the literature, since at the highest impact energies the

failure modes exhibit less petalling and higher fragmentation which leads to more obvious holes.[183, 190, 191] Images of the samples, taken from the high-speed camera confirmed the rebounding (Figure 4.2.14 a), perforation (Figure 4.2.14 b) and higher fragmentation (mass loss) (Figure 4.2.14 c) during the impact at different velocities.
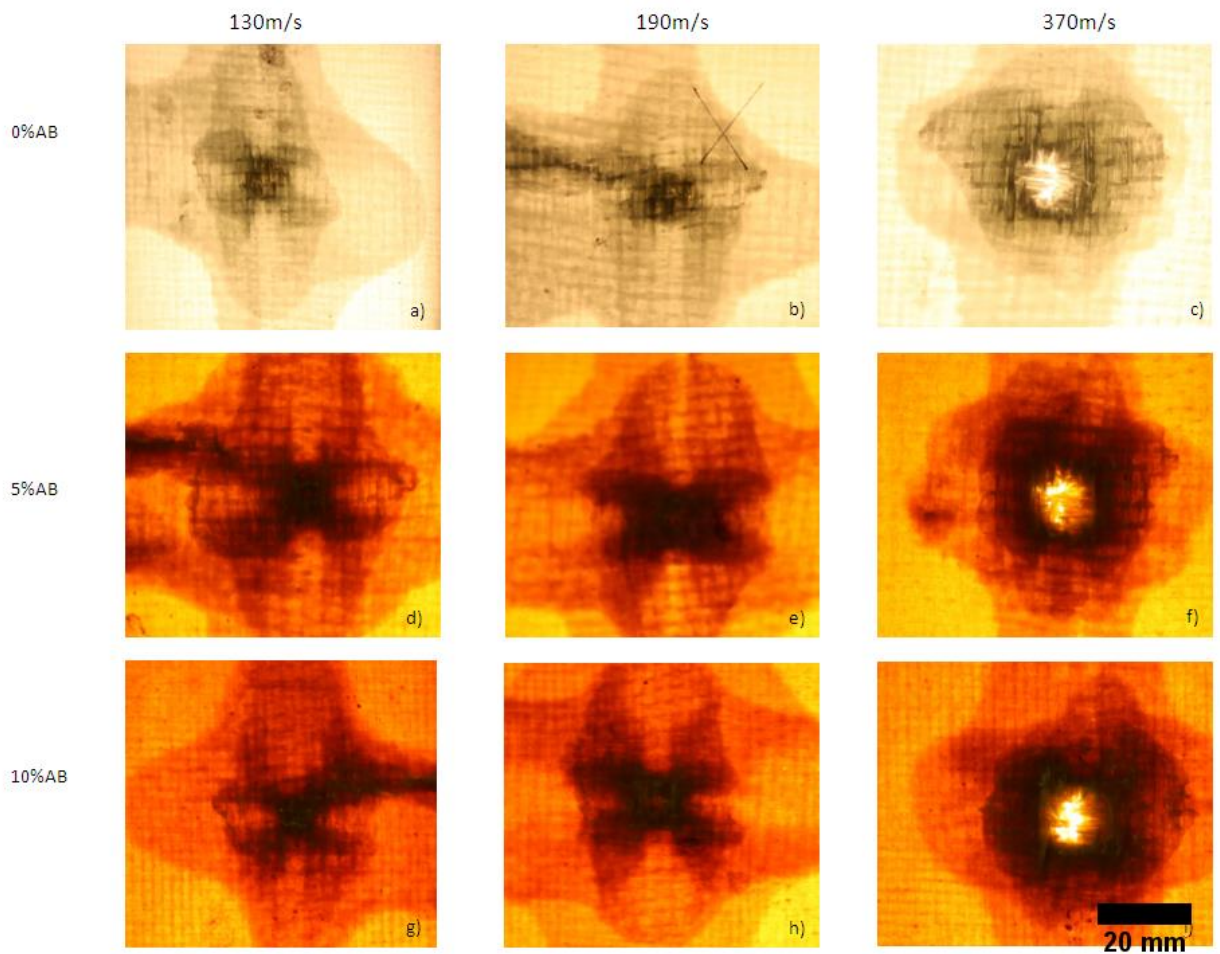
Figure 4.2.13 Post-impact images of non-irradiated composites, with 5%, 10% and without azobenzene, at different velocities
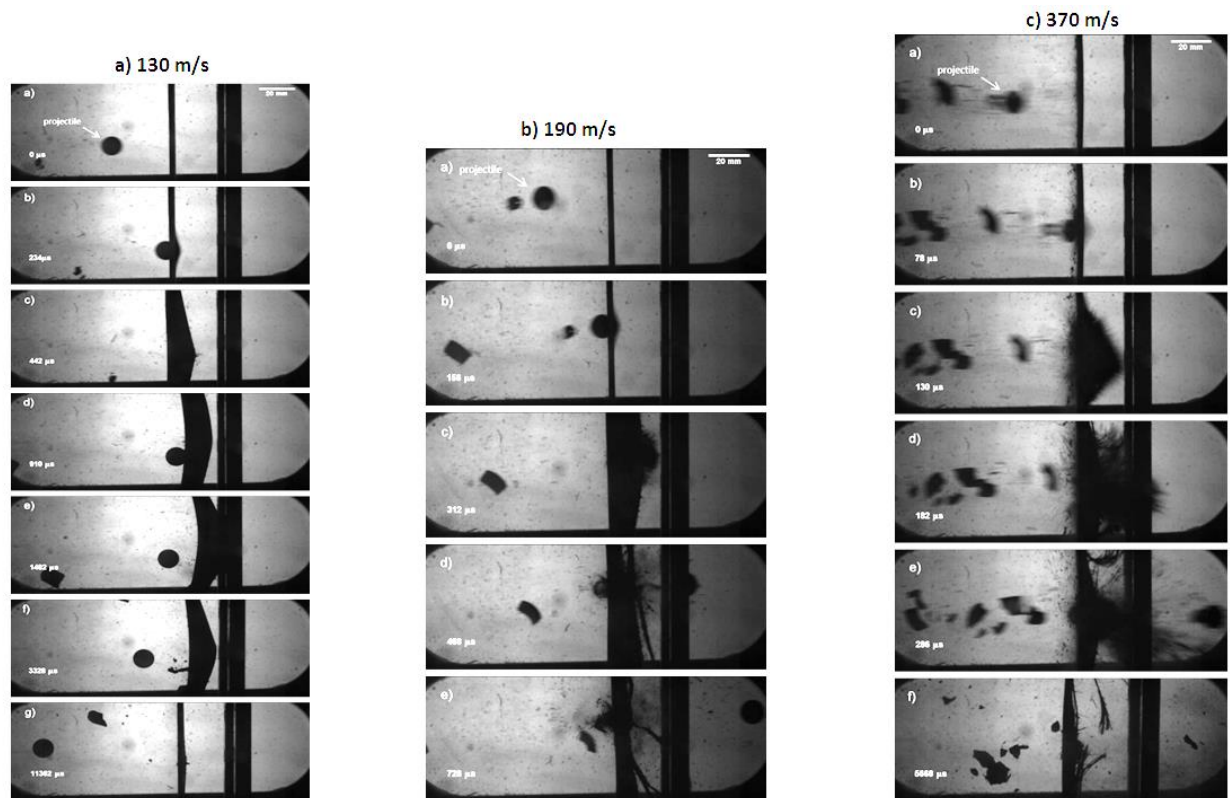
Figure 4.2.14 Photos taken during impact tests at a) 130 m/s, b) 190 m/s and c) 370 m/s of non UV irradiated composites with 5% azobenzene

4.2.7 Post-impact residual strength studies (CAI)

Compression after impact (CAI) tests determine the residual strength of materials damaged by impact.[192] For this study high impact energy was applied to the specimens (190 m/s), delamination occurred and then post impact tests were performed to measure the composites' maximum strength and the damage from the delamination which progressively propagated during the compressive force. CAI tests were performed to composites with 5%, 10% and without azobenzene loading. Each specimen was subjected to UV or visible light exposure before or after CAI and the maximum force was recorded. Exposure to UV light induced the azobenzene isomers to obtain their *cis* form and exposure to visible light converted the azobenzene isomers to their *trans* form into the composites via isomerisation.
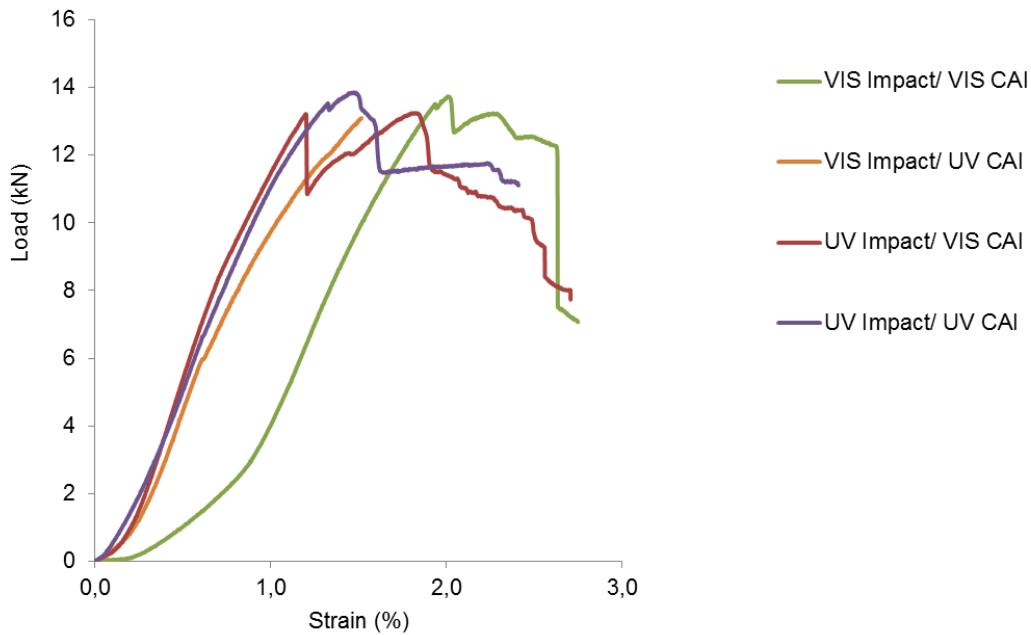
Figure 4.2.15 Typical load vs. strain graph of 10% azobenzene composites under different light conditions

Figure 4.2.15 illustrates typical load vs. strain graphs of composites with 10% azobenzene loading. As it can be seen from the graph the different light treated specimens demonstrated similar compressive strengths. Initially, an increase in strength (elastic region) was observed until a peak was reached (residual strength) and then the composites showed a decrease in stress or plateau until failure (breaking point). During the tests, cracking sounds and growth of the damage after impact of the specimens were noticed.

For better understanding the behaviour and the effect that azobenzene and light have on the epoxy glass fibre composites, two graphs including the residual strength values at all the different light conditions of the 0%, 5% and 10% azobenzene specimens were plotted (Figure 4.2.16 and Figure 4.2.17). Visible irradiation before impact and CAI tests are described as VIS Impact and VIS

CAI accordingly. UV irradiation prior to impact and CAI tests are mentioned in the graph as UV Impact and UV CAI respectively.

Figure 4.2.16 Residual strength vs. azobenzene loading at visible irradiated samples prior to impact tests

The first graph, in Figure 4.2.16, facilitates the identification of any trend that might be revealed from the experiments where the specimens were exposed to visible irradiation before the impact test. A noticeable observation is the decrease of the residual strength with the azobenzene loading of visible-irradiated specimens before impact test and exposed to UV light prior to CAI. This trend is usually observed in CAI tests where the residual strength decreases with the increasing impact energy.[193] However, in these studies a single impact velocity (190 m/s) was applied to all the composites before the CAI tests. The percentage of decrease reached the 9% and 20% for the composites with 5% and 10% azobenzene loading. The decrease of the residual strength was noticed too in composites that were exposed to visible light before impact test and prior to CAI. The percentage of decrease reached

21% and 23% for the composites with 5% and 10% azobenzene loading respectively. The results suggest that *trans* azobenzene (after exposure to visible light) prior to high-velocity impact has a negative effect on the residual strength. The decrease in CAI could be a result of increased interlaminar shear damage.[194] This explanation can be supported by the fact that with increased *trans* azobenzene loading the absorbed energy after impact was found to be increased as well (section 4.2.5.1). As the level of damage increases, the structural strength of the composite after impact also decreases.[186] Therefore, more failure was expected to occur (according to the damage assessment after impact, section 4.2.6) and less residual strength.
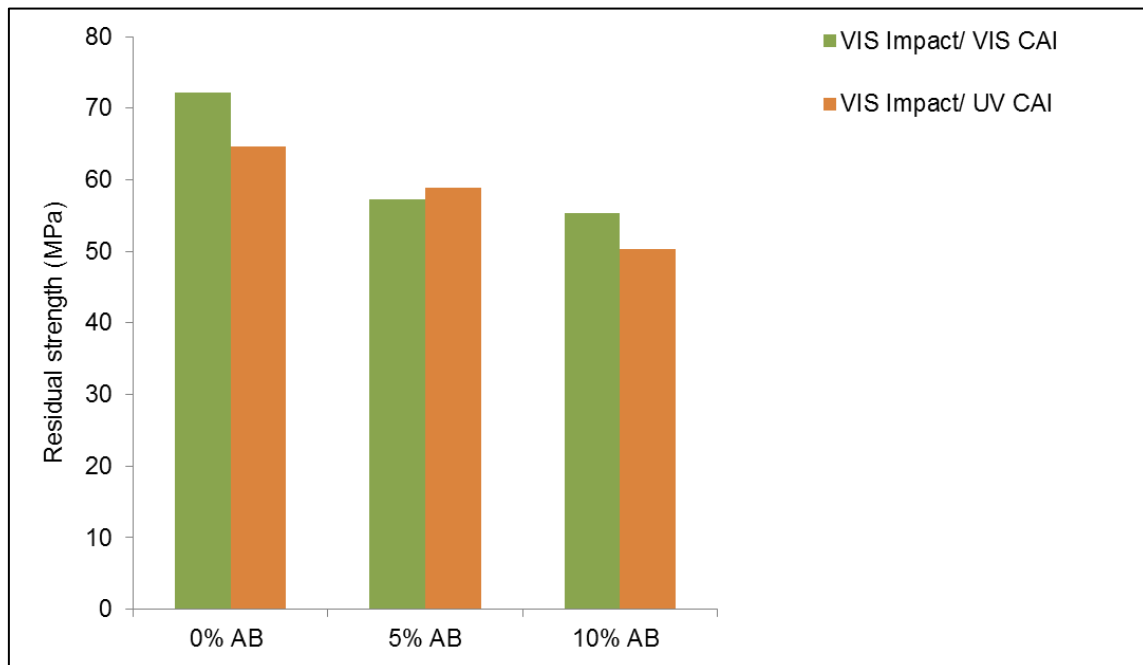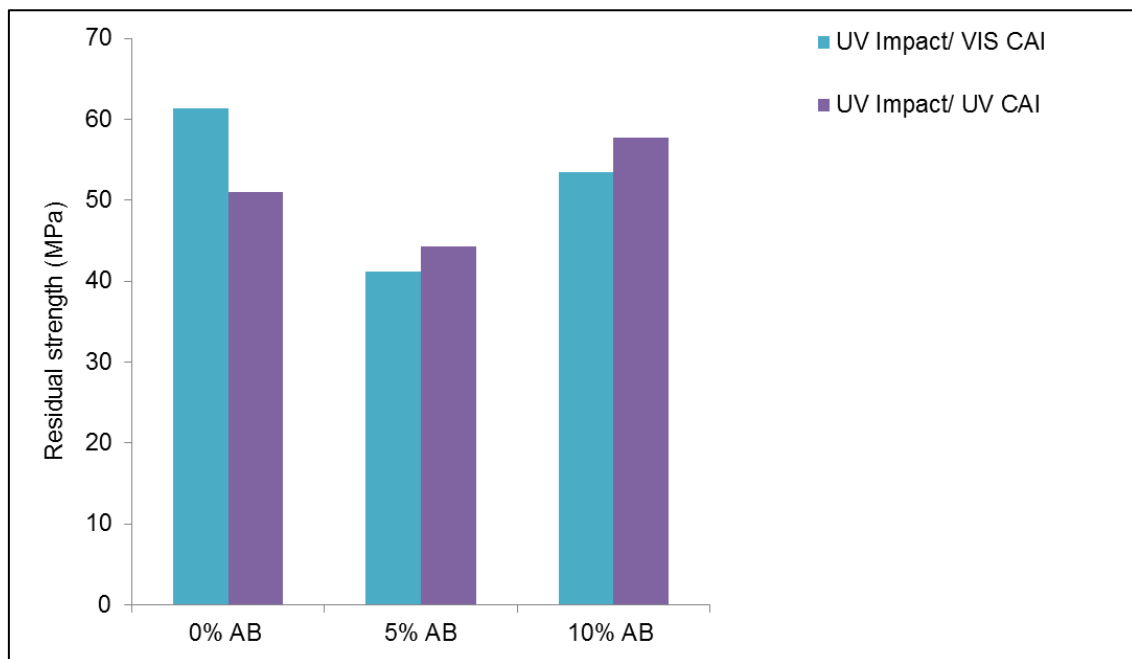

Figure 4.2.17 Residual strength vs. azobenzene loading at UV irradiated samples prior to impact tests

The graph in Figure 4.2.17 demonstrated that there is no apparent trend relating to the CAI experiments where the specimens were exposed to UV irradiation before the impact test. However, this graph (Figure 4.2.17) from CAI tests

demonstrated the same trend with the graph (Figure 4.2.7) from the compression tests (before impact) in section 4.2.4. An important observation is the effect of UV irradiation on the reference samples (0% azobenzene loading). In both graphs (Figure 4.2.16 and Figure 4.2.17) an approximately 10-15% decrease of the residual strength was noticed. These findings come in accordance with the compression tests, in section 4.2.4, where the effect is justified by the degradation of the mechanical properties due to UV irradiation. On the other hand the composites containing azobenzene (5% and 10%) demonstrated a slight increase of 5-8% of the residual strength after further exposure to UV light. The enhancement of composites' residual compressive properties might have occurred due to the polymer chain rearrangement caused by the photoinduced *trans→cis* isomerisation. Another explanation for the increase in residual strength could be a better adhesion between the polar, *cis* azobenzene epoxy resins, with 3 Debye dipole moment, and glass fibres or because the polymeric matrix containing *cis* azobenzene chromophores demonstrate better compressive properties than with the non-polar, *trans* azobenzene with 0 Debye polarity.[154]

4.2.8 Post-impact damage assessment of photoresponsive composites

At the end of all the experiments some post-impacted samples were tested to see if there was any healing effect after UV irradiation. The composites were exposed to UV irradiation for 1 hr but no healing was apparent as seen in Figure 4.2.18 and Figure 4.2.19 possibly due to the large deformation area. As has been discussed earlier in section 4.1.2.8 higher chromophore loading might be required to increase the chain mobility for healing to occur in larger damaged regions.

0% AB epoxy/glass fibres composite

1 hr UV Radiation

After Radiation

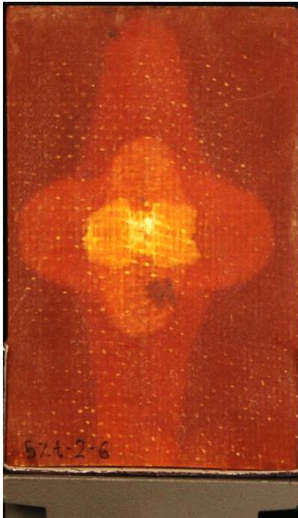**Figure 4.2.18 Impacted specimens with 0% AB before and after UV irradiation**

5% AB epoxy/glass fibres composite

1 hr UV Radiation
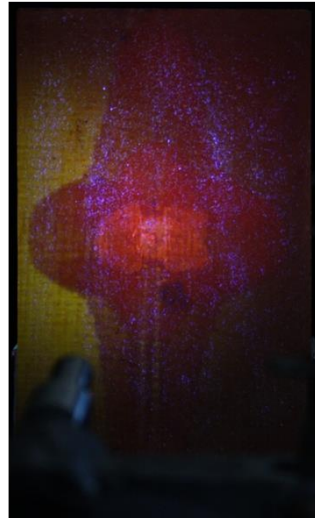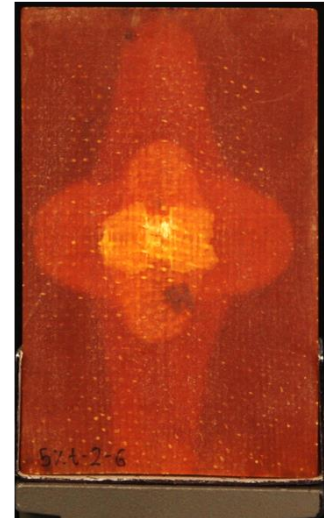
After Radiation

Figure 4.2.19 Impacted specimens with 5% AB before and after UV irradiation

The AFM studies, in section 4.1.2.8, demonstrated the influence of the damage area on the healing efficiency. Azobenzene epoxy resin films with smaller

damage depth (400-770 nm) obtained healing with higher ratios of 68-73%. On the other hand, when the damage depth was increased to 950 nm and 2700 nm the healing ratios decreased respectively to 55% and 40%. The damage recovery was attributed to the *trans→cis* photoisomerisation of the azobenzene, since the films without azobenzene did not indicate healing ratio when exposed the UV light under the same conditions.

This outcome would have been expected because azobenzene isomerisation belongs to the intrinsic healing mechanisms, where a material has self-healing abilities triggered by damage or external stimulus such as heat, light, or pressure.[24] Blaiszik *et al*. have proved that different healing mechanisms demonstrated healing for different damage volume regions.[82] They verified that intrinsic healing systems are corresponding to small damage (0.01-0.5 mm^3) and can potentially heal at the molecular scale. Vascular systems, where healing agents are embedded within a vascular network that has upto 3D connectivity are able to heal much larger damage volumes (0.1-100 mm^3). Capsule-based approaches, where healing agents are dispersed in capsules are able to heal medium sizes damage areas (0.1-50 mm^3). The damaged areas, in this PhD study, after impact, were found to be between 12,000 and 24,000 mm^3, as seen in previous section 4.2.6. The formation of this large damage area explains why healing effect was not obvious in composite matrices.

5 CONCLUSIONS

The concept of photoresponsive composite materials is innovative and encouraging for both the defence and civil platforms due to the use of azobenzene molecules in the materials whose properties can be manipulated by light. This research concerned the synthesis and characterisation of functional photoresponsive polymers that were exploited to improve the mechanical properties of new formulations by UV light.

A number of photoresponsive molecules and their polymers and copolymers have been synthesised. Their physical and mechanical properties were investigated in order to understand the photoresponsive behaviour of azobenzene molecules. Characterisation of these materials by conventional techniques such as NMR, FTIR, DSC and UV/Visible spectroscopy demonstrated some success in synthesising the materials to be used for composites preparation.

It was observed by reflectance, UV/Vis and NMR spectroscopy that *trans* and *cis* isomers of the azobenzene molecules undergo reversible isomerisation from *trans*→*cis* and *cis*→*trans* under the influence of light of appropriate wavelength (UV and visible), sonication and thermal treatment.

DSC analysis showed that the T_g of the azobenzene acrylic-based polymers is higher (by 10-20°C) than that of PMMA. The nanoindentation tests that were conducted in poly(MMA/MOAB) thin films before and after exposure to UV light demonstrated a maximum increase in stiffness of 19% with an optimum 30 mol% azobenzene loading. Remarkable healing of the indents occurred due to the UV triggering which enhanced the polymers' mobility in the damaged region. Photo-triggered volume changes of this class of materials were not observed after gas pycnometry. Ultrasound-induced *cis*→*trans* isomerisation was demonstrated here for the first time in azobenzene materials at solid state. It was found that a 20% of the *cis* isomers were converted to the *trans* form by

CONCLUSIONS

ultrasonic agitation for 2 hrs while an additional 36% were isomerised by the associated temperature rise.

Modified epoxy resins (mono- and di-functional) were synthesised by optimising an existing synthetic route. Investigation of, the monofunctional, 4-GOAB' responses to light and its curing behaviour with diethylenetriamine was undertaken. The rates of *cis→trans* isomerisation in the 4-GOAB and 4-GOAB/DETA systems by visible light, thermal treatment and storage in the dark were studied using UV/Vis spectroscopy. The conformational changes in the two systems are influenced by the chemical structures of both systems and also by the method employed to trigger the isomerisation. The rate of *cis→trans* isomerisation in 4-GOAB is faster by visible light than by heat or storage in the dark although visible irradiation involved smaller amount of energy compared to heat energy. Conversely, the rate of reversible *trans/cis* isomerisation is slower in the cured system (4-GOAB/DETA) than in the individual monomer (4-GOAB). The curing of the azobenzene epoxy resin was successfully accomplished for the first time and was confirmed by ^{1}H-NMR, near-FTIR spectroscopy, and dynamic DSC analyses. It was found that only three molecules of 4-GOAB can react with one molecule of DETA although each DETA molecule possesses five reactive protons.

Cured azobenzene epoxy resin films (with the difunctional 4,4′-DGOAB) were fabricated and penetrated using a common diamond scriber and a pin and AFM analysis demonstrated that after UV light irradiation a significant recovery of 55-73% of the polymers was observed. The healing character of the particular polymers is attributed to the azobenzene isomerisation, which by the geometrical changes that UV light triggers, enables the mobility of the whole polymeric matrix. Reflectance spectroscopy analysis and images after nanoindentation verify the healing effect. Azobenzene-based epoxy polymers could find applications where shape memory materials or self-healing agents are required.

CONCLUSIONS

Fracture mechanics studies on epoxy-based polymeric matrices with 0%, 5% and 10% azobenzene loading were conducted before and after UV irradiation. It was demonstrated that the azobenzene chromophores (in their *trans* form) increase the plasticity of the matrix and crack propagation occurs slower in comparison to the control specimens. An 11% increase in K_{IC} was observed at specimens with 10% azobenzene loading. On the other hand, UV light increases the brittleness of the matrix with higher azobenzene loading. This phenomenon is attributed to the azobenzene isomerisation which might transform to a higher rigidity the matrix by forming physical cross-linking when the chromophores are in the molar polar (3 D) *cis* form.

After having reinforced the modified epoxy resins with glass fibres, the manufactured composites were examined for their quality and void and fibre volume fractions. All the panels demonstrated good quality, with typical fibre volume fractions of 31-43% and slightly higher than the normal void volume fractions of 6-16%. The photoresponsive behaviour of the specimens was analysed with reflectance spectroscopy, which indicated the required UV exposure time for complete conversion of the azobenzene molecules from *trans→cis* is 1 hr. Measurements with a thermal camera showed a temperature increase of 3.5-6°C of the UV irradiated photoresponsive composites and a thermal relaxation to take place within 20 min. The UV treated composites exhibited a 16% increase in compressive strength with the higher azobenzene loading of 10% due to the polymer chain rearrangement caused by the photoinduced *trans→cis* isomerisation. The impact energy at 190 m/s of the glass/epoxy composites with 0%, 5% and 10% azobenzene loading before their failure was measured. The influence of light irradiation on these materials was also evaluated. The results show that *trans* azobenzene is a good impact energy absorbing material, probably due to the geometrical isomerisation that could occur due to the stress of the impact. Nevertheless, the damaged area that occurred during the impact test was higher with azobenzene and in particular without exposure to UV light. The azobenzene loading appeared to decrease the residual strength after exposure to UV light before the CAI tests.

Examination of the fractured specimens by visual/light inspection showed a similar degree of damage for non-irradiated composites with and without azobenzene.

To summarise synthesis, characterisation and analysis were performed to identify materials that would offer optimum performance to be able to use in photoresponsive composites formulation. It is believed that the combination and the comparison of different azobenzene polymers with resins will offer valuable information to the world of smart engineering materials.

5.1 Future work

- It would be extremely useful if low-velocity impact tests were performed in photoresponsive composites. Low-velocity impact tolerance is depending on the target stiffness, material properties and the projectile's mass and stiffness. [105] At low-impact energy (1-5 J) minimal damage would occur and information about matrix cracking and delamination initiation will be revealed. It is expected that higher absorption energy will correspond to composites with higher azobenzene loading.

- The synthesis of 2,2'-diglycidyloxyazobenzene, shown in Figure 5.1.1, will involve functional groups to different positions (2,2') of the phenyl rings. This study will investigate the effect of the location of the azobenzene on the rate of isomerisation and on the stiffness of the polymers. It is expected that this type of molecules may undergo mechanical isomerisation resulting in the similar mechanical properties in response to UV light. If this will be demonstrated there will be no need for UV irradiation to isomerise the azobenzene molecules. This can be a very promising approach because the linkage of the azobenzene with the polymeric matrix would be closer to the nitrogen double bond nitrogen, where the isomerisation occurs. Thus the obtained photomechanical changes can be proven more forceful.
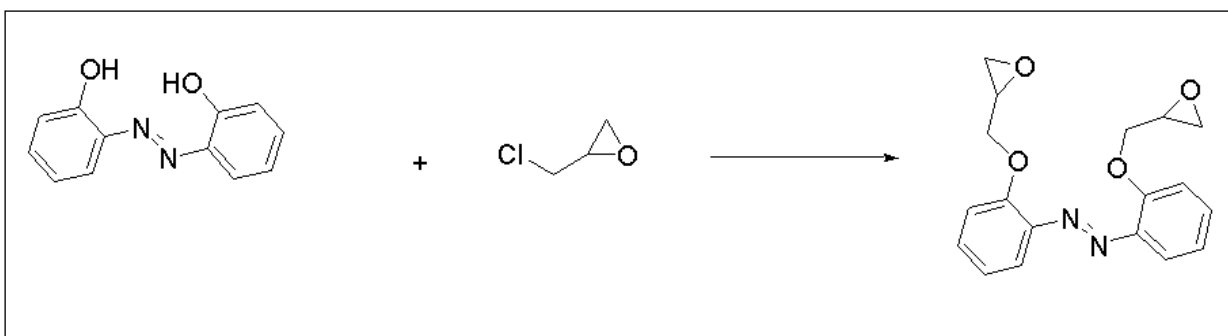
Figure 5.1.1 Synthesis of 2,2'diglycidyloxyazobenzene

- The use of difunctional azobenzene crosslinkers with a short spacer (2-5 ehtylene groups) might lead to an optimum effect of *trans→cis* isomerisation. The photoinduced changes would be able to affect the whole polymer chains but at the same time, because of the spacer, the stresses induced by UV-induced *trans→cis* conversion will be eliminated due to higher free volume space. In this way, the compressive properties of the photoresponsive composites could be enhanced.

- Another possibility for observing healing effect in larger areas would be the use of a hybrid polymer matrix with a more flexible polymer (e.g. polyurethane) than epoxy. The disadvantage of the introduction of increased mobility within the material is the reduction of the mechanical properties.[195] By increasing the flexibility of chains between crosslinks it would facilitate the photochemical *trans→cis* azobenzene isomerisation and lead to higher elastic recovery and scratch resistance but lower chemical resistance. A flexible network with high amounts of urethane linkages would involve physical crosslinks with reversible hydrogen bonding. Since the polymer matrix would be flexible, temperatures beyond the polymer T_g would permit enough flow for surface recovery in a scratch healing mechanism.

APPENDICES

Appendix A

A.1 Isolation and Purification Processes

All the chemical substances purchased or those synthesised in the lab were not always 100% pure. Therefore their purity should be tested before being used for chemical synthesis. The presence of impurities in the reagents could contaminate the target products. Many synthesised products should be isolated in pure form for being characterised. The following techniques were applied to purify the materials in these investigations.[130]

In some synthetic works, such as in sections 3.1.1.2 and 3.1.1.5 solvent extraction technique was used. For the liquid extraction, in order to remove unwanted substances from the crude products, a conical separator funnel fitted with a stopcock was required. The mixture of an organic and an aqueous solution resulted to the isolation of dissolved products into the organic phase from the impurities that have been trapped in the water. This procedure was repeated and the two phases were collected separately every time. The purification of solids was conducted by recrystallisation. Appropriate solvents and temperature ranges were applied to dissolve the impurities and easily separate the latter from the crystals of the product.

When the isolation of the products from impurities was not efficient by solvent extraction or recrystallisation, the column chromatography process was conducted instead.[12] The fundamental equipment for CC was a long narrow glass tube fitted with a glass stopcock. With this technique a desired compound can be isolated from a mixture. During this experimental work, silica gel (SiO_2) with particle size 33-70 μm was the absorbent that was used for column packing. The selection of an efficient solvent was important; not too polar because that would not lead to layers separation from the fast motion of the substances. Alternatively if the eluent was too slow no substances would be eluted from the column. This procedure was very robust and the obtained

product was completely purified. The disadvantages of this technique were that it required enough time and after its completion a respectful amount of the product (~10-20%) was lost through the column, due to interactions with the silica.
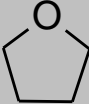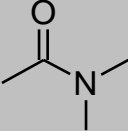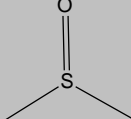
For the removal of bulk amount of solvents after solvent extraction or CC, rotary evaporation was used. The separation of liquids from a reaction mixture was obtained by the use of a Rotevapor BUCHI Vacuum Controller V-805. It is a rapid and simple method. The solution in the rotating flask, with the aid of reduced pressure and heat transfer, was evaporated fast, preventing any local overheating while the content was mixing homogeneously. At the end of this process, only solid particles were present into the flask. The purification of the chemical compounds for the removal of any trapped solvent was achieved by drying the samples under high vacuum at room temperature. This method is based on the high reduced pressure that can eliminate any traces of residual solvent.

A.2 Solvent effect on polymer synthesis

It has been reported that synthesising PMMA with different solvents can affect the mechanical and thermal behaviour of the polymer.[126, 127] Thus, the selection of an appropriate solvent for the synthesis of PMMA incorporated with azobenzene groups would be an essential research attempt. The thermal and spectroscopic properties of azobenzene based polymers synthesised by using THF (sample CV2.1), DMF (sample CV2.2) and DMSO (sample CV2.3) were investigated and evaluated.

Table 5.1.1 Information for THF, DMF and DMSO solvents

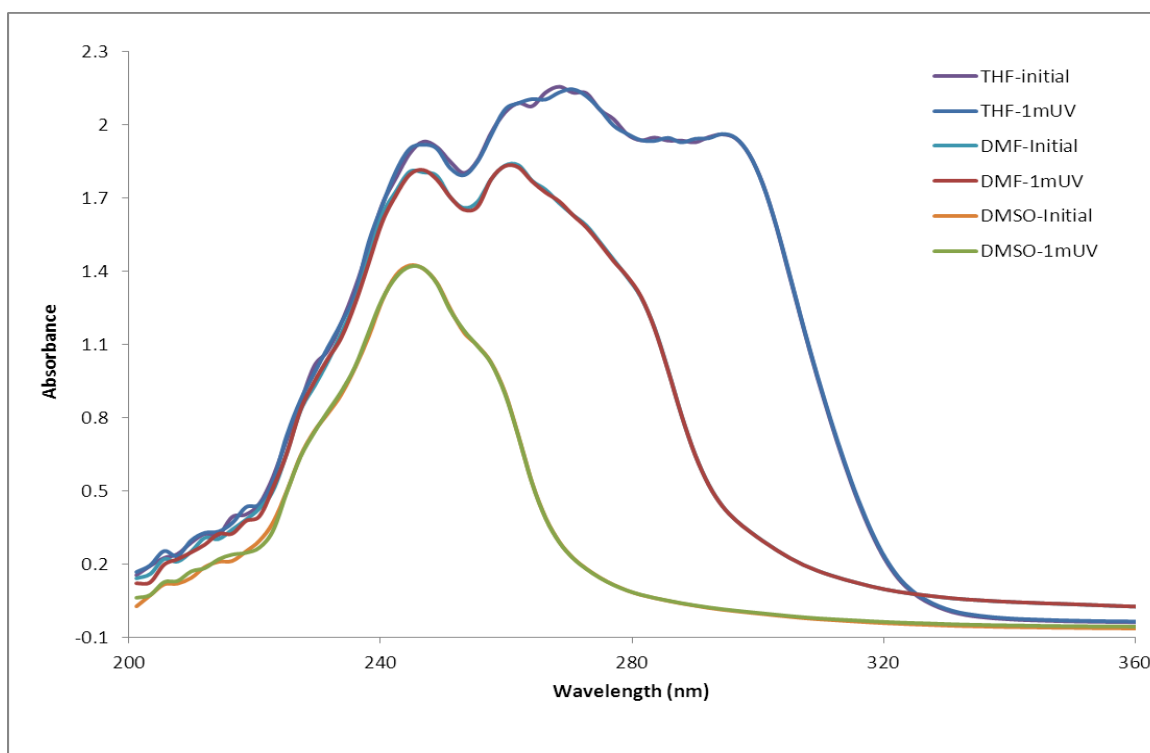| Solvents	THF	DMF	DMSO
Molecular structure			
UV absorbance cut-off (nm)	240	265	265
Polarity Index	4.0	6.4	7.2
Toxicity	Relatively non-toxic	Health hazardous	Low toxicity

Figure 5.1.1 UV/Vis spectra of THF, DMF and DMSO before and after 1 min of UV irradiation at 500 mW/cm^2

These solvents were chosen due to their common usages and were examined by UV/Vis based on their different polarity and their toxicity. The data are illustrated in Table 5.1.1. The characteristic absorbance bands between 240 and 265 nm are shown in Figure 5.1.1. THF, DMF and DMSO's absorbance bands did not change significantly upon 1 min of UV irradiation. DMSO was determined as the most appropriate solvent for the UV/Vis spectroscopy measurements of azobenzene based monomers and polymers as its cut off peak interrupts the azobenzene signals minimally.

A.3 Thin layer chromatography

Thin layer chromatography (TLC) was conducted almost after each step of the reactions due to its reproducible, fast, cheap and highly accurate qualitative character for the detection of substances. It only required chromatographic plates where spots of any known substances and our product were spreading from the bottom to the top of the plates with unique velocities. The choice of suitable solvent or mixture of solvents was crucial in order to provide appropriate characteristic constants for each chromatographic system.

A.4 NMR studies
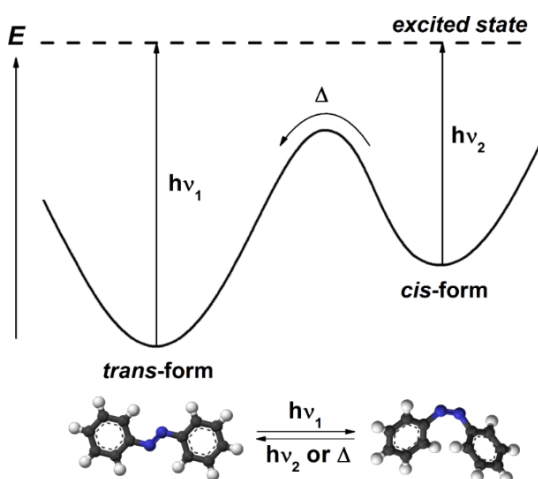
Figure 5.1.2Scematic representation of different energy profiles of azobenzene isomers. (Taken from Ref.[196])
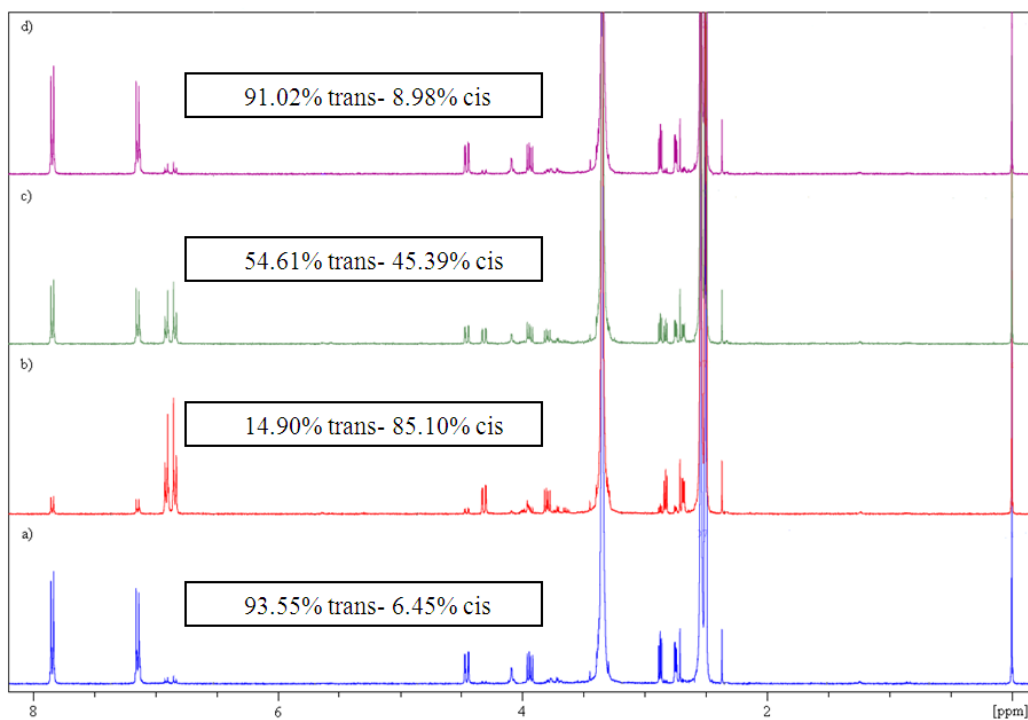
Figure 5.1.3 ^{1}H NMR spectra of 4,4´-DGOAB in DMSO-d$_{6}$ solution a) non-irradiated, b) after 1 min exposure to UV light, c) after exposure to 60 min sonication and d) after exposure to 120 min sonication
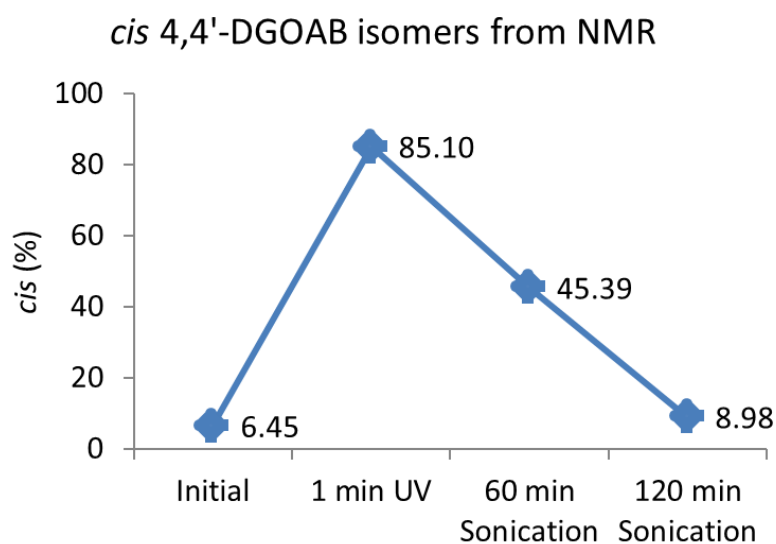
Figure 5.1.4 Concentrations of cis isomers calculated from the integrals of the protons of the cis benzene rings at δ 6.8297-6.927 ppm

A.5 HPLC studies

In this section chromatograms of materials with their characteristics (retention time, peak area and height) after HPLC are presented.

- Initial 4,4´-DGOAB
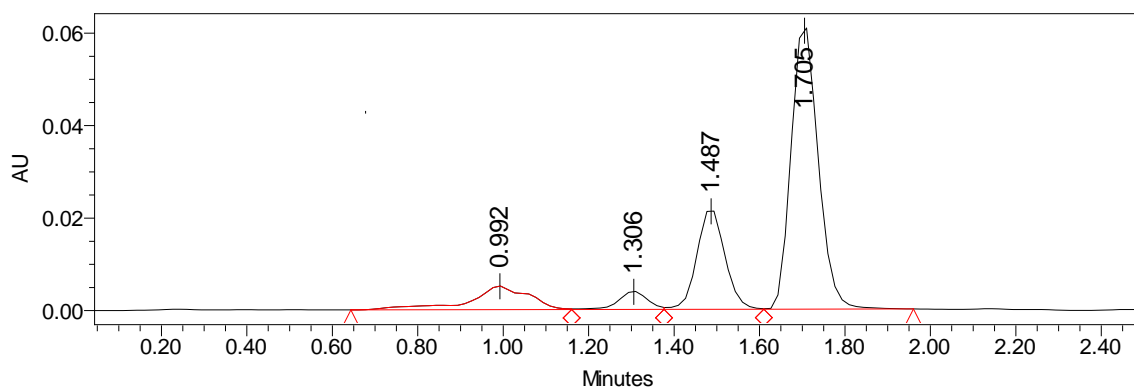
Name	Retention Time	Area	Height
1	0.992	48850	4987
2	1.306	18396	3843
3	1.487	98521	21222
4	1.705	269952	60199

- UV irradiated 4,4´-DGOAB
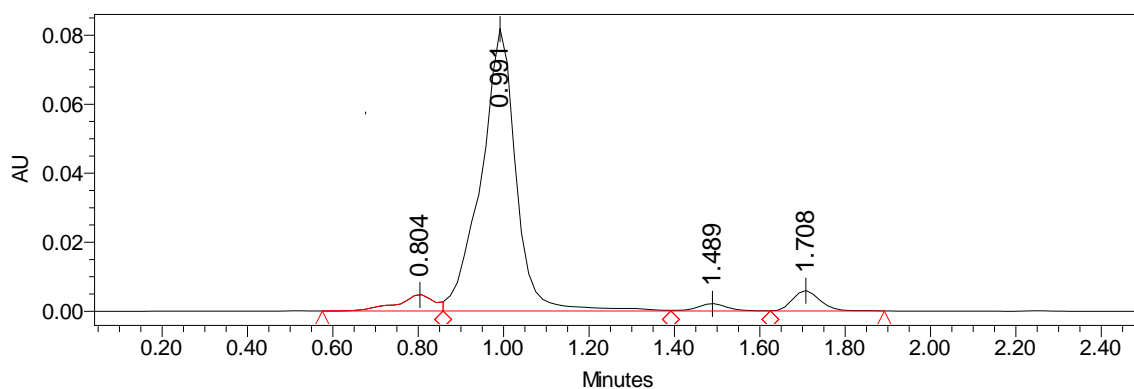
Name	Retention Time	Area	Height
1	0.804	28337	4630
2	0.991	463289	79968
3	1.489	10131	2083
4	1.708	26232	5796

- UV-Sonicated 4,4´-DGOAB
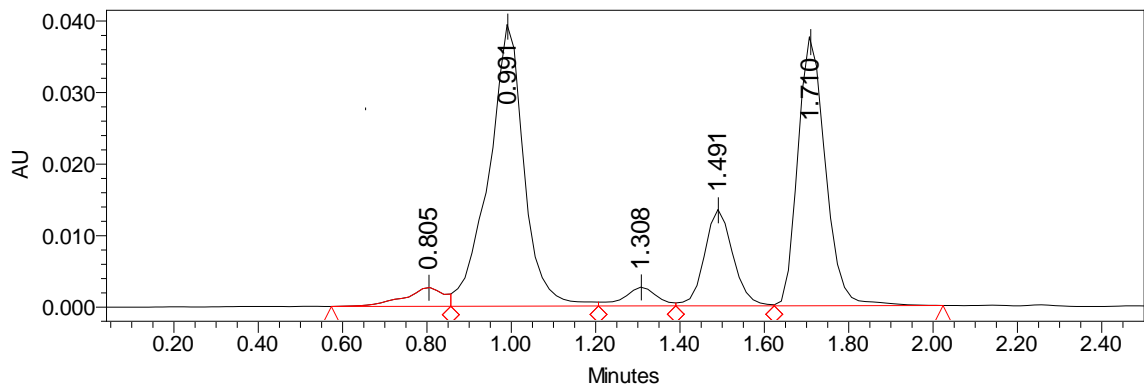
Name	Retention Time	Area	Height
1	0.805	16954	2585
2	0.991	227388	38587
3	1.308	14047	2574
4	1.491	62778	13185
5	1.710	170406	36905

- Initial 4,4´-DHAB
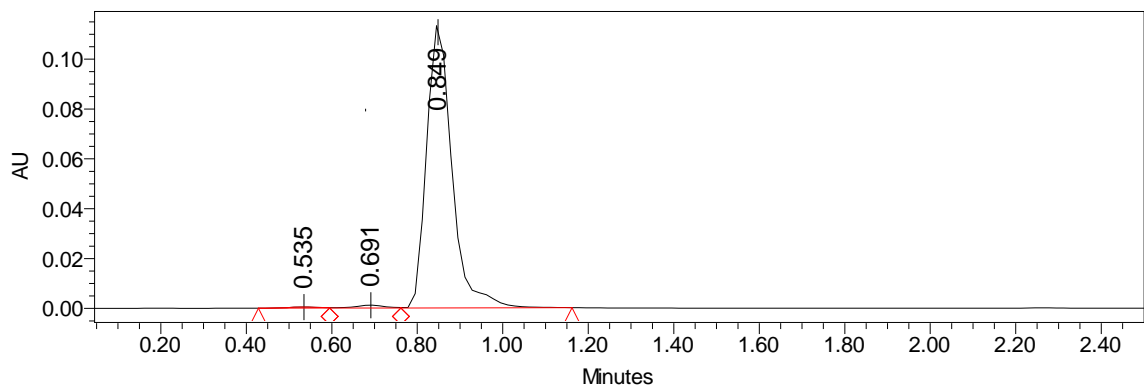
Name	Retention Time	Area	Height
1	0.535	2223	451
2	0.691	5414	1120
3	0.849	467578	110690

- UV irradiated 4,4´-DHAB
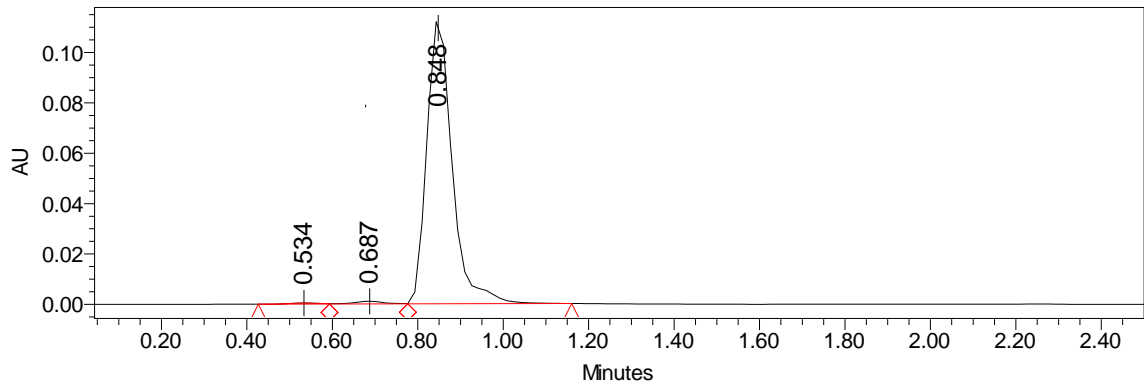
Name	Retention Time	Area	Height
1	0.534	2068	433
2	0.687	5325	1072
3	0.848	464100	109880

UV-Sonicated 4,4´-DHAB
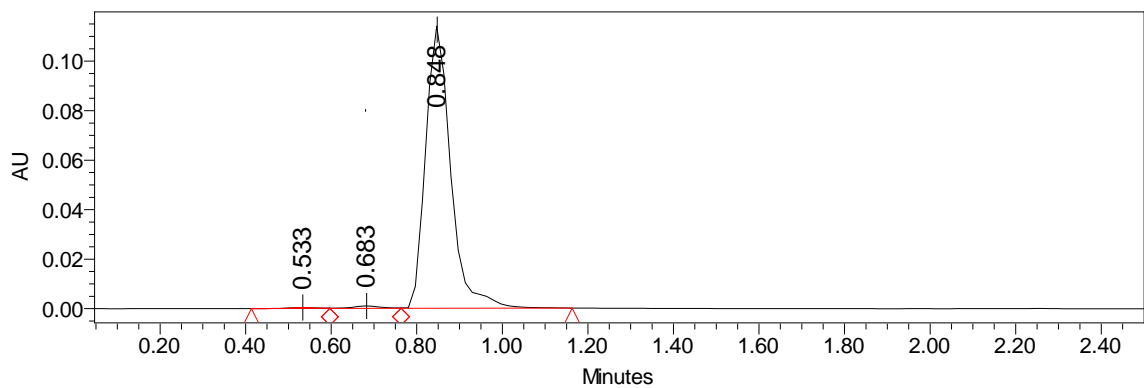
Name	Retention Time	Area	Height
1	0.533	1741	394
2	0.683	4524	968
3	0.848	462862	110658

- Initial ACN
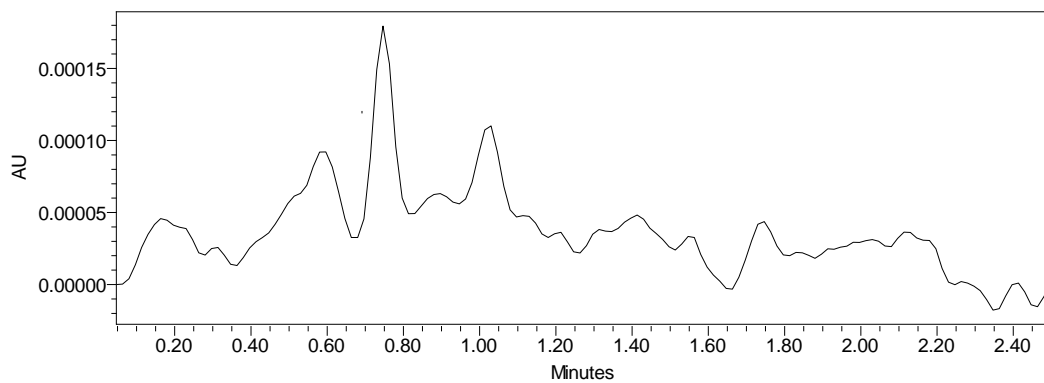
- UV irradiated ACN
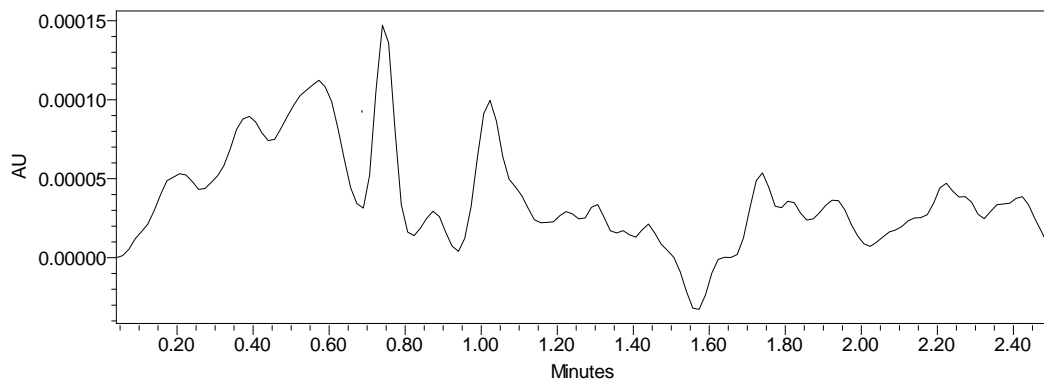
- UV-Sonicated ACN

A.6 Nanoindentation studies

45% AB P(MMA/MOAB) FILM

1st Nanoindentation on unirradiated film

1 hour UV light

2nd Nanoindentation 3 hours after UV irradiation

30 min Visible light
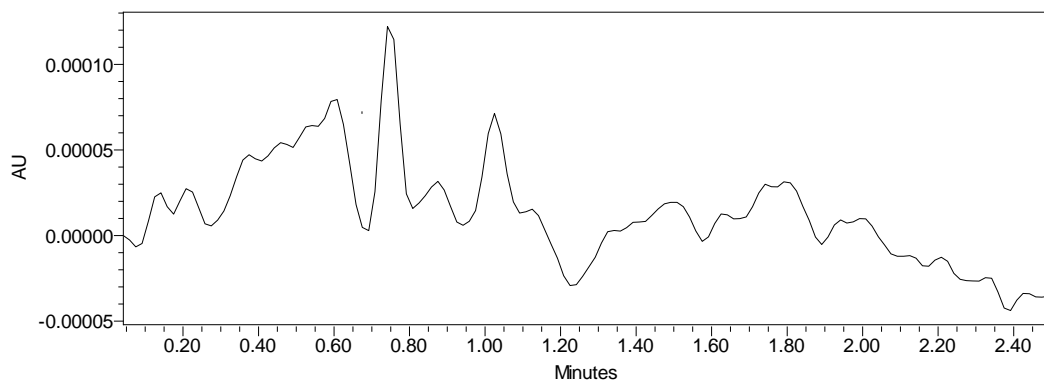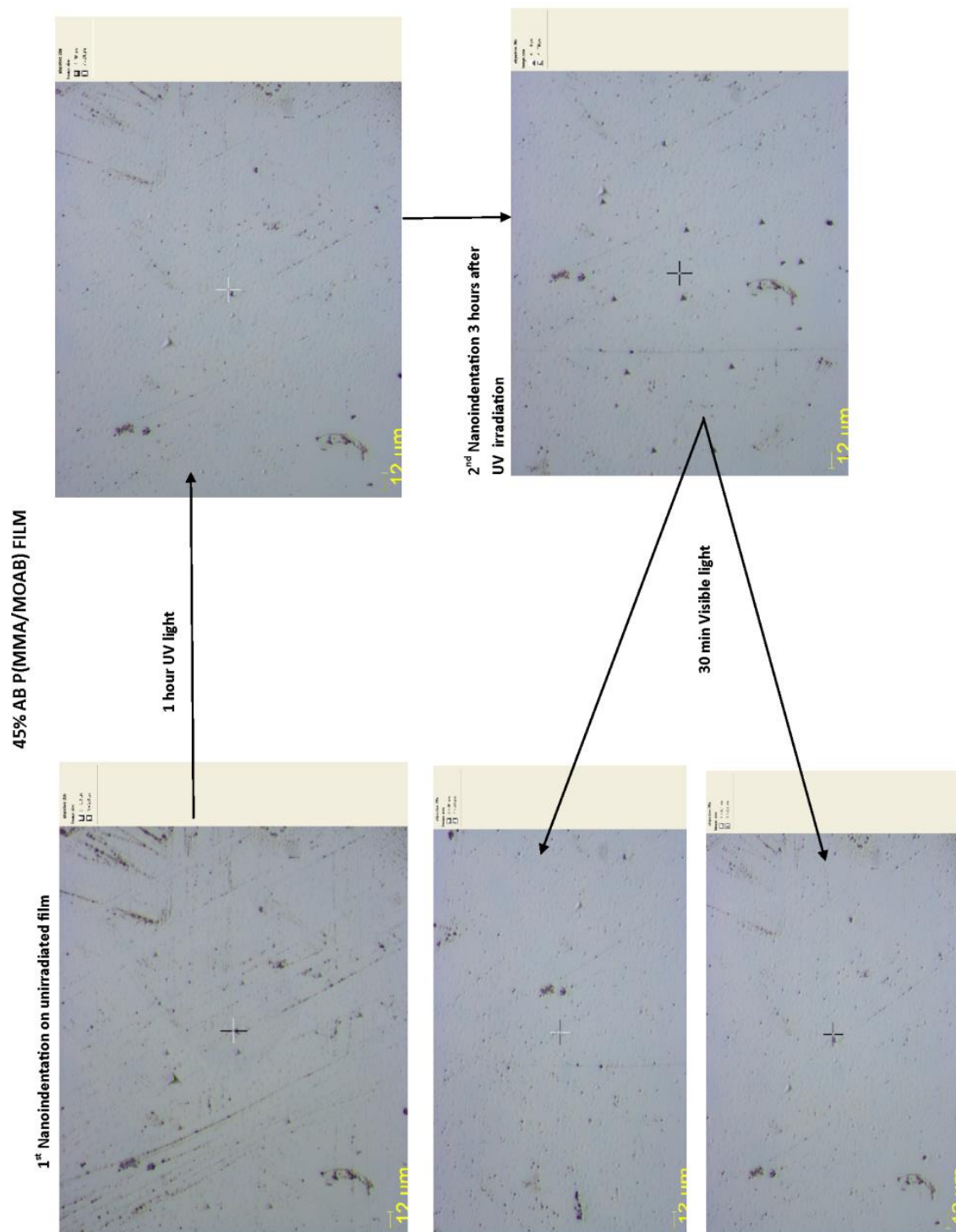
A.7 FTIR studies

In this section FTIR spectra of the materials are presented.
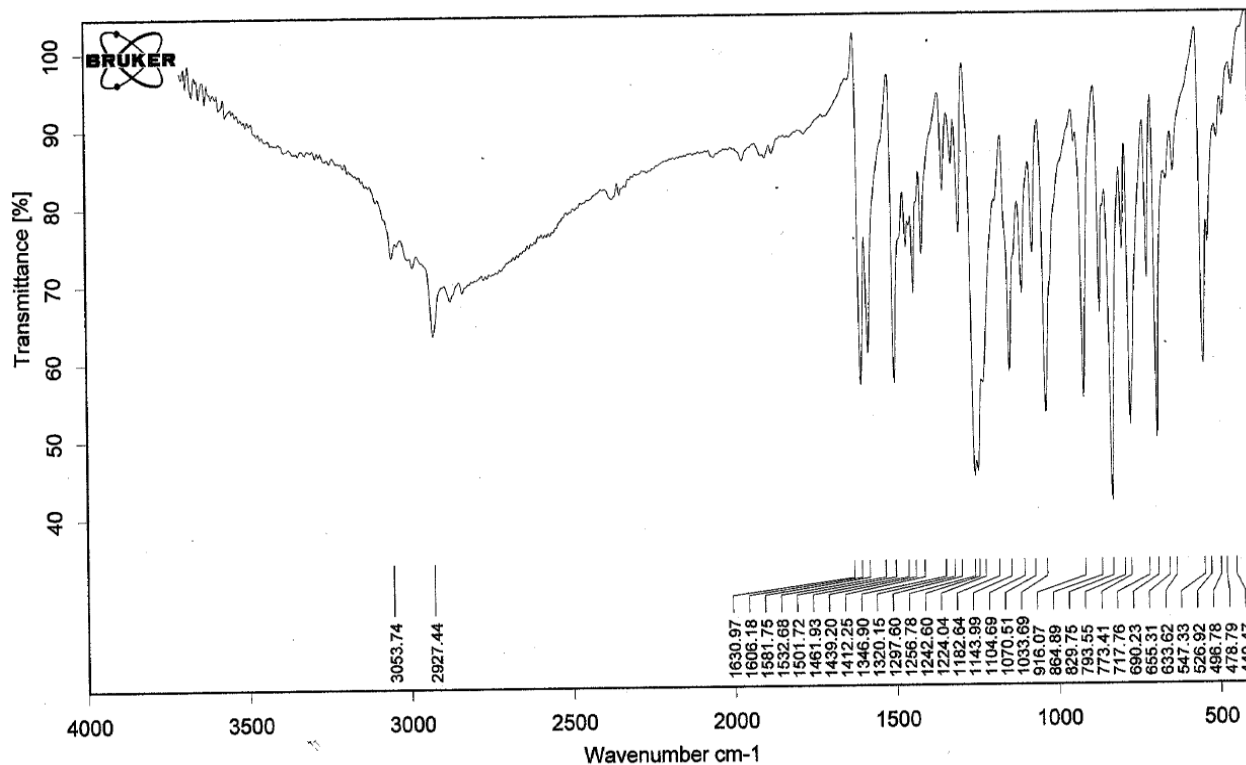
Figure 5.1.5 4-Glycidiloxyazobenzene Infrared spectrum

Bond	Compound Type	Frequency range, cm^{-1}
C-H	aromatic rings	3053.74
	Alcanes	2927.44
C=C	aromatic rings	1500, 1600
N=N	diazo-	1581.75
C-N	amine	1224.04-1256.78
C-O	ether	1070.51-1143.99
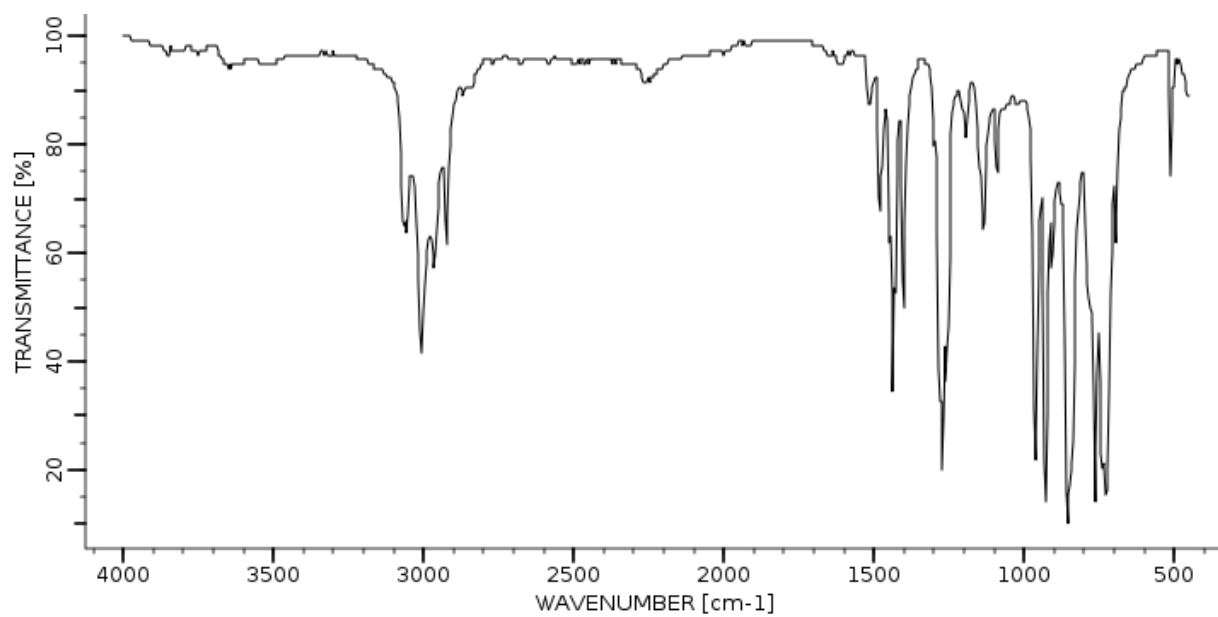
Figure 5.1.6 Epichlorohydrin Infrared spectrum
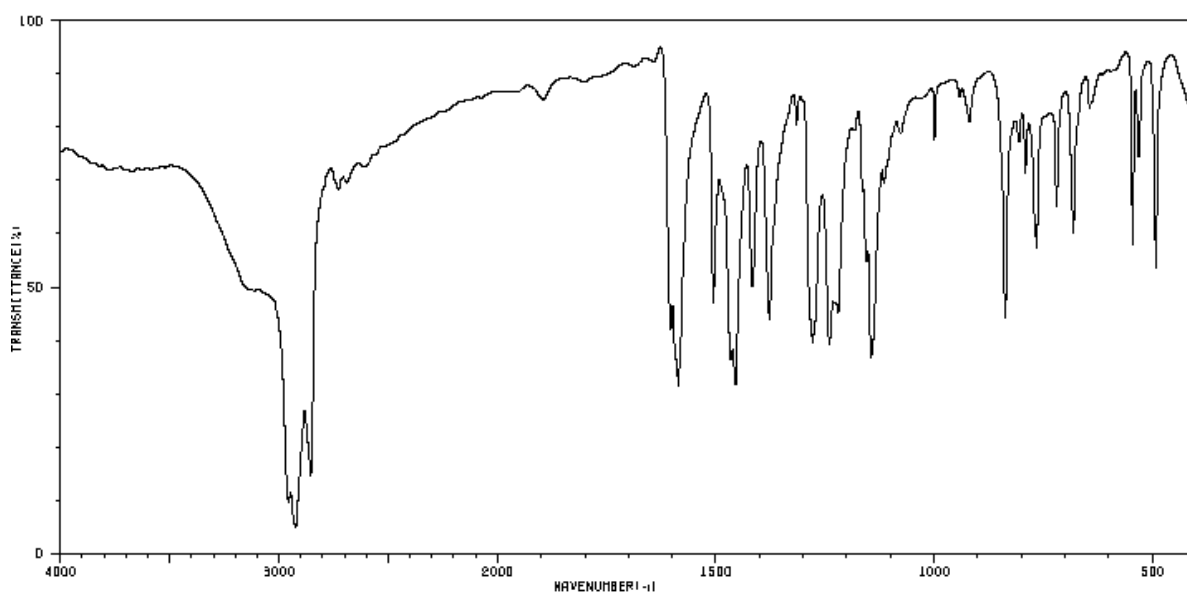
Figure 5.1.7 4-Phenylazophenol Infrared spectrum
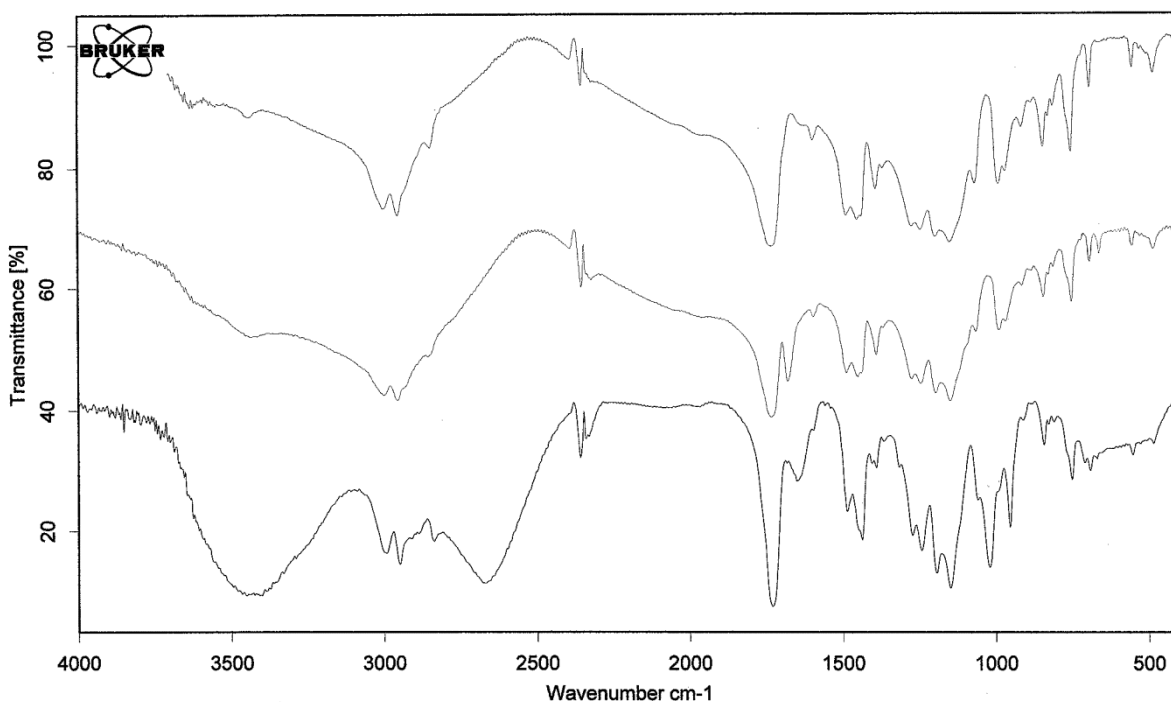
E:\STAFF data\WORK.393	CV2.3	KBr	06/09/2012
E:\STAFF data\WORK.392	CV2.2	KBr	06/09/2012
E:\STAFF data\WORK.391	CV2.1	KBr	06/09/2012

Seite 1 von 1

Figure 5.1.8 CV2.1, 2.2, 2.3 copolymers Infrared spectrum

A.8 UV/Vis studies

In Table 5.1.2 three spectral regions, UV/Vis, IR and radio wave, with their produced phenomena and their associated wavelengths are listed. The identification of the samples in this project was accomplished after collecting and analysing these three spectra.

Spectral Region	Wavelength	Special phenomena
Ultraviolet/ Visible	200-400nm/ 400-750nm	Outer electron transitions
Infrared	13333-400nm	Molecular vibrations
Radio wave	10-50m 190-555m 1000-2000m	Nuclear magnetic resonance

Table 5.1.2 Regions of the electromagnetic spectrum (Taken from Ref.[130])

- UV/vis studies of azobenzene molecules exposed to ultra sound (without UV irradiation).
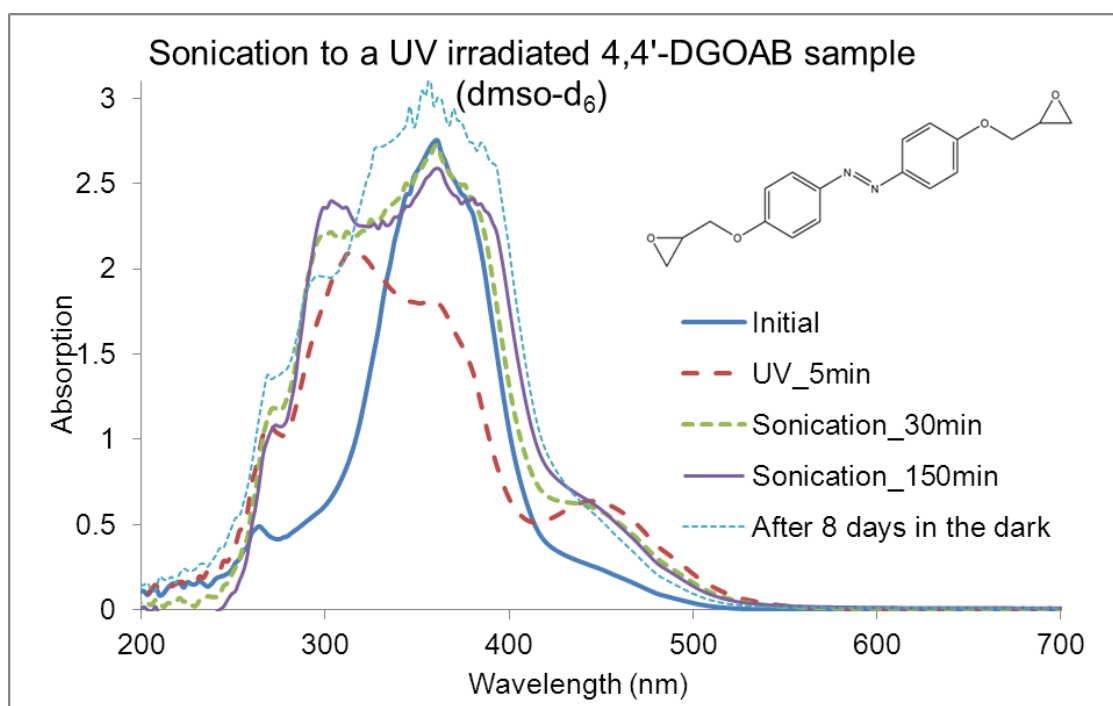
Figure 5.1.9 UV irradiated solution of 4,4´-DGOAB of 0.25 mg/ml in DMSO-d$_6$ after sonication and storage in the dark

Complete *cis* →trans isomerisation occurred upon 30 min sonication (in agreement with lit.). Partially trans→cis isomerisation (6%) occurred upon 150 min sonication. After 8 days in the dark the solution seems more concentrated, probably due to solvent evaporation but here the peak at 300 nm seems to have been decreased.

From UV/Vis measurements (Figure 5.1.9 and Figure 5.1.10) sonication at UV irradiated and non-irradiated 4,4´-DGOAB molecules induces *trans* to *cis* isomerisation ~6% in DMSO solution.
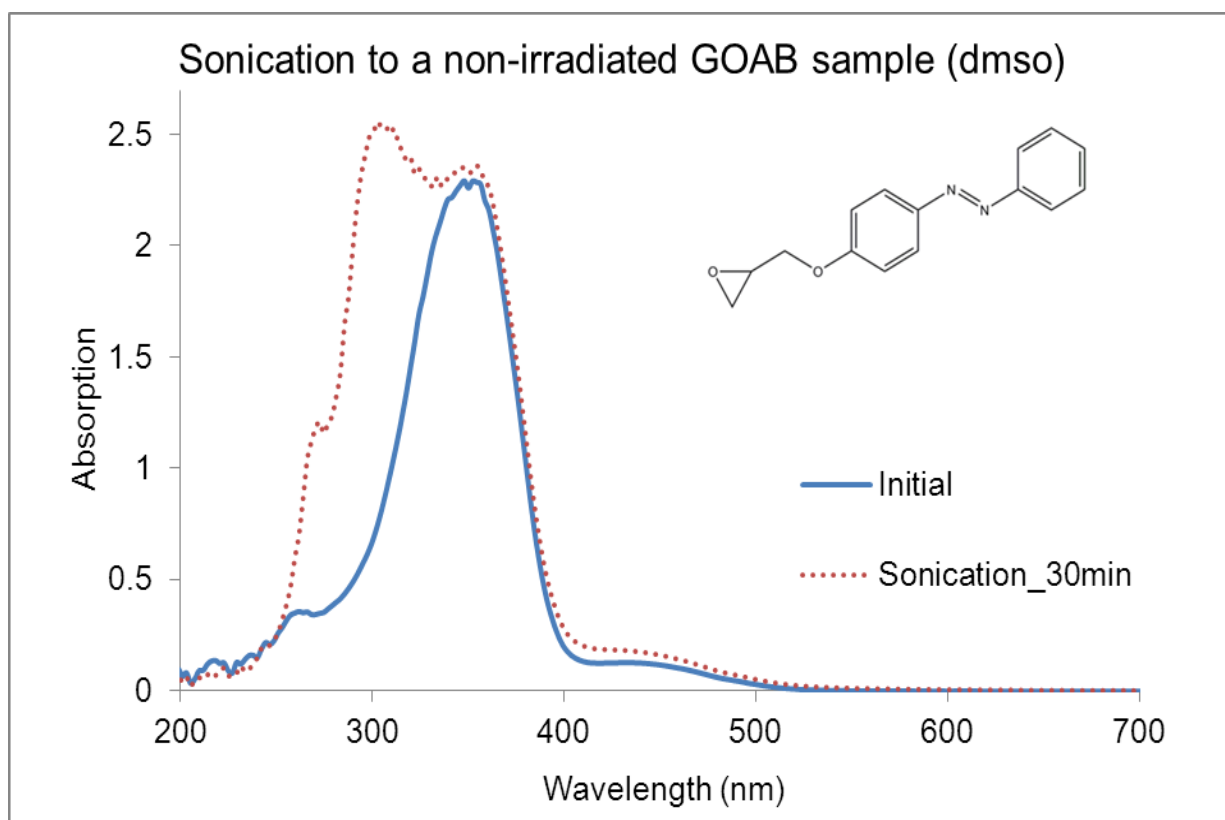
Figure 5.1.10 Non-irradiated solution of 4-GOAB of 0.25 mg/ml in DMSO-d$_6$ after sonication

- UV/vis studies of mono- and di-functional azobenzene molecules.

Photo-switchable molecules such as azobenzene change their molecular conformation when exposed to light irradiation (Figure 5.1.11 and Figure 5.1.12). Azobenzenes have two isomeric states: a thermally stable *trans* configuration, and a meta-stable *cis* form. Under irradiation, a fraction of the trans-azobenzenes will be converted to the *cis* form, which will thermally revert to the more stable *trans* on a timescale determined by the molecule's particular substitution pattern.
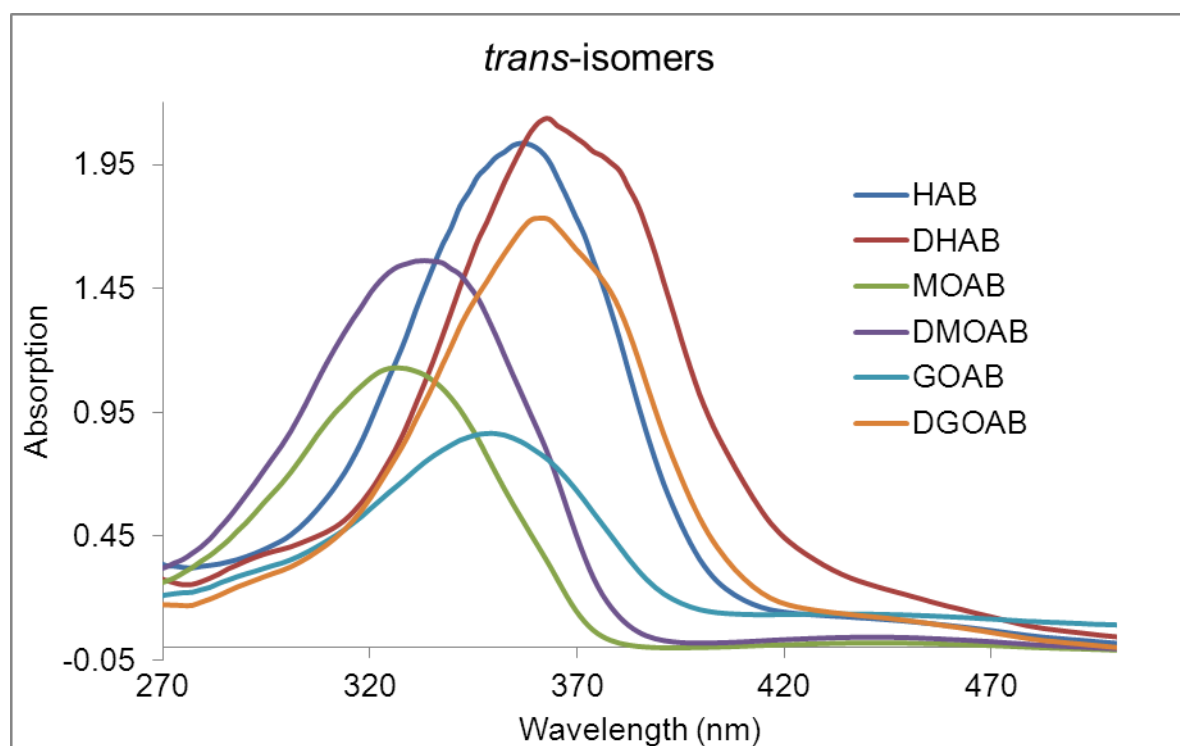
Figure 5.1.11 Non-irradiated solutions of mono- and di-functional azobenzene molecules of 0.25 mg/ml in DMSO
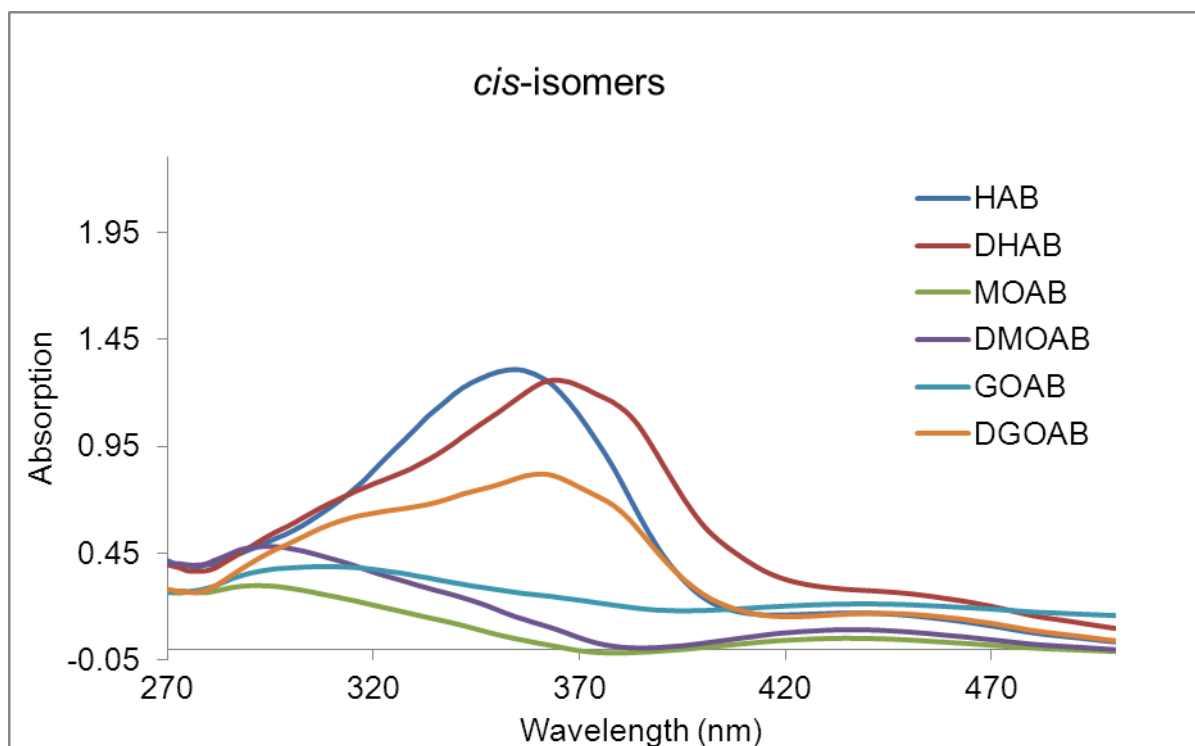
Figure 5.1.12 Solutions of mono- and di-functional azobenzene molecules of 0.25 mg/ml in DMSO upon UV irradiation

Table 5.1.3 Parameters of the first-order trans-to-cis isomerisation reaction of azobenzene molecules

Molecules	$(t=t_{1/2})$ sec	$A_o - A_{max}$	$A_t - A_{max}$	$\ln \{(A_o - A_{max}) /(A_t- A_{max})\}$	$k_{trans->cis}$ (s^{-1})
HAB	4	0.734	0.290	0.929	0.232
4,4´-DHAB	2	0.878	0.120	1.987	0.994
MOAB	9	0.938	0.130	1.974	0.219
4,4´-	11	1.260	0.260	1.578	0.149

DMOAB	12	1.260	0.198	1.853	
GOAB	6	0.578	0.047	2.500	0.421
	7	0.578	0.029	2.976	
4,4´-DGOAB	7	0.908	0.533	0.534	0.076

Appendix B

B.1 Glass fibres–Reinforcement

Glass is the most common and inexpensive fibre for the reinforcement of polymer matrices. It has a high tensile strength and fairly low density.[197] Glass fibres are manufactured by drawing molten glass into very fine threads. They are strong and characterised by lack of rigidity regarding their molecular structure. The main fibre glass, called E-glass, for composite materials is constituted by ordinary borosilicate glass. Another kind of glass fibre is the S-glass, which presents better properties than E-glass, like strength and thermal stability, but its higher cost is the reason for its limited use.[93]

Here, it should be mentioned that one of the important reasons of using glass fibres in the composites is because of their transparency. The goal of our studies is to investigate the photo-mechanical properties of azobenzene composite materials and thus the need of light passing through the material, without being absorbed, is required.

B.2 Epoxy polymer matrices

As has been mentioned previously, most of the reinforced polymers consist of hard fibres, like glass, in a weak, brittle polymer matrix, like epoxy. The optimum result of this combination is that they form tough composites attributed to their heterogeneous structure.[93] The polymer matrix plays an important role in the composites as it is responsible for binding the fibres together.

Epoxy resin are widely used in composite's formulation for aerospace, automotive and electronics industries.[198] They exhibit excellent bonding with glass, higher chemical resistance than the polyesters and are not affected by water (moisture absorbance reduces the composite's mechanical properties). Epoxy/glass fibre composites are prepared by coating glass fibre with epoxy

resin (two parts epoxy resins are mixed before use) and then heating until forming a hard matrix.

B.3 Compression tests

Initial experiments for identifying the influence of azobenzene by using 1 mol% diglycidyloxyazobenzene were performed and their compressive strength was compared with the control samples before and after exposure to UV light. Composite panels of (25 cm x 50 cm) of 20 balanced and symmetrical plies (~4-5 mm thickness) were manufactured. The structure of the laminates is illustrated in Figure 5.1.13. The curing conditions were identical with those mentioned in section 3.2.2 (Vacuum: -27.4 mmHg, Temperature: 25→80°C @ 2°C/min, 80°C for 2 hrs, Pressure: 0→50 psi @ ~1.5-2 psi/min, 50 psi for 2 hrs).
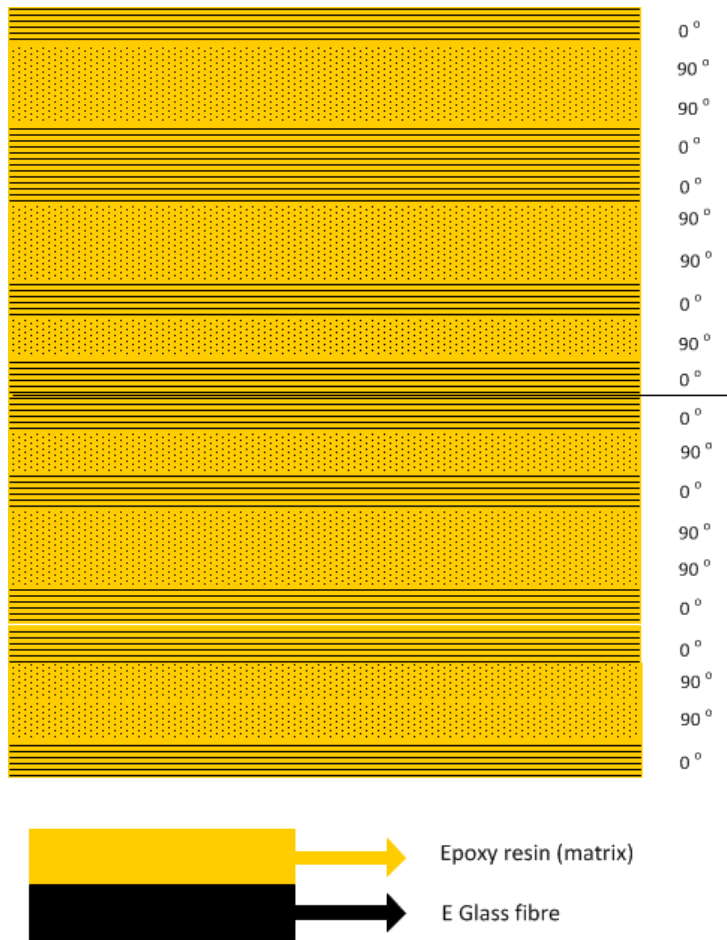
Figure 5.1.13 Laminate's structure

Table 5.1.4 presents the values of the compressive strength at fracture [8] and Young's Modulus of the composites containing 0 and 1 mol% azobenzene, before and after UV irradiation. A slightly decrease in compressive strength was noticed for the composites without azobenzene after have been exposed to UV light. This reduction confirms that UV light is an environmental stress that weakens the mechanical properties of the composites.

On the other hand, a 10.17% increase in compressive strength was observed for the composites with 1 mol% azobenzene after the UV exposure. These results suggested photo-induced enhancement of the composites' mechanical properties and thus panels with higher azobenzene loading were manufactured and more tests were performed to understand this phenomenon.

Table 5.1.4 Compressive strength and Young's Modulus of UV and non-irradiated composites

	N° of samples	Young's Modulus	Compressive fracture strength [8]
Non-irradiated Glass/Epoxy	6	19.83 ± 2.75	70.01 ± 21.65
UV irradiated Glass/Epoxy	3	20.54 ± 0.27	65.92 ± 32.41
Non-irradiated Glass/Epoxy_1%AB	3	16.47 ± 2.15	46.22 ± 3.67
UV irradiated Glass/Epoxy_1%AB	3	16.99 ± 2.86	50.92 ± 14.03

B.4 Impact tests

In this section all the photo-frames of the composites that were penetrated for this Thesis during impact testing are presented.
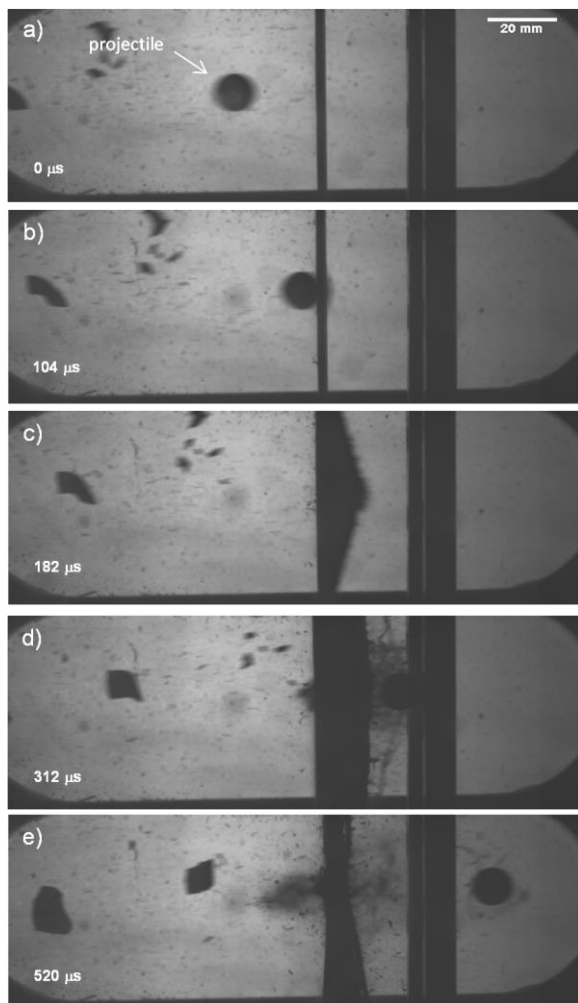
Figure 5.1.14 Impact tests at 190 m/s Control NO UV irradiation
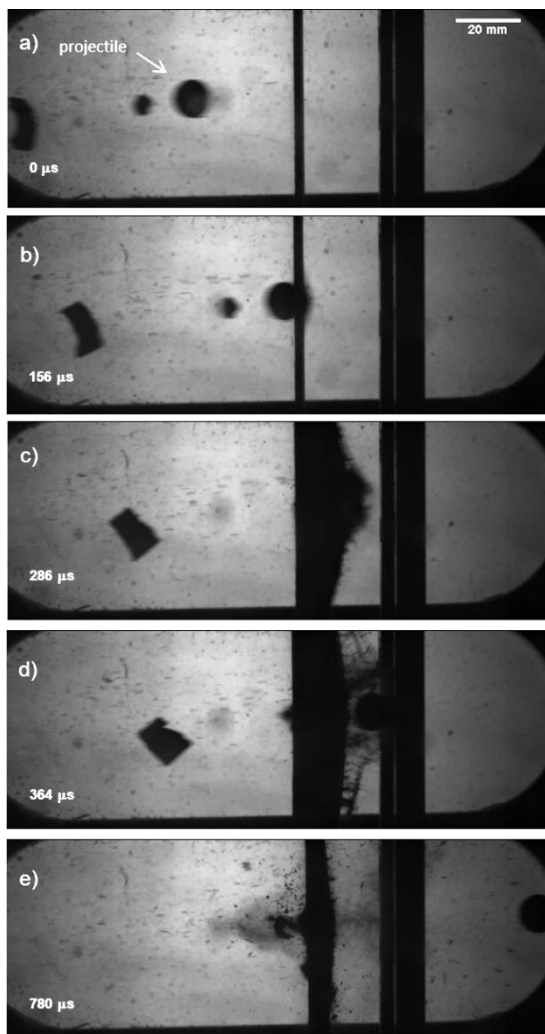
Figure 5.1.15 Impact tests at 190 m/s 5% AB NO UV irradiation
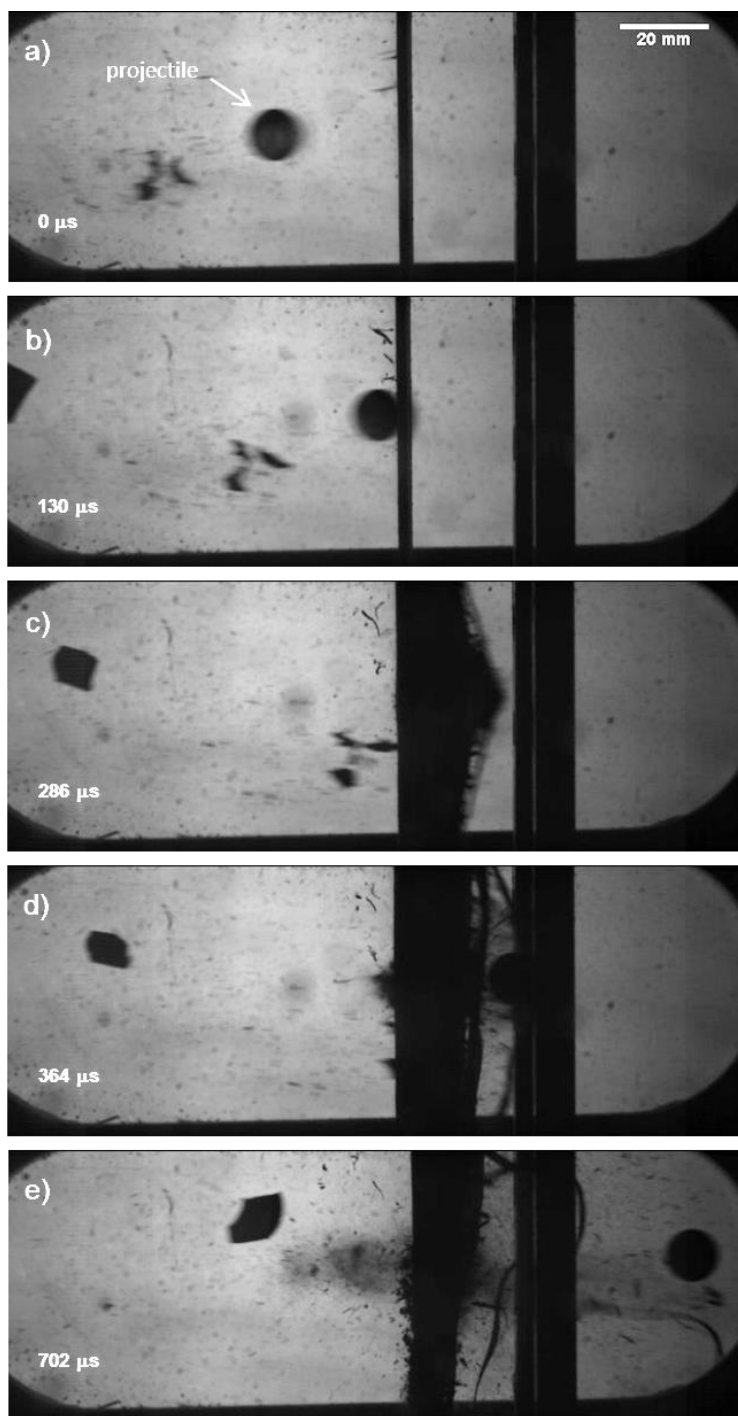
Figure 5.1.16 Impact tests at 190 m/s 10% AB NO UV irradiation
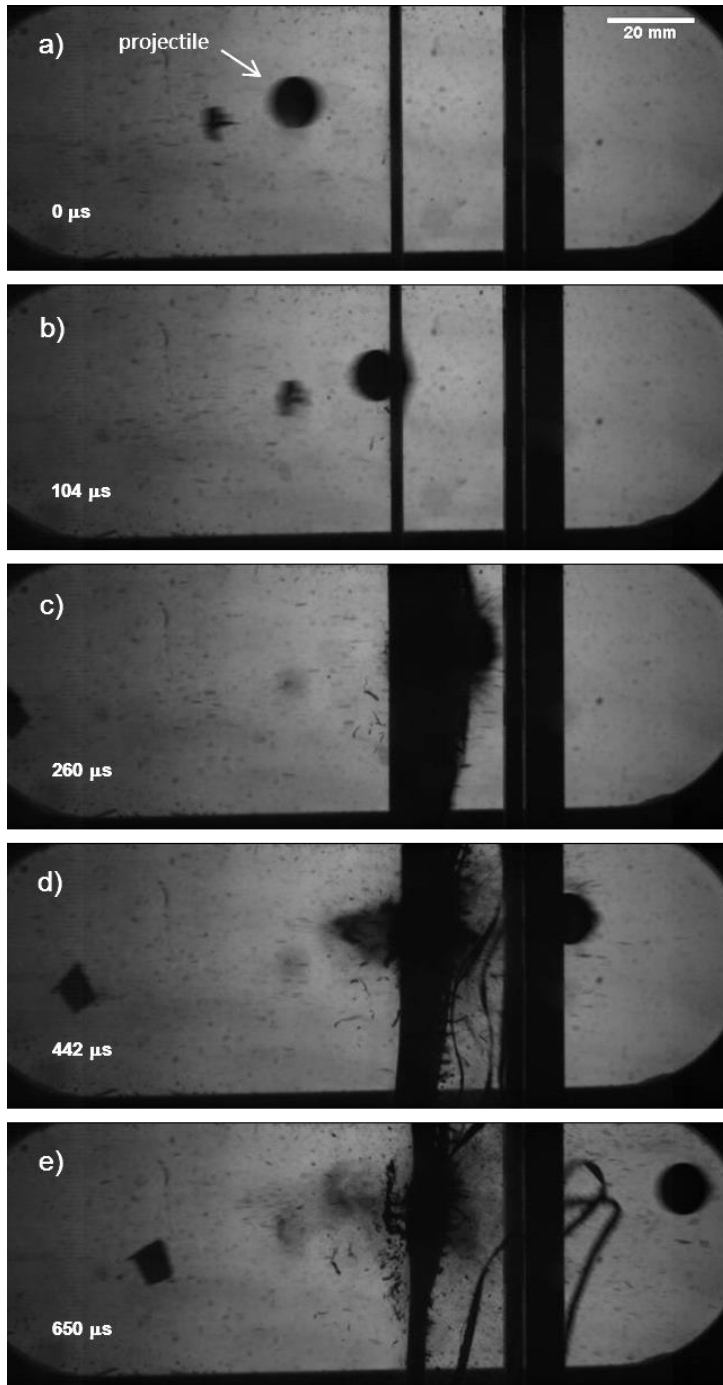
Figure 5.1.17 Impact tests at 190 m/s control after 1hr UV irradiation
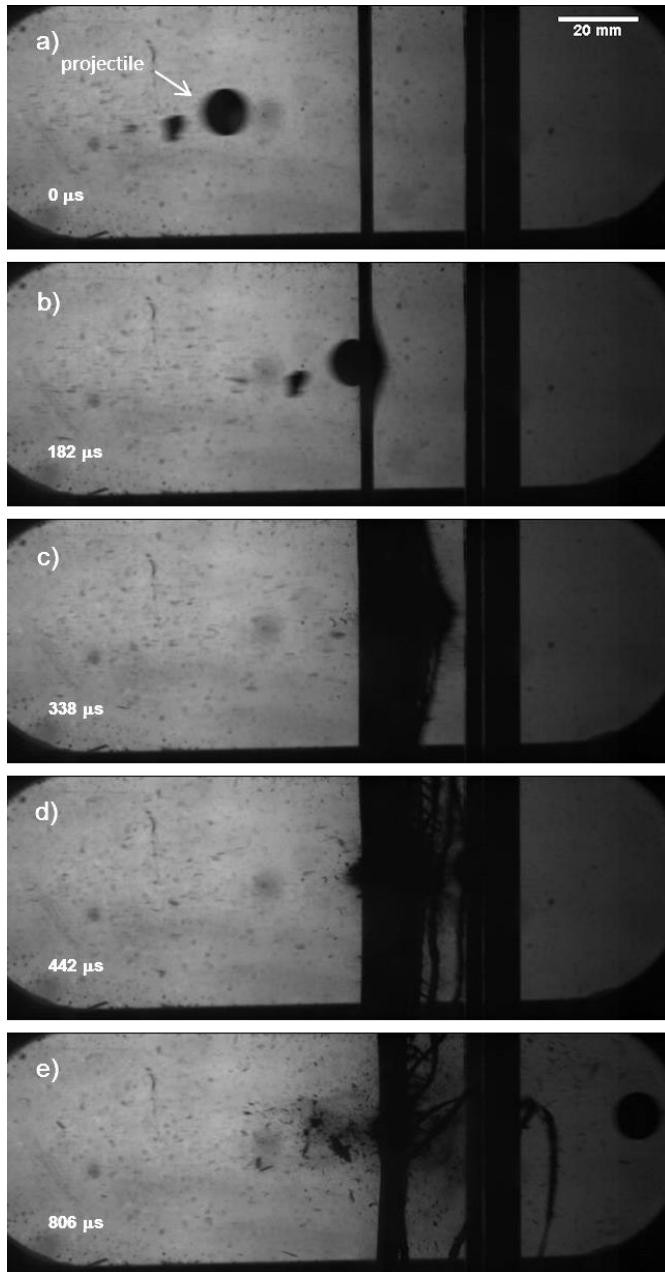
Figure 5.1.18 Impact tests at 190 m/s 10%AB after 1hr UV irradiation
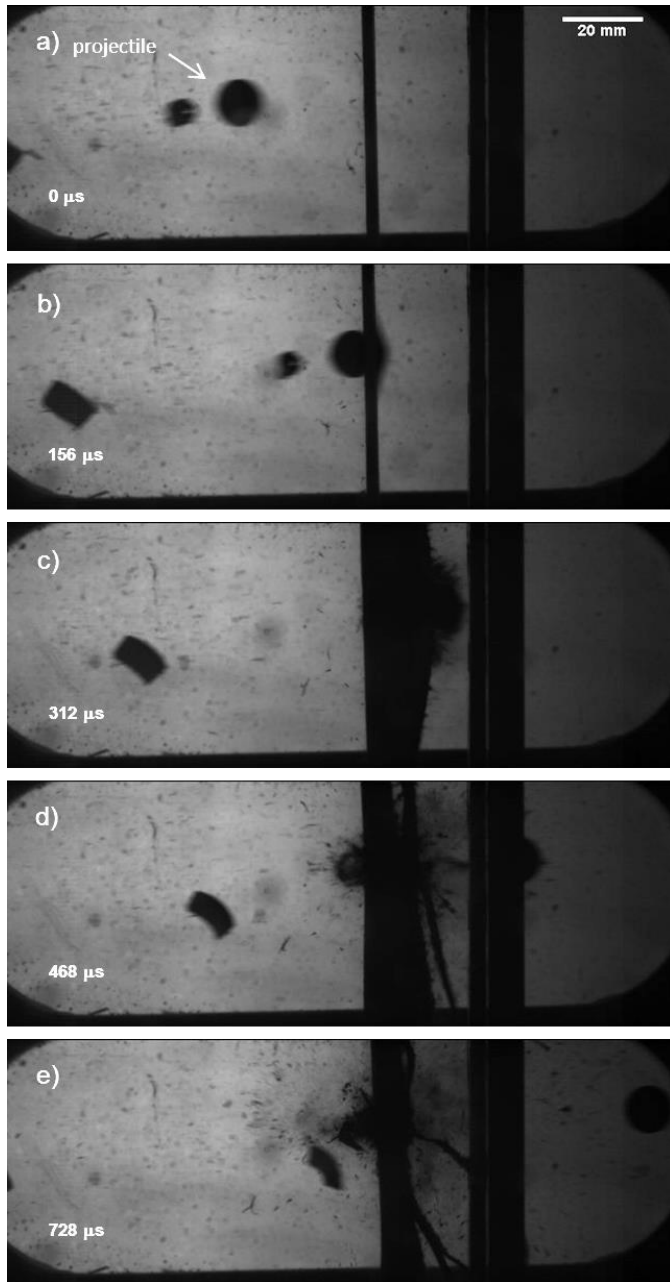
Figure 5.1.19 Impact tests at 190 m/s 5%AB NO UV irradiation (2nd)
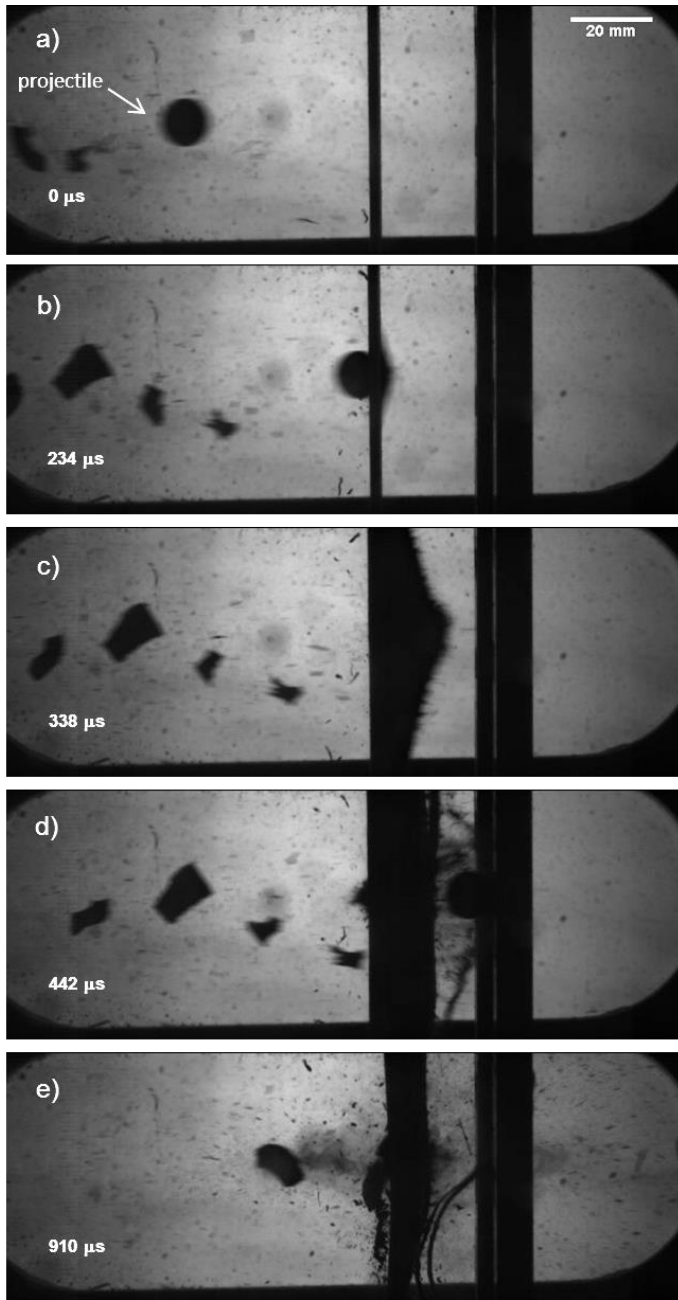
Figure 5.1.20 Impact tests at 190 m/s 10%AB NO UV irradiation (2nd)
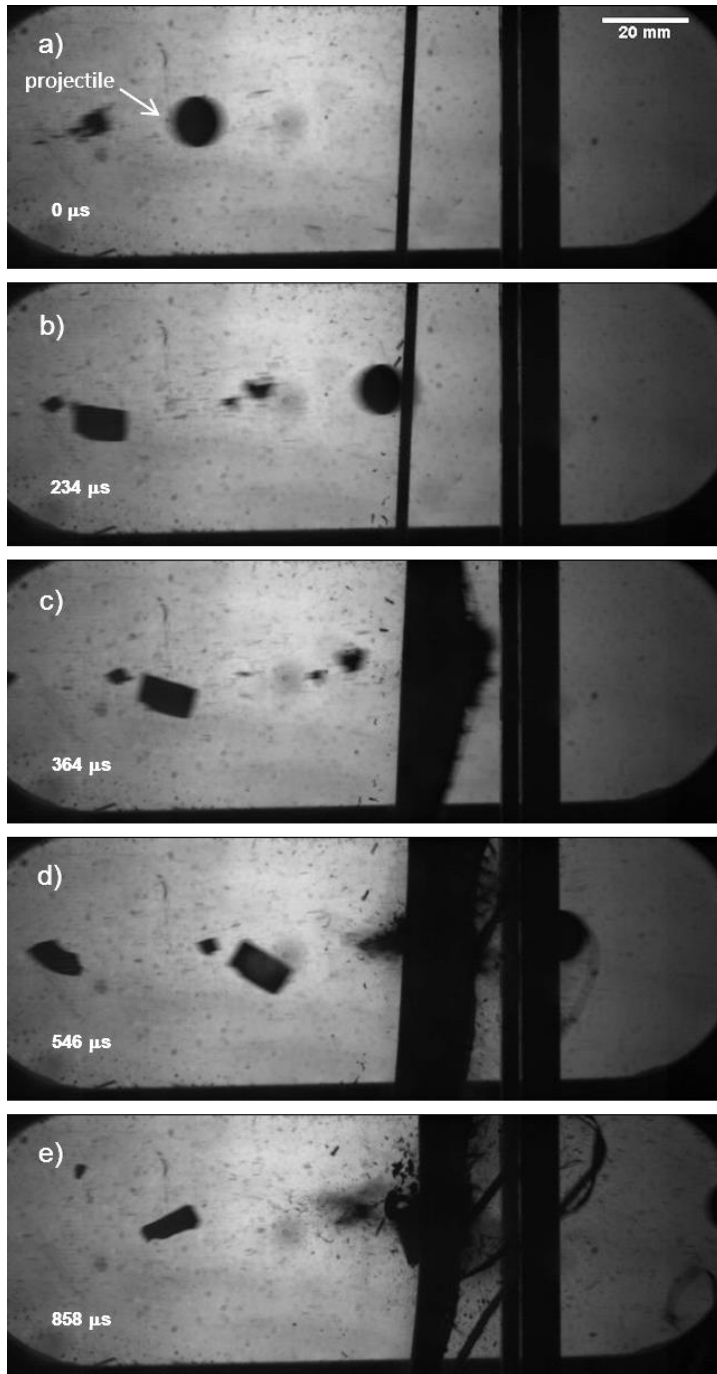
Figure 5.1.21 Impact tests at 190 m/s control NO UV irradiation (2nd)
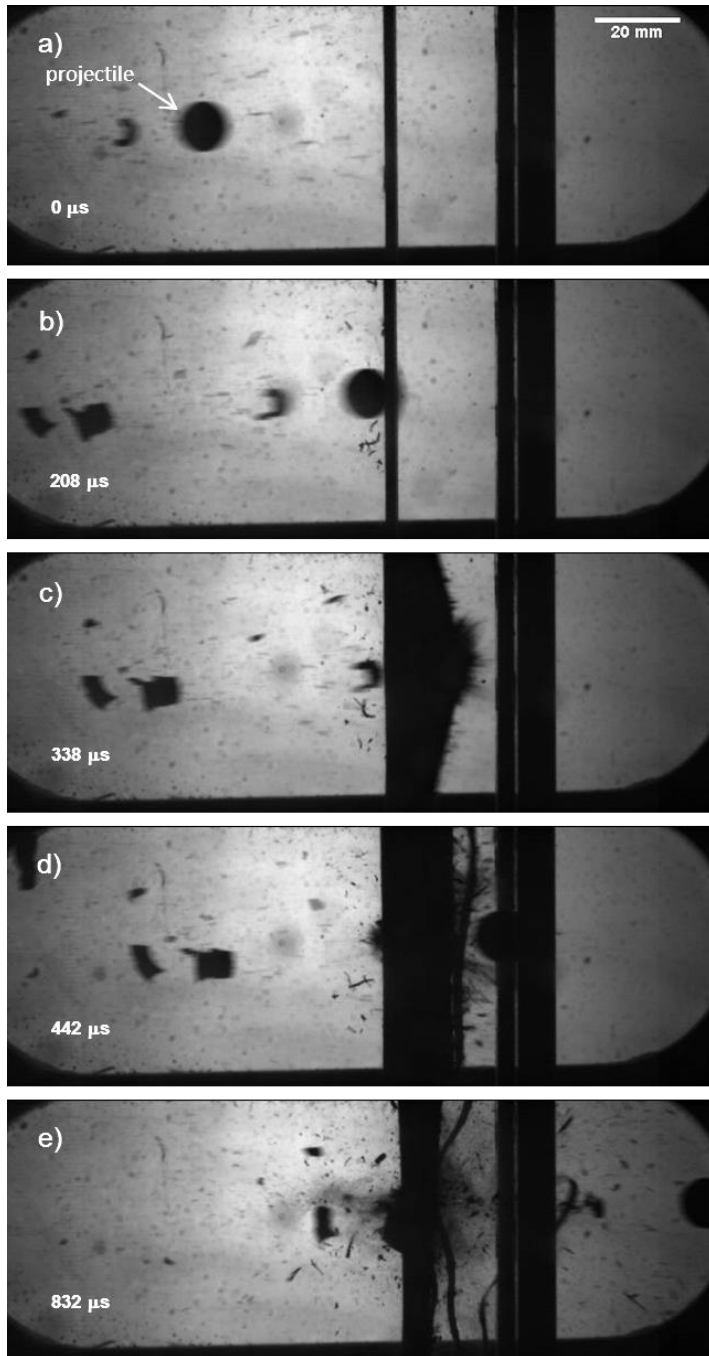
Figure 5.1.22 Impact tests at 190 m/s 5%AB after UV irradiation
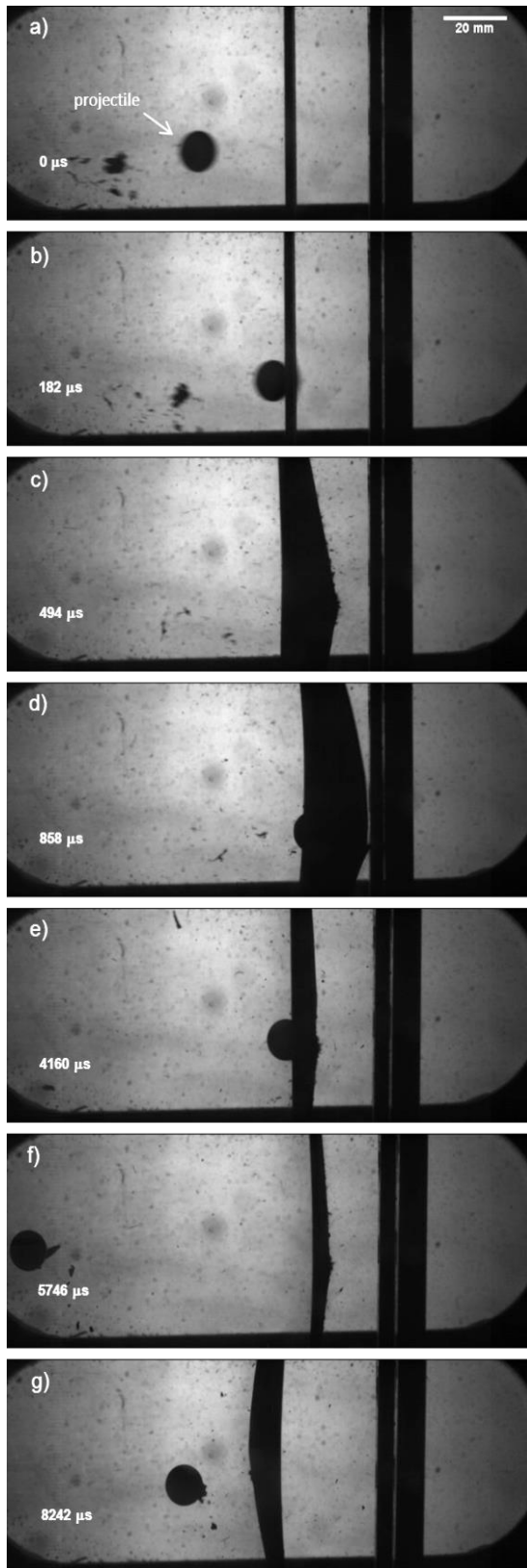
Figure 5.1.23 Impact test at 130 m/s control NO UV irradiation
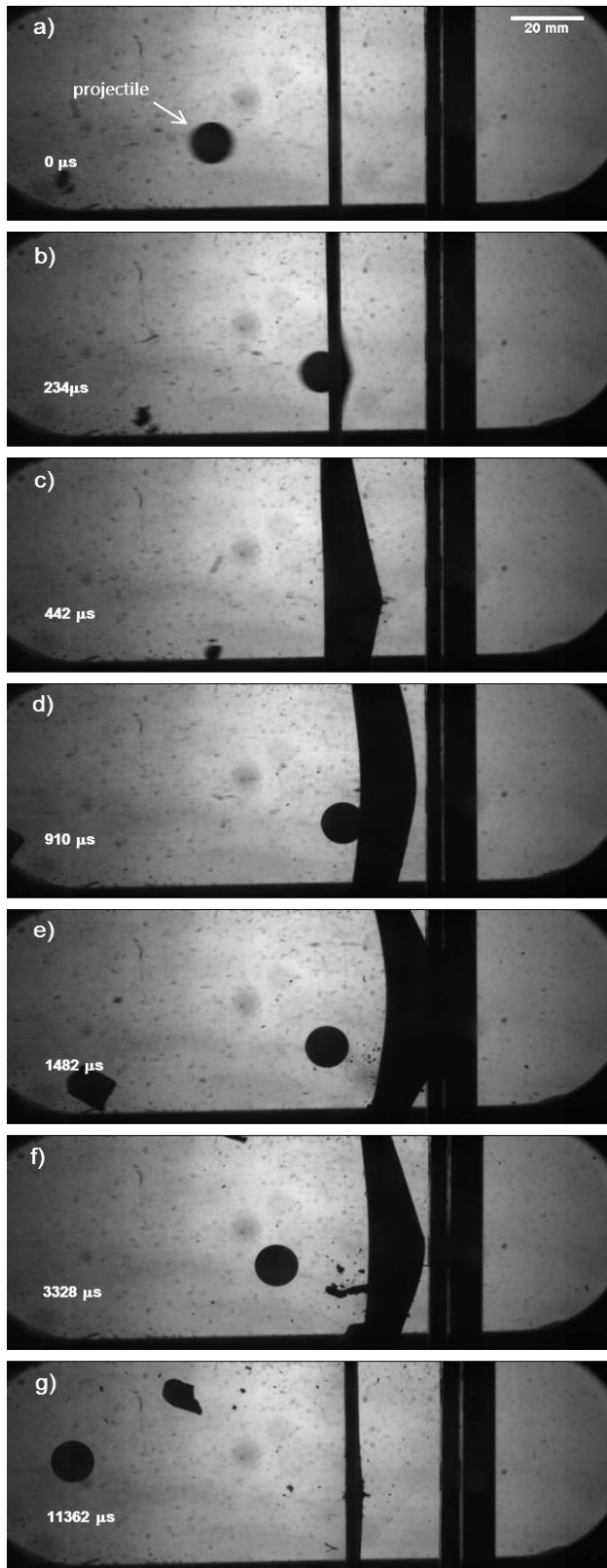
Figure 5.1.24 Impact test at 130 m/s 5%AB NO UV irradiation
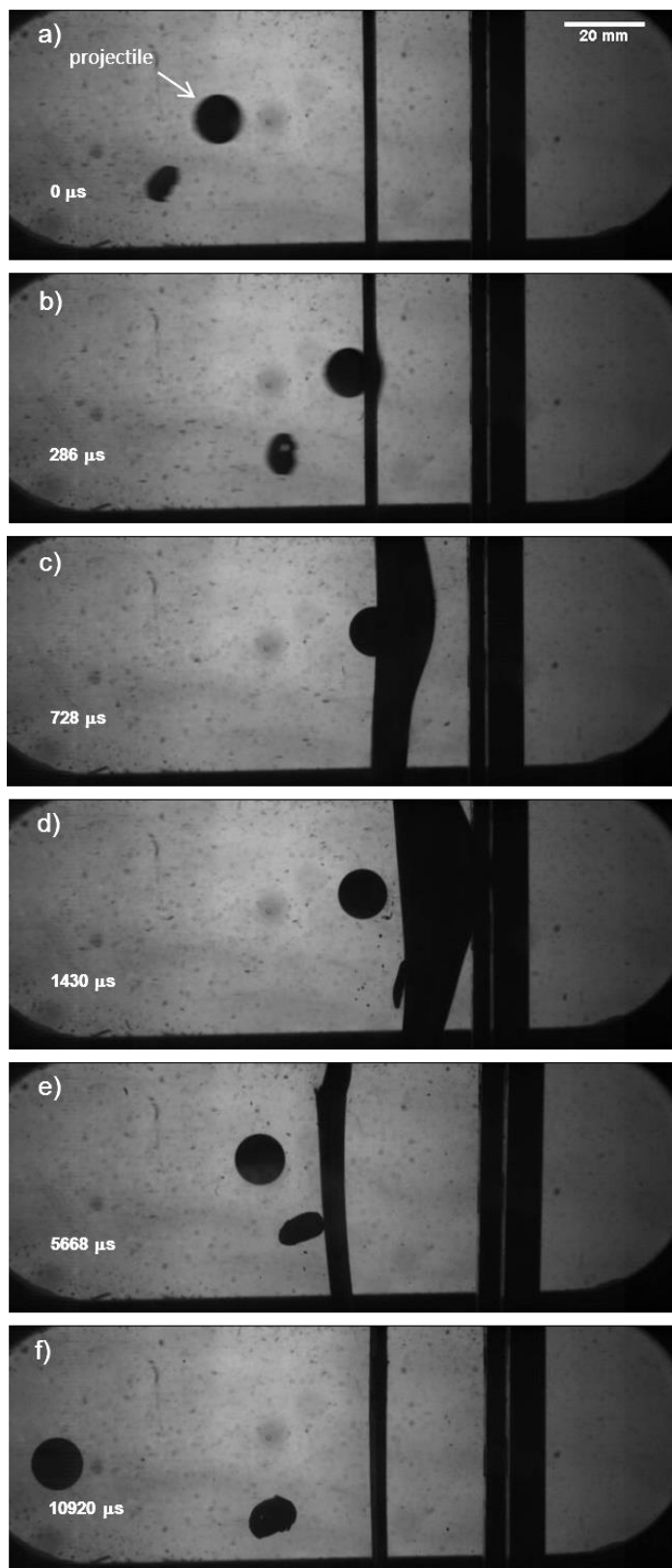
Figure 5.1.25 Impact test at 130 m/s 10%AB NO UV irradiation
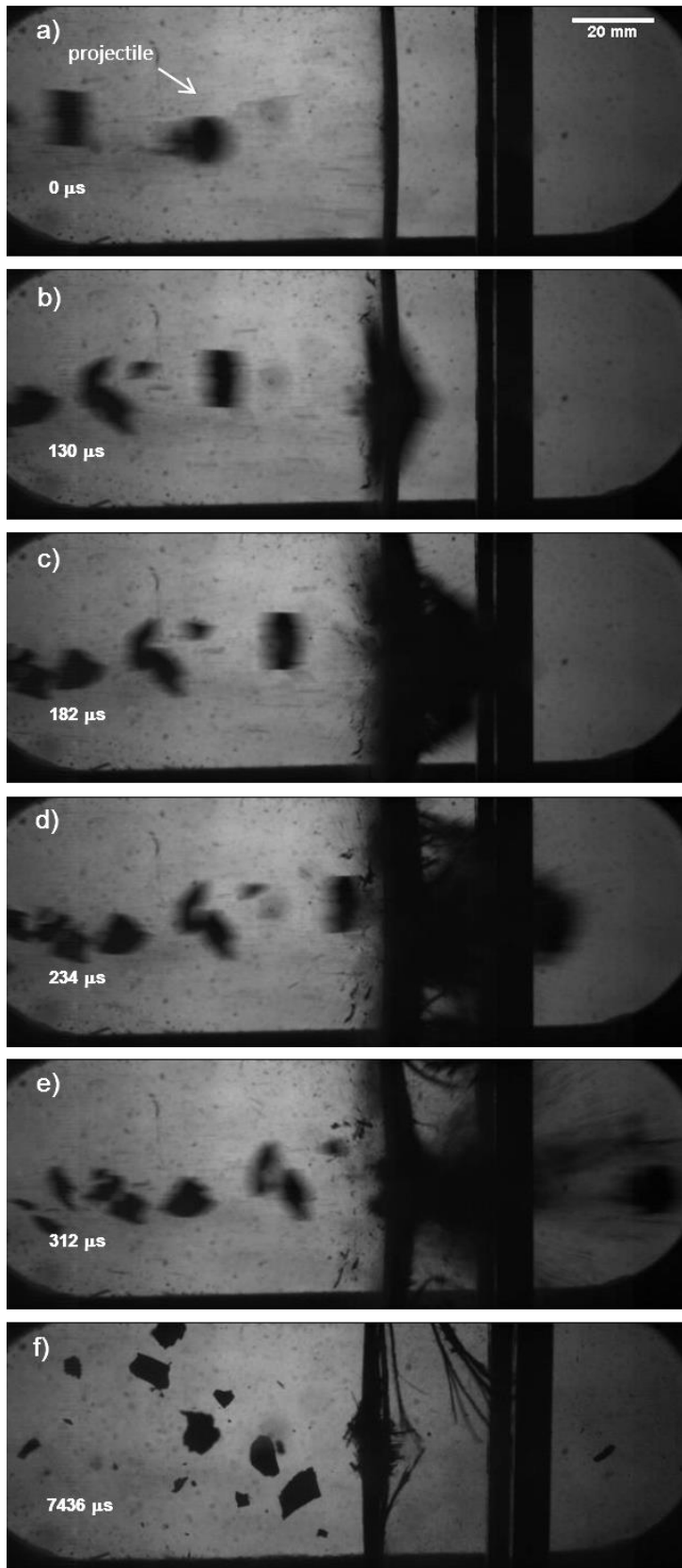
Figure 5.1.26 Impact test at 370 m/s control NO UV irradiation
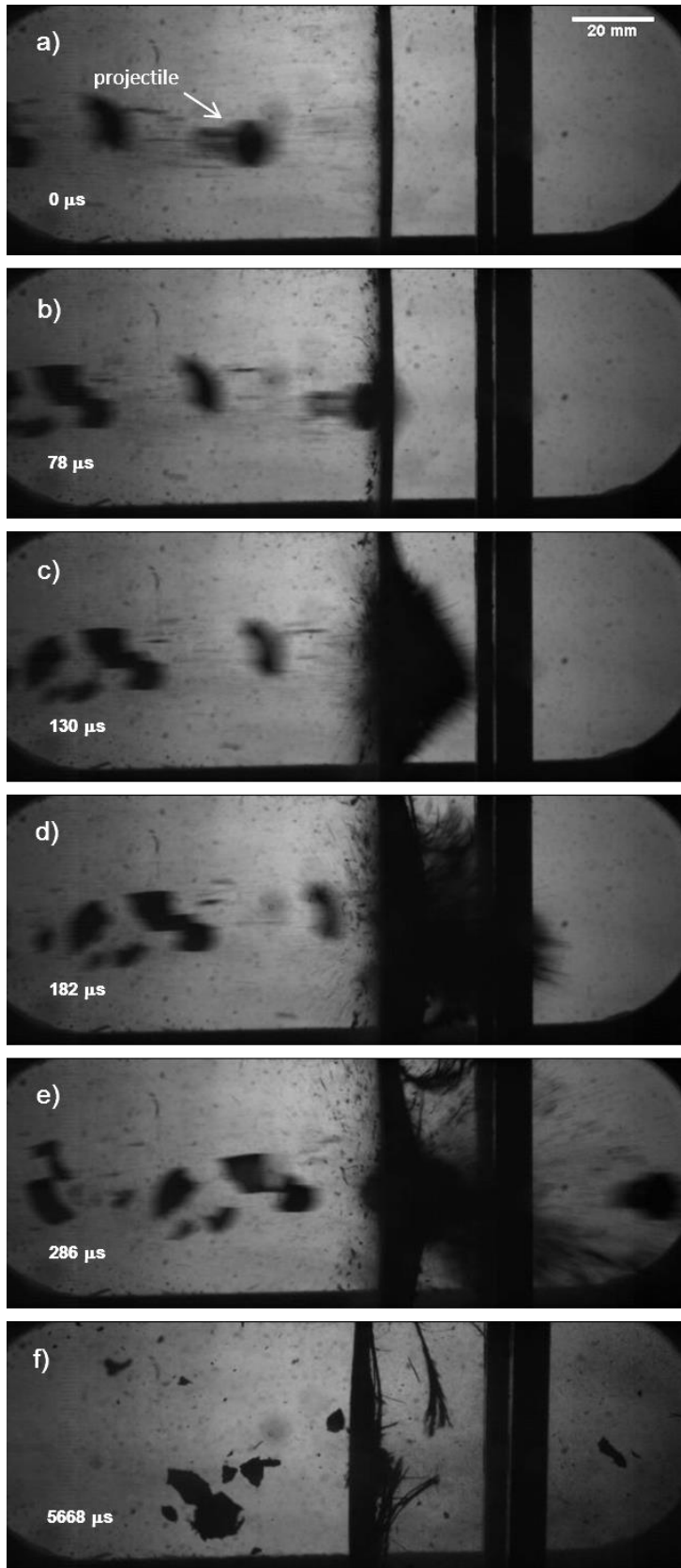
Figure 5.1.27 Impact test at 370 m/s 5%AB NO UV irradiation
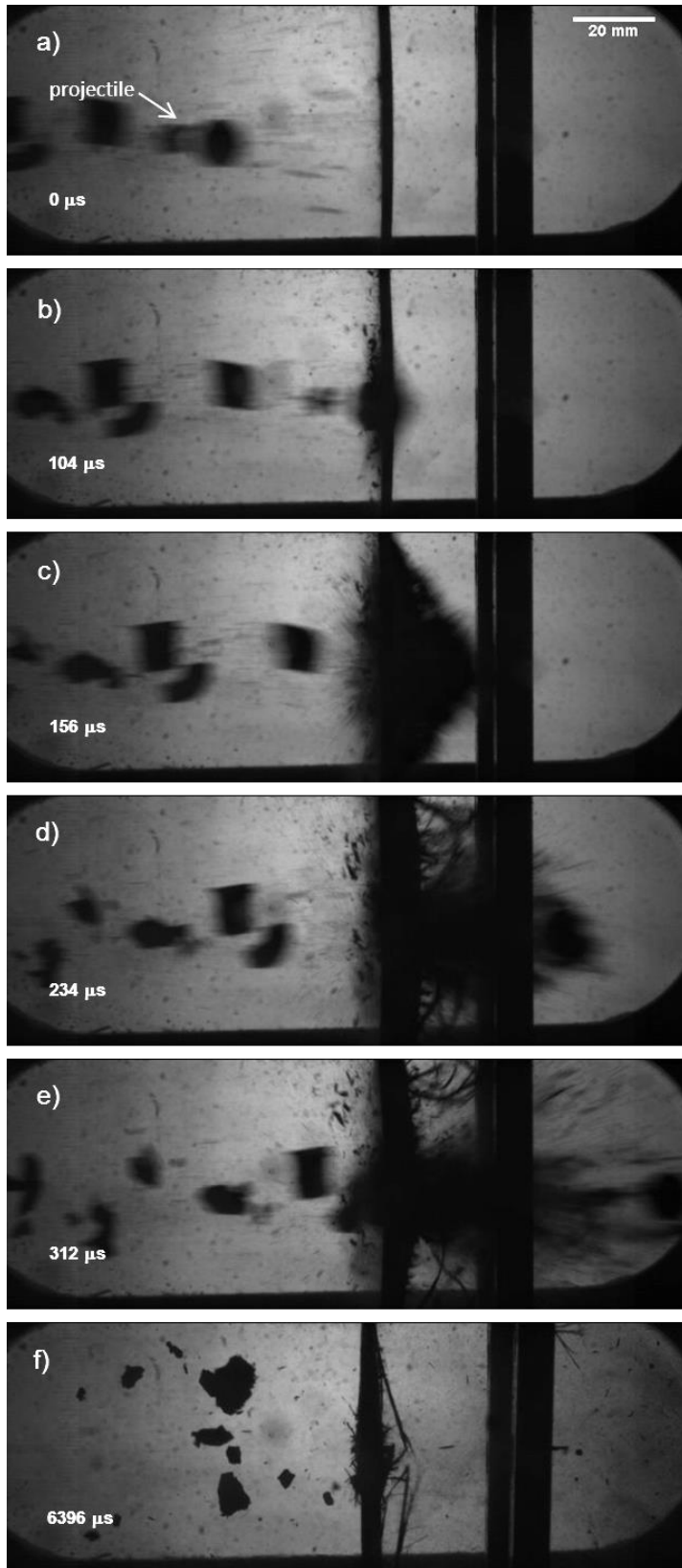
Figure 5.1.28 Impact test at 370 m/s 10%AB NO UV irradiation
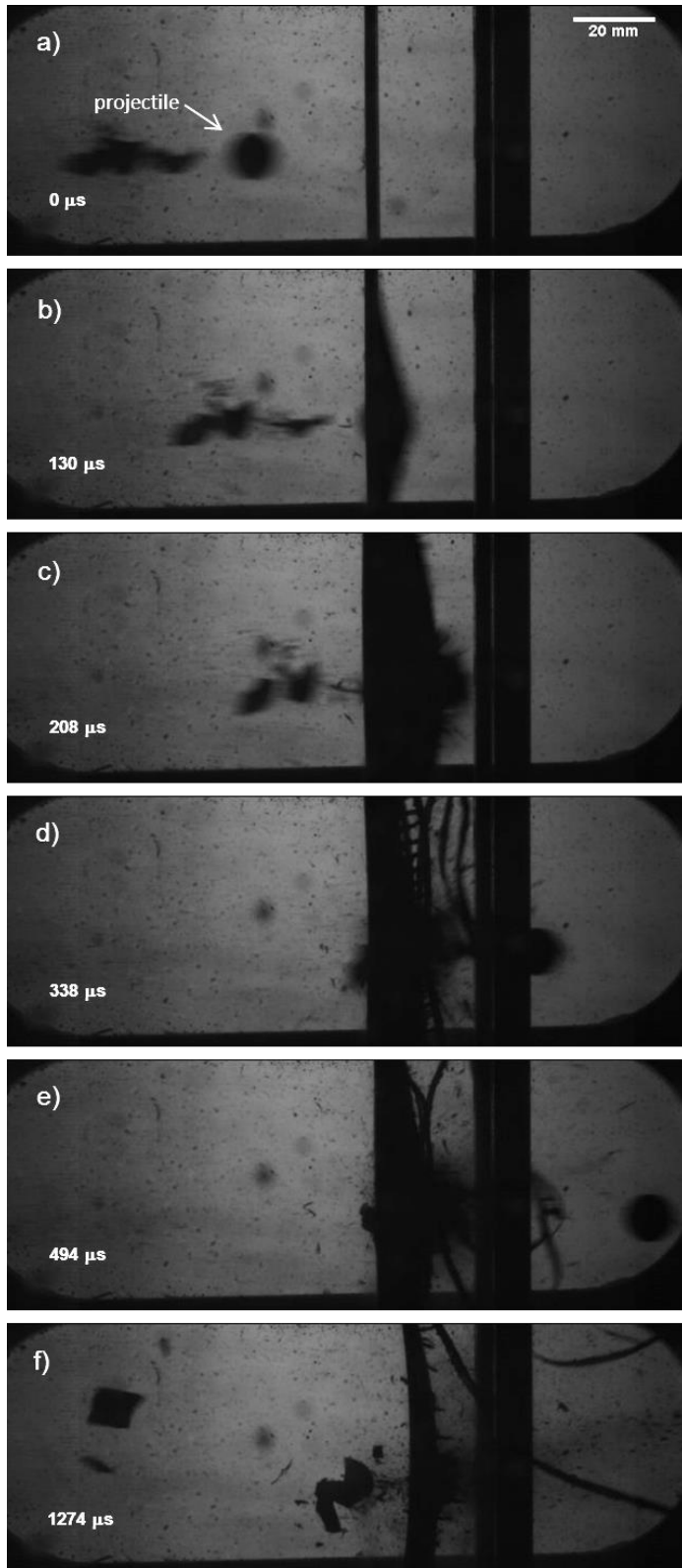
Figure 5.1.29 Impact test at 190 m/s control after UV irradiation (2nd)
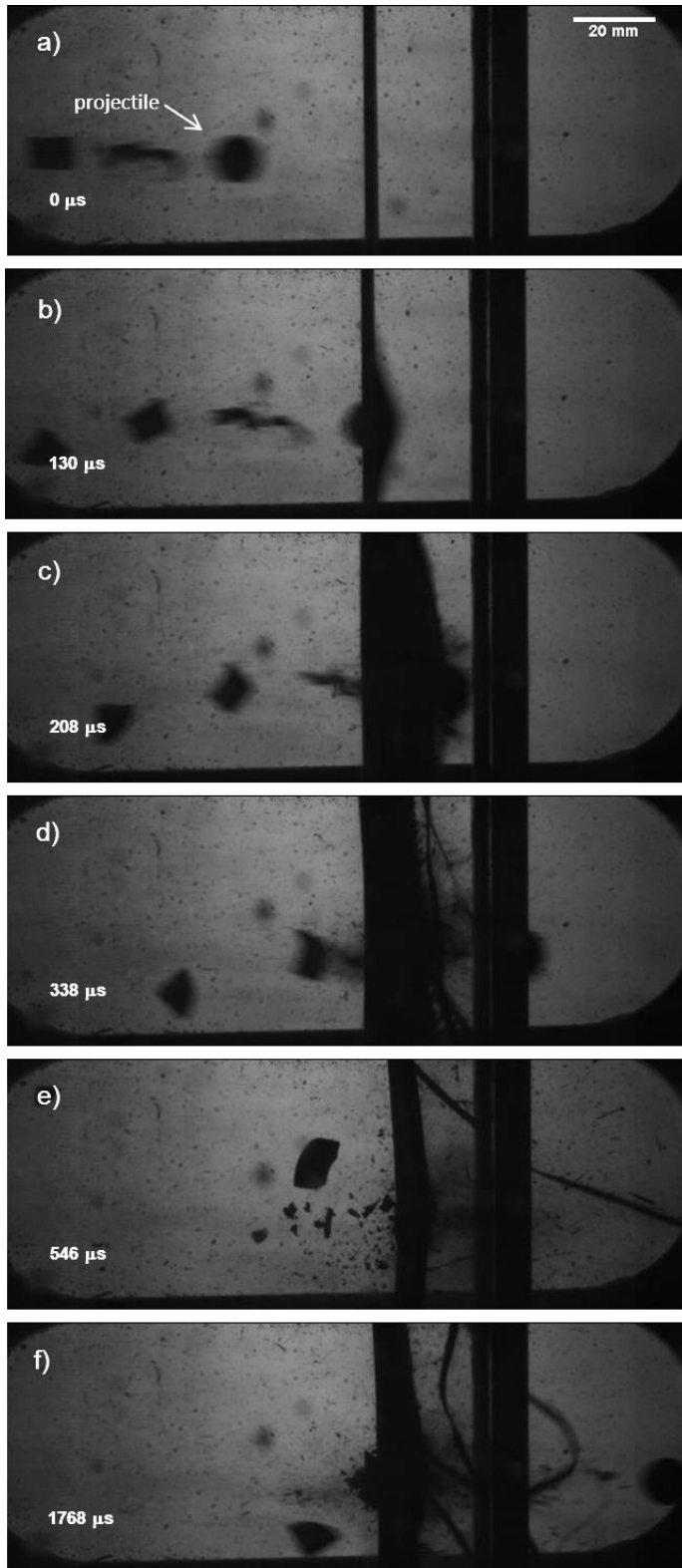
Figure 5.1.30 Impact test at 190 m/s 5%AB after UV irradiation (2nd)
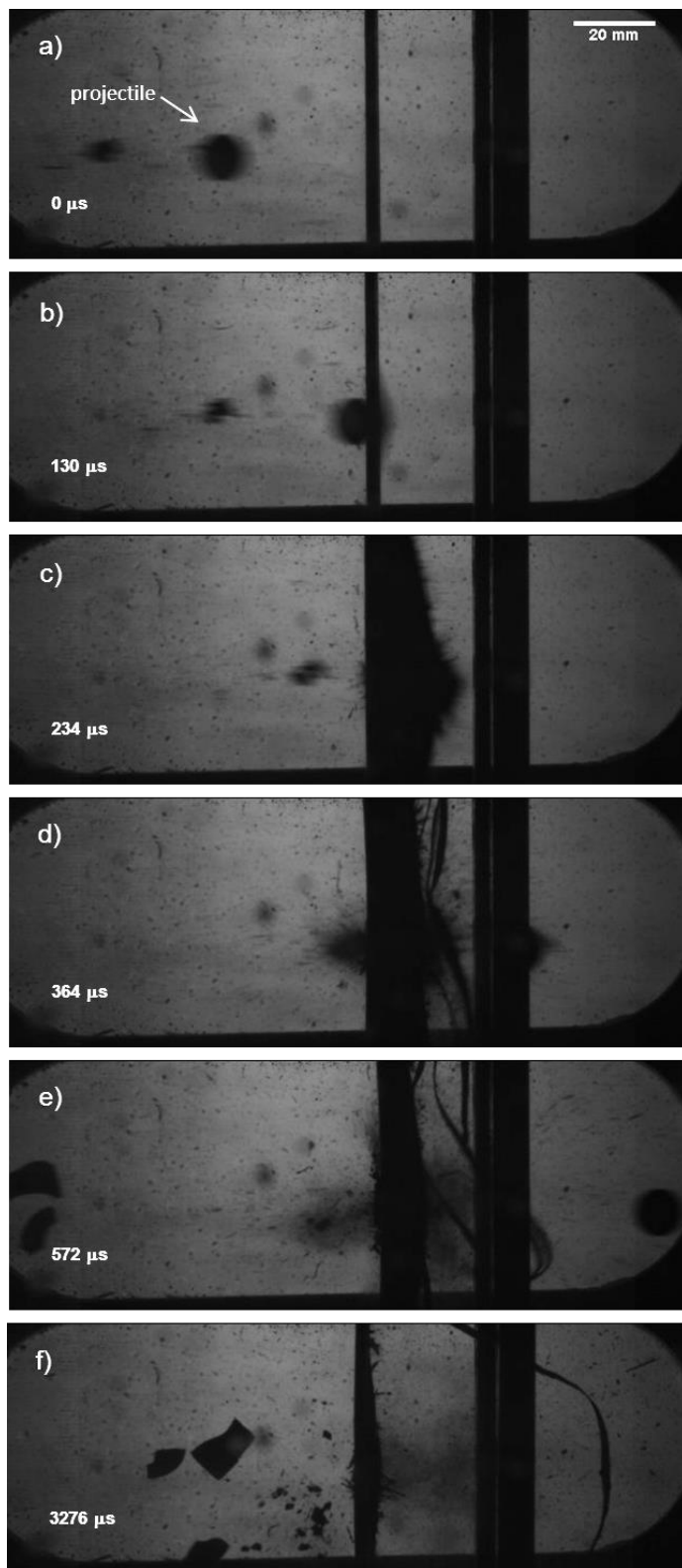
Figure 5.1.31 Impact test at 190 m/s 10%AB after UV irradiation (2nd)

B.5 Hyperspectral analysis

In these studies, we were trying to identify if there are any spectral differences that might occur due to the *trans/cis* isomerisation after exposure to UV light using a hyperspectral camera. Hyperspectral camera uses a spectral sensing technique which captures hundreds of narrow waveband images in the short wave infrared (SWIR) region of the electromagnetic spectrum. An SWIR camera was used on 0% and 5% azobenzene composites.

As can be seen below within this wavelength range the conformational changes weren't obvious.
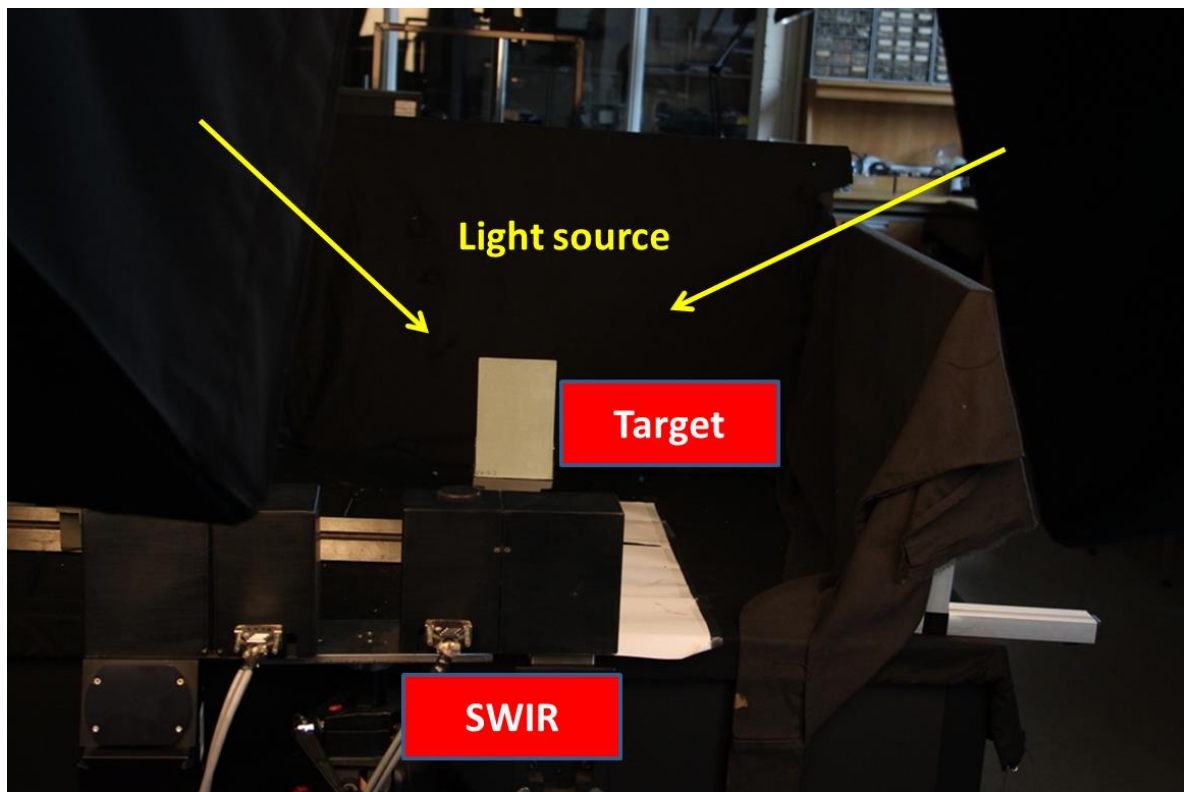
Figure 5.1.32 Experimental setup for SWIR studies on glass fibre composites

Epoxy/glass fibres composite (0% AB)

UV Radiation on same sample

After Radiation Epoxy/glass fibres composite (0% AB)

SWIR Data Taken

15 Min Radiation

SWIR Data Taken
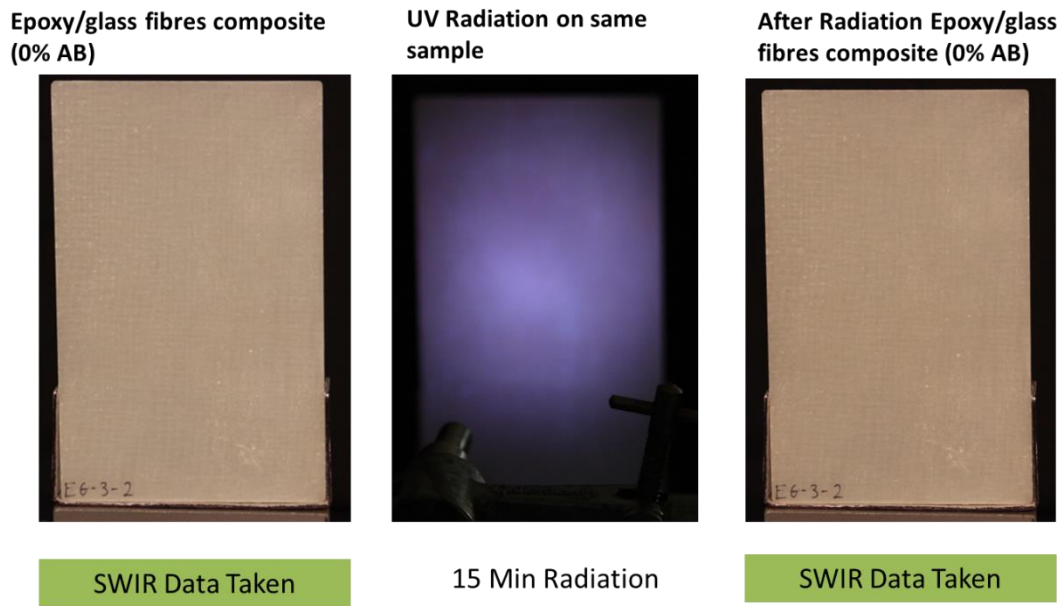
Figure 5.1.33 Images of epoxy/glass fibre composites before, during and after 15 min UV irradiation

5% AB epoxy/glass fibres composite

UV Radiation on same sample

After Radiation 5% AB epoxy/glass fibres composite

SWIR Data Taken

15 Min Radiation

SWIR Data Taken
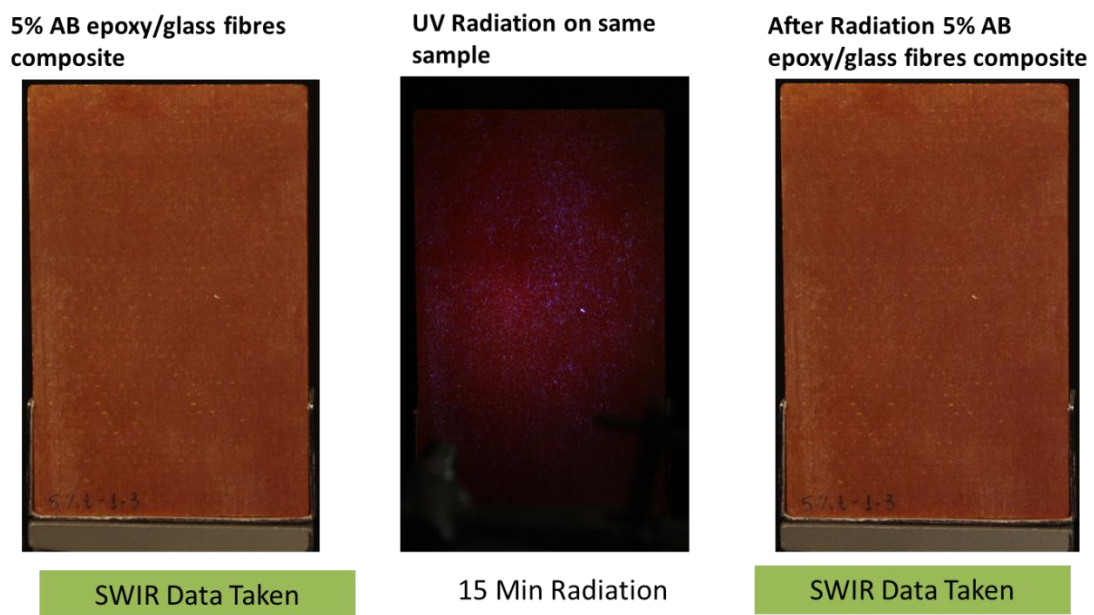
Figure 5.1.34 Images of 5% azobenzene epoxy/glass fibre composites before, during and after 15 min UV irradiation
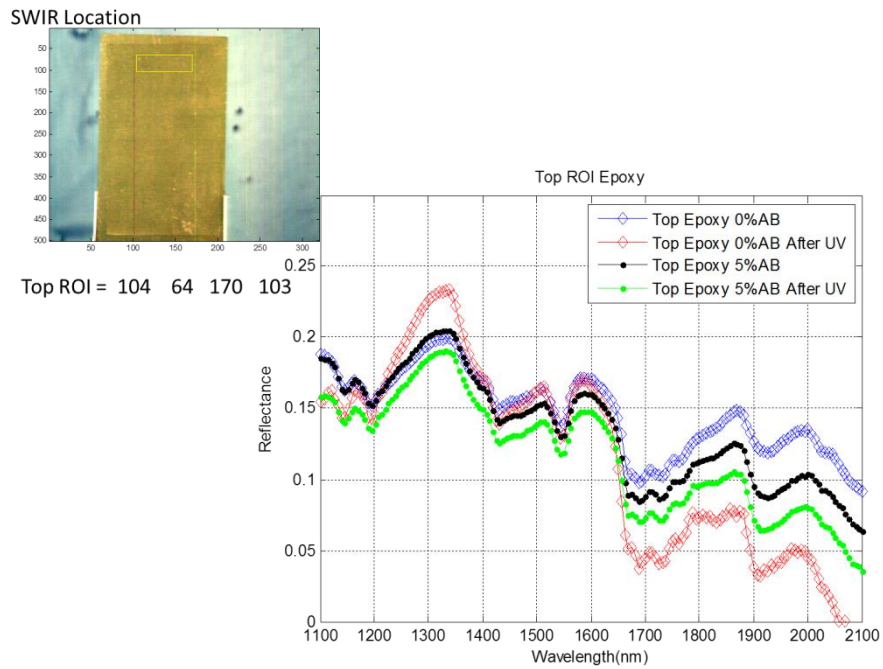
Figure 5.1.35 Combined Reflectance of 0% and 5% AB Epoxy at TOP ROI
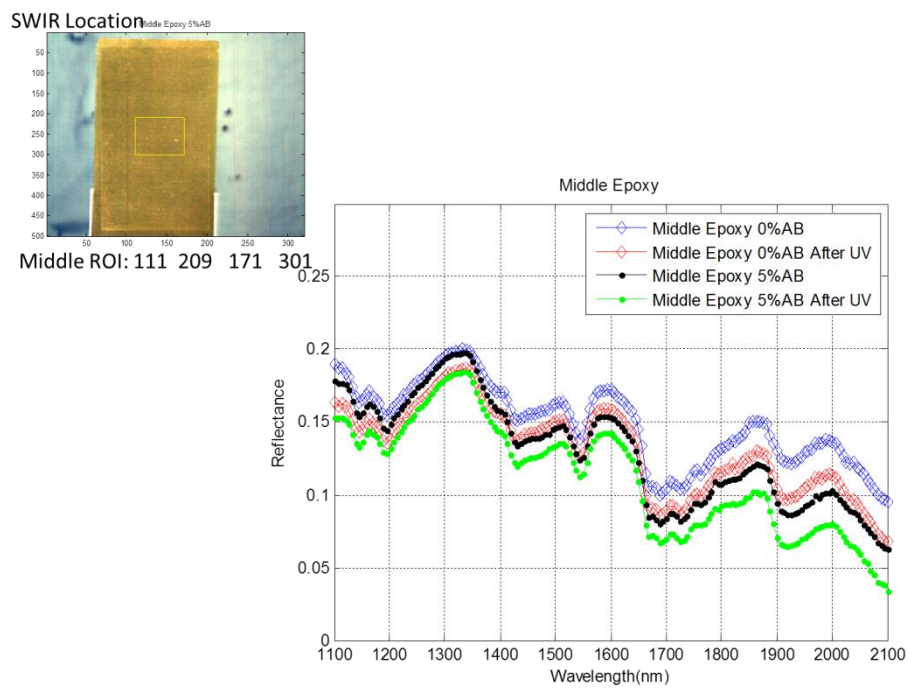
Figure 5.1.36 Combined Reflectance of 0% and 5% AB Epoxy at Middle ROI
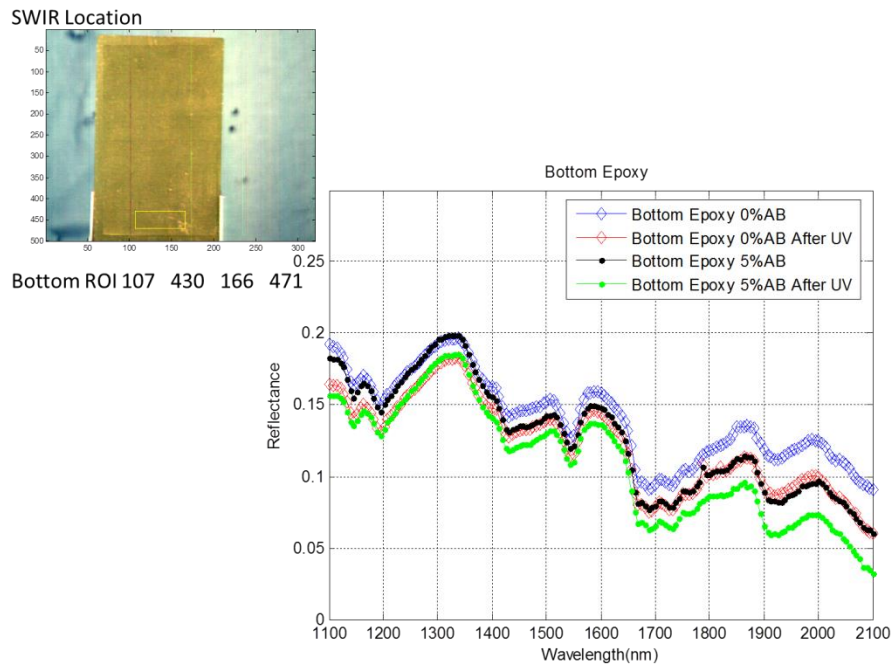
Figure 5.1.37 Combined Reflectance of 0% and 5% AB Epoxy at Bottom ROI

Appendix C

In this section a publication list has been developed with all the novel results of this work is presented. Moreover the attended conferences with the awards that were obtained during this PhD are enlisted below.

C.1 Publications

- M. Moniruzzaman, P. Christogianni, G. Kister "Reversible isomerisation and cure monitoring of epoxy azobenzene resins", Journal of Applied Polymer Science, 2014, Vol 131, 40770

- P. Christogianni, M. Moniruzzaman, G. Kister "Enhancement of Mechanical Properties of Photo-Responsive Polymers", Macromol. Symp., 2015, 354, 55–61

- P. Christogianni, M. Moniruzzaman and G. Kister, Light-triggered enhancement of mechanical properties and healing effect in azobenzene-based polymer films, POLYMER, 2015, 77, 272-277.

- M. Moniruzzaman, P. Christogianni, and G. Kister "Self-healing in epoxy thermoset polymer films triggered by UV light", Procedia Engineering, 2016,148, 114-121,

- P. Christogianni, M. Moniruzzaman, G. Kister, P. Gill "Ultrasound-induced switching of molecular structures in polymer thin films", (Submitted at Chemical Communications RSC Journal/ Feb. 2016)

C.2 Conferences/Symposia/Forums

- November 2015, Defence and Security Doctoral Symposium, Defence Academy of the United Kingdom, Shrivenham, 3 Minutes Thesis Competition: "Characterisation of Photoresponsive Composites for

Defence Applications", Poster Presentation: "Self-healing behaviour of photoresponsive thermosets"

- May 2015, 7th MAST Defence Materials Forum (DMF), Defence Academy of the United Kingdom, Shrivenham, Oral Presentation: "High-velocity impact behaviour of composites enhanced by photosensitive polymers" and Poster Presentation

- September 2014, 5th EuCheMS Chemistry Congress, Istanbul, Turkey, Poster Presentation: "Photo-mechanical properties of epoxy-based resins"

- July 2014, IUPAC World Polymer Congress MACRO2014, Chiang Mai, Thailand, Oral Presentation: "Light-driven enhancement of mechanical properties of polymers"

- February 2013, National PhD Scheme Conference, The Kassam Stadium, Oxford, Poster presentation: "Photo-mechanical properties in acrylic and epoxy based polymers"

C.3 Awards

- May 2015, 7th MAST Defence Materials Forum (DMF), **Best poster prize award**, Poster Presentation

- September 2014, 5th EuCheMS Chemistry Congress, **Travel grants-Student Bursary by Royal Society of Chemistry (£500)**, Istanbul, Turkey, Poster Presentation

- September 2012, Institute of Process, Research & Development (iPRD) Course "Chemistry for Engineers and Scientists", **Award of an RSC-PTG Student Bursary (£300)**, University of Leeds

REFERENCES

[1] J. Comyn, - Adhesion Science, 1997, 14-15.

[2] F. W. Billmeyer, *Textbook of Polymer Science*, 3rd edn., 1984.

[3] S. Thomas and W. Yang, *Advances in Polymer Processing: From Macro to Nano Scales*, Woodhead Publishing, 2009.

[4] J. Izdebska and S. Thomas, *Printing on Polymers: Fundamentals and Applications*, Elsevier Science, 2015.

[5] S. FARBEROV, 2015, American Airlines' new Dreamliner jet was pummeled by hail, 'dropped hundreds of feet' and was forced to return to Beijing, Place of Publication: Available at http://www.dailymail.co.uk/news/article-3177369/American-Airlines-new-Dreamliner-jet-pummeled-hail-forced-return-Beijing-terrified-passengers-plane-dropped-hundreds-feet.html.

[6] I. Maragakis, Bird population trends and their impact on Aviation safety 1999-2008, *European Aviation Safety Agency: Safety Analysis and Research Department*, 2009.

[7] B. G. Kumar, R. P. Singh and T. Nakamura, Degradation of Carbon Fiber-Reinforced Epoxy Composites by Ultraviolet Radiation and Condensation, *Journal of Composite Materials*, 2002, 36, 2713-2733.

[8] M. S. S. R. Kumar, N. Mohana Sundara; Sampath, P.S.; Jayakumari, L.S. , Effects of nanomaterials on polymer composites - an expatiate view, *Rev. Adv. Mater. Sc*, 2014, 38, 40-54.

[9] A. F. Avila, M. I. Soares and A. Silva Neto, A study on nanostructured laminated plates behavior under low-velocity impact loadings, *International Journal of Impact Engineering*, 2007, 34, 28-41.

[10] M. upová, G. Martynková, S. yna and K. Barabaszová, Effect of Nanofillers Dispersion in Polymer Matrices: A Review, *Science of Advanced Materials*, 2011, 3, 1-25.

[11] O. Pieroni and F. Ciardelli, Photoresonsive polymeric Materials, *TRIP*, 2005, 3, 282-287.

[12] Y. Torres, T. White, A. McClung, W. Oates and Asme, *PHOTORESPONSIVE AZOBENZENE LIQUID CRYSTAL POLYMER NETWORKS: IN SITU PHOTOGENERATED STRESS MEASUREMENT*, Amer Soc Mechanical Engineers, New York, 2010.

[13] Y. S. Wang S., L. Jiang, Photoresponsive surfaces with controllable wettability, *Journal of Photochemistry and Photobiology*, 2007, 8, 18-29.

REFERENCES

[14] 2015, Modor Plastics, Place of Publication: Available at www.modorplastics.com/thermoset-vs-thermoplastics.

[15] S. Bader, 2005, Crystic Composites Handbook, Place of Publication: Available at http://www.scottbader.com/uploads/files/3381_crystic-handbook-dec-05.pdf.

[16] N. Mechau, M. Saphiannikova and D. Neher, Dielectric and Mechanical Properties of Azobenzene Polymer Layers under Visible and Ultraviolet Irradiation, *Macromolecules*, 2005, 38, 3894-3902.

[17] R. Halabieh, O. Mermut and C. Barrett, Using light to control physical properties of polymers and surfaces with azobenzene chromophores, *Pure &Appl/,Chem.*, 2004, 76, 1445-1465.

[18] R. H. Lambeth and J. S. Moore, Light-Induced Shape Changes in Azobenzene Functionalized Polymers Prepared by Ring-Opening Metathesis Polymerization, *Macromolecules*, 2007, 40, 1838-1842.

[19] C. J. S. M. Moniruzzaman, G.F. Fernando, Synthesis of azobenzene-based polymers and the in-situ characterization of their photoviscosity effects, *Macromolecules*, 2004, 37, 2572-2577.

[20] M. Moniruzzaman, C. J. Sabey and G. F. Fernando, Photoresponsive polymers: An investigation of their photoinduced temperature changes during photoviscosity measurements, *POLYMER*, 2007, 48, 255-263.

[21] T. Umeyama, K. Kawabata, N. Tezuka, Y. Matano, Y. Miyato, K. Matsushige, M. Tsujimoto, S. Isoda, M. Takano and H. Imahori, Dispersion of carbon nanotubes by photo- and thermal-responsive polymers containing azobenzene unit in the backbone, *Chemical Communications*, 2010, 46, 5969-5971.

[22] C. Vijayakumar, B. Balan, M.-J. Kim and M. Takeuchi, Noncovalent Functionalization of SWNTs with Azobenzene-Containing Polymers: Solubility, Stability, and Enhancement of Photoresponsive Properties, *The Journal of Physical Chemistry C*, 2011, 115, 4533-4539.

[23] P. Imin, M. Imit and A. Adronov, Supramolecular Functionalization of Single-Walled Carbon Nanotubes (SWNTs) with a Photoisomerizable Conjugated Polymer, *Macromolecules*, 2012, 45, 5045-5050.

[24] Y. Kawata, T. Yamamoto, H. Kihara and K. Ohno, Dual Self-Healing Abilities of Composite Gels Consisting of Polymer-Brush-Afforded Particles and an Azobenzene-Doped Liquid Crystal, *ACS Applied Materials & Interfaces*, 2015, 7, 4185-4191.

[25] J. Clayden and S. G. Warren, *Organic chemistry*, Oxford University Press, Oxford, 2001.

REFERENCES

[26] R. G. A. Kumar, *Foundamental of Polymers*, McGraw-Hill Companies, 1998.

[27] M. Kutz, *Applied Plastics Engineering Handbook*, Elsevier, First Edition edn., 2011.

[28] G. Odian, *Principles of polymerization*, 4th edn., 2004.

[29] R. J. Young and P. A. Lovell, *Introduction to Polymers, Third Edition*, Taylor & Francis, 2011.

[30] K. Dušek, *Epoxy Resins and Composites*, Springer-Verlag, 1985.

[31] E. Petrie, *Epoxy Adhesive Formulations*, McGraw-Hill Education, 2005.

[32] S. Peris, B. Tylkowski, J. Carles Ronda, R. Garcia-Valls, J. A. Reina and M. Giamberini, Synthesis, characterization, and photoresponsive behavior of new azobenzene-containing polyethers, *Journal of Polymer Science Part A: Polymer Chemistry*, 2009, 47, 5426-5436.

[33] X. Sun, W. Wang, L. Qiu, W. Guo, Y. Yu and H. Peng, Unusual Reversible Photomechanical Actuation in Polymer/Nanotube Composites, *Angewandte Chemie International Edition*, 2012, 51, 8520-8524.

[34] B. E. Rochon P., Natansohn A., Optically induced surface gratings on azoaromatic polymer films, *Appl. Phys. Lett.*, 1995, 66, 136-138.

[35] P. Z. M. Moniruzzaman, G.F. Fernando, Investigation of reversible photo-mechanical properties of azobenzene- based polymer films by nanoindentation, *Scripta Materialia*, 2006, 54, 257-261.

[36] M. Kondo, R. Miyasato, Y. Naka, J.-i. Mamiya, M. Kinoshita, Y. Yu, C. J. Barrett and T. Ikeda, Photomechanical properties of azobenzene liquid-crystalline elastomers, *Liquid Crystals*, 2009, 36, 1289-1293.

[37] S. M. Kondo M., Yamada M., Naka Y., Mamiya Y., Kinoshita M., Shishido A., Yu Y., Ikeda T., Effect of contraction of photoactive chromophores on photomechanical properties of crosslinked azobenzene liquid-crystalline polymers, *Journal of Materials Chemistry*, 2010, 20, 117-122.

[38] M. H. Li, P. Keller, B. Li, X. G. Wang and M. Brunet, Light-driven side-on nematic elastomer actuators, *Advanced Materials*, 2003, 15, 569-572.

[39] S. J. Kalista, Jr., Self-healing of poly(ethylene-co-methacrylic acid) copolymers following projectile puncture, *Mechanics of Advanced Materials and Structures*, 2007, 14, 391-397.

[40] B. Voit, Principles of polymerization. By George Odian, *Macromolecular Chemistry and Physics*, 2002, 203, 2142-2142.

REFERENCES

[41]   A. Shimamura, A. Priimagi, J.-i. Mamiya, T. Ikeda, Y. Yu, C. J. Barrett and A. Shishido, Simultaneous Analysis of Optical and Mechanical Properties of Cross-Linked Azobenzene-Containing Liquid-Crystalline Polymer Films, *ACS Applied Materials & Interfaces*, 2011, 3, 4190-4196.

[42]   X. Hu, X. Zhao, L. H. Gan and X. Xia, Synthesis, characterization, and photochromic properties of PMMA functionalized with 4,4'-diacryloyloxyazobenzene, *Journal of Applied Polymer Science*, 2002, 83, 1061-1068.

[43]   V. Blomquist, B. Helgee and F. H. J. Maurer, Synthesis and characterization of copolymers of methyl methacrylate and 11-(4-ethoxyazobenzene-4 '-oxy)undecyl methacrylate, *Macromolecular Chemistry and Physics*, 2001, 202, 2742-2749.

[44]   K. H. Tanaka S., Sudo A., Nishida H., Endo T., Anisotropic photomechanical response of stretched blend film made of polycaprolactone-polyvinyl ether with azobenzene group as side chain, *Macromol. Chem. Phys.*, 2008, 209, 2071-2077.

[45]   C. Schuh, N. Lomadze, J. Ruhe, A. Kopyshev and S. Santer, Photomechanical degrafting of azo-functionalized poly(methacrylic acid) (PMAA) brushes, *J Phys Chem B*, 2011, 115, 10431-10438.

[46]   W. X. Kim H., Fujita Y., Sudo A., Nishida H., Fujhii M., Endo T., Reversible photomechanical switching behavior of azobenzene-containing semi- interpenetrating network under UV and visible light irradiation, *Macromol. Chem. Phys.*, 2005, 206, 2106-2111.

[47]   O. Kulikovska, L. M. Goldenberg and J. Stumpe, Supramolecular azobenzene-based materials for optical generation of microstructures, *Chemistry of Materials*, 2007, 19, 3343-3348.

[48]   G. M. Eisenbach, Isomerization of aromatic azo chromophores in poly(ethyl acrylate) networks and photomechanical effect, *POLYMER*, 1980, 21, 1175-1179.

[49]   W. Grellmann and S. Seidler, *Deformation and Fracture Behaviour of Polymers*, Springer Berlin Heidelberg, 2013.

[50]   L. E. Nielsen and R. F. Landel, *Mechanical Properties of Polymers and Composites, Second Edition*, Taylor & Francis, 1993.

[51]   M. Alemani, M. Peters, S. Hecht, K.-H. Rieder, F. Moresco and L. Grill, Electric Field-Induced Isomerization of Azobenzene by STM, *J. Am. Chem. Soc.*, 2006, 128, 14446-14447.

[52]   A. Emoto, E. Uchida and T. Fukuda, Optical and physical applications of photocontrollable materials: Azobenzene-containing and Liquid crystalline polymers, *Polymers*, 2012, DOI: 10.3390/polym4010150, 150-186.

REFERENCES

[53]   D. A. Davis, A. Hamilton, J. Yang, L. D. Cremar, D. Van Gough, S. L. Potisek, M. T. Ong, P. V. Braun, T. J. Martinez, S. R. White, J. S. Moore and N. R. Sottos, Force-induced activation of covalent bonds in mechanoresponsive polymeric materials, *Nature*, 2009, 459, 68-72.

[54]   J. A. Delaire and K. Nakatani, Linear and Nonlinear Optical Properties of Photochromic Molecules and Materials, *Chem Rev*, 2000, 100, 1817-1846.

[55]   J. S. Katz and J. A. Burdick, Light-responsive biomaterials: development and applications, *Macromol Biosci*, 2010, 10, 339-348.

[56]   R. Klajn, P. J. Wesson, K. J. Bishop and B. A. Grzybowski, Writing self-erasing images using metastable nanoparticle "inks", *Angew Chem Int Ed Engl*, 2009, 48, 7035-7039.

[57]   A. Lendlein and V. P. Shastri, Stimuli-sensitive polymers, *Adv Mater*, 2010, 22, 3344-3347.

[58]   M. M. Russew and S. Hecht, Photoswitches: from molecules to materials, *Adv Mater*, 2010, 22, 3348-3360.

[59]   T. Seki, Smart photoresponsive polymer systems organized in two dimensions, *Bull. Chem. Soc. Jpn*, 2007, 80, 2084-2109.

[60]   Z. Sekkat and W. Knoll, *Photoreactive organic thin films*, Academic Press, Amsterdam ; Boston, 2002.

[61]   C. Ho, K. Yang and S. Lee, Mechanistic study of trans-cis isomerization of the substituted azobenzene moiety bound on a Liquid- Crystalline polymer, *Journal of Polymer Science*, 2001, 39, 2296-2307.

[62]   T. Srikhirin and A. Laschitsch, Light-induced softening of azobenzene dye- doped polymer films probed with quartz crystal resonators, *Applied Physics Letters*, 2000, 77, 963-965.

[63]   E. Verploegen, J. Soulages, M. Kozberg, T. Zhang, G. McKinley and P. Hammond, Reversible switching of the shear modulus of photoresponsive liquid-crystalline polymers, *Angew Chem Int Ed Engl*, 2009, 48, 3494-3498.

[64]   Ravve, *Light-associated reactions of synthetic polymers*, Springer edn., 2006.

[65]   R. Lovrien, The photoviscosity effect, *Proc Natl Acad Sci U S A*, 1967, 57, 236-242.

[66]   S. L. Potisek, D. A. Davis, N. R. Sottos, S. R. White and J. S. Moore, Mechanophore-linked addition polymers, *J Am Chem Soc*, 2007, 129, 13808-13809.

REFERENCES

[67]   S. K. Surampudi, H. R. Patel, G. Nagarjuna and D. Venkataraman, Mechano-isomerization of azobenzene, *Chemical Communications*, 2013, 49, 7519-7521.

[68]   J. Garcia-Amorós and D. Velasco, *Polysiloxane Side-Chain Azobenzene-Containing Liquid Single Crystal Elastomers for Photo-Active Artificial Muscle-Like Actuators*, 2012.

[69]   I. T. Zhao Y., *Smart light responsive materials: azobenzene containing polymers and liquid crystals*, 2009.

[70]   E. Merino and M. Ribagorda, Control over molecular motion using the cis–trans photoisomerization of the azo group, *Beilstein Journal of Organic Chemistry*, 2012, 8, 1071-1090.

[71]   Z. Mahimwalla, K. Yager, J.-i. Mamiya, A. Shishido, A. Priimagi and C. Barrett, Azobenzene photomechanics: prospects and potential applications, *Polymer Bulletin*, 2012, 69, 967-1006.

[72]   D. H. Choi, Effect of Temperature on Photoinduced Reorientation of Azobenzene Chromophore in the Side Chain Copolymers, *Bull. Korean Chem. Soc.*, 1999, 20, 1010-1016.

[73]   C. Sanchez, R. Alcala, S. Hvilsted, P. S. Ramanujam, C. Sanchez, R. Alcala, S. Hvilsted and P. S. Ramanujam, Effect of heat and film thickness on a photoinduced phase transition in azobenzene liquid crystalline polyesters, *Journal of Applied Physics*, 2003, 93, 4454-4460.

[74]   N. J. Dunn, W. H. Humphries, A. R. Offenbacher, T. L. King and J. A. Gray, pH-Dependent cis → trans Isomerization Rates for Azobenzene Dyes in Aqueous Solution†, *The Journal of Physical Chemistry A*, 2009, 113, 13144-13151.

[75]   Q. Tang, X. Meng, H. Jiang, T. Zhou, C. Gong, X. Fu and S. Shi, Synthesis and characterization of photo- and pH-responsive nanoparticles containing amino-substituted azobenzene, *Journal of Materials Chemistry*, 2010, 20, 9133-9139.

[76]   T. Yamamoto and M. Yoshida, Viscoelastic and Photoresponsive Properties of Microparticle/Liquid-Crystal Composite Gels: Tunable Mechanical Strength along with Rapid-Recovery Nature and Photochemical Surface Healing using an Azobenzene Dopant, *Langmuir*, 2012, 28, 8463-8469.

[77]   L. Sorelli, F. Fabbri, J. Frech-Baronet, A.-D. Vu, M. Fafard, T. Gacoin, K. Lahlil, L. Martinelli, Y. Lassailly and J. Peretti, A closer look at the light-induced changes in the mechanical properties of azobenzene-containing polymers by statistical nanoindentation, *Journal of Materials Chemistry C*, 2015, 3, 11055-11065.

REFERENCES

[78]   M. J. Barrett C., Yager K., Ikeda T., Photo-mechanical effects in azobenzene-containing soft materials, *Soft Matter*, 2007, 3, 1249-1261.

[79]   H. Finkelmann, E. Nishikawa, G. G. Pereira and M. Warner, A new opto-mechanical effect in solids, *Physical Review Letters*, 2001, 87.

[80]   M. A. Kienzler, A. Reiner, E. Trautman, S. Yoo, D. Trauner and E. Y. Isacoff, A Red-Shifted, Fast-Relaxing Azobenzene Photoswitch for Visible Light Control of an Ionotropic Glutamate Receptor, *Journal of the American Chemical Society*, 2013, 135, 17683-17686.

[81]   T. A. Plaisted and S. Nemat-Nasser, Quantitative evaluation of fracture, healing and re-healing of a reversibly cross-linked polymer, *Acta Materialia*, 2007, 55, 5684-5696.

[82]   B. J. Blaiszik, S. L. B. Kramer, S. C. Olugebefola, J. S. Moore, N. R. Sottos and S. R. White, in *Annual Review of Materials Research, Vol 40*, ed. D. R. R. M. Z. F. Clarke, 2010, vol. 40, pp. 179-211.

[83]   J. Hu, *Advances in Shape Memory Polymers*, Elsevier Science, 2013.

[84]   A. Lendlein and S. Kelch, Shape-Memory Polymers, *Angewandte Chemie International Edition*, 2002, 41, 2034-2057.

[85]   C. Liu, H. Qin and P. T. Mather, Review of progress in shape-memory polymers, *Journal of Materials Chemistry*, 2007, 17, 1543-1558.

[86]   E. D. Rodriguez, X. Luo and P. T. Mather, Linear/Network Poly(ε-caprolactone) Blends Exhibiting Shape Memory Assisted Self-Healing (SMASH), *ACS Applied Materials & Interfaces*, 2011, 3, 152-161.

[87]   A. Lendlein, H. Jiang, O. Junger and R. Langer, Light-induced shape-memory polymers, *Nature*, 2005, 434, 879-882.

[88]   M. Behl and A. Lendlein, Shape-memory polymers, *Materials Today*, 2007, 10, 20-28.

[89]   T. Fukuda, H. Matsuda, T. Shiraga, T. Kimura, M. Kato, N. K. Viswanathan, J. Kumar and S. K. Tripathy, Photofabrication of Surface Relief Grating on Films of Azobenzene Polymer with Different Dye Functionalization, *Macromolecules*, 2000, 33, 4220-4225.

[90]   G. S. Kumar and D. C. Neckers, Photochemistry of azobenzene-containing polymers, *Chemical Reviews*, 1989, 89, 1915-1925.

[91]   C. Weber, T. Liebig, M. Gensler, L. Pithan, S. Bommel, D. Bléger, J. P. Rabe, S. Hecht and S. Kowarik, Light-Controlled "Molecular Zippers" Based on Azobenzene Main Chain Polymers, *Macromolecules*, 2015, 48, 1531-1537.

REFERENCES

[92]   H. S. Kang, H.-T. Kim, J.-K. Park and S. Lee, Light-Powered Healing of a Wearable Electrical Conductor, *Advanced Functional Materials*, 2014, 24, 7273-7283.

[93]   B. Harris and I. o. Materials, *Engineering Composite Materials*, IOM, 1999.

[94]   D. Ratna, *Epoxy Composites: Impact Resistance and Flame Retardancy*, iSmithers Rapra Publishing, 2007.

[95]   NASH, 2010, Nash Pumps for Processing Composites in Autoclaves, Place of Publication: Available at http://gdnash.com.br/ing/pdf/1087%20Autoclaves%20for%20composites.pdf.

[96]   L. Tong, A. P. Mouritz and M. Bannister, *3D Fibre Reinforced Polymer Composites*, Elsevier Science, 2002.

[97]   D. H. Allen, *Damage and Interfacial Debonding in Composites*, Elsevier Science, 1996.

[98]   J. A. Nairn, in *Comprehensive Composite Materials*, Pergamon, Oxford, 2000, DOI: http://dx.doi.org/10.1016/B0-08-042993-9/00069-3, pp. 403-432.

[99]   V. V. Silberschmidt, *Dynamic Deformation, Damage and Fracture in Composite Materials and Structures*, Elsevier Science, 2016.

[100] R. Y. Kim and R. M. Aoki, Transverse cracking and delamination in composite materials, *Fibre Science and Technology*, 1983, 18, 203-216.

[101] J.-L. Rebière, Matrix cracking and delamination evolution in composite cross-ply laminates, *Cogent Engineering*, 2014, 1, 943547.

[102] E. Randjbaran, R. Zahari, N. A. Abdul Jalil and D. L. Abang Abdul Majid, Hybrid Composite Laminates Reinforced with Kevlar/Carbon/Glass Woven Fabrics for Ballistic Impact Testing, *The Scientific World Journal*, 2014, 2014, 413753.

[103] A. Varvani-Farahani and A. Shirazi, A Fatigue Damage Model for (0/90) FRP Composites based on Stiffness Degradation of 0° and 90° Composite Plies, *Journal of Reinforced Plastics and Composites*, 2007, DOI: 10.1177/0731684407079771.

[104] W. J. Cantwell and J. Morton, The impact resistance of composite materials — a review, *Composites*, 1991, 22, 347-362.

[105] M. O. W. Richardson and M. J. Wisheart, Review of low-velocity impact properties of composite materials, *Composites Part A: Applied Science and Manufacturing*, 1996, 27, 1123-1131.

REFERENCES

[106] A. P. Mouritz, *Introduction to Aerospace Materials*, Elsevier Science, 2012.

[107] H. F. Mark, *Encyclopedia of Polymer Science and Technology, Concise*, Wiley, 2013.

[108] A. A. M. Badawy, Impact behavior of glass fibers reinforced composite laminates at different temperatures, *Ain Shams Engineering Journal*, 2012, 3, 105-111.

[109] S. A. Hayes, F. R. Jones, K. Marshiya and W. Zhang, A self-healing thermosetting composite material, *Composites Part A: Applied Science and Manufacturing*, 2007, 38, 1116-1120.

[110] Impact modifiers: how to make your compound tougher, *Plastics, Additives and Compounding*, 2004, 6, 46-49.

[111] S. E. Amos and B. Yalcin, *Hollow Glass Microspheres for Plastics, Elastomers, and Adhesives Compounds*, Elsevier Science, 2015.

[112] A. C. Garg and Y.-W. Mai, Failure mechanisms in toughened epoxy resins—A review, *Composites Science and Technology*, 1988, 31, 179-223.

[113] P. Wang, X. Zhang, G. Lim, H. Neo, A. A. Malcolm, Y. Xiang, G. Lu and J. Yang, Improvement of impact-resistant property of glass fiber-reinforced composites by carbon nanotube-modified epoxy and pre-stretched fiber fabrics, *Journal of Materials Science*, 2015, 50, 5978-5992.

[114] M. J. Pawar, A. Patnaik and R. Nagar, Experimental investigation and numerical simulation of granite powder filled polymer composites for wind turbine blade: A comparative analysis, *Polymer Composites*, 2015, DOI: 10.1002/pc.23700, n/a-n/a.

[115] M. Sudheer, R. Prabhu, K. Raju and T. Bhat, Effect of Filler Content on the Performance of Epoxy/PTW Composites, *Advances in Materials Science and Engineering*, 2014, 2014, 11.

[116] J. Gibson, J. McKee, G. Freihofer, S. Raghavan and J. Gou, Enhancement in ballistic performance of composite hard armor through carbon nanotubes, *International Journal of Smart and Nano Materials*, 2013, 4, 212-228.

[117] N.-I. M. Mohammad, Latifi; Mohammad, Amani-Tehran, Enhancement of Composite Performance by Hollow Polyester Fibers *JOURNAL OF TEXTILES AND POLYMERS*, 2014, 2, 45-50.

[118] H. Wiebeck, D. F. Borrelly, C. Xavier, P. S. Santos, S. A. Asciutti and M. P. Corrêa, The Effect of Silane Coupling Agents on a Composite

Polyamide-6/Talc, *Brazilian Journal of Chemical Engineering*, 1998, 15, 406-409.

[119] S. R. White, N. R. Sottos, P. H. Geubelle, J. S. Moore, M. R. Kessler, S. R. Sriram, E. N. Brown and S. Viswanathan, Autonomic healing of polymer composites, *Nature*, 2001, 409, 794-797.

[120] D. A. McIlroy, B. J. Blaiszik, M. M. Caruso, S. R. White, J. S. Moore and N. R. Sottos, Microencapsulation of a Reactive Liquid-Phase Amine for Self-Healing Epoxy Composites, *Macromolecules*, 2010, 43, 1855-1859.

[121] T. Yin, M. Z. Rong, M. Q. Zhang and G. C. Yang, Self-healing epoxy composites – Preparation and effect of the healant consisting of microencapsulated epoxy and latent curing agent, *Composites Science and Technology*, 2007, 67, 201-212.

[122] S. M. Bleay, C. B. Loader, V. J. Hawyes, L. Humberstone and P. T. Curtis, A smart repair system for polymer matrix composites, *Composites Part A: Applied Science and Manufacturing*, 2001, 32, 1767-1776.

[123] N. K. Mehta, Self-healing Fiber-reinforced Epoxy Composites: Solvent-epoxy Filled Hollow Glass Fibers, *International Journal of Composite Materials*, 2013, 3, 145-155.

[124] R. S. Trask, G. J. Williams and I. P. Bond, Bioinspired self-healing of advanced composite structures using hollow glass fibres, *Journal of the Royal Society Interface*, 2007, 4, 363-371.

[125] S. A. Hayes, W. Zhang, M. Branthwaite and F. R. Jones, Self-healing of damage in fibre-reinforced polymer-matrix composites, *Journal of the Royal Society Interface*, 2007, 4, 381-387.

[126] N. Patra, M. Salerno, A. Diaspro and A. Athanassiou, Effect of solvents on the dynamic viscoelastic behavior of poly(methyl methacrylate) film prepared by solvent casting, *Journal of Materials Science*, 2011, 46, 5044-5049.

[127] N. Patra, A. C. Barone and M. Salerno, Solvent effects on the thermal and mechanical properties of poly(methyl methacrylate) casted from concentrated solutions, *Advances in Polymer Technology*, 2011, 30, 12-20.

[128] Y. Kondo, A. Matsumoto, K. Fukuyasu, K. Nakajima and Y. Takahashi, Gold-Colored Organic Crystals of an Azobenzene Derivative, *Langmuir*, 2014, 30, 4422-4426.

[129] H. R. Kricheldorf, O. Nuyken and G. Swift, *Handbook of Polymer Synthesis: Second Edition*, CRC Press, 2004.

[130] A. I. Vogel and B. S. Furniss, *Vogel's textbook of practical organic chemistry*, Longman, 1989.

REFERENCES

[131] J. Clayden, N. Greeves and S. G. Warren, *Organic chemistry*, Oxford University Press, Oxford, 2nd edn., 2012.

[132] B. M. Trost, C. R. Hutchinson, International Union of Pure and Applied Chemistry. Organic Chemistry Division., American Chemical Society. Division of Organic Chemistry. and University of Wisconsin. Department of Chemistry., *Organic synthesis, today and tomorrow : proceedings of the 3rd IUPAC Symposium on Organic Synthesis, Madison, Wisconsin, USA, 15-20 June 1980*, Pergamon Press, Oxford ; New York, 1st edn., 1981.

[133] B. Standard, *BS/EN ISO 14577-1*, British Standard, 2002.

[134] *AccuPycTM 1330 Pycnometer Operator's Manual V3.03*, 2001.

[135] R. B. Cook and P. Zioupos, The fracture toughness of cancellous bone, *Journal of Biomechanics*, 2009, 42, 2054-2060.

[136] N. Domun, H. Hadavinia, T. Zhang, T. Sainsbury, G. H. Liaghat and S. Vahid, Improving the fracture toughness and the strength of epoxy using nanomaterials ? a review of the current status, *Nanoscale*, 2015, 7, 10294-10329.

[137] H. Taoda, K. Hayakawa, K. Kawase and H. Yamakita, PHOTOCHEMICAL CONVERSION AND STORAGE OF SOLAR ENERGY BY AZOBENZENE, *Journal of Chemical Engineering of Japan*, 1987, 20, 265-270.

[138] *Spectrophotometer CM-700d/600d Instruction Manual*.

[139] J. M. Lloyd, *Thermal Imaging Systems*, Springer US, 2013.

[140] D. Bates, G. Smith, D. Lu and J. Hewitt, Rapid thermal non-destructive testing of aircraft components, *Composites Part B: Engineering*, 2000, 31, 175-185.

[141] M. Vollmer and K. P. Möllmann, *Infrared Thermal Imaging: Fundamentals, Research and Applications*, Wiley, 2010.

[142] R. K. Fruehmann, D. A. Crump and J. M. Dulieu-Barton, in *Thermomechanics and Infra-Red Imaging, Volume 7*, Springer New York, 2011, DOI: 10.1007/978-1-4614-0207-7_2, ch. 2, pp. 9-15.

[143] G. J. Dvorak, *Inelastic Deformation of Composite Materials: IUTAM Symposium, Troy, New York, May 29 – June 1, 1990*, Springer New York, 2012.

[144] B. Standard, *BS/EN ISO 18352 Determination of compression-after-impact properties at a specified impact-energy level*, British Standard, 2009.

REFERENCES

[145] A. Matsumoto, M. Kawaharazuka, Y. Takahashi, N. Yoshino, T. Kawai and Y. Kondo, Gold-Colored Organic Crystals Formed from an Azobenzene Derivative, *Journal of Oleo Science*, 2010, 59, 151-156.

[146] P. URBEN, *Bretherick's Handbook of Reactive Chemical Hazards: 2-Volume Set*, Elsevier Science, 2013.

[147] M. J. Monteiro and H. de Brouwer, Intermediate Radical Termination as the Mechanism for Retardation in Reversible Addition−Fragmentation Chain Transfer Polymerization, *Macromolecules*, 2001, 34, 349-352.

[148] J. D. R. T. M. Moniruzzaman, C.J. Sabey, G.F. Fernando, The use of ^{1}H NMR and UV/vis measurements for quantitive determination of trans/cis isomerization of a photo-responsive monomer and its copolymer, *Applied Polymer Science*, 2006, 100, 1103-1112.

[149] F. F. De Nograro, P. Guerrero, M. A. Corcuera and I. Mondragon, Effects of chemical structure of hardener on curing evolution and on the dynamic mechanical behavior of epoxy resins, *Journal of Applied Polymer Science*, 1995, 56, 177-192.

[150] J. Y. Lee, J. Jang, S. S. Hwang, S. M. Hong and K. U. Kim, Synthesis and curing of liquid crystalline epoxy resins based on 4,4′-biphenol, *POLYMER*, 1998, 39, 6121-6126.

[151] A. V. Zemskov, G. N. Rodionova, Y. G. Tuchin and V. V. Karpov, IR spectra and structure of some azo dyes — p-azobenzene derivatives — In various aggregate states, *Journal of Applied Spectroscopy*, 49, 1020-1024.

[152] J. M. G. Cowie, Glass transition temperatures of stereoblock, isotactic and atactic polypropylenes of various chain lengths, *European Polymer Journal*, 1973, 9, 1041-1049.

[153] A. Richter, M. Nowicki and B. Wolf, A nanoindentation study of photo-induced changes in polymers containing azobenzene, *Molecular Crystals and Liquid Crystals*, 2008, 483, 49-61.

[154] Y. Zhao and T. Ikeda, *Smart Light-Responsive Materials: Azobenzene-Containing Polymers and Liquid Crystals*, Wiley, 2009.

[155] P. Christogianni, M. Moniruzzaman and G. Kister, Light-triggered enhancement of mechanical properties and healing effect in azobenzene-based polymer films, *POLYMER*, 2015, 77, 272-277.

[156] K. M. Lee, H. Koerner, R. A. Vaia, T. J. Bunning and T. J. White, Light-activated shape memory of glassy, azobenzene liquid crystalline polymer networks, *Soft Matter*, 2011, 7, 4318-4324.

REFERENCES

[157] O. M. Tanchak and C. J. Barrett, Light-Induced Reversible Volume Changes in Thin Films of Azo Polymers: The Photomechanical Effect, *Macromolecules*, 2005, 38, 10566-10570.

[158] M. Matsumoto, S. Terrettaz and H. Tachibana, Photo-induced structural changes of azobenzene Langmuir–Blodgett films, *Advances in Colloid and Interface Science*, 2000, 87, 147-164.

[159] H. Y. Jiang, S. Kelch and A. Lendlein, Polymers Move in Response to Light, *Advanced Materials*, 2006, 18, 1471-1475.

[160] T. Mason and D. Peters, in *Practical Sonochemistry (Second Edition)*, Woodhead Publishing, 2002, DOI: http://dx.doi.org/10.1533/9781782420620.49, pp. 49-63.

[161] E. Rusu, N. Tudorachi and G. Rusu, Investigation on structure and thermal behavior of 4,4′-dihydroxyazobenzene functionalized with epoxy groups, *Journal of Analytical and Applied Pyrolysis*, 2012, 98, 144-150.

[162] L. Yang, N. Takisawa, T. Hayashita and K. Shirahama, Colloid Chemical Characterization of the Photosurfactant 4-Ethylazobenzene 4'-(Oxyethyl)trimethylammonium Bromide, *The Journal of Physical Chemistry*, 1995, 99, 8799-8803.

[163] D. Fujita, M. Murai, T. Nishioka and H. Miyoshi, Light Control of Mitochondrial Complex I Activity by a Photoresponsive Inhibitor†, *Biochemistry*, 2006, 45, 6581-6586.

[164] J. C. Murphy and L. C. Aamodt, Google Patents, 1984.

[165] Q. Wang, B. K. Storm and L. P. Houmøller, Study of the isothermal curing of an epoxy prepreg by near-infrared spectroscopy, *Journal of Applied Polymer Science*, 2003, 87, 2295-2305.

[166] O. S. Bushuyev, T. C. Corkery, C. J. Barrett and T. Fri??i, Photo-mechanical azobenzene cocrystals and in situ X-ray diffraction monitoring of their optically-induced crystal-to-crystal isomerisation, *Chemical Science*, 2014, 5, 3158-3164.

[167] G. A. Maier, G. Wallner, R. W. Lang and P. Fratzl, Structural Changes during Plastic Deformation at Crack Tips in PVDF Films: A Scanning X-ray Scattering Study, *Macromolecules*, 2005, 38, 6099-6105.

[168] B. J. Cardwell and A. F. Yee, Rate and temperature effects on the fracture toughness of a rubber-modified epoxy, *POLYMER*, 1993, 34, 1695-1701.

[169] C. Guerra, J. Scheibert, D. Bonamy and D. Dalmas, Understanding fast macroscale fracture from microcrack post mortem patterns, *Proceedings of the National Academy of Sciences*, 2012, 109, 390-394.

REFERENCES

[170] C. L. Yeung, S. Charlesworth, P. Iqbal, J. Bowen, J. A. Preece and P. M. Mendes, Different formation kinetics and photoisomerization behavior of self-assembled monolayers of thiols and dithiolanes bearing azobenzene moieties, *Physical Chemistry Chemical Physics*, 2013, 15, 11014-11024.

[171] R. Wanhill and S. Barter, in *Fatigue of Beta Processed and Beta Heat-treated Titanium Alloys*, Springer Netherlands, Dordrecht, 2012, DOI: 10.1007/978-94-007-2524-9_5, pp. 27-40.

[172] P. Musto, G. Ragosta, M. Abbate and G. Scarinzi, Photo-Oxidation of High Performance Epoxy Networks: Correlation between the Molecular Mechanisms of Degradation and the Viscoelastic and Mechanical Response, *Macromolecules*, 2008, 41, 5729-5743.

[173] B. T. Astrom, *Manufacturing of Polymer Composites*, Taylor & Francis, 1997.

[174] C. S. Grimmer and B. University of California, *The Cyclic Strength of Carbon Nanotube/glass Fiber Hybrid Composites*, University of California, Berkeley, 2008.

[175] N. J. Dovichi, T. G. Nolan and W. A. Weimer, Theory for laser-induced photothermal refraction, *Analytical Chemistry*, 1984, 56, 1700-1704.

[176] S. Gowthaman and S. Kunigal, in *46th AIAA/ASME/ASCE/AHS/ASC Structures, Structural Dynamics and Materials Conference*, American Institute of Aeronautics and Astronautics, 2005, DOI: doi:10.2514/6.2005-1997

10.2514/6.2005-1997.

[177] X.-L. Xie, C.-Y. Tang, X.-P. Zhou, R. K.-Y. Li, Z.-Z. Yu, Q.-X. Zhang and Y.-W. Mai, Enhanced Interfacial Adhesion between PPO and Glass Beads in Composites by Surface Modification of Glass Beads via In Situ Polymerization and Copolymerization, *Chemistry of Materials*, 2004, 16, 133-138.

[178] *Adhesives in Manufacturing*, Taylor & Francis, 1983.

[179] F. Nielsen, Google Patents, 2014.

[180] J. M. Esfahani, M. Esfandeh and A. R. Sabet, High-velocity impact behavior of glass fiber-reinforced polyester filled with nanoclay, *Journal of Applied Polymer Science*, 2012, 125, E583-E591.

[181] J. L. Thomason and M. A. Vlug, Influence of fibre length and concentration on the properties of glass fibre-reinforced polypropylene: 1. Tensile and flexural modulus, *Composites Part A: Applied Science and Manufacturing*, 1996, 27, 477-484.

REFERENCES

[182] M. N. Tamin, *Damage and Fracture of Composite Materials and Structures*, Springer Berlin Heidelberg, 2012.

[183] P. J. Hazell and G. Appleby-Thomas, A study on the energy dissipation of several different CFRP-based targets completely penetrated by a high velocity projectile, *Composite Structures*, 2009, 91, 103-109.

[184] S. K. Garcia-Castillo, S. Sánchez-Sáez and E. Barbero, Influence of areal density on the energy absorbed by thin composite plates subjected to high-velocity impacts, *The Journal of Strain Analysis for Engineering Design*, 2012, DOI: 10.1177/0309324712454996.

[185] D. G. Lee and N. P. Suh, *Axiomatic Design and Fabrication of Composite Structures: Applications in Robots, Machine Tools, and Automobiles*, Oxford University Press, USA, 2006.

[186] W. J. Cantwell and J. Morton, Comparison of the low and high velocity impact response of cfrp, *Composites*, 1989, 20, 545-551.

[187] R. Hosseinzadeh, M. M. Shokrieh and L. Lessard, Damage behavior of fiber reinforced composite plates subjected to drop weight impacts, *Composites Science and Technology*, 2006, 66, 61-68.

[188] R. S. Sikarwar, R. Velmurugan and V. Madhu, Experimental and analytical study of high velocity impact on Kevlar/Epoxy composite plates, *Central European Journal of Engineering*, 2012, 2, 638-649.

[189] M. E. Backman and W. Goldsmith, The mechanics of penetration of projectiles into targets, *International Journal of Engineering Science*, 1978, 16, 1-99.

[190] N. R. Mathivanan and J. Jerald, Experimental Investigation of Woven E-Glass Epoxy Composite Laminates Subjected to Low-Velocity Impact at Different Energy Levels, *Journal of Minerals and Materials Characterization and Engineering*, 2010, Vol.09No.07, 10.

[191] P. J. Hazell, G. J. Appleby-Thomas and G. Kister, Impact, penetration, and perforation of a bonded carbon-fibre-reinforced plastic composite panel by a high-velocity steel sphere: An experimental study, *The Journal of Strain Analysis for Engineering Design*, 2010, 45, 439-450.

[192] G. J. Williams, I. P. Bond and R. S. Trask, Compression after impact assessment of self-healing CFRP, *Composites Part A: Applied Science and Manufacturing*, 2009, 40, 1399-1406.

[193] G. C. Grimes, *Composite Materials: Testing and Design (tenth Volume)*, ASTM, 1992.

[194] P. Grant and C. Q. Rousseau, *Composite Structures: Theory and Practice*, ASTM, 2001.

[195] S. J. Garcia, Effect of polymer architecture on the intrinsic self-healing character of polymers, *European Polymer Journal*, 2014, 53, 118-125.

[196] J. García-Amorós and D. Velasco, Recent advances towards azobenzene-based light-driven real-time information-transmitting materials, *Beilstein Journal of Organic Chemistry*, 2012, 8, 1003-1017.

[197] N. E. R. Center, 2012, Materials and Processes, Place of Publication: Available at https://www.nde-ed.org/EducationResources/CommunityCollege/Materials/Structure/composite_class.htm.

[198] A. Kumar and R. K. Gupta, *Fundamentals of Polymer Engineering, Revised and Expanded*, CRC Press, 2003.